DTU Technical University of Denmark

Quantification of Radiation-induced DNA Damage following intracellular Auger-Cascades

Ph.D. Thesis by

Pil Møntegaard Fredericia

June 2017

The Hevesy Laboratory, Center for Nuclear Technologies, DTU

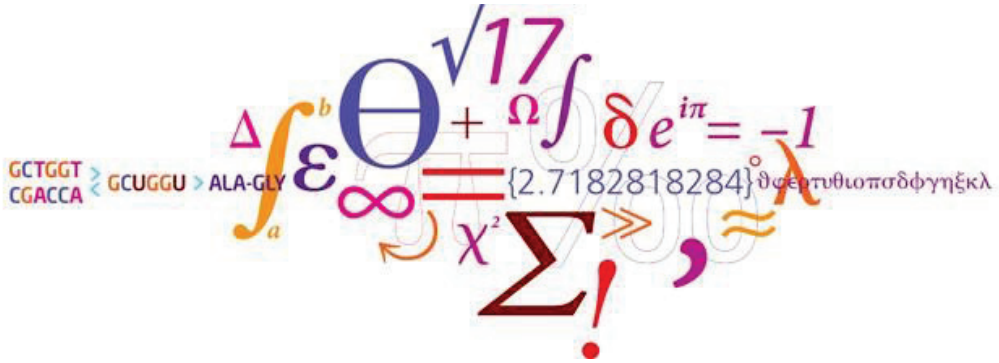

Preface

This thesis is the result of 3 years graduate work carried out carried at the Hevesy Laboratory, part of the Center for Nuclear Technologies, at the Technical University of Denmark, under the supervision of Dr. Torsten Groesser and Prof. Mikael Jensen.

The work has focused on investigating the biological response following intracellular Auger emitter decays and comparing these results with external reference radiation. ^{131}Cs has been developed as a new model for use in cell studies of radiation damage following Auger-emitter decays. This radionuclide is gamma-silent, has no nuclear beta emissions, has a good Auger cascade and internalises into cells by a natural process. Special attention has been given to the experimental design to establish a reliable calculation of the absorbed dose and dose rate from internalised ^{131}Cs. In order to obtain valid RBE-values, care has been taken to deliver the reference radiation at dose rates comparable to that of the internal ^{131}Cs test radiation.

The work is presented as fulfillment of the requirements for obtaining a PhD at the Technical University. It is composed as a monograph and divided into chapters comprising: Introduction, background overview, materials and methods, results, discussion, conclusions and outlook.

Acknowledgement

I will especially like to thank my main supervisor Mikael Jensen. I am thankful for the support and guidance he has provide during these 3 years of my PhD study and not at least for many challenging and inspiring discussions. I am especially grateful to him for giving me the chance to do a PhD in a field combining my educational background in human biology with my interest in physics. Moreover, he has been a role model for me, not just in the role as a professional teacher, but also as a researcher with an open mind.

I would like to thank my co-supervisor Dr. Torsten Groesser, for guidance on biological issues and discussions on research and laboratory procedures.

Gregory Severin (now Michigan State University and FRIB) has as a post-doc at the Hevesy Laboratory, helped the entire project by developing the production radiochemistry of ^{131}Cs . Boon Quan Lee from Dept. Nuclear Physics at Australian National University, Canberra, has shared with me important results from a theoretical calculation of the ^{131}Cs Auger electron yields. Ulli Koester from ILL, Grenoble, France has provided inspiration and the essential fuel for my studies: high flux neutron irradiations of barium for ^{131}Cs production. My research presented here is standing on the shoulders of Greg, Boon, and Ulli.

Special thanks should be given to the Hevesy Laboratory technicians for their hard work in our production of radiopharmaceuticals, which has provided part of the funding for this study. I am amazed by their helpfulness, spirit and hard work.
In addition I would like to thank the remaining staff at the Hevesy Laboratory, and especially my fellow PhD students (Anders Frellsen, Bente Mathiessen, Jesper Fonslet and Mattia Siragusa).

Acknowledgement

Last but not least, I would like to thank my absolutely amazing family, for their support during very stressful time. My dad, Johnny Fredericia deserves special thanks, for introducing me to the natural sciences in a very early age. He has been my teacher and role model!

I would not have made it without you!

-*Pil Møntegaard Fredericia*

Abstract

Purpose: The aim my PhD study and the topic of this thesis is to investigate the radiotoxicity and the Relative Biological effectiveness (RBE) of intracellular Auger cascades. A special focus is kept on obtaining reliable absorbed dose calculations and using matched dose rate profiles for the Auger exposed cells and cells exposed to the reference radiation.

In order to accomplish this, a new experimental model was developed. The Auger cascades were induced by intracellular decays of the electron-capture radionuclide ^{131}Cs. The use of radiocaesium allowed me to develop new version of the cellular S-values (S_C-values).

The work can be divided into three steps; Examination of the bio-kinetics of the Auger emitter ^{131}Cs used in the study, calculations of the S_C-values and finally the measurement of the RBE of intracellular ^{131}Cs decays, through yH2AX and clonogenic cell survival assay.

Methods: A series of experiments examining the cellular uptake, release rate and cellular accumulations of ^{131}Cs in HeLa and V79 cell cultures were performed. The intracellular ^{131}Cs activity was measured using liquid scintillation counting. The geometry used for the S_C-values calculations were a confluent cellular monolayer, with the nuclei dispersed within. The height of this cellular monolayer and the size and shape of the nuclei were determined by confocal microscopy for both HeLa and V79 cell cultures. S_C-values values were obtained for whole cell to nucleus, S_C(N←C), with ^{131}Cs distributed homogeneously throughout the entire cellular monolayer. Monoenergetic electron emission dose kernels for a point source were calculated using the method applied by MIRD for cellular S-values and using Cole´s pseudo stopping power for electrons in water. K- and L-Auger electron energies and intensities (24.6 keV (9.3 %) and 3.43 keV (79.7 %) respectively) with an intensity normalisation factor of 1.17 were used as input for the S_C value calculation. To measure the RBE of intracellular ^{131}Cs decays, confluent cellular monolayers of HeLa and V79 cells were incubated with ^{131}Cs containing medium. Using the obtained results of the ^{131}Cs bio-kinetics, and the S_C-values, dose rate profiles and absorbed doses for the ^{131}Cs exposed cells could be calculated. HeLa and V79 cell cultures were then exposed to matched dose rate profiles using ^{137}Cs y-rays as the reference

Abstract

radiation. The biological effects of the two exposures were evaluated using yH2AX and clonogenic cell survival.

Results: ^{131}Cs was taken up, accumulated and then released by both cell lines. The uptake and release could be described by exponential equations ($A = A_0 * (1 - e^{-t*k_c})$ and $A = A_0 * e^{-t*k_{out}}$) with k_c and k_{out} having values of 1/283 min^{-1} (HeLa), 1/204 min^{-1} (V79) and 1/339 min^{-1} (HeLa) , 1/256 min^{-1} (V79) respectively. The cellular uptake of ^{131}Cs was found to be mediated by the Na^+/K^+-ATPase, supporting the hypothesis of a homogenous, intracellular distribution of ^{131}Cs. The S_C-values for 29 and 50 different sized nuclei were found to range from 7.78*10^{-4} to 7.83*10^{-4} Gy/(Bq*Sec)/pL for HeLa nuclei and from 7.45*10^{-4} to 7.63 *10^{-4} Gy/(Bq*Sec)/pL for V79 nuclei. The S_C-values were shown to be were very robust and almost independent of cellular and nuclear size. A RBE value of 1 was obtained for HeLa cells using yH2AX assays. RBE values of 4.5 ± 0.5 and 3.8 ± 0.8 were obtained for HeLa and V79 cells respectively, using clonogenic cell survival. The RBE values obtained in this study are higher than expected for Auger emitters located intracellularly but not directly intercalated to the DNA.

Conclusions: The implication of this study is two-fold. The obtained RBE values give further hope for the development of future Auger therapy, as the Auger emitters might not be needed to bind to the DNA in order to achieve high radiotoxicity. At the same time these RBE values should raise concerns about in the ignorance of Auger electrons in dosimetry of diagnostic nuclear medicine procedures, as the risk associated with these might be underestimated. The RBE of Auger emitter decays clearly need to be further investigated. My new experimental method with the robust absorbed dose calculations, the new concept of S_C-values, and the applicability to most cells types and all Auger emitters with homogeneous intracellular distribution, could be a valuable tool for such investigations.

Resume (in Danish)

Formål: Formålet med mit PhD studie og emnet for denne afhandling er en undersøgelse af radiotoksiciteten og den Relative Biologiske Effektivitet (RBE) af intracellulære Auger-kaskader. Særlig fokus har været rettet mod at opnå pålidelige beregninger af absorberet dosis og brugen af sammenlignelige dosishastigheder for både de celler, der blev bestrålet med Auger elektroner og de celler der blev bestrålet med reference strålingen. For at kunne opnå dette har jeg udviklet en ny eksperimental metode. Den radioaktive isotop ^{131}Cs, der henfalder via elektron indfangning, blev brugt til at frembringe disse Auger-kaskader. Brugen af ^{131}Cs tillod mig at udvikle en ny version af de cellulære S-værdier. Arbejdet kan inddeles i tre dele;

- Undersøgelse af bio-kinetikken af ^{131}Cs, der var den Auger-emitter, som blev brugt i studiet
- Beregning af S_C-værdierne
- Måling af RBE for intracellulære ^{131}Cs henfald, med to anerkendte metoder: *γH2AX* og *clonogenic cell survival*.

Metode: Der er udført undersøgelser over optagelsen, frigivelseshastigheden og akkumuleringen af ^{131}Cs in HeLa og V79 celler. Den intracellulære ^{131}Cs aktivitet blev målt via væskescintillation. Geometrien, der blev brugt til beregning af de cellulære S_C-værdier, var et konfluent cellulært enkeltlag, hvori cellekernerne var placeret. Højden af dette cellelag (for både HeLa og V79 cellekulturer) samt cellekernernes størrelse og form, blev målt ved hjælp af konfokal mikroskopi. ^{131}Cs var homogent fordelt i hele dette cellelag og de cellulære S_C-værdier blev beregnet for "hele cellen til kernen". *Dose-kernel* for monoenergetiske elektroner fra en punktkilde, blev beregnet ved brug af samme metode, som anvendes af MIRD ved beregning af cellulære S-værdier, og ved brug af Cole's "pseudo stopping power" for elektroner i vand. Energien af K- og L- elektronerne og deres intensitet (24,6 keV (9,3 %) og 3,43 keV (79,7 %) blev intensitets-normaliseret med en faktor 1.17, og herefter brugt som input til beregning af S_C-værdierne. For at finde RBEen blev HeLa og V79 cellekulturer inkuberet med vækstmedium tilsat ^{131}Cs. Baseret på den opnåede viden om ^{131}Cs´ biokinetik og de beregnede S_c-værdier, kunne dosis-hastighedes-profilerne og den absorberede dosis beregnes. Disse

dosishastighedsprofiler blev brugt til at planlægge ekstern bestråling af celler med ^{137}Cs γ-stråling, således at cellerne blev udsat for den samme dosishastighedsprofil. Den biologiske effekt af den interne og den eksterne bestråling blev målt med γH2AX og *clonogenic cell survival assay*.

Resultater: Begge cellelinjer var i stand til at optage, akkumulere og derefter frigive ^{131}Cs. Optaget og frigivelsen kunne beskrives ved brug af simple eksponentielle udtryk ($A = A_0 * (1 - e^{-t*k_c})$ og $A = A_0 * e^{-t*k_{out}}$) hvor k_c og k_{out} var henholdsvis 1/283 min^{-1} (HeLa), 1/204 min^{-1} (V79) og 1/339 min^{-1} (HeLa) , 1/256 min^{-1} (V79). ^{131}Cs blev taget op af cellerne via Na^+/K^+-ATPasen, hvilket understøtter hypotesen om den homogene intracellulære fordeling af ^{131}Cs. S_C-værdierne for 29 HeLa og 50 V79 cellekerner af varierende volumen, blev beregnet til 7,78*10^{-4} -7,83*10^{-4} Gy/(Bq*Sec)/pL (HeLa) og 7,45*10^{-4} - 7.63 *10^{-4} Gy/(Bq*Sec)/pL (V79). S_C-værdierne viste sig at være meget robuste som beregnings-værktøj, fordi de næsten er uafhængige af celle og cellekernes størrelse.
En RBE-værdi på 1 blev fundet for HeLa celler ved brug af γH2AX metoden.
RBE-værdier på 4,5 ± 0,5 og 3,8 ± 0,8 blev fundet for HeLa henholdsvis V79 ved at undersøge overlevelsesraten med *clonogenic cell survival.*
RBE-værdierne fundet i dette studie er højere end, hvad der normalt forventes for Auger-emitterer der er lokaliseret intracellulært, men ikke er bundet mellem DNA-strengene.
Konklusion: Betydningen af dette studie todelt. De fundne RBE-værdier giver håb for udviklingen af fremtidig Auger-terapi, da Auger-emitteren muligvis ikke behøver at være bundet til DNAet for at opnå en høj radiotoksicitet. På samme tid burde disse RBE-værdier også give grund til bekymring over den nuværende undervurdering af Auger-elektroner i dosimetrien for isotoper anvendt i diagnostisk nuklearmedicin. Der er et klart behov for videre undersøgelse af RBEen af Auger-emitter henfald. Min nye eksperimentelle metode, med dens robuste beregning af absorberede dosis, de nye S_c værdier, anvendeligheden på de fleste celletyper og på alle Auger-emittere med en homogen intracellulær fordeling, vil være et brugbart redskab for sådanne undersøgelser.

Table of Contents

Table of Contents

Table of Contents

List of Figures

List of Abbreviations and Acronyms

AAPM	American Association of Physicist in Medicine¨
ATP	Adenosine triphosphate
BER	Base excision repair (pathway)
CK	Coster-Kronig
CPS	Count per second
CSDA	Continues slowing down approximation
D_{37}	Dose at 37 % survival
DDR	DNA damage response
DMEM	Dulbeccos's modified eagle medium
DMSO	Dimethylsulfoxid
DNA	Deoxyribonucleic acid
DPS	Disintegration per second
DSBs	Double strand breaks
EC	Electron capture
ECACC	The European Collection of Cell Cultures
EDTA	Ethylenediaminetetraacetic acid
FBS	Fetal bovine serum
FISH	Fluorescence in situ hybridization
GRF	Geometric reduction factor
HBSS	Hank´s balanced salt solution
HHR	Homologues recombination repair
HPV	Human papilloma virus

IC	Internal conversion
IC_{50}	Half maximal inhibitory concentration
ICRP	International Commission of Radiation Protection
IUdR	Idoxuridine
LET	Linear energy transfer
LMDS	Locally multiple damage sites
LSC	Liquid scintillation counting
LSM	Laser scanning microscope
MEM	Minimum essential medium eagle
MIRD	Medical Internal Radiation Dose (committee)
NHEJ	Non-homologues end joining
OER	Oxygen enhancement ratio
PBS	Phosphate buffered saline
pRb	Retinoblastoma protein
RBE	Relative biological effectiveness
SCK	Super Coster-Kronig
s.d.	Standard deviation
SPECT	Single photon emission computed tomography
SSBs	Single strand breaks
SSBR	Single strand break repair
w_R	Radiation weighting factor
w_T	Tissue weighting factor
w_x	Fluorescent yield

1. Introduction

Ionising radiation was discovered in 1895 by the German physicist Wilhelm Conrad Röntgen and named X-rays, and were shortly thereafter, used for medical diagnostic purposes (radiology). Similarly, the discovery of radioactivity by Henri Becquerel and of radium by Marie and Pierre Curie quickly led to the treatment of cancer by radium preparations and ionizing radiation. However, in addition to the benefits gained in cancer treatment, these new types of radiation also possessed detrimental properties. In 1928 "The International X-ray and Radium Protection Commission" (later known as "International Commission of Radiation Protection", ICRP) was established [1].

Today ionizing radiation is widely used for both diagnostic and therapeutic purposes. Over 40 million nuclear medicine procedures are performed each year spread over more than 10.000 hospitals. Many of these procedures are part of the diagnosis and treatment of cancer and nuclear medicine has been a major contributor to the increased survival rate of cancer patients [2][3]. However one of the current challenges in today's radiotherapy is to limit the collateral damage to the healthy tissue near the irradiated tumor(s). It is the hope that the use of Auger emitters in targeted cancer therapy can overcome this problem. As an Auger emitter decays, several low energy electrons are released. These electrons have a range of only nanometers to micrometers and are therefore able to hit only the targeted cells, while sparing nearby healthy tissue [4][5]. In addition, the simultaneous release of multiple low energy electrons and their contorted path can cause clustered and complex DNA damage, resulting in a significantly increased radiotoxicity compared to photons at similar absorbed doses and a consequently very high relative biological effectiveness (RBE). It is these characteristics of the Auger cascade that are thought to be of advantage in a cancer treatment [6]. Still, for Auger therapy to ever become a reality, more experimental data on their increased radiotoxicity and their RBE have to be provided.

90 % of the nuclear medicine procedures performed today, is part of diagnostic examinations, and here radioisotopes that also emit Auger electrons are already in use. These radioisotopes include

^{111}In, ^{123}I, ^{67}Ga and ^{99m}Tc which photons emissions (not their Auger electrons) are utilized in diagnostic gamma-camera and single photon emission computer tomography (SPECT) imaging [2]. Despite the fact, that the simultaneous release of Auger electrons from these radioisotopes, are known to cause DNA damage disproportional to their energy deposition (absorbed dose), risk estimations for these diagnostic procedures still treats Auger electrons as "normal" electrons, and their contribution to the dose calculation is therefore minimal even though their biological effect could be significant[7][8][9]. It could be argued that the dose received by a patient during a diagnostic procedure is low (μSv – mSv). However, considering the number of patients undergoing a diagnostic procedure each year, an underestimation of the risk associated with these could affect a substantial amount of people [10].

The interest in and the need to know more about the cellular effects and RBE of Auger emitters are therefore not only related to a potential future cancer treatment, but also to nuclear medicine procedures extensively used each day.

Even though the increased RBE of Auger emitters has been studied and acknowledge since the late 1960s [11][12], it is only recently that the official organizations involved in risk assessments of low doses of ionizing radiation, has begun to practically acknowledge this. In Publication 92 published in 2003 by the International Commission of Radiation Protection (ICRP) it is stated that a radiation weighting factor (w_R) of 20 or more is appropriate for Auger emitter bound to the DNA and that a radiation weighting factor for Auger emitters not bound to the DNA should also be considered [13]. This change has been underway for a long time, as it was already proposed by Pomplun et al in 1987 to assign a quality factor of 20 for Auger emitters bound to the DNA and of 1 for emitters not bound to the DNA [14]. However later, values above much higher than 1 for Auger emitters incorporated into cells, but not the DNA, have been recommended for use in risk estimations for specific cases and for deterministic effect [15][9]. Even though the American Association of Physicists in Medicine (AAPM), have proposed an alternative method for estimating equivalent doses, the official recommendation for ICRP are still that microdosimetry should be used to assess the effect of Auger emitters. However, several "issues" related to microdosimetric calculations are present, and no recommendations have so far been given on how the microdosimetric assessment is to be performed

[13][15][16]. The delayed action, in assigning an official radiation weighting factor for Auger electrons, is probably more a consequence of existing challenges and unanswered questions than due to a lack of interest.

These challenges especially relate to the absorbed dose calculations and to the experimental conditions applied when investigating the RBE. The challenges related to the absorbed dose calculation can be divided into two groups, comprising the problems in the calculations of the cellular S-values (computational, correct stopping powers etc. not covered here) and the compliance between the assumption made in the cellular S-value and absorbed dose calculations and the experimental reality [17][18].

The absorbed dose to cellular targets is formally calculated using the cellular S-values from the Medical Internal Radiation Dose Committee (MIRDs). Due to the complexity of these cellular S-values calculations, S-values for some commonly used radioisotopes have been published by MIRD, in the report on cellular S-values [17]. The cellular S-values are calculated for cells and nuclei of different dimensions. Due to the short range of the Auger electrons these cellular S-values are very dependent on the cellular and nuclear dimensions and therefore very sensitive to small changes in them. In addition, the cellular S-values are only calculated for spherical cells (except a few for low energy electrons), a geometry which is suitable for cells in suspension but not for adherent cells [17][18]. One of the crucial assumptions in the MIRD cellular S-value calculations is the homogenous distribution of the radioisotope in one or more of the defined source compartments; cell surface, cytoplasm and nucleus [17][18]. This requirement is not easily met as the Auger emitting radioisotopes often have non-trivial intracellular organometallic chemistry.

It is well known that the dose rate is an important factor for the biological effect observed, especially for low linear energy transfer (LET) radiation which is often used as reference radiation [13][20]. If the dose rate of the reference and test radiation are significantly different and the cells type are sensitive to this effect the obtained RBE can change dramatically. In studies investigating the cellular effect of Auger emitters, the dose rate of the reference radiation is often in the order of Gy/min while the dose

rate of the reference radiations is in the order of Gy/h (due to the uptake kinetics) potentially underestimating their RBE [21].

The dose rate of the test radiation can be influenced by several factors including the kinetics of the cellular uptake and intracellular distribution of the radiochemical, its possible release from the cell and its subcellular distribution over time. These factors should therefore be elucidated for correct dose and dose rate calculation. In addition, depending on the bio-kinetics of the radioisotope and the biological endpoint used, the cell might be exposed to significant doses after the radiochemical is removed from the culture medium. Care should especially be given to this when clonogenic cell survival is used as an endpoint after exposure from a radioisotope with a relatively long half-life.

All these dynamics will influence the dose, the dose rate and in the end the biological effect observed. When investigating the RBE, it is therefore of high importance that the experimental conditions for the cells exposed to the reference or test radiations are similar. At the moment, these components are only minor addressed and sometimes completely ignored, in studies investigating the radiotoxicity and RBE of Auger emitters [22][23][24]. However if reliable and consisting RBE values for Auger emitters can ever be obtained these vital parameters in the experimental setup will have to be consistently addressed.

1.1 Aim of the work

The main aim of this study is to investigate the radiotoxicity and relative biological effectiveness of the Auger emitter ^{131}Cs, based on an understanding of the in the introduction mentioned challenges.

To accomplish this I will establish an experimental setup and develop new cellular S-values, named S_C-values which are much less sensitive to small changes in cellular and nuclear volumes. By using these robust S_C-values I can obtained reliable absorbed dose calculations, and significantly decrease the (often high) uncertainty associated with these calculations using the MIRD cellular S-values.

As my aim is to investigate Auger emitter decays and not a specific medical radioisotope, I have chosen the pure Auger emitter ^{131}Cs, which decays by 100% electron capture (EC), for the work. It has no γ-ray emission (but of course some X-ray emission) and a relatively high abundance of Auger events [25]. In addition ^{131}Cs, being an alkali metal, has some bio-chemical properties which are crucial for the developed S_C-values.

In order to properly calculate absorbed doses and dose rates for the ^{131}Cs exposed cells, it is crucial to know the bio-kinetics of ^{131}Cs. Thus, I will investigate the uptake and release of ^{131}Cs in order to know the activity concentration in the cells over time. Also the cellular location of ^{131}Cs (intracellular or bound to the cell surface) is examined, as this is also crucial parameter for the S_C-value calculations, due to the short range of Auger electrons.

In the end, to obtain RBE values for ^{131}Cs decays, I will compare the observed biological effect of ^{131}Cs exposed cells, to that of cells exposed to a reference radiation (γ-rays). RBE values for two different biological assays (γH2AX and clonogenic cell survival) along with two different cell lines (HeLa and V79 cells) will be obtained. In addition, as several parameters are known to influence the biological response, applying a similar experimental setup for the two different exposures (test and reference radiation) will be highly prioritized. This will include using similar cell densities and absorbed doses, with a special focus on using similar dose rate profiles for the two exposures, in order to correct for any dose rate effects.

1.2 Outline of the work

To provide a better overview of the main work, a flow chart showing the different experimental steps is presented in Figure 1.1

1: Using the natural uptake of ^{131}Cs in cells, the radiotoxicity and RBE for intracellular Auger decays in two cell lines (HeLa and V79 cells) will be studied.

2: Production and chemical separation of ^{131}Cs to get a ^{131}CsCl solution used in the study.

3: Cells were incubated with ^{131}Cs (produced in step 2) in order to investigate its bio-kinetics including uptake, release and cellular localization. For the RBE experiments cells were incubated with ^{131}Cs and the cellular activity concentration measured at the end of incubation

Step 4 and 5 were performed in parallel, with the other steps.

4: Cells were grown to a confluent monolayer and the cell membrane and the nucleus were stained with fluorescent dyes. Images were taken (by confocal microscopy) of the stained cells, and these pictures were used to estimate the height of the cellular monolayer and the size of the nuclei.

5: Using the results of the cell layer and nuclei geometry (obtained in step 4), S_C-values were calculated for both cell lines.

6. Using the measured cellular ^{131}Cs concentration obtained in step 3 and the S_C-values obtained in step 5, the absorbed dose and dose rate profiles were calculated.

7. Knowing the absorbed dose and dose rate profile for the ^{131}Cs exposed cells, the dose rate profile for the external γ-ray exposed (reference radiation) cells were matched, in order to avoid a dose rate effect.

8. γH2AX assay and clonogenic cell survival were used to measure the RBE.

-These steps were performed independently for the two cells lines.

Flow chart

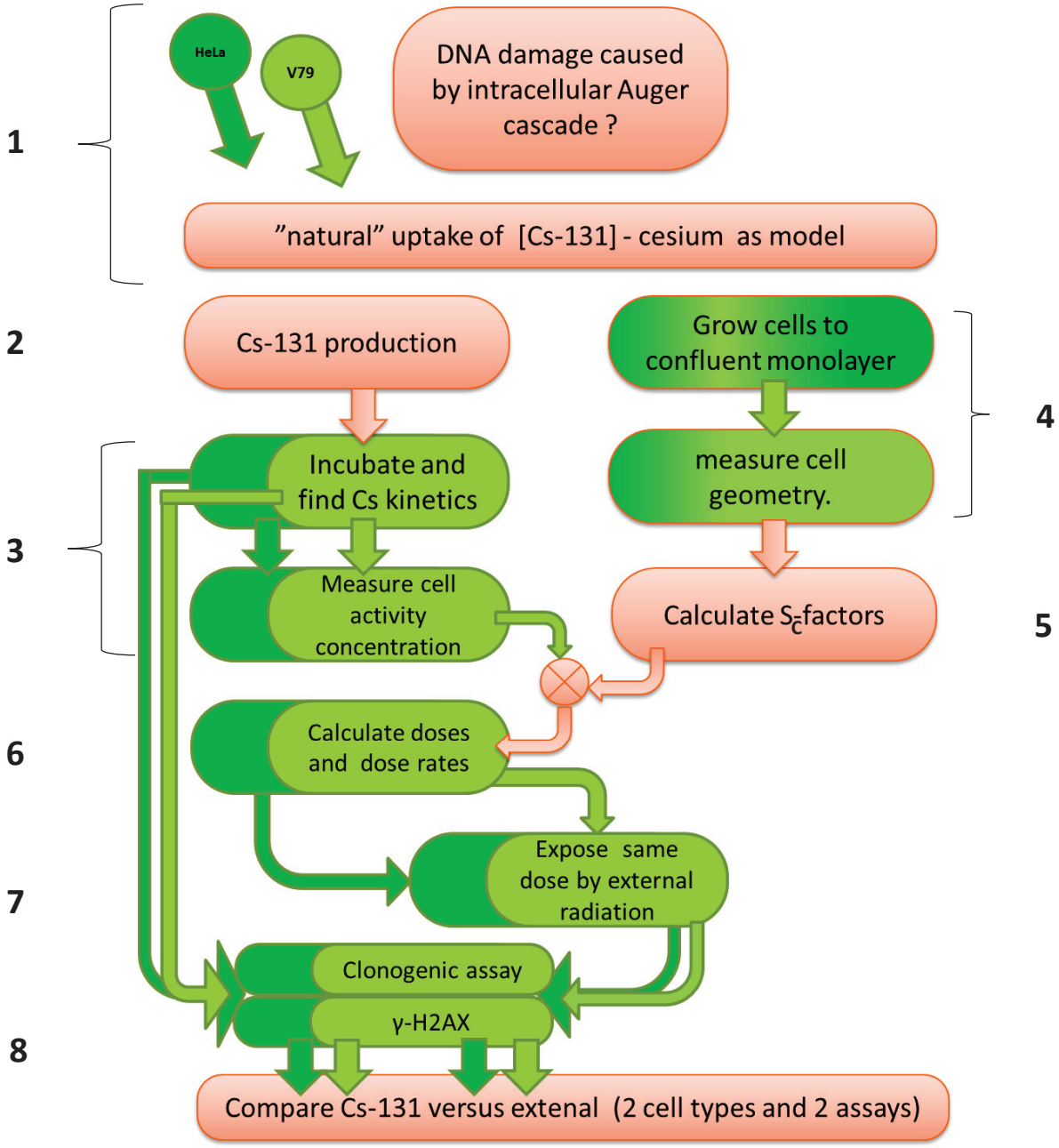

Figure 1.1 Flow Chart

2. Background

2.1 Auger emitters

2.1.1 Auger cascade

The Auger effect was discovered in 1923 by Lise Meitner and later in 1925 by the French physicist Pierre Victor Auger, whom it was also named after[26][27]. Pierre Victor Auger was investigating electron tracks produced in a cloud chamber by low energy photons, when he noticed that several of the electron tracks emanated from the same spot. He concluded that these electrons were the result of inner shell transition, in which the excess energy was transferred to orbital electrons instead of being released as photons. This process of release of multiple orbital electrons arising from inner shell transition is called the Auger effect, Auger process or the Auger cascade [27][15].

The Auger cascade begins with the creation of a vacancy in one of the inner shells. To relax the atom, an electron from a higher energy orbital will fill the vacancy. In that process, the energy resulting from the energy difference between the two orbitals, will either be emitted as a characteristic X-ray or be transferred to another orbital electron which is ejected from the atom, creating another vacancy (Figure 2.1) This result in a cascade of electrons, being emitted from the atom and ends with the highly ionized atom absorbing electrons from the nearby environment in a process called charge neutralization [28][29].

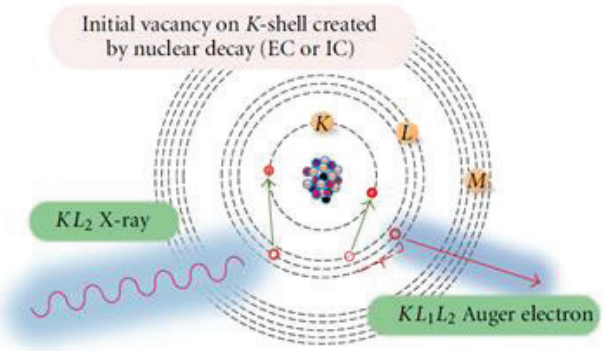

Figure 2.1 Relaxation of an atom with a vacancy in the K-shell

Relaxation of a vacancy in the K-shell can result in two scenarios. Either an electron from a higher shell, here the L-shell transits to the K-shell and the energy difference between the two shell is emitted as an X-ray (KL X-ray) or the energy is transferred to another orbital electron, which gets ejected (KLL Auger electron) (courtesy by B. Q. Lee [30]).

Depending on the orbitals involved in the transitions, the emitted electrons are called Auger-, Coster-Kronig (CK) - or Super Coster-Kronig (SCK) electrons, but are often all referred to as Auger electrons (Figure 2.2). Their energy range from just below the K-shell binding energy (of the isotope) down to a few eV. [29][8].

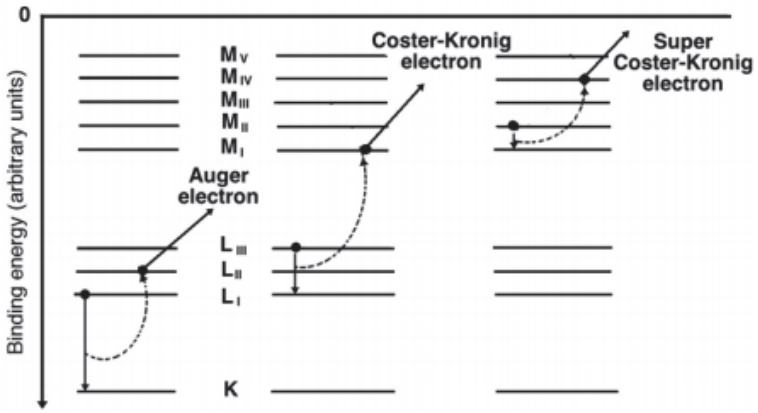

Figure 2.2 Production of Auger-, Coster-Kronig- and Super Coster-Kronig electrons

The ejected electron is called an Auger electron when the electron transition occurs between shells. Coster-Kronig and Super Coster-Kronig electrons are produced when the transition occurs between sub shells and the energy is transferred to an electron in the same shell (Super Coster-Kronig) or to an electron in a higher shell (Coster-Kronig). Figure is taken from [31].

The emitted X-ray(s) has an energy corresponding to the difference in electrons binding energies in the two orbitals involved;

$$E_{(X-ray)} = E_{(BE,x)} - E_{(BE,y)} \quad \text{(Eq. 1)}$$

While the ejected electron(s) has energy corresponding to the differences in electron binding energies in the three orbitals involved;

$$E_{(z,\text{Auger electron})} = E_{(BE,x)} - E_{(BE,y)} - E_{(BE,z)} \quad \text{(Eq. 2)}$$

$E_{(X-ray)}$ and $E_{(z,\text{Auger electron})}$ being the energy of the emitted X-ray and Auger electron respectively, $E_{(BE,x)}$ and $E_{(BE,y)}$ the electron binding energies in the two orbitals (x, y) involved in the transition and $E_{(BE,z)}$ being the electron binding energy for the ejected Auger electron in orbital z [29].

The emission of X-rays and Auger electrons (including Coster-Kronig & Super Coster-Kronig) after the creation of a vacancy are competing processes. The probability that an X-ray will be emitted (radiative transitions) after filling of the vacancy is called the fluorescence yield (ω), while the probability that an Auger electron will be emitted (non-radiative transitions) is called the Auger yield (a)[32] . It follows that;

$$\omega + a = 1 \quad \text{(Eq. 3)}$$

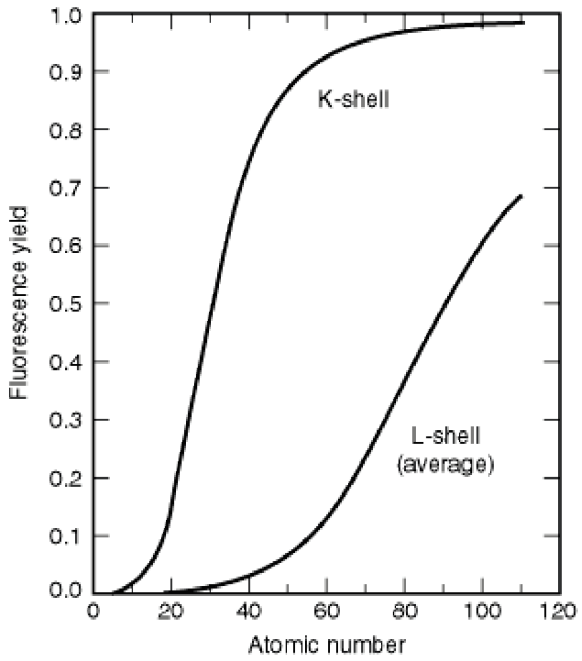

Figure 2.3 Fluorescence yield for K- and L-shells

The fluorescence yield equals the number of X-rays emitted per vacancy. The fluorescence yield increases with increasing atomic number and becomes the dominating process for K-shells in elements with an atomic number above ~30. For L-shells it becomes the dominating process in elements with an atomic number above ~90. Figure is taken from [33].

The fluorescence yield depends (among other factors) on the atomic number (Z) and the orbitals involved in the transition. It increases with increasing atomic number and the radiative transition becomes dominant for K shells in elements with Z > 30. For the L shell the radiative transition first becomes dominant in elements with atomic number around 90 (Figure 2.3)[32] [34].

The inner shell vacancy that starts the Auger cascade can be created by several mechanisms including coulomb interactions between an energetic charged particle and an orbital electron, photon interactions (photoelectric effect, Compton effect, triplet production), electron capture and internal conversion. Electron capture and internal conversion, being the only two processes that involve nuclear transitions are described below [35].

2.1.1.1 Electron Capture

Radioactive isotopes that decay by electron capture are often proton-rich and lie to the left of the stability line. These isotopes can stabilize by converting a proton into a neutron, thereby increasing their proton/neutron ratio. In essence, a proton in the nucleus captures one of the inner shell electrons and transforms into a neutron and a neutrino. A vacancy is thereby created, which can lead to an Auger cascade;

$$ {}^{A}_{Z}X + e^{-} \rightarrow {}^{A}_{Z-1}Y + \nu_e \qquad \text{(Eq. 4)} $$

For electron capture to occur the decay energy should be greater than the binding energy of the captured electron. The decay energy (much of which is carried away by the neutrino) is equivalent to the difference in the mass between the mother and daughter isotopes. As the daughter isotope is relatively heavy, the recoil energy is very small [35].

2.1.1.2 Internal conversion

After beta decay the nucleus can be left in an excited state. To relax, the nucleus can emit a photon (γ-decay) or it can interact with an orbital electron, “transferring” enough energy to it, to eject it from the atom. Thereby a hole in the shell is created, which can lead to an Auger cascade;

$$ {}^{A}_{Z}X^{*} \rightarrow {}^{A}_{Z}X + e^{-}_{K} \qquad \text{(Eq. 5)} $$

The energy of the ejected electron is almost equal to the excitation energy minus the binding energy of the electron;

$$ E_e \approx E^{*} - E_B \qquad \text{(Eq. 6)} $$

E_e being the energy of the ejected electron, E^{*} he excitation energy and E_B the binding energy of the ejected electron. The process competes with gamma emission but dominates in heavy nuclei at low excitation energies [35].

2.2 Radiobiological effects of Auger emitters

2.2.1 Radiotoxicity and Relative biological effectiveness of Auger emitters

The radiotoxicity of Auger emitters has been investigated since the late 1960s where the first cell studies incorporating ^{125}I into DNA were performed. These studies reported an increase in radiotoxicity around 4-5 fold and even up to 20 fold when compared to ^{3}H and sparked the idea of using Auger emitters in cancer therapy [12][28][36]. Carlson & White published a paper in 1963 showing a high degree of fragmentation (99%) after the decay of ^{125}I incorporated into CH_3I and C_2H_5I molecules [37]. These data were at that time used to explain the underlying mechanism of the increased biological effect that was experimentally observed. Since then, several experiments investigating the radiotoxicity of Auger emitters have been performed and the understanding of its effect has increased [28].

A way of reporting radiotoxicity for different types of radiation is the "relative biological effectiveness" (RBE). The RBE was defined by The National Bureau of Standards in 1954 as; "*The RBE of some test radiation (r) compared with X-rays is defined by the ratio D250/Dr, where D250 and Dr are, respectively, the absorbed doses of 250 kV X-rays and the test radiation required for the equal biological effects*" [38][39].

$$\mathrm{RBE} = \frac{\text{abosrbed dose of 250 kV X-ray}}{\text{absorbed dose of test radiaiton}} \text{ , required to produce equal biological effect} \qquad \text{(Eq. 7)}$$

The RBE is an empirical value. The RBE-value obtained by an experiment is linked to that specific experiment and the conditions used. It is therefore not only dependent on the radiation quality, but also on experimental variables such as cell type, dose, dose rate, oxygenation status, and the biological endpoint used. Differences in the experimental setup between studies investigating the radiotoxicity of Auger emitters can therefore (at least partly) explain the variations in the RBE-values obtained [13].

However, it is agreed that the radiotoxicity of Auger emitters is highly dependent on the location of the decay in respect to DNA. When the Auger emitter is incorporated into the DNA, such as when using ^{125}IUdR, the RBE-value is considered to be around 7. However, values between 2 and 20 have also been reported. In contrast, when the Auger emitter is not incorporated into the DNA, but still in close proximity to it (e.g. intercalated), the RBE-value is considered to be around 4. Auger emitters located in the cytoplasm or outside the cells, is thought the be much less radiotoxic with RBE-values around 1 [21][40].

The high radiotoxicity of Auger emitters (located close to the DNA) is thought to be caused by the simultaneous release of several low energy electrons. In the case where the Auger emitter is incorporated into the DNA, charge neutralisation is also thought to significantly contribute to the high RBE. Low energy electrons travel in contorted paths and deliver a considerable amount of energy in a very small volume. These low energy electrons only travel nanometres to micrometres, and can consequently deposits their energy close together. Monte-Carlo simulations have shown, that the energy deposited within 2 nm from a ^{125}I decay site, and the free radicals species concentration around the decay, can exceed that of a 5 MeV alpha particle track passing the DNA. However the energy deposition density sharply decreases with distance from the decay site. This is thought to be the underlying reason for the dependency of RBE-values on the cellular location of the Auger emitter[15][21][41][42].

Beside the release of several electrons, the short range of these makes it possible to damage/kill only the targeted cells while sparing the neighbouring cells. The K-Auger electrons have a range in the micrometre order, while the electrons with the lowest energies, the Super Coster-Kronig have a range of only a few nanometres. This ability to only hit targeted cells is in sharp contrast to the radioisotopes currently used in the clinic where the collateral damage to the healthy tissue is of great concern, as it can limit the activity used and hence the dose to the tumour cells [15].

2.2.2 Linear Energy Transfer (LET) and RBE

Ionising radiation is often divided into high LET (e.g. heavy charge particles, alpha) and low LET (e.g. γ-rays, X-rays) radiation also denoted densely- and sparsely ionising radiation respectively. LET stands for linear energy transfer and describes the average energy locally deposited to the medium per unit length of track. In other words it relates to the ionisation density of the track [38][43]. The unit used is keV/µm

$$\mathrm{LET} = \frac{\mathrm{dE}}{\mathrm{dl}} \qquad \text{(Eq. 8)}$$

High LET radiation shows an increased biological effect compared to low LET radiation at similar absorbed doses. This increase in the biological response is due to the differences in the spatial pattern of ionisations and excitations event and ultimately in the pattern of DNA damage. Several DNA lesions close to each other can results in clustered and complex DNA damage, which is much more harmful to a cell than the same amount of DNA lesion well separated [6][44].

As the LET increases, the energy deposition per unit length of track and ionisations density increases, which result in an increased RBE. The RBE increases slowly with increasing LET up to a LET value of 10 keV/µm. From here the increase in RBE with LET occurs more rapidly until it reaches a maximum at a LET of 100 keV/µm. Above this value the RBE decreases with increasing LET (Figure 2.4) [39].

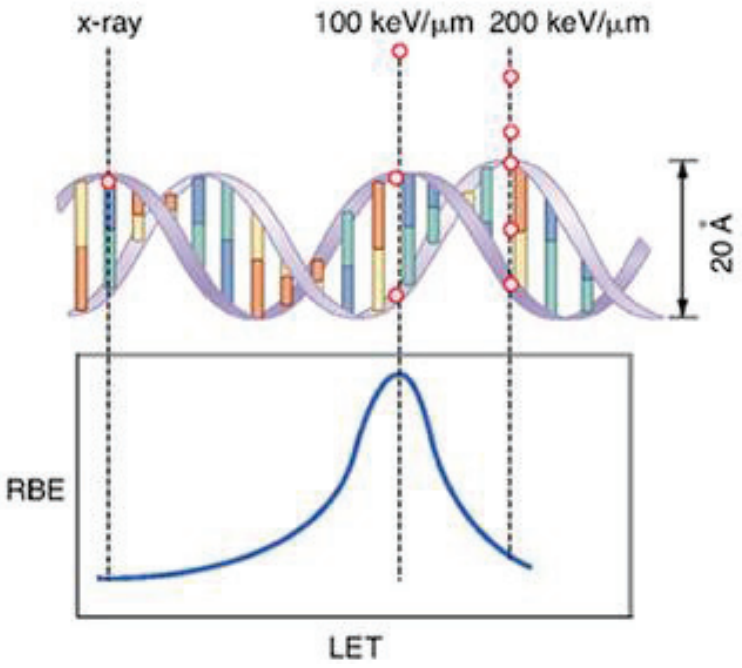

Figure 2.4 Relative biological effectiveness in relation to LET

The relationship between RBE and LET, and the average distance between events by radiation with different LET values are shown. As illustrated in the figure a particle with a LET of 100 keV/µm will have two events separated by a distance 20 Å (which corresponding to the distance between the two DNA strands) and therefore have a high probability of producing a DNA DSB. In contrast, a particle with a LET of 200 keV/µm will (on average) have three events separated by the 20 Å. The particle with a LET of 200 keV/µm will deposits more energy, but will not cause a proportional higher biological response. As absorbed dose is incorporated in the RBE, the RBE of the particle with a LET 200 keV/µm will be lower than the RBE of a particle with a LET of 100 keV/µm. Figure is taken from [39].

The LET value of 100 keV/µm corresponds to two ionisation events separated on average by a distance of 20 Å -the diameter of the DNA helix. It is thought that radiation with this LET is most efficient in producing DNA double strand breaks (DSBs). Radiation with LET values above 100 KeV/µm will also produce DNA DSBs. However as the absorbed dose is incorporated into the RBE-value, energy will be "wasted" in additional ionisations that do not cause a proportional increase in biological effect [39].

2.2.3 Mechanisms of DNA damage

Ionising radiation mainly causes DNA damage by two mechanisms; direct action and indirect action. For photons it is of course the secondary electrons that are involved in the interactions. In direct action the ionising radiation interacts directly with the target (DNA). In indirect action the ionising radiation interacts with a molecule other than the DNA. As cells consist mainly of water the radiation will very often produce free radicals in the process of water radiolysis. These free radicals then interact with the DNA causing DNA damage. The primary free radicals are e_{aq}, $OH^{\cdot}$ and $H^{\cdot}$ [43][6](Figure 2.5).

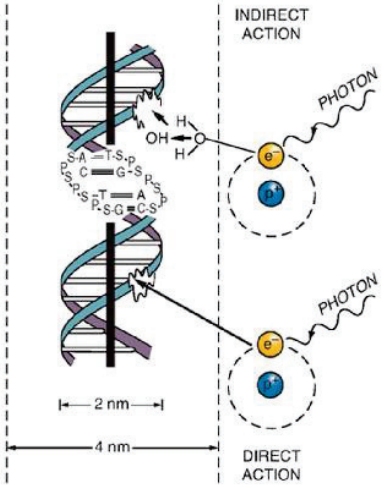

Figure 2.5 Representation of the direct and indirect action of DNA damage by ionising radiation

Ionising radiation can produce DNA damage by different mechanisms. An ejected electron can either ionise the DNA directly (direct action), or it can produce free radicals by radiolysis, which then interact with the DNA, resulting in DNA damage (indirect action). Figure is taken from [39]

Which of these two processes (direct and indirect) that dominates, depends on the LET of the radiation. For high LET radiation the direct action dominates, while for low LET radiation the indirect action is dominant. Auger emitters can also produce DNA damage by a third mechanism called charge neutralization [43]. During the Auger cascade several electrons are released, leaving the atom highly charged. If the Auger emitter is incorporated into the DNA (as when using covalently labelled DNA

bases with ^{125}I) electrons from surrounding molecules (the DNA) will be transferred to the Auger emitter, leaving the donor molecules ionised. In addition DNA damage can be caused by the recoil energy and chemical transmutations [45]. However these last two processes are not thought to be contributing significantly to the radiotoxicity of ionising radiation. The dominant mechanism behind DNA damage by Auger decays depends on the location of the decays in relation to the DNA. If the Auger emitter is incorporated into the DNA, charge neutralisation and direct action have been found to be the dominating actions. In contrast, if the Auger emitter is located just a few Angstroms to few nanometres away, most of the DNA damage is produced by indirect actions [28][46][47].

2.2.4 Clustered and complex DNA damage and repair

DNA damage caused by ionising radiation can be divided into base damage, single strand breaks (SSBs) and double strand breaks (DSBs). Because of the relatively simple nature and effective repair of base damage and single strand breaks, these are thought not to be particularly harmful to the cell. In contrast double strand breaks are thought to be the main contributor to cytotoxicity and the amount of DSBs are sometimes used to predict the biological response and the severity of a treatment [48]. However, this view is too simplistic. Several DNA lesions occurring close to each other produce clustered and/or complex DNA damage. These types of DNA damage have been shown to be highly detrimental to a cell (Figure 2.6). The term clustered DNA damage or locally multiple damage sites (LMDS) was introduced by Ward in 1981. The term sought to explain an underlying reason for a disproportionally high biological response in comparison to the amount of DSBs observed [49][50]. Clustered DNA damage is defined as two or more lesion within one or two helical turns, made by a single track. The complexity of the damage depends on the number of lesion within the cluster. These lesions can be of different nature (e.g. DSB, SSB, base damage, cross linking). Clustered DNA damage can be divided into DSB-clustered DNA damage and non-DSB-clustered DNA damage [51] [52].

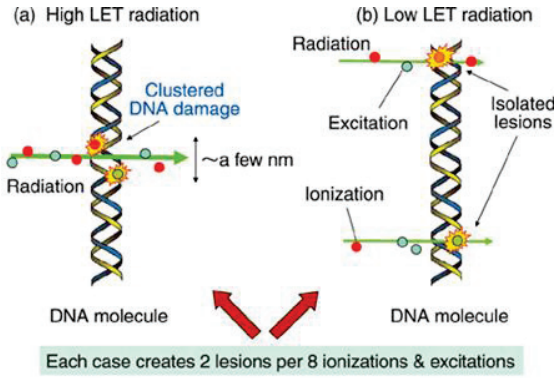

Figure 2.6 Clustered and complex DNA damage

The spatial distribution of DNA damage is important for the biological response. In the figure, both pieces of DNA have 2 DNA lesions created by 8 events (ionisation or excitation). However the DNA lesions produced by the high LET are in close proximity to each other, resulting in clustered DNA damage, while the 2 lesions created by the low LET radiation are well separated. The DNA lesions produced by the high LET radiation will be more difficult to repair, and consequently more detrimental to the cell. Figure is taken from [53]

The increased biological effect of clustered DNA damage is thought to be a result of poor or error-prone repair [50]. DSB are repaired through one of the two main repair pathways; Homologues recombination repair (HRR) and non-homologues end joining (NHEJ). HRR can only take place during the late S-phase and in G2-phase where a full replicate of the chromatid is present. HHR uses this sister chromatid as a template and is therefore relatively error-free but slow. In contrast, NHEJ repair process can be utilized in all the cell cycle phases. As no template is needed (for NHEJ), the repair process is fast but error-prone [48]. Base damage is repaired by the base excision repair (BER) pathway, where either a single nucleotide is removed (short patch BER) or several nucleotides are removed (long-patch BER). DNA SSBs are repaired through a fast single strand break repair (SSBR) process, which involves the last steps of the BER. The repair of these types of DNA damages can use the opposing strand as a template and the DNA lesions are therefore effectively repaired [54][55].

When base damage and SSBs are located within a cluster (of DNA lesions), the repair of these DNA damages is less efficient. When multiple types of DNA lesions are located in a cluster, the DNA damaging repair mechanisms used for each lesion must interplay, which might affect the repair efficiency. The severity of this reduction in repair efficiency is dependent on the complexity of the

cluster; number of lesions, inter-lesion separation and the types of lesions present [44]. A hierarchy between the DNA lesions exist, and so the DSBs and SSBs within a cluster will be repaired before base damages. In addition, the first base lesion encountered in a cluster will be repaired before the next occurring base damage. The reduced repair efficiency can result in an increase in the life-time of the clustered lesion (up to 8 hours compared to single lesion) and increase the risk of error-prone repair. Moreover, during the repair of base lesions and SSBs present in a cluster, de novo DSBs can be generated. It has been estimated that 10 % of non-DSB clustered lesions is converted into DSB clustered lesions during repair processing [44][56][57].

The amount of clustered DNA lesions and the complexity of these lesions increase with the LET of the radiation. 30-40 % of DSBs induced by low LET radiation are found to be complex while for high LET radiation the fraction has been found to be up to 90 % [51] [58]. This increase with LET is quite intuitive as a higher ionisation density will have a higher probability of creating multiple DNA lesions in close proximity to each other. Moreover, the repair of DNA damage induced by high LET and high LET –like radiation shows a considerably decrease in repair efficiency compared to DNA damage produced by low LET radiation [59] [60] [61].

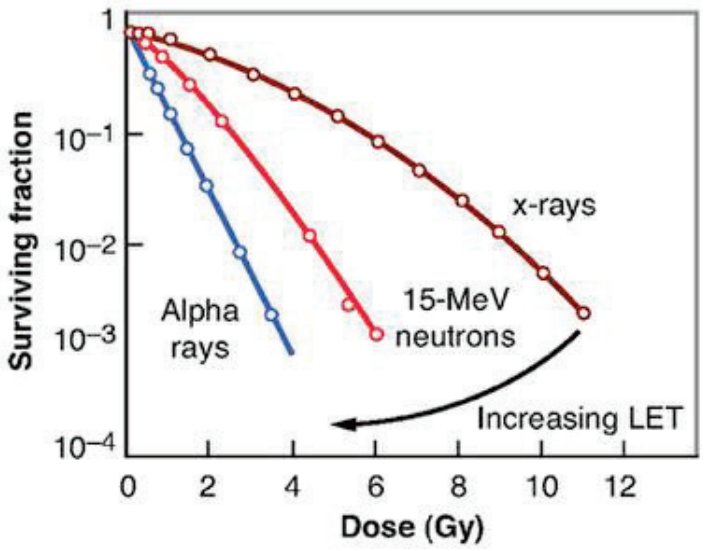

Figure 2.7 Relationship between cell survival and LET

Typical survival curves for cells exposed to radiation with increasing LET is showed. The survival curve for X-ray exposed cells shows a typical shoulder, representing repair of sub-lethal DNA damage. As the LET increases, the size of the shoulder decreases and for cells exposed to alpha radiation (high LET), no shoulder is evident. Figure is taken from [39]

The high induction of clustered DNA damage with the subsequently reduced repair is also evident in survival curves. The typical shoulder seen in cell survival curves when cells are exposed to low LET radiation represents repair of sublethal DNA damage. This shoulder is getting smaller as the LET of the radiation increases (Figure 2.7). For Auger emitters the shape of the survival curve is not yet fully determined and reported survival curves reflect both high LET- and low LET like behaviour [62][63][22]. However, the current view is that Auger emitters covalently bound to DNA produce survival curves with no shoulder, while Auger emitters, that are not covalently bound to the DNA can exhibit survival curves with and without shoulders [28].

2.2.5 Cell cycle arrest and sensitivity

The cell cycle consists of four phases; G1-phase, S-phase, G2-phase and M-phase. Between the different cell cycle phases are checkpoints. These checkpoints are controlled by cyclin and cyclin-

dependent kinases and control, that (DNA) damaged cells do not progress through the cell cycle. The check points between the G1/S -phase and the G2/M –phase completely arrest the cells, while the intra S-phase the check point just slows down the progression through the phase so the cell gets time to repair their DNA damage [64].

In response to DNA damage, a mechanism called DNA Damage Response (DDR) is activated. This consists of a complex signalling network, which activates several pathways involved in DNA repair, transcription, cell cycle checkpoints, and apoptosis. Several of the main proteins in this network are not confined to a single pathway, but can be involved in several of them (BRACA1, 53BP1, etc.). Two main players in the DDR are ATM and ATR. These are involved in the G1/S, intra S-phase check point and the G2/M check point, and through several mediators (53BP1, BRACA1), transducers (Chk1/2) and effectors (p53), they try to retain the cell in cell cycle arrest. The proteins p53 and BRACA1 are especially important in the DDR response and cells lacking a functional copy of one of them often transform into cancerous cells [48][65].

The sensitivity of a cell for radiation varies between cell cycle phases. The cell is most sensitive in the mitotic phase and most resistant in the last part of the S phase. The G2 phase often shows a high sensitivity too, while the G1 phase shows intermediate sensitivity. If the G1 phase is long, as for HeLa cells, the G1 can be divided into a resistant period in the beginning and a more sensitive period in the end [66] (Figure 2.8).

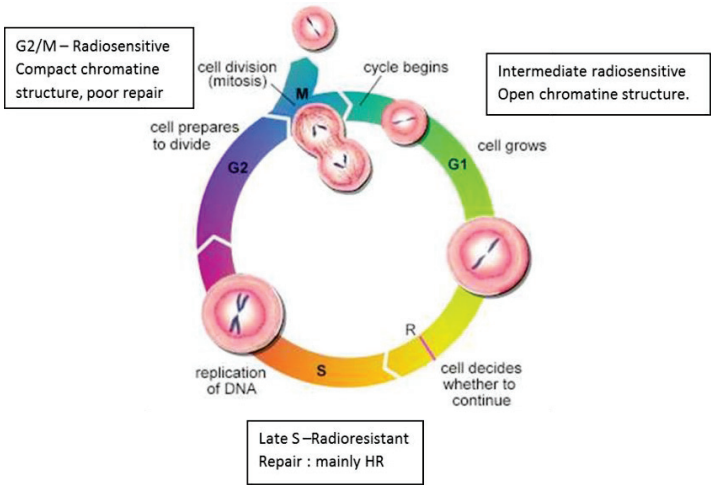

Figure 2.8 Representation of radiation sensitivity of cells in the different cell cycle phases

The sensitivity to ionising radiations varies between cells cycles phases. The G2-phase and the M-phase is thought to be the most radiation sensitive, while the late S-phase is the most radiation resistant. This difference is thought to be related to the DNA damaging repair pathways available and the chromatin structure in the different phases. Figure is modified from [67]

The difference in sensitivity between the cell cycle phases is not well understood, but several factors are known to play a role. The S-phase is the most radiation resistant. Indeed, if DNA replication has taken place, DNA damage can be repaired through homologue recombination, which is less prone to errors (than non-homologue end joining). However, this does not explain why the G2 phase is radiosensitive. Another parameter that could play a role in the sensitivity to radiation of the different cell cycle phases, is the topology of the chromatin structure. The DNA in the G1 phase has a very open chromatin structure, which gives relatively easy access for the repair proteins to the DNA lesion. In contrast, the chromatin structure in G2/M is compact, which could result in less efficient repair and consequently a higher sensitivity. Although the underlying mechanisms for the differences in radiation sensitivity between the different cell cycle phases are not fully understood, this feature is still one of the basic ideas underlying fractionation in the clinic [66][68].

The G1/S checkpoint is a sensitive but slow process. Cells have been observed to enter the S-phase even after high doses of radiation. Cells irradiated in the G1-phase might enter the S-phase even with a high amount of DNA damage. However, if the G1/S check point is fully activated it is very sensitive.

This could be an explanation for the division of G1-phase into a radiation resistant and a more radiation sensitive period [64].

The G2/M checkpoint is passed relatively fast, and has a low sensitivity to DNA damage. Only at high absorbed doses does the check point succeed in arresting all the damaged cells. Still, the check point does not managed to arrest the cells until all the DNA damage has been repaired, but releases them when a small amout of DNA damage are still present. Cells can therefore enter the mitotic phase with unrepaired DNA damage [64].

If the DNA damage is too severe to be properly repaired, the cell can go into senescence, where it loses its ability to divide but maintain its normal functions, or it can go into apoptosis. Proteins involved in senescence are generally also part of the DNA damage response and cell cycle check points. These include p53 and the retinoblastomas protein (pRb)[69][70].

2.2.6 Dose rate effects & inverse dose rate effects

The rate at which the radiation is deposited is called the dose rate and has the unit Gy/Sec or more practically for internal radiation Gy/h. Especially for low LET radiation, the dose rate is an important factor for the biological response . In general the lower the dose rate, the lower the biological effect. When cells are exposed to low dose rates, they will have time and capacity to repair the sublethal DNA damage and thereby avoid acummulations of DNA lesions [20].

However a phenomenon called the inverse dose rate effect has been observed. Here lowering the dose rate will decrease cell survival, and can be just as effective as an acute exposure [71][20]. If the dose rate is low the cell will not be arrested in the G1-phase, but can continue into the G2-phase where it will be arrested. At a continuous low dose rate, a normal asynchronous cell population can thereby become a synchronous cell population, all arrested in the radiation sensitive G2-phase. Due the increased radiation sensitivity of cells in this phase, the exposure will results in a higher cell killing compared to an asynchrome cell populations [20]. The inverse dose rate effect seems to be more pronounced when cells are exposed to high LET radiation. The mechanims for this inverse dose rate

effect is not fully understood, but thought to be a results of a complex interaction of dose, dose rate and radiation quality and might be related to exposure of cells in the different cell cycle phases [72][73].

2.2.7 The oxygen effect

The indirect action of DNA damage is mediated by free radicals. These free radicals can interact with the DNA and turn it into a DNA radical. If the area is hypoxic (reducing) the DNA can be restored by reduction by a sulfhydryl (SH) group. However, if oxygen (O_2) is present the DNA radical will interact with the oxygen and become oxidized (DNA-O_2). This DNA derivate cannot be chemically restored and are therefore said to be "fixed". These "fixed" DNA lesions are very difficult to repair. This is the underlying mechanism of the oxygen effect, and the increased resistant to radiation observed in hypoxic tumours (Figure 2.9) [74].

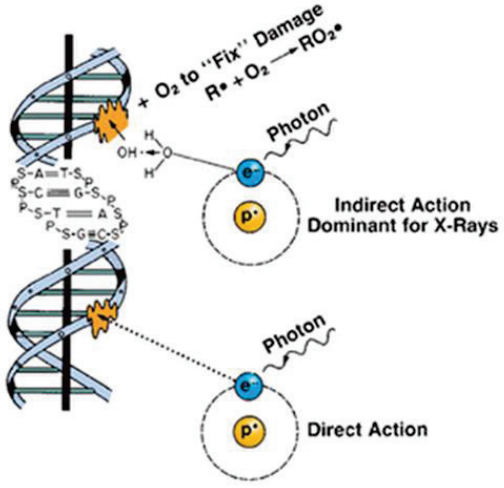

Figure 2.9 Mechaisnm of the oxygen effect.

In the presence of O_2 DNA radicals created by free radiacals can become oxidized to produced DNA-O_2. This type of DNA damage cannot be chemically repair and are therefore referred to as "fixed".

The ratio between the absorbed doses needed to achieve the same biological effect under hypoxic and aerated conditions is called the oxygen enhancement ratio (OER)

$$\mathrm{OER} = \frac{\text{absorbed dose under hypoxic condition}}{\text{absorbed dose under aerated conditions}}$$, required to produce equal biological effect (Eq. 9)

For high abosrbed doses of low LET radiation, the OER are typically around 2.5 to 3, while for high LET radiation (alpha) it is close to 1. In contrast to low LET radiaiton, of which most DNA lesions are produced by free radicals (indirect action), the dominant mechaims for high LET radiation is direct action [39].

Not many experiments have investigated the oxygen effect for Auger emitter decays. However an OER around 1 have been found for ^{125}I incorporated into DNA [75][76]. The oxygen fixation hypothesis is dependent on the indirect action. With this low OER for Auger emitters, it could be thought that Auger emitters mainly produce DNA damage by direct action or charge neutralisation. However the OER of Auger decays could, like the RBE, be dependent on the distance between the decay site and the DNA.

2.3 Dosimetry

The term dosimetry used in the field of health and medical physics, is the calculation or measurement of absorbed dose in the human body or other biological entity. The absorbed dose is an essential component in the prediction of the effect of a radiation treatment, the risk assessment associated with a diagnostic procedure (in nuclear medicine) or after exposure to ionising radiation in circumstances relevant for radiation protection.

2.3.1 Internal Radiation Dosimetry

In 1965 the MIRD (Medical Internal Radiation Dose) Committee was established in order to develop a unified approach to calculate absorbed doses to organs from internal distributed radionuclides during diagnostic procedures. This resulted in the publication of MIRD Pamphlet No. 1 which was published in 1968. It was later revised (1976) and re-published in 1988 and 1991. In 2009 the MIRD Pamphlet No. 21 was publish with the aim of standardizing the nomenclature within nuclear medicine and radiation protection and adopting the dosimetric quantities; "equivalent dose" and "effective dose" formulated by the International Commission of Radiological Protection (ICRP) [77].
The medical internal radiation dose (MIRD) committee has developed a general formalism for calculating the mean absorbed dose ($\overline{\mathrm{D}}\mathrm{k}$) to the target ($r_k$) from the source ($\mathrm{r_h}$):

$$\overline{D}(r_k \leftarrow r_h) = \tilde{A}_h S(r_k \leftarrow r_h) \qquad \text{(Eq. 10)}$$

$\tilde{A}_\mathrm{h}$ being the cumulated activity (total number of decays) in the source region ($\mathrm{r_h}$) and S the absorbed dose to the target region per unit cumulated activity in the source region [78].
S is defined as

$$S(r_k \leftarrow r_h) = \sum_i \frac{\Delta_i \emptyset_i (r_k \leftarrow r_h)}{m_k} \qquad \text{(Eq. 11)}$$

Δ_i being the mean energy emitted per nuclear transition, $\emptyset_\mathrm{i}$ the fraction of energy emitted by the source region that is absorbed in the target region for the i^{th} radiation component, and $\mathrm{m_k}$the mass of the target region. Ø depends on the quality and energy of the radiation plus the volume and composition of the target and its distance to the source [78]. This formalism was developed by MIRD to calculate absorbed doses to organs during diagnostic procedures and Ø for several organ pairs (source & target) has therefore been calculated and tabulated using a standard human model [77] [79] (Figure 2.10). It is only recently that MIRD has moved from a very "schematic" standard human model composed of boxes, spheres and cones into the present "anatomical" model. The MIRD cellular

model described below can still be seen as a very primitive “non biological” model, far from real biological variation.

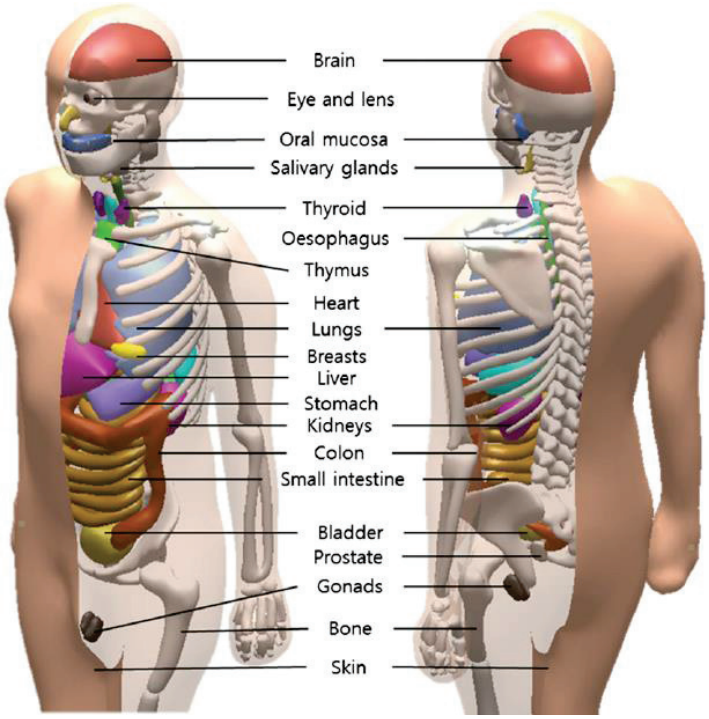

Figure 2.10 Representation of the standard human model
Figure taken from [80]

In parallel the ICRP established guidelines regarding risk estimation for stochastic effects (cancer and hereditary effects). These guidelines also involved calculations of the absorbed dose using similar principles as MIRD and differs more in nomenclature than in substance. The ICRP established the concepts equivalent dose and effective dose (later adopted by MIRD) relating the radiation quality and tissue “sensitivity” respectively to the absorbed dose and to the risk of stochastic effects. To get the equivalent dose, the absorbed dose is multiplied by the radiation weighting factor (w_R) [77].

$$\text{Equivalent dose} = \text{Absorbed dose} * w_R \quad \text{(Eq. 12)}$$

The radiation weighting factor is based on relevant RBE-values for stochastic effects and is conservatively set by the ICRP. The w_R can therefore NOT be used to estimate deterministic effect as it might (in such case) result in an overestimation of occurrence and severity. The w_R is set to 1 for electrons and (hence) photons, 20 for α-particles and is energy dependent for neutrons. The current recommendation regarding radiation weighting factors for Auger emitters is that a w_R of 20 or more is appropriate if the Auger emitter is incorporated into the DNA and that a w_R for Auger emitters more uniformly distributed should be addressed in the future. The ICRP states that the effect of Auger electrons should be assessed by microdosimetry, even though several "issues" related to microdosimetric calculations exist, and no recommendation for how this assessment should be performed has been given [13][77]. However the American Association of Physicists in Medicine has proposed an alternative approach for estimating equivalent doses for Auger emitters. As the decay scheme for different Auger emitters are so diverse, a w_R should ideally be ascribed to each individually Auger emitter [15][16]. Using the equation below (eq.13) the equivalent dose to an organ ($H_{T.R_{Auger}}$) from Auger emitters taken into account its subcellular distribution.

$$\mathrm{H_{T.R_{Auger}}} = \left[1 + \mathrm{f_0(W_{R_{Auger}} - 1)}\right] \sum\nolimits_{\mathrm{R_{Auger}}} \mathrm{D_{T.R_{Auger}}} \qquad \text{(Eq. 13)}$$

w_R being the radiation weighing factor (for stochastics effect) for Auger electrons only, f_0 the fraction of organ activity that is bound to the DNA and $D_{T.R}$ the mean absorbed dose from radiation R_{Auger} [15][16].

The effective dose incorporates the sensitivity of a given organ or tissue to radiation. To get the effective dose, the equivalent dose is multiplied by the tissue weighting factor (w_T).

$$\text{Effective dose} = \text{Equivalent dose} * \ w_{\mathrm{T}} \qquad \text{(Eq. 14)}$$

The tissue weighting factor states the relative risk of stochastic effects in the giving organ or tissue compared to the whole body. The sum of all the tissue weighting factors is therefore 1. The effective dose for the organs/tissue irradiated, can be summed to give the effective dose for the whole body [77].

2.3.2 Cellular dosimetry

During the 1970'es the special problem of the Auger-cascade in dosimetry and in estimations of the biological effects became clear to many medical physicists. While diagnostic nuclear medicine at that time focused on the nuclear emissions of gamma rays for imaging, it now became clear that many diagnostically important isotopes (^{99m}Tc, ^{123}I and ^{111}In) had strong Auger emissions. Also, as targeted radionuclide therapy developed through better bio-vectors and better understanding of the targeting problem *in vivo*, more precise dosimetry at the cellular level was needed for better prediction of biological effect and risk assessment. This was especially relevant for "radiation" with ranges on the cellular scale. Obviously, for some radiation types and energies (e.g. Auger electrons) the range are so short that dosimetry on a cellular level is needed. For that reason the MIRD S-value formalism was extended to treat the cellular dosimetry [17].

2.3.2.1 Cellular S-values

The principal behind the MIRD absorbed dose calculations on the organ and cellular level are the same [78]. The cellular S-value is still defined by;

$$S(r_k \leftarrow r_h) = \sum_i \frac{\Delta_i \emptyset_i (r_k \leftarrow r_h)}{m_k} \qquad \text{(Eq. 15)}$$

However the absorbed fraction ($\emptyset(r_k \leftarrow r_h)$) has now incorporated a geometrical reduction factor (GRF) and electron stopping powers;

$$\emptyset(\mathrm{r_k} \leftarrow \mathrm{r_h}) = \int_0^\infty \Psi_{\mathrm{rk}\leftarrow\mathrm{rh}}\,(\mathrm{x}) \frac{1}{\mathrm{E_i}} \frac{\mathrm{dE}}{\mathrm{dX}}\Big|_{\mathrm{X(Ei)\text{-}X}}\ \mathrm{dX} \qquad \text{(Eq. 16)}$$

E_i being the initial energy of the i^{th} particle, $\Psi_{rk\leftarrow rh}(X)$ the geometrical reduction factor and $\frac{1}{E_i}\frac{dE}{dX}\Big|_{\text{X(Ei)-X}} dX$ is the stopping power evaluated at X(E_i). The geometrical reduction factor is the mean probability that a randomly directed vector of length (X) from a random point in the source region will end within the target region. The value of the geometrical reduction factor depends on the length X, the geometrical shape of the source and target regions and their dimensions [77][78].

As the calculation of GRF is complex, only cellular S-values for simple geometrical shapes (spheres and ellipsoids) have been calculated by MIRD. The geometrical shape of the cell is customary assumed to be two concentric spheres. The radionuclide is assumed to be evenly distributed within one of the source compartments: whole cell (C), cell surface (CS) cytoplasm (Cy) or nucleus (N). Cellular S-values for monoenergetic electrons (1 keV to 1 MeV), for alpha particles and for the continuous electron spectrum emitted from certain radionuclides have been calculated using either the nucleus or the whole cell as target region. The calculation has been done for various combinations of cell sizes (R_c 3-10 µm) and nucleus sizes (R_N 1-9 µm). Surprisingly, cellular S-values for the combination of whole cell as source and nucleus as target (S(N←C)) is missing [17][18]. The MIRD publication states that when the source compartment constitutes more than one of the above mentioned compartments, the S-values can be found by multiplying the cellular S-values (that in combination gives the source and target combinations, you seek) with the fraction of the total radioactivity present in their source compartment. [17]

$$\overline{\mathrm{D}}_{\mathrm{N}} = \widetilde{\mathrm{A}}_{\mathrm{C}} \left[\mathrm{f}_{\mathrm{N}}\, \mathrm{S}(\mathrm{N} \leftarrow \mathrm{N}) + \mathrm{f}_{\mathrm{Cy}}\, \mathrm{S}(\mathrm{N} \leftarrow \mathrm{Cy})\right] \qquad \text{(Eq. 17)}$$

The “missing” cellular S-values for ^{131}Cs with the combination of whole cell as source and nucleus as target (S(N←C)), have been calculated and is shown in appendix 8.2.1 p. 196.

While the geometrical reduction factors (GRF) are just a computational problem (the GRFs have only been tabulated for a very limited set of cellular sizes and geometries), the need for a correct electron stopping power is a true physics problem. The electrons do not move in straight paths, and especially

low energy (few keVs) electrons will have a very twisted and bent track. Standard Continuously Slowing Down Approximations (CSDA) for the electron stopping cannot be used to calculate the absorbed dose distribution around a hypothetical point source of monoenergetic electrons in the low range [81]. The MIRD cellular S-values authors turned to an experimental solution. They based their "electron stopping powers" recommendation on an extended experimental set of measurements published by Author Cole [18][82]. Cole actually measured the penetration depth of monoenergetic electrons in plastic (placeholder for water or tissue), and gave polynomial approximations to the measured range versus energy. This range versus energy polynomial can be inverted to formally give energy versus penetration depth expression, that has the dimension of stopping power and look like a stopping power [82]. It is this expression of "electron stopping power" that the MIRD cellular S-value publication endorses for cellular dosimetry [18].

The tabulated MIRD cellular S-value states the mean absorbed dose to the target (cell or nucleus). This means that in a given cell population, some of the cells will have been exposed to a higher absorbed dose, while other will have been exposed to a lower absorbed dose. This variation in absorbed dose is caused by heterogeneity in the cell population, in cellular and nuclear sizes and shapes and in differences in their uptake of the radioisotope as well as stochastic effects related to energy deposition. This is important to keep in mind especially if the uptake of the radioisotope varies a lot between the cells. This variation is an additional complication in the dosimetry and should ideally be taken into account as well as the true microdosimetric variation (see section 2.3.3 p. 49).

The tabulated cellular S-values are, as said, calculated for cells with the geometry of two concentric spheres. However this geometry is not always a suitable representation of a cell. Cellular S-values for cells with the geometry of two concentric ellipsoids have therefore also been calculated for a limited set of electron energies and compared to the cellular S-values with the standard geometry (spherical) (Figure 2.11 & Figure 2.12). The comparisons were done for monoenergetic electrons with four different energies and for two ellipsoids geometries [17].

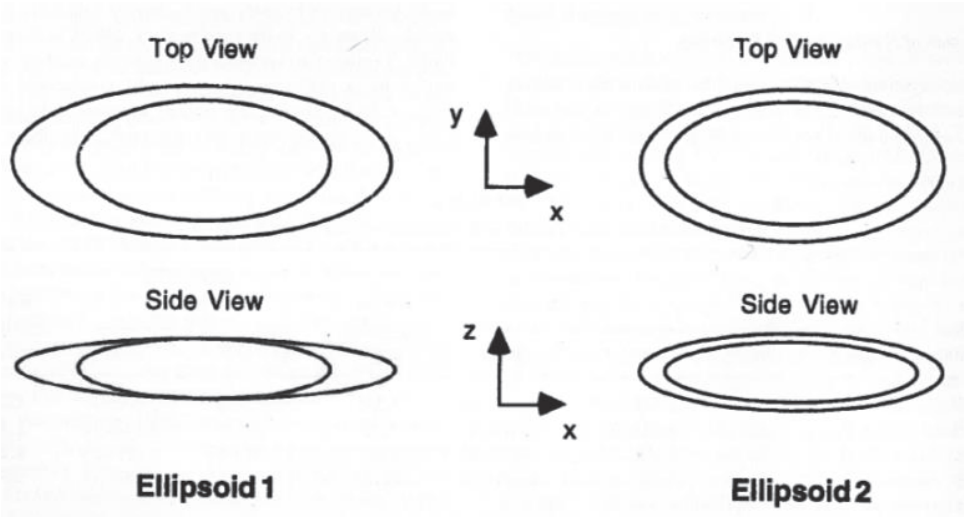

Figure 2.11 Geometries of the two ellipsoids used for the MIRD Cellular S-values, for non-spherical cells

For ellipsoids 1, the semi-axes of the whole cell in the x,y and z direction are 12.5 µm, 5 µm and 2 µm respectively, while the semi-axes (x, y, z) of the nucleus are 8 µm, 4 µm and 2 µm. For ellipsoid 2, the semi- axes of the whole cell are 10 µm, 5 µm and 2.5 µm, while the semi-axes for the nucleus are 8 µm, 4 µm and 2 µm. The total volume of these two ellipsoids geometry equals that of a sphere with a cell diameter of 10 µm and a nuclear diameter of 8 µm [17].

Dependence of S value on Cellular Geometry

Electron Energy (MeV)	Cellular Geometry	$\frac{S_{sphere}(N \leftarrow N)}{S_{ellipsoid}(N \leftarrow N)}$	$\frac{S_{sphere}(N \leftarrow Cy)}{S_{ellipsoid}(N \leftarrow Cy)}$	$\frac{S_{sphere}(N \leftarrow CS)}{S_{ellipsoid}(N \leftarrow CS)}$
0.005	ellipsoid 1	1.03	1.10	0.017
0.01	ellipsoid 1	1.10	1.53	0.645
0.100	ellipsoid 1	1.14	1.53	0.992
2.5	ellipsoid 1	1.13	1.53	0.991
0.005	ellipsoid 2	1.03	0.816	0.085
0.01	ellipsoid 2	1.10	1.02	0.713
0.100	ellipsoid 2	1.13	1.13	0.945
2.5	ellipsoid 2	1.14	1.13	0.992

Figure 2.12 Comparison of MIRD Cellular S-values for two different geometries (spherical & ellipsoid)
Table taken from [17]

When the “electrons” were “located” on the cells surface the cellular S-values were higher for the cells with the ellipsoid geometry, while the cellular S-values were higher for the cells with the spherical geometry when the “electrons” were “located” inside the cell. When the ”electrons” were

"located" in the nucleus the change in geometry did not change the cellular S-values considerably. The difference in the cellular S-values was especially high when the energy of the electrons was low, the they were "located" on the cells surface and the ellipsoid was very elongated [17]. The stated variability between the cellular S-values demonstrates how important it is to take the actual realistic cellular and nuclear geometries into account if precise absorbed doses are to be calculated.

2.3.3 Microdosimetry

The need for microdosimetry relates to the stochastic nature of energy deposition by ionising radiation. As ionising radiation traverse matter, it interacts and deposits energy in a discontinuous way. In contrast to the conventional dosimetry where these fluctuations in energy deposition can be ignored (due to the high number of events) they cannot be neglected in microdosimetry. Therefore microdosimetry must utilize the probability distribution of energy deposition, instead of the average energy deposition used in conventional dosimetry [83]. This raises the need for some new quantities substituting the macrodosimetric quantities "absorbed dose" and "LET" with their stochastic equivalents; the specific dose (z) and lineal energy (y) [84]. The specific dose is defined as the energy imparted (ε) by one or more events in a volume of mass (m) and has the unit Gy;

$$\boldsymbol{z = \frac{\varepsilon}{m}} \qquad \text{(Eq. 18)}$$

The lineal energy (y) is defined as the energy imparted in a given volume by a single energy deposition event (ε_s), divided by the mean chord length ($\bar{l}$) of that volume and has the unit keV/µm;

$$\mathbf{y = \frac{\varepsilon_s}{\bar{l}}} \qquad \text{(Eq. 19)}$$

During the Auger cascade, several low energy electrons (Auger, CK and SCK), with very different energies are released. In contrast to cellular dosimetry, where the K-and L-Auger electrons (being the most energetic) are the ones that almost exclusively contribute to the calculated absorbed dose, it is the very low energy electrons (higher shell Auger electrons, CK and SCK) that are of most interest in microdosimetry [85].Due to the very short range (in the order of nm) of these very low energy

electrons, their contorted paths and especially their multiplicity, the energy deposition density near the decay site of an Auger emitter can be very high and equivalent to that of an alpha particle [42]. Microdosimetry of Auger emitters deals with these very low energy electrons and their "track structures", in order to predict/estimate and understand the biological effect of Auger emitter decays [85].

The official recommendation from ICRP in assessing the effect of Auger electrons is explicitly to use microdosimetry. However, no official recommendation on how this assessment should be performed has been given [13]. This is a problem as there are several parameters needed for the microdosimetric calculations for these special Auger emitters, for which the details are not know. As an Auger emitter decays, several low energy electrons are released. As these electrons and their tracks are correlated in time and space they constitute a single event. However the number of electrons and their respective energies released per single decay, has not been mapped. Several energy spectrums for different Auger emitters have been calculated, but these are all obtained as averages from several thousands of decays and do not contain information of the distribution of the actual number of electrons and their energies in the individual decay. Equally important is the lack of knowledge on the possible angular correlations between the emitted electrons ([85] [86]and personal communication with prof. Mikael Jensen). Another issue relates to the size of the target. In cellular dosimetry the cell nucleus in often considered to be the target (as it contains the DNA) and its mass therefore used for the absorbed dose calculations. However, as is evident by the RBE >1 for high LET radiation, the "real" target must be smaller than the nucleus [87]. For microdosimetry, a more accurate representation of the target (the DNA) must therefore be used. This is however not easy, as the DNA is highly organized in a complex chromatin structure. The DNA double helix has a diameter of about 2 nm, but is wrapped around histones (with a diameter of 11 nm), which in turn makes up a nucleosome cluster (with a diameter of 30 nm), that again is packed in 300 nm sized sections. The size of the "real" target that should be used in the microdosimetric calculations is therefore not obvious [87][88]. Unfortunately, these unresolved questions hinder "true" microdosimetric calculations of the precise energy deposition density and hence microscopic dose calculation for Auger decays.

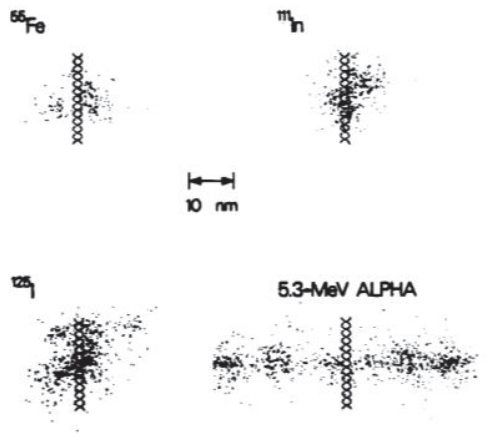

Figure 2.13 Monte Carlo simulations of the position of reactive species produced by Auger emitter decays

The initial positions of reactive chemical species in relation to the DNA double helix, produced by the decay (of a representative cascade) of different Auger emitters and by a passing (perpendicular) 5.3 MeV alpha particle. Figure taken from [42]

Nevertheless, by using Monte Carlo codes, the localized energy deposition following the decay of an Auger emitter has been simulated. Figure 2.13 from [42] shows the localized energy deposition (illustrated by the position of the reactive chemical species) following the decay of the three Auger emitters (^{55}Fe, ^{111}In and ^{125}I) and the passage of a 3.5 MeV alpha particle. As can be seen, the energy deposition density after a ^{125}I or ^{111}In decay is comparable to that produced by the passing 3.5 MeV alpha particle, while the energy deposition density following a ^{55}Fe decay much is smaller [42]. However, the decay of ^{55}Fe only emits 5.1 Auger electrons (on average) per decay, while ^{125}I and ^{111}In on average emit 24.9 and 14.7 electrons per decay respectively [86] and so a much higher energy deposition density for ^{125}I and ^{111}In would also be expected. The figure clearly illustrates the potential of an Auger emitter (positioned very close to the DNA) to produced DNA damage comparable to that of an alpha particle.

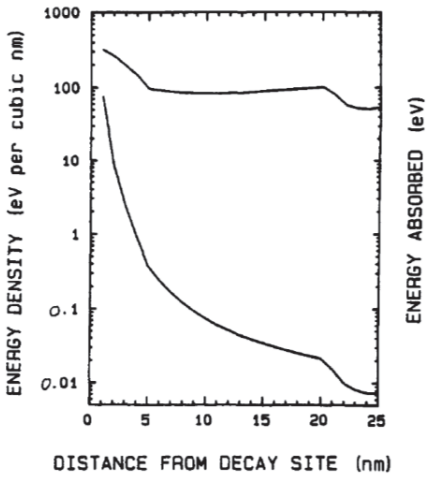

Figure 2.14 Monte Carlo simulation of localized energy deposition

Figure shows the localized energy deposition around the decay site of the Auger emitter ^{125}I. The top curve shows the energy absorbed by 1 nm thick concentric spherical shells of unit density. The lower curve shows the average absorbed energy density with distance for the decays site. Note that an energy density of 10 eV/µm^3 corresponds to a locally absorbed dose of 1.6 MGy. Figure & text taken from [63] *&* [89]

Another calculation, now of the energy deposition density for ^{125}I with increasing distance to the decay site has been given by Kassis and Sastry et al [63] and is pictured in Figure 2.14. As can be seen the energy density decreases rapidly with increasing distance to the decays site (in nm), illustrating the very short range of the lowest energy electrons (released from the ^{125}I decay). This rapidly decrease in energy density can explain the difference in biological effect between Auger emitters incorporated into and intercalated with the DNA. It is noteworthy that the energy density, within the first few nanometres (~ 0-3 nm) from the decay site corresponds to an incredible high absorbed dose in the order of MGy [63].

2.4 Physical and biochemical characteristics of Caesium and ^{131}Cs

2.4.1 Physical characteristics

The alkali metal caesium has many radioactive isotopes, with a range of half-lives and emissions [25]. The highly published and rightfully feared radiotoxic fission product ^{137}Cs with a 30 year half-life, is a good example of the combined effect of decay characteristics, chemical availability and biological uptake. It is well know that nuclear accidents (and bombs) have spread large activities of ^{137}Cs into the biosphere, leading to continental scale food chain contamination and measurable human uptake. Because of the very large populations exposed, this more or less homogeneous internal radiation from ^{137}Cs has been a major radiological concern after the major accidents at Chernobyl and Fukushima [90][91][92].

However, ^{137}Cs like most of the other radioactive caesium isotopes, decay by particular beta emission and very often companied by strong gamma branches. This makes the ^{137}Cs dosimetry simpler, and much less localised, and the intracellular distribution becomes unimportant because the ranges of all radiations are long compared to cell sizes. It is only the organ distribution that has been studied for such fission product [92].

As we are interested in studying the isolated effect of the Auger cascade, the “standard” long half-life caesium isotopes ^{137}Cs and ^{134}Cs are not useful. They both have weak Auger branches, but the overwhelming part of the local and distant absorbed dose from these isotopes comes from radiation that is not localised at the cellular scale.

^{131}Cs is a rather unique isotope which turns out to suit our purpose well. It has a decent half-life (9.689 +/- 0.016 days [25]) making it easy to work with in the laboratory, easy to use for exposure, and making activity measurements possible at a not too stressing timetable.

^{131}Cs decays by pure and absolutely gamma-silent electron capture directly to the ground state of ^{131}Xe. The only ionising radiation comes from the Auger cascade following the K-shell capture (dominating) and the competing X-ray emission [25].

The Auger yields and energy is tabulated in the NuDat 2.7 database [25]:

Auger L	3.43 keV	79.7 %
Auger K	24.6 keV	9.3 %

Of course there are more Auger cascade electrons than these, but of much lower energy. There are strong branches of Coster-Kronig and Super Coster-Kronig electrons.The total electron emission multiplicity is unkown, but now estimated to be 10.1, with an average energy of 613 eV (personal communication with Quan Lee Boon, based on Monte Carlo calculations as described in his paper [93])

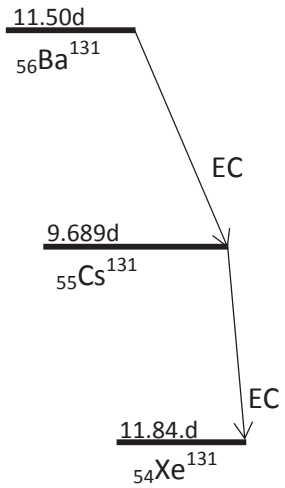

Figure 2.15 ^{131}Cs decay scheme.
Data from NuDat 2.7 [25]

The finer details and the lower energy branches of the ^{131}Cs cascade are not at all important for our S_C-value calculations (section 2.5 p. 57), where the above two branches (from NuDat 2.7) are more

than enough. However the knowledge that there are many more low energy electrons in the cascade is important, if there is more damage observed than the pure "absorbed dose" can account for.

2.4.2 Biochemical characteristics

As said, the release of ^{134}Cs and ^{137}Cs under nuclear accidents (and by nuclear bombs) lead to major radiological concerns including food chain contaminations. Due to the importance of microorganism in the biogeochemical cycle and primary production, forming the basis of all food chains, the cellular kinetics and biochemistry of caesium in microorganism, became of importance to human health and were therefore investigated. Although microorganism (bacteria, algae and fungi) are very different from mammalian cells, the knowledge about the bio-kinetics of caesium in these organisms, has given some clues to the bio- kinetics of caesium in mammalian cells [91] [92]. Caesium is taken up and accumulated through similar routes as potassium in cyanobacteria [90], bacteria [94] algea [95]and fungi [91] and has also been shown to compete with potassium uptake in cells from higher organisms [96][97]. In human erythrocytes caesium has been found (in 1964) to be transported by an active pump, that also transported potassium and sodium [98]. This description of the pump sounds very familiar to the pump that today is called the Na^+/K^+-ATPase.

2.4.2.1 Homogenous distribution of caesium

As stated, caesium mimics potassium in biological settings and since they are both group 1 elements, the intracellular chemistry of caesium, might be similar to that of potassium. They both have low first ionizations energies and therefore give off their valence electrons very easily. They also have a low tendency to form complexes with other ions, consequently making them highly soluble in water [91][99][100]. The difference between the extracellular and intracellular potassium concentration and its transport across the plasma membrane, form the basis for the electrochemical potential across the cell membrane [88]. In contrast to other metals involved in the biochemistry of cells, such as Zn^{2+}

(that form tightly bound complexes), potassium ions only form weak bindings to other biomolecules and exert its biological function primary as a charge carrier. As it is known that potassium is an ion that is highly mobile in the cell, mainly unbound and exist in its ionic state and it is justified to assume that caesium, will also be freely moveable, unbound and inside the cell, if it gets taken up as an ion. [91][99][100].

To summarise, ^{131}Cs is a pure Auger emitter which decays by electron capture (100%). It has a half-life of 9. 689 days, which is highly suitable for biological experiments. It has been shown to mimic potassium in biological settings, and might be taken up by the cells through the Na^+/K^+-ATPase. Its alkali chemistry makes it unlikely to get incorporated into biological molecules and a homogenous distribution inside the cells can be assumed, if it gets taken up as an ion.

All these characteristics make ^{131}Cs an ideal radioisotope for investigating the radiotoxicity of intracellular Auger decays.

^{131}Cs is not commercially available and is seldom used as an open radioactive source. The production of pure ^{131}Cs with high molar activity is difficult and the availability therefore limited.

2.5 Introduction to S_C-values

In this work I would like to introduce a new type of S-values, which I have chosen to name S_C-values. In the results and discussion sections, I will talk more about these S_C-values, which we have "developed" and used for this work. I will show results and discussed the difference between these S_C-values and the MIRD cellular S-values (see section 2.3.2.1 p. 45) and the implications of using these S_C-values. I will also show results, to back the statements I will make below. However, I would like already now to give a short description to these S_C-values and their qualities.

The S_C-values have the unit Gy/(Bq*Sec)/pL. The S_C-values are denoted with a subscript C, as they relate the activity concentration of the radioisotope to the absorbed dose. This is in contrast to the MIRD cellular S-values that use the total activity in a given cellular compartment to calculate the absorbed dose.
The computation of S_C-values uses the same "input" ("stopping power" ect.) as the MIRD cellular S-values, but differs from them in two important ways; the assumed geometry and the unit.

In order to be able to use these S_C-values, the geometry has to be a relatively big cell layer (big, when compared to the range of the Auger electrons). In addition the radioisotope has to be homogeneously distributed throughout this cellular layer, both in the cytoplasm and the nuclei. However, if these requirements are met, there are benefits of using these S_C-values instead of the MIRD cellular S-values.

First of all, our S_C-values are almost independent of the cellular and cell nuclear sizes. This is a very big difference from the MIRD cellular S-values that are very sensitive to small changes in these. A change in the size of the nucleus of only 1 µm changed the tabulated cellular S-values on average by a factor 2. Dependent on the precise geometry, this change varied from a factor 1.3 to 6.3 (for ^{131}Cs S(N←C)) (for these cellular S-values see appendix 8.2.1 p. 196). Such a difference will accordingly, change the absorbed dose by the same factor. In sharp contrast, our S_C-values only change with a few percent

over this range of nuclear sizes. In addition the shape of the cell and the nucleus is not important either. The concentric spheres model most often used by MIRD, does not fit the geometry of adherent cells. The ellipsoid geometry used in a few MIRD cellular S-value calculations comes somewhat closer to reality. However, every biologist having looked into a microscope knows that the shape of attached cells and the nuclei are diverse and very difficult (if not impossible) to model. Our S_C-values do not depend on the shape and size of the nucleus and the individual cells, but only on the height of the cell layer. The only thing that these S_C-values are dependent on is therefore the height of the cellular monolayer and the position of the nucleus in respect to the monolayer top and bottom. All this makes the S_C-values robust to use and significantly decreases the uncertainty in absorbed dose calculations. This in turn, will considerably reduce the uncertainty in the RBE-values obtained for Auger emitter decays.

3. Materials & Methods

3.1 Biological assays

3.1.1 The γH2AX assay

The γH2AX assay is widely used within the ionizing radiation field as a marker for DNA double strand break. The DNA DSB is in contrast to other DNA lesion (base damage, single strand break) considered to be highly detrimental to the cell. This is due to the high risk of destabilization of the chromatin structure, sequence loss and incorrect repair. The amount of DNA DBS is therefore thought to be a good indicator for the severity of cellular damage and the radiotoxicity of an irradiation [48].

As the name of the assay indicates the method involves the specific phosphorylation (γ) of the histone H2AX on the serine 139th residue. H2AX belong to the H2A histones that are one of the five histone families (H1/H5, H2A, H2B, H3 & H4) that together make up the nucleosome, the core unit, which the DNA double helix is wrapped around (Figure 3.1). The H2AX differs from the rest of the H2A histones, as it is the only one that is phosphorylated after DNA DSB formation. This is due to a highly conserved sequence of a serine 139th and a glutamine 140th, known as the SQ motif. The phosphorylated version of 139th serine on the H2AX (histone) is called γH2AX [101]. The amount of H2A histones, which are of the variant H2AX, varies between cell lines, constituting between 2-20 % of the total H2A histones. Dependent on the cell line and their fraction of H2AX histones the response observed after an irradiation can be more or less pronounced [102].

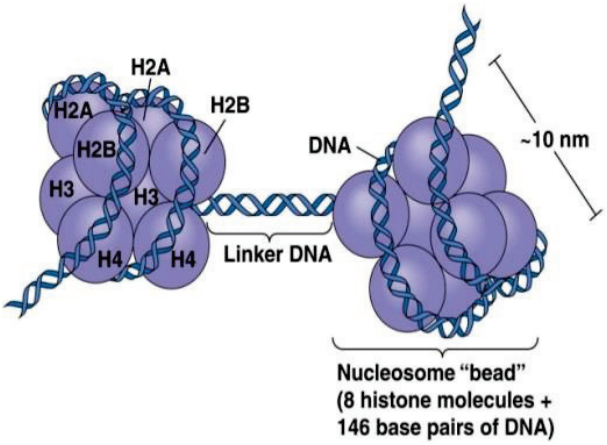

Figure 3.1 Representation of the nucleosome

The DNA double helix (blue) is wrapped around the nucleosome. Each nucleosome consists of 8 histones (purple spheres), belonging to 5 different families. After the formation of a DNA DSB, the H2AX histone (belonging to the H2A family) gets phosphorylated and plays a crucial part in the DNA damage repair process. Figure taken from [103]

Upon the formation of a DNA DSB, the serine 139th on the (nearby) H2AX is phosphorylated. This phosphorylation is carried out by the ATM/ATR and MRN complex, which have recognized the DNA DSB. The phosphorylation of the serine 139th is one of the first steps in the DNA damage repair process and serves to recruit mediators and repair proteins to the damaged site. To amplify the "signal", the phosphorylation of H2AX then propagates to neighboring H2AX histones, and spread along the DNA resulting in several hundreds to thousands H2AX histones getting phosphorylated per DNA DSB. The phosphorylation of H2AX does not occur immediately after irradiation. Rather, the amount of detected γH2AX foci increases over the first 30-60 min until it peaks. Thereafter, as the DNA DSBs gets repaired, the γH2AX (foci) become dephosphorylated and the amount of γH2AX foci decreases [102] [104].

In the γH2AX assay, it is the cluster (foci) of phosphorylated Serine 139th that is detected using the immune-fluorescence technique. The γH2AX method does therefore not detect the DNA DSB directly but rather detects the initiation of the DNA DSB repair process (Figure 3.2).

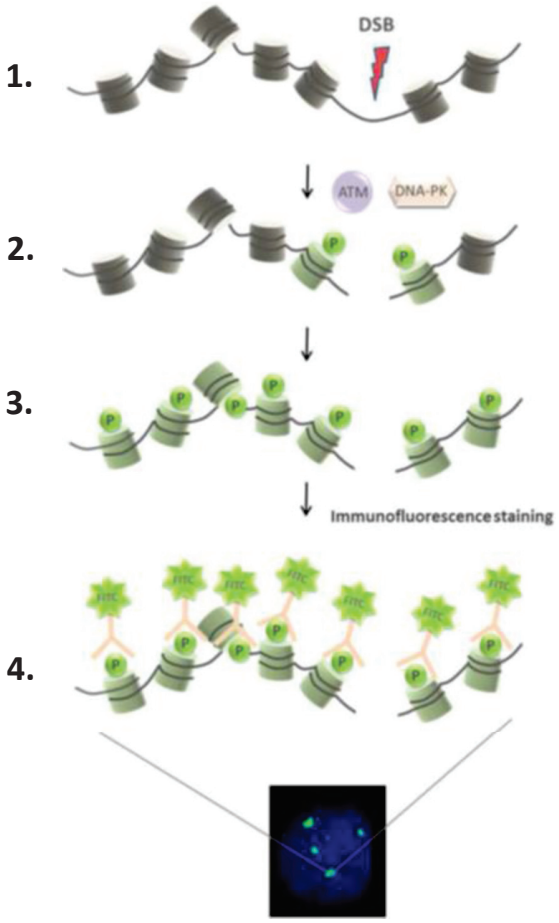

Figure 3.2 Representation of the γH2AXimmunofluorescence technique

The DNA represented by black lines is wrapped around the histones represented by grey cylinders. In step 1 a DNA DSB is produced by ionizing radiation. The ATM DNA-PK and MRN complex recognizes the DSB and phosphorylates the serine 139th on H2AX (step 2). In step 3, the phosphorylation (of H2AX) is propagated along the DNA, in order to amplify the signal. In step 4, the γH2AX focus is detected by fluorescent antibodies binding specific to the phosphorylated serine 139th. The γH2AX foci, can then be detected, counted and the fluorescence intensities measured. Figure modified from [105]

The γH2AX assay used in this work was developed by Merck Millipore. The assay is provided as a kit produced to run on the "MUSE", a small tabletop "flow cytometer" (Figure 3.3).

Figure 3.3 A picture of the "muse", a small table top flowcytometer that was used to obtain the data in the γH2AX assay
Figure taken from [106]

Besides permeabilization- fixation and washing -buffers, the kit contains two fluorescent antibodies; anti-phospho-Histone H2A.X (Ser139)-Alexa Fluor®555 and an anti-Histone H2A.XPECy5 conjugated antibody. The former specifically recognizes the phosphorylated serine 139th on histone 2AX (γH2AX) and the latter recognizes the unphosphorylated H2AX.

This assay measures the intensity of the two antibodies, representing the amount of phosphorylated and non-phosphorylated histone 2AX in each cell. It does not, as other γH2AX assays, count the number of γH2AX foci.
The data is presented in a on a plot with arbitrary scales, representing the intensities of phosphorylated H2AX (γH2AX) (x-axis) and the non-phosphorylated H2AX (y-axis) (Figure 3.4. A, C). A "red dot" represents a cell. The threshold (represented as red lines) for cells to be included in the categories non-expressing, inactivated and activated can be set and modified manually after all test samples and control samples have been analyses. The results are also presented in a bar plot (Figure 3.4. B, D) and in an excel table, stating the total cell number in each category. Before the analysis is run, a minimum cell size is chosen, and so, most cellular debris should have been excluded from the test.

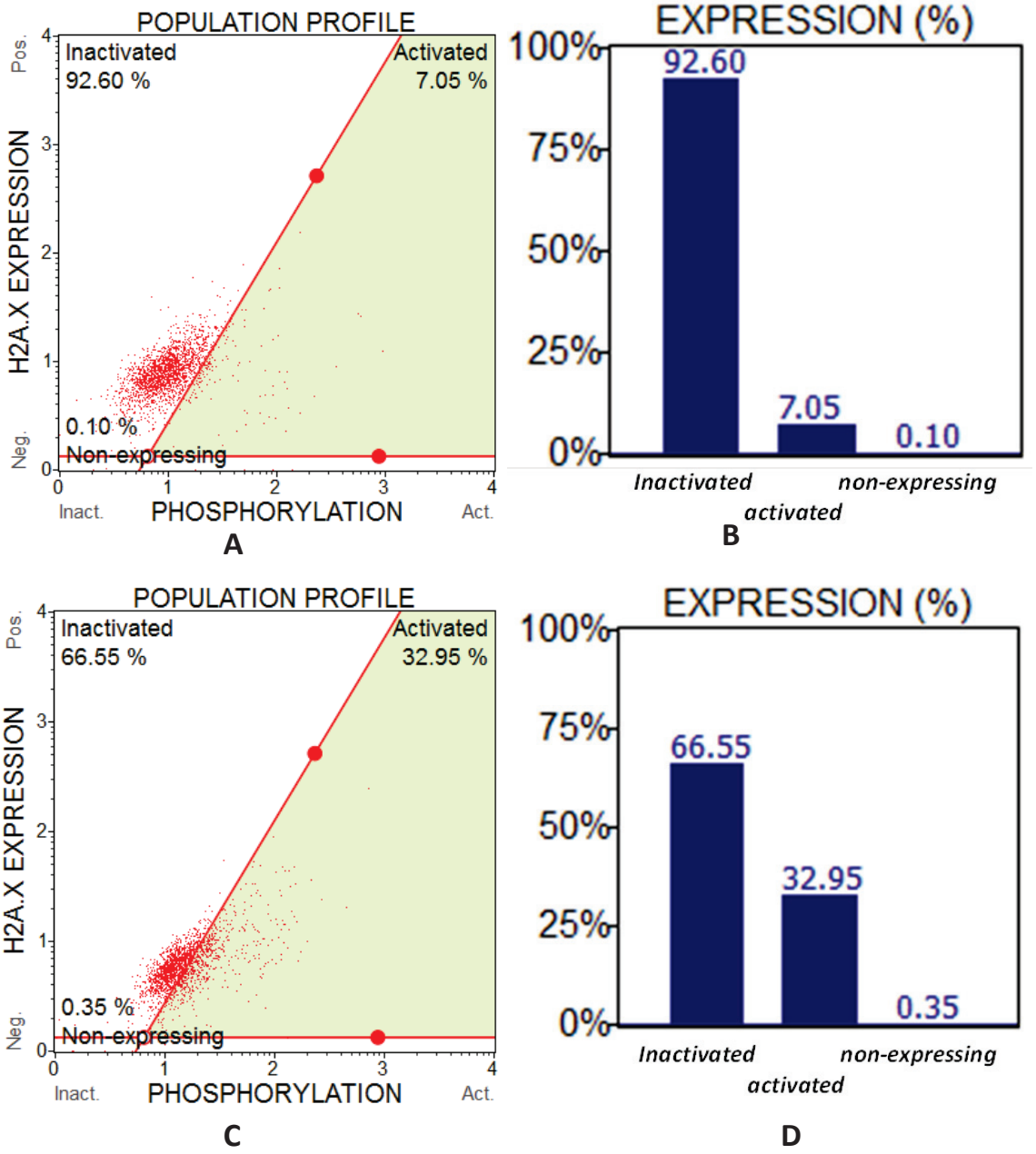

Figure 3.4 Representation of the data analysis in the γH2AX assay used in this work

The data is presented in a Cartesian coordinate system with arbitrary scales representing intensities of phosphorylated H2AX (γH2AX) (x-axis) and the non-phosphorylated H2AX (y-axis). Each red dot represents a cell. The cells are group into three categorized (inactivated, activated and non-expressing) based on their fluorescent intensities. The amount of cells in each group (in percentage) is given in a bar plot (B,D). The data presented in A & B shows the distribution of HeLa cells in a sample not exposed to any ionizing radiation. The data in C & D shows the distribution of cells in a sample, ~30 min after receiving 5Gy (γ-rays) from a Co^{60} source, using a dose rate of 1.5 Gy/min. As can be seen the cells have moved to the right (along the x-axis) and a higher percentage of the cells now lie in the green area representing activated cells.

As the cell are exposed to higher doses of radiation, the cell population move to the right along the x-axis indicating a higher amount of γH2AX-specific antibody binding and consequently more DNA DSBs. Sometimes the cell population is also observed to move up and down along the y-axis.

In this assay the number γH2AX foci in each cell are not directly counted. Instead the fluorescent intensities of the two antibodies in each cell are measured, indicating the level/amount of DNA DSBs present. A threshold for the intensities of the antibodies are manually decided, and groups the cells into three categories; non-expressing, inactivated and activated cells.
It is important to note, that the cells categorized as inactivated, will most likely still have DNA DSBs and γH2AX foci, however they will not have as many (or as big) as the cells categorized as activated cells. The cells categorized as non-expressing, are cells which did not bind "enough" of the two antibodies, representing a lack of Histone 2AX. This group should contain almost no cells.
For more information see *http://www.merckmillipore.com/DK/en/product/Muse-H2A.X-Activation-Dual-Detection-Kit,MM_NF-MCH200101*

In the thesis, the results are presented as γH2AX response "fold over control level", (as a function of absorbed dose) representing the percentage of cells categorized as activated in the test sample over the percentage of cells categorized as activated in the control sample;

$$\gamma\text{H2AX response, fold over control level} = \frac{\%\text{ cells catagogrized as activated in test sample}}{\%\text{ cells catagogrized as activated in control sample}} \qquad \text{(Eq. 20)}$$

3.1.2 Clonogenic cell survival assay

The clonogenic cell survival assay was developed by Puck and Marcus in the 1950s to study the effect of ionizing radiation on cells and is still considered by many the golden standard [107]. The clonogenic cell survival assay is used to study the effect of a treatment or an insult on the reproductive capability of cells. The assay is simple and does not required special equipment, but still gives the most important information when investigating potential cancer therapies; whether a cell will be able to continuously proliferate or not. A cell that has lost its ability to continuously proliferate is said to have lost its reproductive integrity or to be reproductively dead [39].

The mechanisms behind this loss of reproductive integrity are many incl. apoptosis, mitotic catastrophe and senescence. A cell that is reproductively dead is therefore not necessarily dead. It can still have maintained its ability to synthesize proteins, and fulfill its normal function. It can even be able to divide a couple of times before this capability cease [39] [108]. In the clonogenic cell survival assay, a cell that is able to form a colony of at least 50 cells is considered to be clonogenic, and is thought to have maintained its ability to divide and proliferate.

The clonogenic cell survival assay can be performed with both cells that grow attached or in suspension. The cells can be seeded either after or before the treatment. In the latter case, it is important to begin the treatment shortly after seeding (or after the cells have attached, if the cells grow adherent), so the cells will as little time as possible to divide. However in the case where the radioisotope is internalised or in other ways bound to the cells, the cells will also be exposed during the attachment phase, which might have an influence on the observed effect.

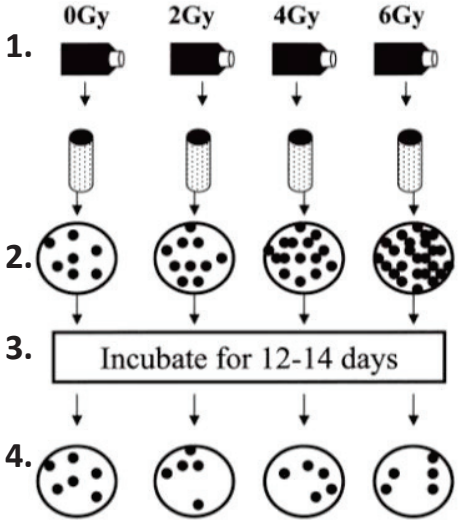

Figure 3.5 Representation of the clonogenic cell survival assay

In step 1 the cells are exposed to different absorbed doses of ionizing radiation. Thereafter (step 2) an appropriate number of cells are seeded. Sometimes, however, the cells are seeded before they are exposed. In this work, the cells were exposed both before and after seeding, due to the intracellular location of the radioisotope. The appropriate amount of cells seeded is different for the different absorbed doses. The appropriate number is estimated based on the expected survival fraction. After the cells are seeded and exposed they are incubated for several days in order to form colonies (step 3). The incubation time depends on the cell cycle time of the cell lines used. A group of cells (all originating from one cell) is defined as a colony if it consists of 50 cells or more. At the end of the incubation time, the number of colonies formed is counted (step 4) and the plating efficiency and survival fraction are calculated. Figure taken from [108]

A schematic representation of the different steps in the assay can be seen in (Figure 3.5). Either before or after the exposure, an appropriate number of cells are seeded. The appropriate number of cells differs within the experiments, and is estimated based on the expected survival fraction (SF). Preferably ~100 colonies should be present in each sample. A control sample, where the cells have not been exposed to the treatment, but otherwise handled in the same way, is always prepared together with the test samples. The control is used to determine the plating efficiency. The plating efficiency (PE) can vary between experiments, and is used to correct for factors other than the radiation, that could have an influence on the clonogenic cell survival [109].

The plating efficiency (PE) is defined for the control sample as;

$$\mathrm{PE} = \frac{\text{colonies counted}}{\text{number of cells plated}} \qquad \text{(Eq. 21)}$$

The survival fraction (SF) is defined as;

$$\mathrm{SF} = \frac{\text{colonies counted}}{\text{number of cells plated x PE}} \qquad \text{(Eq. 22)}$$

A survival curve represents the relationship between the survival fraction and the absorbed dose and is usually plotted on a semi-logarithmic plot. Dependent on the shape of the survival curve, the curve is fitted to the linear model ($y = e^{-\alpha x}$) or the linear quadratic model($y = e^{-(\alpha x + \beta x^2)}$), where y is the survival fraction and x the absorbed dose [39].

3.2 Materials

3.2.1 Chemicals & Solutions

Accutase, StemPro, (cat# A11105), (Gibco by Life Technologies, Brand owned and represented by Thermo-Fischer, NY, USA) (“ready to use solution”)

AG 1x8 ion exchange material 200-400 mesh, Dowex© , supplied by Sigma Aldrich, St. Louis, MO, USA

Americium-241 source, ISOTRAK calibration source, traceable to Deutsches kalibrerungs Dienst.

Ammonium carbonate, p.a., ACS reagent, (Sigma Aldrich, St. Louis, MO, USA)

Antibiotic Antimycotic Solution, (cat# A5955) (Sigma Aldrich, St. Louis, MO, USA)

Barium-130, 49 % enriched, as nitrate (Supplied by ILL, Grenoble, France)

Barium carbonate 99.999% pure on trace metal basis, (Sigma Aldrich, St. Louis, MO, USA)

Bovine Albumin Fraction V Solution (BSA, 7.5%) (cat# 15260-037) (Gibco by Life Technologies, Brand owned and represented by Thermo-Fischer, NY, USA)

Crystal violet (Sigma-Aldrich, St. Louis, MO, USA)

Dimethyl sulfoxide, anhydrous 99.9% (DMSO) (Cat # 27.685(Sigma-Aldrich, St. Louis, MO, USA)

Dulbecco´s Modified Eagle´s Medium (DMEM) (cat# D6546), (Sigma Aldrich, St. Louis, MO, USA)

EDTA (0.5 M), ultra-pure (Cat# 15575-038) (Invitrogen by Life Technologies, Grand Island, NY, USA)

Fetal Bovine Serum (FBS) (Cat# F22442) (Sigma-Aldrich, St. Louis, MO, USA)

Giemsa Stain, Modified Solution (cat# 48900) (Fluka Analytical by Sigma-Aldrich, St. Louis, MO, USA)

Hank’s balanced salt solution (HBSS) (Cat# 14025-0.50)(Thermo Fisher Scientific, Waltham, MA, USA)

Hoechst 33342 (Sigma-Aldrich, St. Louis, MO, USA)

L-Glutamine (200 mM) (cat# G7513) (Sigma Aldrich, St. Louis, MO, USA)

Minimum Essential Medium Eagle (MEM), (cat# M2279), (Sigma Aldrich, St. Louis, MO, USA)

MUSE kit: H2A.X Activation Dual Detection Kit (Cat # MCH200101) (Merck Millipore, Billerica, MA, USA)

Count & Viability Kit (Cat# MCH600103) (Merck Millipore, Billerica, MA, USA)

Ouabain Octahydrate (Cat # 03125) (Sigma Aldrich, St. Louis, MO, USA)

Phosphate buffered saline (PBS) 10x (Cat # P5493)(Sigma-Aldrich, St. Louis, MO, USA)

Scintillation fluid Ultima Gold (cCat # 6013329) (Perkin Elmer, Waltham, MA, USA)

Trypsin, 2.5% (cat# 15090-046) (Gibco by Thermo Fisher Scientific, Waltham, MA, USA)

Ultra pure water. FLUKA Trace Select Ultra Pure Water (via Sigma-Aldrich, St. Louis, MO, USA)

Wheat Germ Agglutinin Sampler kit, Oregon Green® 488, Alexa Fluor® 488 conjugate (cat # W7024) (Thermo Fisher scientific , Waltham, MA, USA)

3.2.2 Cell culture medium

Freeze medium (HeLa): MEM medium, 14 % FBS, 7,8% DMSO

Freeze medium (V79): 40% normal growth medium (DMEM), 50% FBS, 10% DMSO

Growth medium (HeLa): DMEM medium supplemented with 10% FBS, 4 mM L-glutamine and 1% antibiotic antimycotic

Growth medium (HeLa): MEM medium supplemented with 10% FBS, 4 mM L-glutamine and 1% antibiotic antimycotic

Growth medium (V79): DMEM medium supplemented with 10% FBS, 4 mM L-glutamine and 1% antibiotic antimycotic

3.2.3 Equipment & instruments

Centrifuge: Micro CL 17 (Thermo Fisher Scientific, Waltham, MA, USA)

Cell culture microscope: Olympus CKX41 (Olympus, Tokyo, Japan)

Confocal Laser Scanning Microscope LSM780 (Zeiss, Oberkochen, Germany)

HP-GE X-ray spectroscope/detector (Canberra, now Mirion, Uppsala, Sweden)

Incubator (calibration facility): Cell culture CO_2 incubator Compact Midi 40 (VWR, Søborg, Denmark)

Incubator (cell lab): Cell culture CO_2 Incubator, model CCL-170B-8 (ESCO, Singapore)

MUSE analyser (Merck Millipore Corporation, Billerica, MA, USA)

Passive cooler with isopropanol (Nalgene by Thermo Fisher Scientific, Waltham, MA, USA)

Sceptor 2.0 (Merck Millipore, Billerica, MA, USA)

Scintillation Counter Hidex 300SL (Hidex, Turku, Finnland)

3.2.4 Software

GraphPad Prism 7 (GraphPad Software, Inc. La Jolla, CA, USA)

Matlab R2014b (Mathworks, Natick, MA, USA)

Microsoft Excel 2010, with Data Analysis Tool Package.

MUSE 1.4 cell analysis

NuDat 2.7 database at Brookhaven National Laboratory (*www.nndc.bnl.gov/nudat2/*)

Zeiss ZEN-light version 2.3 (Carl Zeiss, Microscopy GmbH, Jena, Germany)

3.2.5 External radiation sources

Caesium-137:

CANBERRA NUCOMAT UNIVERSAL CALIBRATOR SYSTEM, Nutech Building 201, room K17. Nominal source strength: ^{137}Cs 200 Ci 8 TBq, Dose rate at 100 cm distance: 664 ± 8.4 mGy / h with reference date 25 October 2001. Calibration traceable to SIS, Herlev, Denmark

Cobalt-60:

Terabalt T100 Dosimetric Irradiator, UJP, Praha, Czec Republic with a GK60T03 ^{60}Co source. Nominal activity 455 TBq in 2012, 1 Gy/min at 100 cm distance April 2017.

3.2.6 Cell lines

Two cell lines were chosen for the experiments. These were HeLa cells and V79 cells. Both cells lines are easy to grow in the laboratory and are often used in biological research.

3.2.6.1 HeLa cells

HeLa cells are famous for being the first human cell line to be continuously grown in the laboratory. Despite nearly a decade of experience and success in establishing continuously rodent cell lines, nobody had succeeded in keeping human cells growing in culture for more than a few weeks. In 1951 an especially aggressive cervical cancer (adenocarcinoma) was isolated from the 30-year old black woman Henrietta Lacks (Figure 3.6) and given to George Gey at The John Hopkins Hospital in Maryland, who managed to culture these cells continuously. Despite the tragic passing of Henrietta Lacks only a few months later, and the heavy debated ethical circumstances in obtaining the cells, the HeLa cells have undoubtedly contributed to the understanding and treatment of various human conditions including cancer [110].

Figure 3.6 A picture of Henrietta Lack, the women from whom the HeLa cell line was isolated from
Picture taken from [111]

HeLa cells are a cervical cancer cell line. Even though they are epithelial cell they are fibroblast like and grow adherent as a monolayer. HeLa cells have a cell cycle time of ~24 hours which is divided between the four cell cycle phases; G1-phase (11 hours), S-phase (8 hours), G2-phase (4 hours) and M-phase (1 hours)[39]. HeLa cells express a low level of p53. This might be due to the presence of Human Papilloma virus type 18, (HPV18) and the expression and production of HPV E6 onco-protein which destabilizes p53 [112]. The HeLa cells are positive for the retinoblastoma protein (pRb) a tumour suppressor protein dysfunctional in many cancer [113]

3.2.6.2 V79 cells

V79 cells are a lung fibroblast cell line. It was isolated after a spontaneous transformation from a young male Chinese hamster and was developed by Ford and Yerganian in 1958. The cell line was originally designated Strain V, but got renamed by Elkind to V79. V79 cells were originally grown as an adherent monolayer but can also be grown in suspension in the right medium. The cell cycle of V79 has a cell cycle time of ~12 hours divide into G1-phase (1 hours), S-phase (6 hours), G2-phase (3 hours) and M-phase(1 hours). The V79 cells used here were p53 negative and pRb positive [39][114].

3.3 Methods

3.3.1 Production of ^{131}Cs

^{131}Ba (11.5 d half-life) was produced by high flux neutron irradiation at the ILL reactor (Institut Laue-Langevin, Grenoble, France) with 6 to 10 days irradiations at a flux of (1.1-1.3) * 10^{15} n cm^{-2} Sec^{-1} of either natural Ba (17-25 mg as carbonate) or 49 % enriched ^{130}Ba (0.15 mg as nitrate, supplied by ILL). Upon reception at Hevesy Laboratory (1-2 weeks after end of irradiation), the outside of the quartz ampules were washed in 2 M HCl and ultra-pure water (to remove significant amounts of ^{65}Zn, ^{60}Co etc, but also to remove possible external contamination with salts). After breaking the ampules open, the target materials were dissolved in 2 M ultrapure hydrochloric acid. The clear solution was immediately re-precipitated by addition of a saturated solution of ammonium carbonate. This forces barium carbonate (with > 95% of the barium activity) to settle within a few minutes as heavy, well defined precipitate while initially produced caesium activity was discarded with the supernatant. This caesium fraction was found to be radionuclidic impure due to 1-2 % ^{132}Cs made by either (n,p) or second order capture during the irradiation. Discarding the first caesium fraction proved important for a reliable and high cellular uptake in the following incubation experiments. The precipitate was washed with 2-3 ml of ultra-pure water, the water decanted and discarded after spinning at 3000 rpm, after which the precipitate was left to stand for 2-7 days for build of new caesium activity. Shortly before time of use, the barium carbonate precipitate was dissolved in the smallest possible amount of 2 M hydrochloric acid, and then precipitated with saturated ammonium carbonate. The supernatant at this stage contains only ^{131}Cs, with barium effectively removed by the total absence of any ^{131}Ba or ^{133}Ba activity in the final ^{131}Cs. The decontamination factor from barium in one precipitation was found to be bigger than 30.000 – in accordance with the low solubility of barium carbonate at room temperature and neutral pH.

The supernatant was dried out at 85°C under nitrogen flow, leaving all the caesium activity and a slight white skirt of ammonium chloride in the upper, coldest part of the drying vessel. Drying and

firing at higher temperatures than 85 °C led to significant loss of caesium activity to the gas and was subsequently avoided.

The dry caesium fraction was dissolved in 2-4 ml ultrapure water and then passed over a small ion exchange column AG 1x8 to remove remaining ammonium ion. The column eluate was evaporated in a clean, carefully weighed 10 ml glass vial, and then dried at 80 °C to absolute dryness. At this stage, visual inspection of the vial showed no residuals whatsoever, and the mass balance invariable showed a total mass less than 0.2 mg at this stage. (This corresponds to less than 1 µmol of ammonium chloride).

The activity was recovered from the vial by the ready dissolution in 100-200 µl PBS. Activity concentration and radionuclidic purity was established by HP-GE X-ray spectroscopy of a 1 µl sample.

The re-precipitated targets were stored for 1-2 weeks for build-up of ^{131}Cs, and then the process could be repeated. We have milked up to 4 batches of useful ^{131}Cs activity from a single activated barium batch from ILL. The harvested, ^{131}Cs in PBS was added the HeLa and V79 cells in normal growth medium.

Using natural barium as target and 10 days for transport/decay before first ^{131}Cs extraction, 80 MBq ^{131}Cs could be obtained. With an enriched ^{130}Ba target, more than 500 MBq were obtained from first extraction. The ^{131}Cs harvesting has been repeated up to 4 times on each neutron activated sample. No difference was seen in the purity or the cellular uptake profile whether the ^{131}Cs came from enriched or natural barium targets. In principle, the specific activity should be equally high in both methods and should approach carrier free conditions.

3.3.2 Liquid Scintillation Counting (LSC) of ^{131}Cs

^{131}Cs activity was counted using Liquid scintillation counting. The machine used for counting was a Hidex 300SL (Hidex, Turku, Finland). The ^{131}Cs sample to be counted was added to 10 ml scintillation fluid, in oximate glass vial. For counting a maximum of 1ml sample solution was added each vials.

Before counting, the LSC vials were shaken thoroughly to ensure a proper mixing of the sample and scintillation fluid. The counting was done using channel 218-480 (covering the K-Auger branch and possible K- X-ray interactions in the scintillation cocktail) The spectrometer was operated in the triple-double coincidence mode to minimise background and lower any quenching effects. A blank was always counted with the samples to measure the background.

3.3.3 Standard curve

A standard curve was made in order to calculate the real ^{131}Cs activity in a sample based on counts per second (CPS). A standard sample of ^{131}Cs was first measured on the germanium X-ray detector that was efficiency calibrated against a standard ^{241}Am source to know the real activity in the sample. A linear extrapolation between the 26.3 keV and the 59.5 keV X-ray emitted by ^{241}Am was used to "calibrate" against the two 29.5 keV and 29.8 keV X-rays emitted by ^{131}Cs

A small amount (49.3 mg) of the ^{131}Cs standard sample was mixed with 197.6 mg of ultra-pure water. From this, a dilution series was made by mixing 200 µl of the previous ^{131}Cs sample with 200 µl of ultra-pure water. In this way every new sample had an activity around half of the previous. For each sample both the amount of ^{131}Cs containing solution and the amount of ultra-pure water added were measured using a scale. The mass was converted to volume assuming a density of 1 mg/µl. 15 samples were made ranging in activity from 1 CPS to 4000 CPS. 100 µl of each 400 µl sample was transferred to LCS vials containing 10 ml scintillation fluid. The samples were counted for either 20 min or untill 10.000 counts were registered. The measured CPS was corrected for background and decay during the measurement protocol.

To find the dead time of the LSC, the 15 samples were allowed to decay for 24 days (~2.5 half-life) and were thereafter counted using the same settings. Based on the CPS of the two countings, the dead time of the LSC was found using solver in Excel. Samples which activity was so low, that the background had a significant influence, were not used in the fitting.

To convert CPS to disintegration per second (DPS or formally Bq) the counting efficiency was found. The CPS from the first counting of the samples was first corrected for the dead time. Then the Bq in each sample were calculated using the known activity in the ^{131}Cs standard sample and the known amounts of ^{131}Cs containing solution and water added to each sample. The count efficiency was then calculated by dividing CPS with Bq and finding the average, excluding outline samples that had a too high or too low activity.

3.3.4 Cell cultures and storage

3.3.4.1 HeLa cells

HeLa cells were obtained from The European Collection of Cell Cultures (ECACC) (93021013), as passage (P5). They were grown in MEM or DMEM medium supplemented with 10 % FBS, 4 mM L-glutamine and 1 % antibiotic antimycotic. They were cultured in a humidified atmosphere containing 5 % CO_2 at 37°C. The HeLa cells were passaged 1-2 times a week when reaching 80-90 % confluency or when needed for experiments. For passage the cells were washed with PBS and either accutase ("ready to use solution") or 0.1 % trypsin containing 0.5 mM EDTA in PBS was used to detach the cells. If accutase was used the cells were centrifuged at 200 G for 5 min and the supernatant was removed before resuspension of the cells in growth medium. Otherwise cells were trypsinizated for 5 min at 5 % CO_2, 37 °C. The trypsinization was stopped by addition of growth medium to the cells.

For long time storage, HeLa cells were grown in T25 flask to 90 % confluency. The old medium was discarded and the cells were washed with PBS. To release the cells from the culture flask surface, they were incubated with 5 ml accutase for 5 min. Thereafter the cells were centrifuged at 200 G for 5 min and the supernatant was removed. The cells were re-suspended in ~1.5 ml HeLa freeze medium consisting of MEM medium, FBS (14 %) and DMSO (7.8 %) and transferred to cryo-tubes (~2x10^6 cells/ml). The cells were pre-cooled at -80 °C in a passive cooler over night before long-time storage in liquid nitrogen (-196 °C).

3.3.4.2 V79 cells

The V79 cells were a generous gift from Dr. Priscilla K. Cooper (Lawrence Berkeley National Laboratory, USA). They were grown in DMEM medium supplemented with 10 % FBS, 4 mM L-glutamine and 1 % antibiotic antimycotic. They were cultured in a humidified atmosphere containing 5 % CO_2 at 37 °C. The V79 cells were passaged 1-2 times a week when reaching 80-90 % confluency or when needed for experiments. For passage the cells were washed with PBS before being trypsinized for 5 min at 5 % CO_2, 37°C, using 0.1 % trypsin/EDTA (0.5 mM) in PBS. Trypsinization was stopped by addition of growth medium to the cells.

For long time storage the V79 cells were kept in a liquid nitrogen tank. The old medium was discarded and the cells were washed with PBS. To release the cells from the culture flask surface the cells were trypsinated using 0.1 % trypsin/EDTA (0.5 mM) in PBS. Freeze medium consisting of 40 % normal growth medium (DMEM medium supplemented with 10 % FBS, 4 mM L-glutamine and 1 % antibiotic antimycotic), 50 % FBS and 10 % DMSO were added to the cells. 1 ml cell suspension was transferred to cryo-tubes (max. $4*10^6$ cells/ml). The cells were either pre-cooled at -80 °C in a passive cooler over night or cooled at dry ice with isopropanol (-77 °C) for 3-4 hours, before being transferred to liquid nitrogen (-196 °C) for long time storage.

3.3.5 ^{131}Cs bio-kinetics

3.3.5.1 Experimental setup

All experiments were carried out using 48-well plates. 48-well plates were chosen in order to use the smallest amount of medium and thereby as little ^{131}Cs as possible (as ^{131}Cs was not easily available), while still having enough cells for the experiments. As both the HeLa and V79 cells grow attached, each sample (e.g. time point) in each experiment was obtained using separate wells (Figure 3.7).

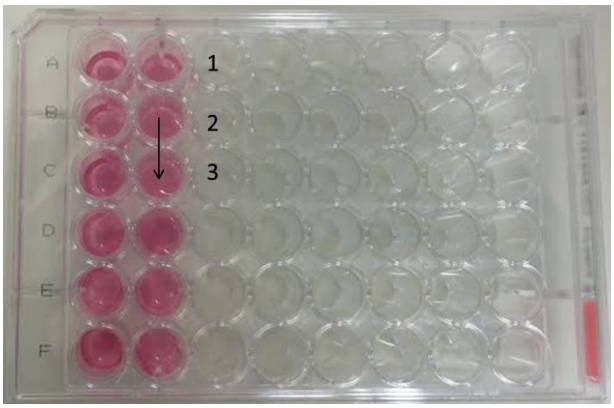

Figure 3.7 Experimental setup for HeLa and V79 cells incubated with ^{131}Cs in 48-well plates

A volume of 200 µl ^{131}Cs containing medium was added each well. As the cells grow attached each sample (e.g. time points) in an experiment was obtained from different wells (e.g. well nr. 1 being time point x, while well nr. 2 would be time point y). Cross dose from neighbouring wells (e.g. from well nr. 2 to well nr. 3) was ignored.

In this geometry of closely spaced wells, a cross-dose effect from one well to the next should in principle be considered. However, cross dose resulting from the Auger electrons can immediately be dismissed because the electron ranges are smaller than the thickness of the plastic walls. The X-ray cross-dose can be disregarded for the same reasons that cell-to-cell and medium to cell X-ray dose could be neglected. Due to the geometry of the wells (cylinders) with shallow layers of (radioactive) cells, there is only a very small solid angle for interaction of one cell layer with the X-rays from the other wells.

3.3.5.2 Uptake of ^{131}Cs in HeLa and V79 cells

HeLa and V79 cells were seeded in 48-well plates and incubated overnight at 37 °C, 5 % CO_2. ^{131}Cs in the form of CsCl (dissolved in saline or PBS) was mixed with growth medium to get an activity concentration of ~25 kBq/ml. The cells were washed with PBS before 200 µl ^{131}Cs containing growth medium was added. The cells were incubated for up to 12 hours (24 hours in one experiment) at 37 °C, 5 % CO_2. As the cells were grown attached, ^{131}Cs uptake for each time point was obtained using separate wells. After incubation the ^{131}Cs containing medium was removed and the cells were washed with PBS before trypsinization (0.1 % trypsin/EDTA (0.5 mM) in PBS for 3-5 min, at 37 °C, 5 % CO_2). The cells were thereafter re-suspended in growth medium. To determine the ^{131}Cs uptake in the cells, a part of the cell suspension was transferred to LSC vials for counting. The LSC counting was performed as described in section 3.3.2 p. 74. The number of cells in each sample and the sizes of the cells were measured using the Sceptor 2.0 from Millipore. In each experiment a control for the washing efficiency was made by adding and immediately afterwards removing the ^{131}Cs containing medium from the control cells. The ^{131}Cs activity measured in this control was subtracted from the other samples. The cellular activity of ^{131}Cs (the intracellular ^{131}Cs activity concentration, Bq/pL cell) for all time points (in each experiment) was calculated by dividing the total ^{131}Cs activity (obtained by LSC counting) by the total cellular volume (number of cells * average cell volume, measured by the Sceptor 2.0).

$$\text{Cellular } ^{131}\text{Cs actvity concentration at time (t)} = \frac{\text{total } ^{131}\text{Cs activity in the cells at time (t)}}{\text{total cellular volume at time (t)}} \qquad \text{(Eq. 23)}$$

To calculate the accumulation of ^{131}Cs in the cells compared to the medium, this cellular activity concentration was dividing by the activity concentration in the medium. The cellular ^{131}Cs activity concentration at each time point (for each experiment) was normalized to the cellular ^{131}Cs activity concentration at time (T) 380 min (HeLa cells) or 480 min (V79 cells) to get the relative ^{131}Cs activity concentration.

$$\text{Relative } ^{131}\text{Cs actvity concentration at time (t)} = \frac{\text{cellular } ^{131}\text{Cs activity concentration at time (t)}}{\text{cellular } ^{131}\text{Cs activity concentration at time (T)}} \qquad \text{(Eq. 24)}$$

T, being time point 380 min for HeLa cells, and 480 min for V79 cells. These two time points were chosen in order to include as many "uptake experiments" as possible in the fitting analysis, but did not otherwise affect the exponential constant (k_c).

The data from all the experiments was fitted together as a single fit to the below exponential equation (Eq. 25) using the curve fitting toolbox in Matlab and k_c determined.

$$A = A_0 * (1 - e^{-t*k_c}) \quad \text{(Eq. 25)}$$

A, being the relative activity concentration in cells at time t, A_0 the relative activity concentration in cells at equilibrium and k_c the exponential constant.

3.3.5.3 Release of ^{131}Cs from HeLa and V79 cells

HeLa and V79 cells in 48-well plates were incubated with ^{131}Cs containing growth medium (~20 kBq/ml) over night (13-16 hours) at 37°C, 5 % CO_2, in order for them accumulate a suitable amount of ^{131}Cs. The cells were thereafter washed and fresh growth medium (not containing any ^{131}Cs) was added. The cells incubated (at 37°C, 5% CO_2) for different time periods (0-10 hours) before being trypsinized (0.1 % trypsin/EDTA (0.5 mM) in PBS for 3-5 min, at 37 °C, 5 % CO_2). The ^{131}Cs activity in the cell sample was measured by LSC (see section 3.3.2 p. 74). The cell number and size was measured using the Sceptor2.0 from Millipore. The cellular ^{131}Cs activity concentration in the cells at the different time points was calculated as above (Eq. 23) and normalized to the ^{131}Cs activity concentration in the cells at time point zero.

The data were fitted to an exponentially decreasing function using both solver in Excel and Matlab and the rate constant k_{out} was found for both HeLa and V79 cells.

$$A = A_0 * e^{-t*k_{out}} \quad \text{(Eq. 26)}$$

A, being the activity concentration in the cells at time (t), A_0, the activity concentration in the cells at time 0, and k_{out} being the rate constant. The results from three independent experiments were fitted

independently in Excel using solver and the least square method. The results were also fitted as a single fit in Matlab (using the fitting toolbox) to obtain confidence intervals. The two different fitting methods used had a small influence of the obtained k_{out} for HeLa cells, but had no effect on k_{out} for V79 cells. For reasons of the chronological progression of the experimental work, the k_{out} value for HeLa cells obtained by Excel solver was used in later calculations.

3.3.5.4 Inhibition of ^{131}Cs uptake by Ouabain

HeLa and V79 cells were seeded in 48-well plates and incubated overnight. The cells were washed in PBS and incubated for 5.5 & 6.5 hours in growth medium containing ~20 kBq/ml ^{131}Cs and different ouabain concentrations ((HeLa: 10 nM, 50 nM, 0.1 µM, 0.5 µM, 1 µM, 5 µM),(V79: 10 µM, 50 µM, 0.1 mM, 0.5 mM, 1 mM). After incubation the cells were washed with PBS and trypsinized (0.1 % trypsin/EDTA (0.5 mM) in PBS for 3-5 min, at 37 °C, 5 % CO_2). The cellular ^{131}Cs activity in each sample were measured by LSC (see section 3.3.2 p. 74) and cell number and their sizes were measured with the Scepter 2.0 from millipore. The cellular ^{131}Cs activity concentration was calculated (using Eq. 23) and normalised to a control sample in which only ^{131}Cs but no ouabain had been added. The data was fitted to a sigmoid curve using the least square fit methods in GraphPad prism 7.03

3.3.6 S_C-values

3.3.6.1 Cell layer height and nuclei volumes

The height of the cellular monolayer and the nuclear sizes of the HeLa and V79 cells were determined by confocal microscopy. The microscope used was a Laser Scanning Microscope (LSM 780) from Zeiss provided by and operated by the Core Facility for Integrated Microscopy (CFIM), at the University of Copenhagen. The cells were seeded on high precision cover glasses with a thickness of 0.17 ± 0.01 mm and grown to full confluency overnight at 5% CO_2, 37°C. The living cells were stained with Wheat Germ Agglutinin (WGA) Oregon Green® 488 and Hoechst 33342. WGA Oregon Green® 488 is a green fluorescent dye, which selectively binds to N-acetylglucosamine and N-acetylneuraminic acid residues, and can thereby be used to stain the plasmamembrane. Hoechst 33342 is a blue fluorescent dye that binds to the minor groove of the DNA and can be used to stain the nucleus. Both fluorescent dyes can be used to stain living cells. The staining were performed using a WGA concentration of 5 µg/mL, diluted in growth medium and a Hoechst 33342 concentration of 20 µg/ml diluted in growth medium. Cells were stained for 10-20 min at 5% CO_2, 37°C. After the staining the cells were washed with Hank´s balanced salt solution (HBSS) before being view in the microscope (alive) still submerge in HBSS. A 10x objective was used. 71 pictures with a spacing of 0.37 µm, covering an axial length of 26.08 µm were taken of the HeLa cell culture. 59 pictures with a spacing of 0.3, covering an axial length of 21.6 µm were taken of the V79 cells. The height of the cell layer and the nucleus sizes were afterwards determined using the Zeiss ZEN-light software package operating directly on these image stacks (Z-stack) obtained by CFIM. Due to limitations in the confocal microscopy technique, the precise location (within 1-2 µm) of the top and bottom of the cellular monolayer and thereby its height were difficult to estimate. However, by scrolling through the Z-stack (image stacks), a sudden drop in the green fluorescent intensity were observed. This drop in fluorescent intensity appeared near what seemed to be the top and bottom of the cellular monolayer (displayed by the picture bars showing an axial cross section of the cell layer) and coincided with the appearance of plasma membrane “overlying” the nuclei and so these locations were chosen as the top and bottom of cellular monolayer, and its height found as the distance between these two position given by the

inbuilt scale in the Zen software. To determine the volume of a nucleus, the image in the Z-stack in which the nucleus appeared largest was first found. Its two different axes in the x-y plane were then measured using the tools in the Zen software. The length of the third axis (in the z-direction) was measured by finding the first and last image in the Z-stack in which the nucleus was present and taking the distance between them again using the tools in the Zen software. The shape of the nucleus was assumed to be an ellipsoid and using the standard formula for volume for such geometry ($V = \frac{4}{3}\pi abc$), in which a, b & c are the semi-axes, the nucleus volume was calculated. This was done for all nuclei that were completely contained inside the confocal images, in order to obtain the nuclear volumes and their distribution. Although this axis measurement is not necessarily completely geometrical correct (the horizontal imaging planes are not necessarily aligned with the ellipsoid axes), it is a fair approximation given the otherwise big biological variations in shape.

3.3.6.2 Calculation of the ^{131}Cs S_C-values, $S_C(N \leftarrow C)$.

The geometry used was a confluent cellular monolayer with a height of 10 µM (HeLa) or 8 µM (V79). This geometry is not treated by MIRD Cell. The cell nuclei were approximated by ellipsoids with 3 axes. The axis lengths as measured above were used to calculate the volume of each nucleus, but also to make a scoring volume in Matlab, inside which the deposited energy was sampled. The energy deposited in each volume element of the cell monolayer is given by the 3 dimensional convolution of the ^{131}Cs dose kernel with a simple rectangular slab representation of the uniform activity concentration in cell monolayer. The average of the S_c-values found (from each cell line) from the individually measured and modelled nuclei, also corresponded to the S_c-value for the average nucleus size (for each cell line) and so this (these) value(s) was used in the dose calculations.

The ^{131}Cs was assumed to be equally distributed throughout the entire cellular monolayer, including the cytoplasm and the nucleus. The K- and L-Auger electron energies and intensities (24.6 keV (9.3 %) and 3.43 keV (79.7 %) respectively) provided by the NuDat 2.7 database [25] were used in the calculations. Monoenergetic electron emission dose kernels (as 3-dimensional matrices centred on

the point of emission) for a point source were calculated using the same method applied by MIRD for cellular S-values, using Cole´s inverted formula for energy versus range as a stopping power [17][82].

To do this for a given single electron energy E, the maximum penetration depth (Cole's "range" is found from the numerical expression in [17][82] for E as function of range R:

$$\mathrm{E} = 5.9 * (\mathrm{R} + 0.0007)^{0.565} + 0.00413 * \mathrm{R}^{1.33} - 0.367 \qquad \text{(Eq. 27)}$$

Where E is given in keV and rang e in µm. Cole states the expression to be valid in the range from 20 eV to 20 MeV.

This expression does not lend itself easily to inversion by analytical methods, but ranges at given energies can be found by successive approximations. In practice, however, for ^{131}Cs with maximum electron energy below 40 keV, a good third degree polynomial approximation was found to be:

$$\mathrm{R} = -0.0001353 * \mathrm{E}^3 + 0.0214 * \mathrm{E}^2 + 0.07272 * \mathrm{E} \qquad \text{(Eq. 28)}$$

Having found the maximum range of each electron branch (Rm), the Cole "stopping power" equation

$$\frac{\mathrm{dE}}{\mathrm{dx}} = 3.333 * (\mathrm{R} + 0.007)^{-0.435} + 0.0055 * \mathrm{R}^{0.33} \qquad \text{(Eq. 29)}$$

is used to find the energy loss per radial distance length from the point source.
Again, this formula has $\boldsymbol{E}$ in keV and R in µm. Cole and "MIRD Cellular S values" uses this expression over the range from 20 eV to 20 MeV.

The expression for the dose at a given distance Rx < Rm from the point source is now

$$\mathrm{D(Rx)} = \frac{\left.\frac{\mathrm{dE}}{\mathrm{dx}}\right|_{\mathrm{R=Rm-Rx}}}{\text{Volume of sperical shell between Rx and Rx+dx}} \qquad \text{(Eq. 30)}$$

This expression is the radial dose kernel. It is used to fill a three cubical Matlab matrix $\mathbf{D}$ centered around the emission point with doses according to the above formula and its distance from the center

of the matrix. The matrix has voxel sizes dx^3, with dx = 0.2 µm. The "Cole" range of K electrons from ^{131} Cs is 12.7 µm or 64 voxels, while L electrons have substantially shorter range.
The matrix elements inside this"dose matrix" $\mathbf{D}$ have dose values when closer than Rm to the matrix center, and zero otherwise. A consistency check is always made that the total energy contained in the dose matrix is equal to the electron energy emitted.

For each Auger electron branch, the monoenergetic dose matrix $\mathbf{D}$ is thus calculated, then weighted by the emission probability for that branch, and finally all individual dose matrixes summed over branches to the composite dose matrix $\mathbf{DT}$ for the decay. This matrix is calculated with the energies and emission rates given in NuDat 2.7 and accordingly only contain a K-Auger and L-Auger branch. The more modern calculations by Boon [93] give energies and intensities for many more Auger branches. The total Auger electron energy released per decay as calculated by Boon is a factor of about 1.2 higher than the total of the K and L branches in NuDat 2.7. Of course the total energy in the EC decay is known, but the distribution between X-ray and Auger emissions is not necessarily known. As explained in appendix 8.3.2 p. 204 I do not want to underestimate the absorbed dose (to the nuclei), as this will lead to apparently higher RBE values. Based on the available knowledge of the Auger branching ratios we (I and supervisor Mikael Jensen) have decided to use a scaling factor of 1.17 to the dose matrix $\mathbf{DT}$, hereby slightly changing the magnitude of the matrix elements, but not the shape and extension of the dose kernel.
The final size of the $\mathbf{DT}$ matrix was 131x131x 131 elements corresponding to 13x13x13 µm^3.

The homogeneous activity concentration in the confluent cellular monolayer is represented by another three dimensional matrix $\mathbf{A}$. It is a large rectangular slab matrix, with x and y dimensions much larger than the size of the $\mathbf{DT}$ but with z (height dimension) equal to the cell layer height.
Inside this matrix, a uniform activity concentration of 1 Bq/pL is represented by the value 1/ voxelvolume, where voxelvolume is the number of µm^3 per pL.

Now the dose distribution $\mathbf{DCellayer}$ inside the cell layer can be found be the three dimensional convolution in Matlab:

$$\mathbf{DCellayer} = \mathbf{DT} \otimes \mathbf{A} \qquad \text{(Eq. 31)}$$

In this geometry, the absorbed dose only depends on the depth position in the cell layer (z-direction) and not the horizontal position (x-y direction), because the horizontal extension of the layer is very large compared to the electron ranges. Any absorbed dose to a nucleus volume inside this monolayer could be calculated by collecting dose from all the matrix elements within a given mathematically defined nucleus shape (spherical or ellipsoid) (Figure 3.8). The absorbed dose to nucleus was scored[1] for each nucleus measured (30 HeLa and 50 V79).

Results were expressed as S_C-values (monolayer to nucleus) with the units Gy/ (Bq*Sec)/pL or Gy Bq^{-1} Sec^{-1} pL. The direct X-ray contribution to the cell nuclei from the ^{131}Cs inside the monolayer could safely be ignored because the cell layer thickness is very small compared with the mean free path of the relevant X-ray photons (29-34 keV) in water (0.01 mm versus 25 mm). Likewise, the X-ray absorbed dose contribution (and the dose contribution from the Auger electrons incl. SCK and CK) from the ^{131}Cs in the medium could be ignored.

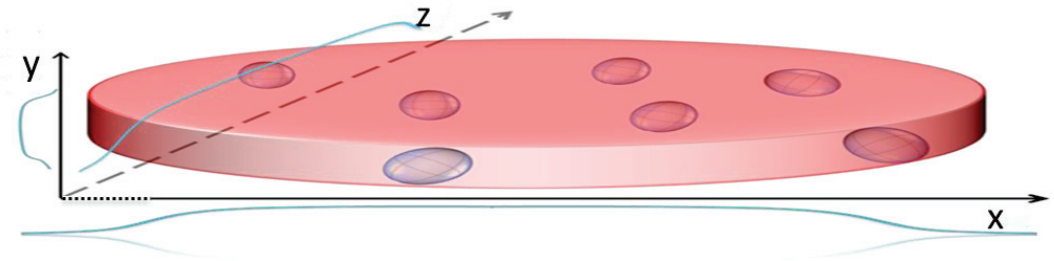

Figure 3.8 Representation of the geometrical model of the cellular monolayer used to calculate the S_C-value, S_C(N←C), and the dose kernels

Because of the evenly distributed ^{131}Cs in cytoplasm and nucleus and the confluency of the cells, the cell culture can be thought of as a "sea" of cytoplasm in which the cell nucleus is floating. The dose kernels (blue lines) for direction x and y are constant through most of the cell layer, and only change close to the edge. The dose kernel for the z direction depends on the height of the cell layer and is the only one that is important for the calculation of the composite dose kernel.

[1] Actual calculations in Matlab done by supervisor Mikael Jensen.

3.3.7 Absorbed dose and dose rate calculations

To calculate the absorbed dose and dose rate profiles, the intracellular ^{131}Cs activity concentration (at at least one time point), the exponential/rate constants (k_c & k_{out}) and the S_C-value had to be known. The constants (k_c & k_{out}) have been found by the uptake and release experiments described above. If the ^{131}Cs activity concentration at more than one time point was known, activity concentration used for further calculations were first found by fitting the known values to the equation $A = A_0 * (1 - e^{-t*k_c})$ applying the least square method using solver in Excel.

3.3.7.1 Dose rate profile

The dose rate to any time point (x) can be found by multiplying the ^{131}Cs activity concentration at time (x) with the S_c-value;

$$\text{Dose rate (x)} = {}^{131}\text{Cs activity concentration at time (x)} * S_C\text{value} \qquad \text{(Eq. 32)}$$

Using the "natural" unit of Bq/pL for the activity concentration this equation gives us dose rate as Gy/s. For ease the dose rates using approximations of 10 min time intervals were used in the subsequent dose rate profiling.

Extrapolating activity concentration measured at one time point to other time points is done by using equation 47 (section 8.3.1. p. 201)

3.3.7.2 Total absorbed dose and integration period for the total absorbed dose.

To calculate the absorbed dose relevant for the the yH2AX experiments, integration of activity and dose rate should be stopped at the time when the cells are removed from the medium.

For the clonogenic survival experiments, exposure actually continues after removal of activity from the medium, and a cummulative activity and dose should in principle be extended to infinity. In section 4.3.1 it is argued that the integration is stopped at t=1440 minutes, without significant error.

A more elaborate example is given in section 4.3 p. 122.

3.3.8 Radiotoxicity and RBE of intracellular ^{131}Cs exposure

3.3.8.1 Radiotoxicity of intracellular and extracellular ^{131}Cs exposure

HeLa cells (~55. 000) were seeded in 48-well plates and incubated overnight at 37°C, 5% CO_2. The cells were washed in growth medium before 200 µl ^{131}Cs containing medium (9.5 MBq/ml -15 MBq/ml) with or without 8.45 µM ouabain was added. A control sample for the effect of ouabain (cells incubated with ouabain, but with no ^{131}Cs) was also made. The cells incubated at 37°C, 5% CO_2 for different periods of time (0 – 8 h). Thereafter the cells were washed with PBS before being trypsinized (0.1% trypsin/EDTA (0.5 mM) in PBS for 3-5 min, at 37°C, 5% CO_2). The trypsinization was stopped using growth medium. The number of cells and their sizes were measured by the Scepter 2.0 from Millipore and the ^{131}Cs activity in the cells was measured by LSC (see section 3.3.2 p. 74). The ^{131}Cs activity concentration was calculated (Eq 23). Around 100.000 cells were used to measured DNA double strand breaks by γH2AX assay on the Muse cell analyser (see section 3.3.8.3 p. 90) Three independent experiments were performed.

3.3.8.2 RBE of Intracellular ^{131}Cs exposure (γH2AX)

3.3.8.2.1 Intracellular ^{131}Cs exposure.

The cells exposed to intracellular ^{131}Cs (without ouabain) in the experiment investigating the effect of intracellular versus extracellular ^{131}Cs decays (section 3.3.8.1 p. 88) are the same cells used in this experiment investigating the RBE of intracellular ^{131}Cs exposure. The methods applied are therefore exactly the same.

HeLa cells (~55. 000) were seeded in 48-well plates and incubated overnight at 37°C, 5% CO_2. The cells were washed in growth medium before 200 µl ^{131}Cs containing medium (9.5 MBq/ml -15 MBq/ml). The cells incubated at 37°C, 5% CO_2 for different periods of time (0 – 8 h). Thereafter the cells were washed with PBS before being trypsinized (0.1% trypsin/EDTA (0.5 mM) in PBS for 3-5 min, at 37°C, 5% CO_2). The trypsinization was stopped using growth medium. The number of cells and their sizes were measured by the Scepter 2.0 from Millipore and the ^{131}Cs activity in the cells was measured by LSC (see section 3.3.2 p. 74). The ^{131}Cs activity concentration was calculated (Eq. 23). Around 100.000 cells were used to measured DNA double strand breaks by γH2AX assay on the Muse cell analyser. The absorbed dose and dose rate profiles were calculated based on the obtained exponential constant (k_c) for ^{131}Cs uptake. Three independent experiments were performed.

3.3.8.2.2 External γ-ray exposure (reference radiation),

HeLa cells (~55.000) were seeded in 48-well plates and incubated overnight at 37°C, 5% CO_2 The cells had reach nearly 100 % confluency at that point (90-100% of the surface of the well was covered with cells). The cells were washed in growth medium and 200 µl growth medium was added the cells. The cells were placed in an incubator in our calibration facility and were thereby exposed at 37°C, 5% CO_2. The cells were exposed to γ-rays from ^{137}Cs at increasing dose rates according to the corresponding dose rate profile (from the ^{131}Cs experiments) by moving the incubator closer to the source. After 120 min, 250 min 370 min and 490 min the samples were removed from the incubator. The cells were washed in PBS and trypsinized(0.1% trypsin/EDTA (0.5 mM) in PBS for 3-5 min, at 37°C, 5% CO_2). The

trypsinization was stopped using growth medium and the cell numbers and cell sizes were counted by the Scepter 2.0 from Millipore. Around 100.000 cells were used to measured DNA double strand breaks by γH2AX on the MUSE cell analyser. Three independent experiments were performed.

3.3.8.3 γH2AX assay

The H2A.X Activation Dual Detection Kit from Millipore was used to analyse DNA double strand break in HeLa cells following exposure to either ^{131}Cs or external γ-rays. The cells were treated according to the protocol provided by the manufacture with minor modifications.

The protocol was divided into two parts. The first part was performed immediately after the end of exposure and included fixation of the cells. The second part included permeabilisation, staining and analysis of the cells and was performed later (1-3 days). This was done in order to stain and analyse all samples in a giving experimental series together. Between the 1st and 2nd part the samples were stored at 4°C

1st part

Approximately 100.000 cells were transferred to Eppendorf tubes. The cells were spun down at 300 G for 5 min and the supernatant discarded. The pellet was re-suspended in 100 µl assay buffer and centrifuged again at 300 G for 5 min. The supernatant was discarded and the pellet was re-suspended in a mixture of 100 µl assay buffer and 100 µl fixation buffer. The cells were fixed for 5 min on ice, before the cells were spun down and the fixation solution was removed. The cells were re-suspended in 200 µl assay buffer and stored at 4°C

2nd part

The cells were centrifuged at 300 G for 5 min and the supernatant was removed. The cells was re-suspended in 200 µl ice cold permeabilisation buffer and incubated on ice for 5 min. The cells were spun down again and re-suspended in 90 µl assay buffer. 50 µl of equal parts of the two antibodies directed against non-phosphorylated histone H2AX (anti-Histone H2A.X-PECy5 conjugated antibody)

and the phosphorylated serine-139 H2AX (anti-phospho-Histone H2A.X (Ser139)-Alexa Fluor®555) were added and the cells incubated 30 min at RT in the dark. A negative control with only the anti-Histone H2A.X-PECy5 conjugated antibody added was also prepared. After incubation 100 µl assay buffer was added to the cells whereafter they were spun down and the supernatant was removed. The cells were washed one more time with 200 µl assay buffer. The cells were re-suspended in a suitable volume (100-200µl) assay buffer and analysed on the Muse cell analyser from Millipore. For elaboration of this particular assay see section 3.1.1 p. 59.

3.3.9 RBE of intracellular ^{131}Cs exposure (clonogenic cell survival)

3.3.9.1 Intracellular ^{131}Cs exposure

HeLa and V79 cells (approximately 85.000 and 100.000 cells respectively) were seeded in 48 well plates and incubated overnight. At that point, the cell cultures had reached nearly 100% confluency and 90-100% well bottom was covered by cells. The cells were washed with PBS before ~15 MBq/ml (HeLa) or ~7.5 MBq/ml (V79) of sterile ^{131}Cs containing growth medium was added. The cells were incubated at 37°C, 5% CO_2 for either 420 min or 480 min. After incubation the cells were washed with PBS, trypsinized (0.1% trypsin/EDTA (0.5 mM) in PBS for 3-5 min, at 37°C, 5% CO_2) and re-suspended in growth medium. A control for the washing efficiency was made by adding and immediately afterwards removing the ^{131}Cs containing medium. The ^{131}Cs activity measured in this control was subtracted from the other samples. The ^{131}Cs uptake was measured by LSC and cell number and sizes were measured by the Scepter 2.0 from Millipore. The cells were also counted and the viability measured using the Muse Count & Viability Kit and the Muse cell analyser from Millipore. The cell counts obtained by this Count & Viability Kit were used to seed the right amount of cells for the clonogenic cell survival assay. 50 µl of the cell suspension were added 450 µl of the count & viability reagent and incubated for 5 min at RT in the dark before it was analysed on the MUSE giving the cell concentration and the proportion of live and dead cells. Cells were seeded in T25 flask and incubated at 37°C, 5% CO_2 for 7 days (V79) or 14 days (HeLa). The HeLa cells were seeded in triplicates using 200 or 300 cells for control samples and 10.000 or 20.000 cells for the ^{131}Cs exposed samples. The V79 cells were also seeded in triplicated using 200 for control samples and 500 or 1000 for the ^{137}Cs exposed samples. After incubation the cells were stained with Crystal violet (0.5 %) in methanol for 30 min – 1 h and thereafter washed in normal tap water. Three independent experiments were performed. A colony was defined as a group of minimum 50 cells, all originating from a single seeded cell. Due to the high number of HeLa cells seeded, the colonies were counted under a light microscope using a 5X objective. The colonies in the control samples, as well as the colonies in the

V79 samples were however counted by eye. The absorbed dose and dose rate profiles were calculated based on the obtained "rate" constants (k_c & k_{out}) for ^{131}Cs uptake and release obtained from the experiments investigating the ^{131}Cs bio-kinetics. (For a more throughout description of these calculations, see section 4.3 p. 122). The survival fraction was obtained as explained in section 3.1.2 p. 65. The survival curve was fitted to the linear model ($y = e^{-ax}$), using the curve fitting tool in Matlab.

3.3.9.2 Protracted external γ-ray exposure (reference radiation)

HeLa and V79 cells (approximately 85.000 and 100.000 cells respectively) were seeded in 48 well plates and incubated overnight so the cells would be close to 100% confluent the next day. The cells were washed with PBS and 200 µl medium containing the same proportion of PBS as the corresponding ^{131}Cs experiment was added the cells. The cells were placed in an incubator in our calibration facility and were thereby exposed at 37°C, 5% CO_2. The cells were exposed to γ-rays from ^{137}Cs at increasing dose rates according to the corresponding dose rate profile (matched to the dose rate experience by the ^{131}Cs incubated cells) by moving the incubator closer to or further away from the source. After 420 min and 480 min the samples were removed from the incubator. The cells were washed in PBS and trypsinized(0.1% trypsin/EDTA (0.5 mM) in PBS for 3-5 min, at 37°C, 5% CO_2). The number of cells and their sizes were counted by the Scepter 2.0 from Millipore. In addition the number of cells and the viability was measured using the Muse Count & Viability Kit and (as explained above). These cell counts were used to seed an appropriate number of cells (for clonogenic cell survival). The cells seeded in T25 flask were placed back into the incubator in the calibration facility for further exposure (This break in exposure was around 30-45 min long). The HeLa cells were seeded in triplicates using 300 cells for control samples and 2000, 5000 or 10.000 cells for the exposed samples. The V79 cells were also seeded in triplicates using 100 cells for control samples and 300 or 400 cells for the exposed samples. The cells were exposed to γ-rays at decreasing dose rates for another 15-16 hours.

After end of exposure the cells were incubated at 37°C, 5% CO_2 (with no exposure) for a total of 8-9 days (V79) or 14 days (HeLa) to form colonies. The colonies were stained with Crystal violet (0,5%) in

methanol for 30 min – 1 hour and thereafter washed in normal tap water. A colony was defined as a group of minimum 50 cells, all originating from a single seeded cell. The V79 colonies were easily scored by eye. Due to the high number of Hela cells seeded, the colonies were counted using a light microscope and a 5X-objective. The T25 flask were (if needed) divided into two equally big and geometrically similar parts. Only colonies in one of the two parts were counted and multiply by 2 to get the total number of colonies. Three independent experiments were performed. The survival fraction (as calculated by Eq. 22 p. 657) Page, was plotted against the absorbed dose and the data were fitted to the linear model ($y = e^{-ax}$) using the curve fitting tool in Matlab.

3.3.9.3 Acute external y-ray exposure

HeLa and V79 cells were sparsely seeded in T-25 flask and incubated at 37°C, 5% CO_2. The cells were exposed at room temperature in T25 flask to y-rays from a ^{60}Co source with a dose rate of 1.5 Gy/min, 1 m from the source. 5 mm of plastic was used as build-up. The cells were exposed to doses between 0-10 Gy. After exposure a suitable amount of cells were seeded in T-25 flask containing a total of 6 ml growth medium. The HeLa cells were seeded in triplicates using 150 cells for control samples, 200 cells (0.5Gy), 300 cells (0.75, 1 & 2 Gy), 500 cells (3 & 4 Gy), 1000 cells (5 Gy), 2000 cells (8 Gy) and 5000 cells (10 Gy). The V79 cells were also seeded in triplicated using 100 cells for the control samples, 100 cells (0.5 Gy), 200 cells (0.75, 1 & 2 Gy), 300 or 500 cells (3 Gy), 300 or 500 cells (4 Gy), 500 or 1000 cells (5 Gy) 2000 cells (8 Gy) and 2000 or 5000 cells (10 Gy). The cells incubated at 37°C, 5% CO_2 for 7 days (V79) or 12 days (HeLa) without any medium change. The cells were stained with Crystal violet (0,5%) in methanol for 20 min – 1 hour and thereafter washed in normal tap water. A colony was defined as a group of minimum 50 cells, all originating from a single seeded cell and were easily scored by eye. Three independent experiments were performed. The survival fraction was obtained as explained in section 3.1.2 p. 65. The obtained survival curve was fitted to the linear quadratic model ($y = e^{-ax+bx^2}$), using the curve fitting tool in Matlab.

4. Results

Recapitulation: The aim of this study is to investigate the RBE of the Auger emitter ^{131}Cs. The RBE is obtained by comparing dose-effect curves for the test and reference radiation. Obviously as the absorbed dose constitute one of the two key parameters (absorbed dose & biological effect) in obtaining the RBE it is vital that this quantity is correctly calculated. In order to calculate the absorbed dose of internal Auger emitters, the S_C-value (introduced in section 2.5 p. 57) and the bio-kinetics of the Auger emitter used needs to be known. Results have been found for the subcellular distribution, the uptake kinetics, cellular accumulation and release kinetics of ^{131}Cs. With this in hand HeLa and V79 cells were exposed to intracellular ^{131}Cs decays and absorbed dose and dose rates calculated. Cells were also exposed to external y-rays (reference radiation) at similar absorbed doses and dose rates. The biological effect of the exposures was examined using the yH2AX assay and clonogenic cell survival. In the end RBE values of intracellular ^{131}Cs decays were obtained.

4.1 ^{131}Cs bio-kinetics

In order to be able to calculate reliable absorbed doses and dose rates, it is important to have knowledge about the ^{131}Cs bio-kinetics. The uptake and release of ^{131}Cs over time were therefore investigated. Because of the short range of Auger electrons it is essential for the calculation of the S_C-values to know if the ^{131}Cs is located intracellularly or extracellularly (perhaps bound to the cell surface) and therefore this was also examined. In addition, the cellular accumulation of ^{131}Cs compared to the medium is also important for the S_C-value calculations. The intracellular activity concentration (Bq/pL) of ^{131}Cs over time is used in the absorbed dose calculations and is therefore also studied. Since all these processes can differ between different cells line, they were all investigated for both the HeLa and V79 cells used in this work.

4.1.1 Uptake of ^{131}Cs in HeLa and V79 cells

To investigate ^{131}Cs uptake by HeLa and V79 cells, the cells were incubated with ^{131}Cs, in the form of (non-carrier added) CsCl, which was added to the medium (in activity concentrations of ~25 kBq/mL) for various time periods. The activity concentration of ^{131}Cs in the cells (Bq/pL cell), at various time points, were measured (by LSC) and the data from 8 (HeLa) or 7 (V79) independent experiments were used to find and fit the "uptake curves".

As can be seen on Figure 4.1 ^{131}Cs is taken up by both the HeLa and V79 cells. The activity concentration in the cells increases over time until it reaches equilibrium after ~800 min for HeLa cells and ~600 min for V79 cells. The data were first normalised to an internal time point (380 min for HeLa cells, and 480 min for V79 cells) and thereafter fitted (in Matlab) to the exponential function;

$$A = A_0 * (1 - e^{-t*k_c}) \quad \text{(Eq. 33)}$$

A, being the relative (due to the normalisation) activity concentration in the cells at time (t). A_0, the activity concentration in cells at equilibrium and k_c, the exponential constant. The exponential constant (k_c) for HeLa and V79 cells were determined to be 1/283 min^{-1} and 1/204 min^{-1} respectively. (For confidence intervals see 4.1.5 p. 103). Figure 4.1 shows the increase in the relative intracellular activity concentration of ^{131}Cs over time. The exponential constant k_c is not to be confused with the classical influx rate constant.

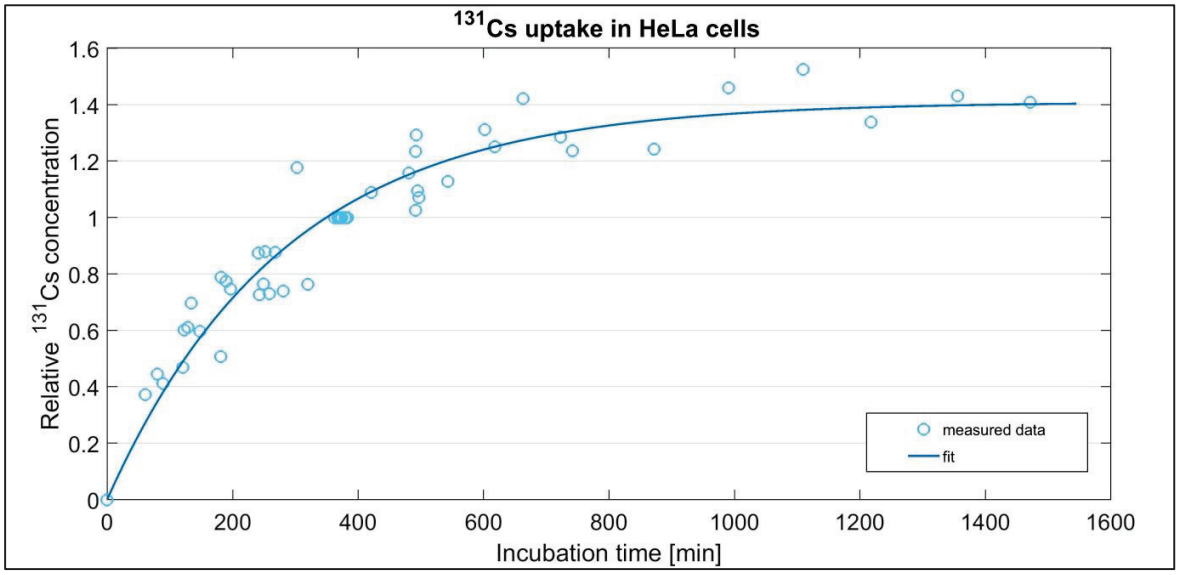

A

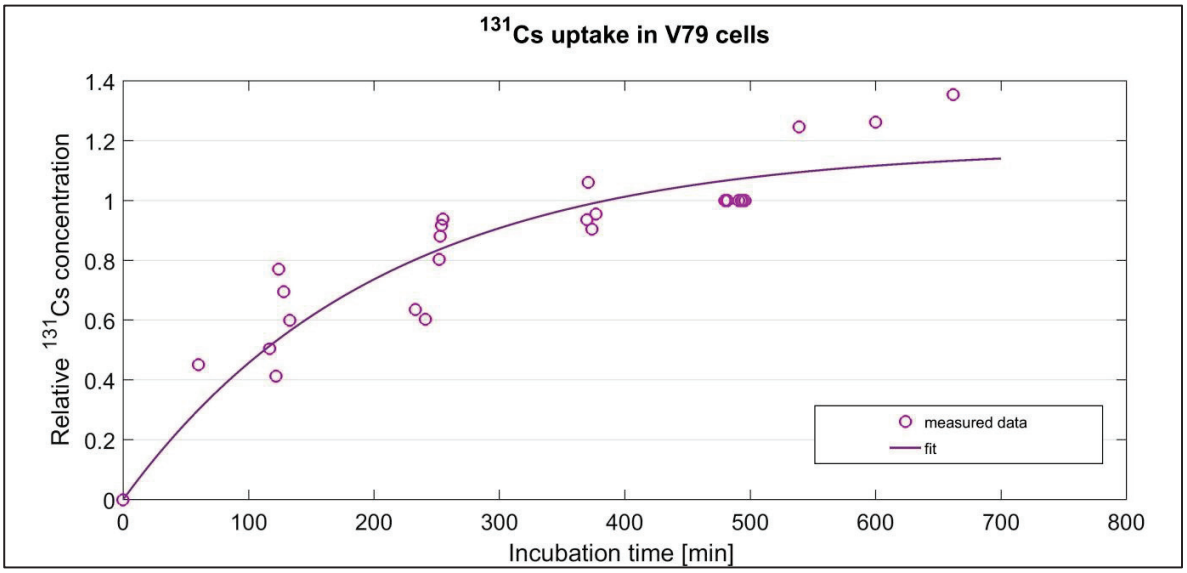

B

Figure 4.1 Uptake of ^{131}Cs in HeLa and V79 cells over time

The cellular activity concentration (relative to A_{380}, or A_{480} respectively) of ^{131}Cs in HeLa cells (A) and V79 cells (B) over time is shown. The cellular activity concentration in the cells increases over time until it reaches equilibrium after ~800 min for HeLa cells and ~600 min for V79 cells. The data were fitted to the exponential equation ($A = A_0 * (1 - e^{-t*k_c}$). The circles represent the obtained data points for HeLa (blue) and V79 (purple), and the lines represent the fitted functions. The exponential constants (k_c) were found to be 1/283 min^{-1} for HeLa cells and 1/204 min^{-1} for V79 cells. Note that the exponential constant k_c is not the classical influx rate constant.

4.1.2 Accumulation of ^{131}Cs in HeLa and V79 cells

To quantify the accumulation of ^{131}Cs in the cells (compared to the medium) over time, the activity concentrations in the cells were measured at different time points. This was done by measuring the activity of ^{131}Cs in the cells along with the cell number and their sizes in 9 independent experiments (the data from 8 (HeLa) or 7 (V79) of these were also used to establish the ^{131}Cs uptake shown in Figure 4.1). The cellular accumulation factor of ^{131}Cs over time was found by dividing the activity concentration in the cells by the activity concentration in the medium (Figure 4.2).

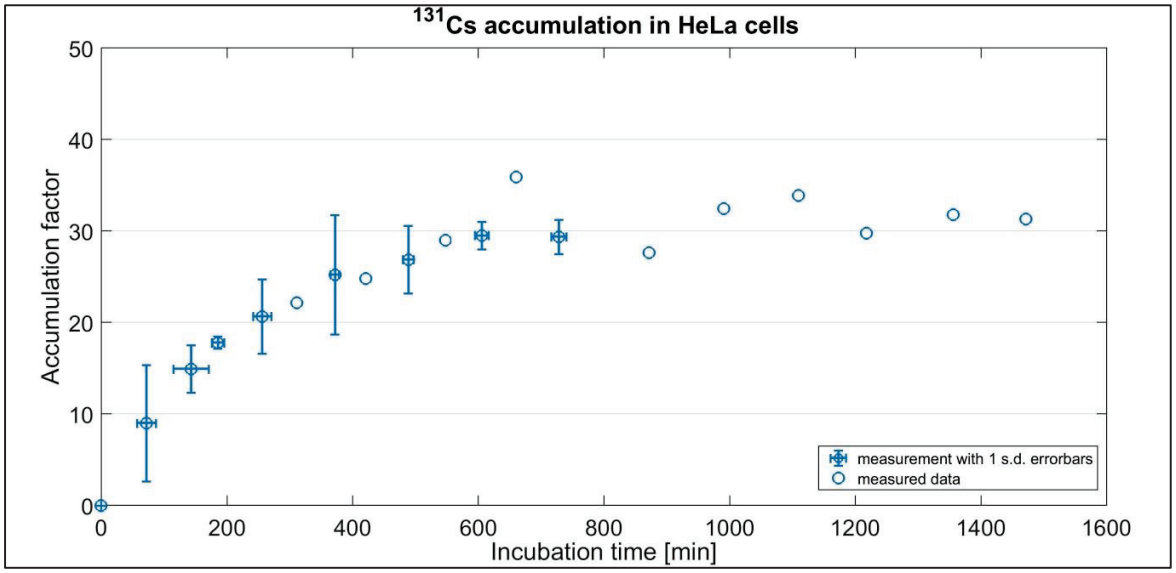

A

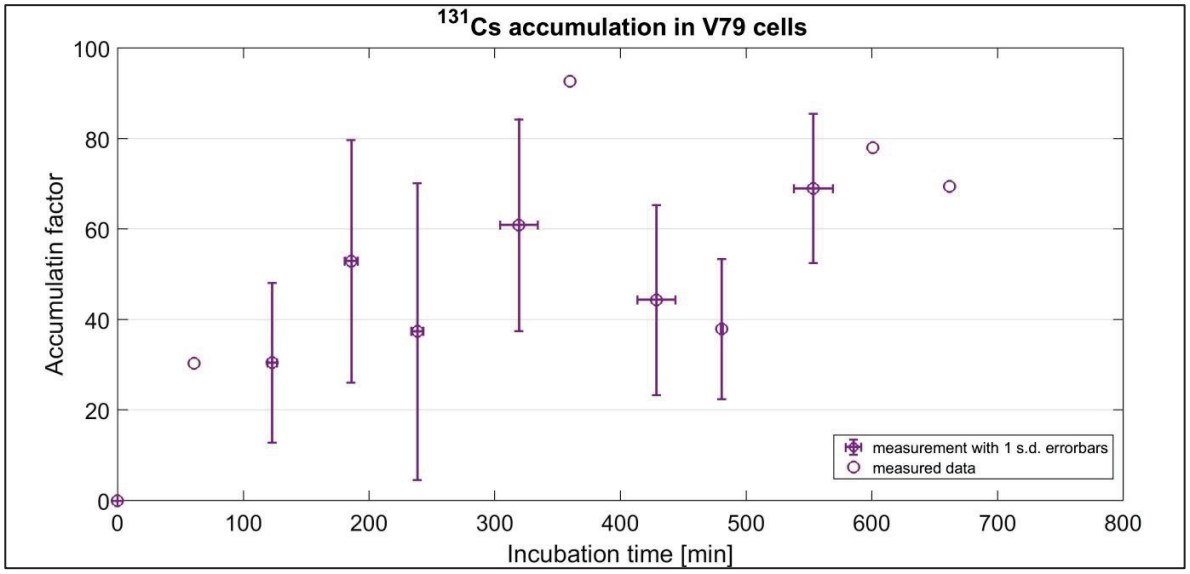

B

Figure 4.2 Cellular accumulation of ^{131}Cs in HeLa and V79 cells

Cellular accumulation of ^{131}Cs in HeLa cells (A) and V79 cells (B) over incubation time is shown. The activity concentration of ^{131}Cs in the cells were measured at different time points and compared to the activity concentration in the medium to find the accumulation factor. An accumulation factor of ~30 was reach after 800 min in Hela cells (A), while an accumulation factor of ~70 was reach after 600 min in V79 cells (B). The data is presented as average ± s.d. of a least 3 independent experiments. The data points (circles) without any visible error bars are result of one or two observations and a standard deviation could therefore not be calculated.

In HeLa cells, the accumulation factor increases over time until it reaches a plateau around a factor 30 after 800 min. In V79 cells, the accumulations factor also increases over time and reaches an accumulation factor around 70 after 600 min. However the clear plateau seen in the HeLa cells is not that evident in V79 cells and the variation between the samples is also higher. This could be an effect of a possible difference in the chemical purity of the ^{131}CsCl solutions used in the experiments.

4.1.3 Release of ^{131}Cs from HeLa and V79 cells

To determine the rate of ^{131}Cs release from the cells, HeLa and V79 cells were first allowed to accumulate ^{131}Cs. Thereafter, the ^{131}Cs containing medium was removed and the cells were incubated in fresh medium. The amount of ^{131}Cs remaining in the cells was measured at various time points and normalized to the sample, that was taken just after medium change (time point zero) and therefore had the highest ^{131}Cs activity concentration.

The activity concentration of intracellular ^{131}Cs decreased exponential over time, confirming the release of ^{131}Cs from the HeLa and V79 cells (Figure 4.3). The data were fitted to the exponential decreasing function;

$$A = A_0 * e^{-t*k_{out}} \quad \text{(Eq. 34)}$$

The data were first fitted in independently in Excel using solver and the least square method using solver later fitted as a single fit in Matlab (using the fitting toolbox) to obtain confidence intervals. The two different fitting methods used had an influence of the obtained k_{out} for HeLa cells, but had no effect on k_{out} for V79 cells. The rate constants (k_{out}) for the ^{131}Cs release were found to be 1/339 min^{-1} (using solver in Excel) and 1/337 min^{-1} (using Matlab) for HeLa cells and 1/256 min^{-1} (using Matlab) for V79 cells. (For confidence intervals see section 4.1.5 p. 103)

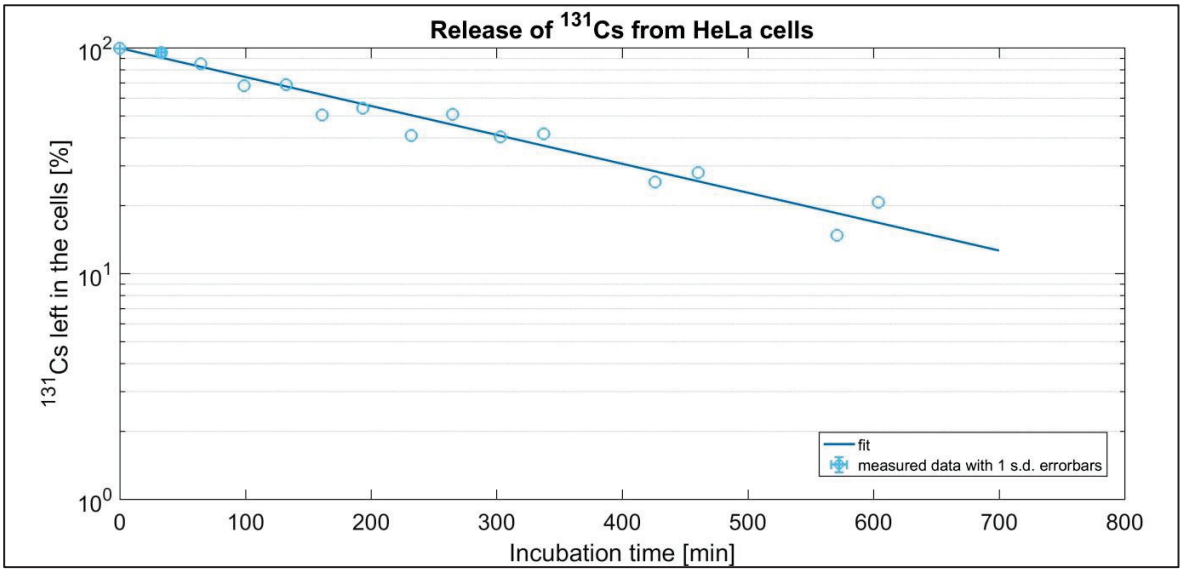

A

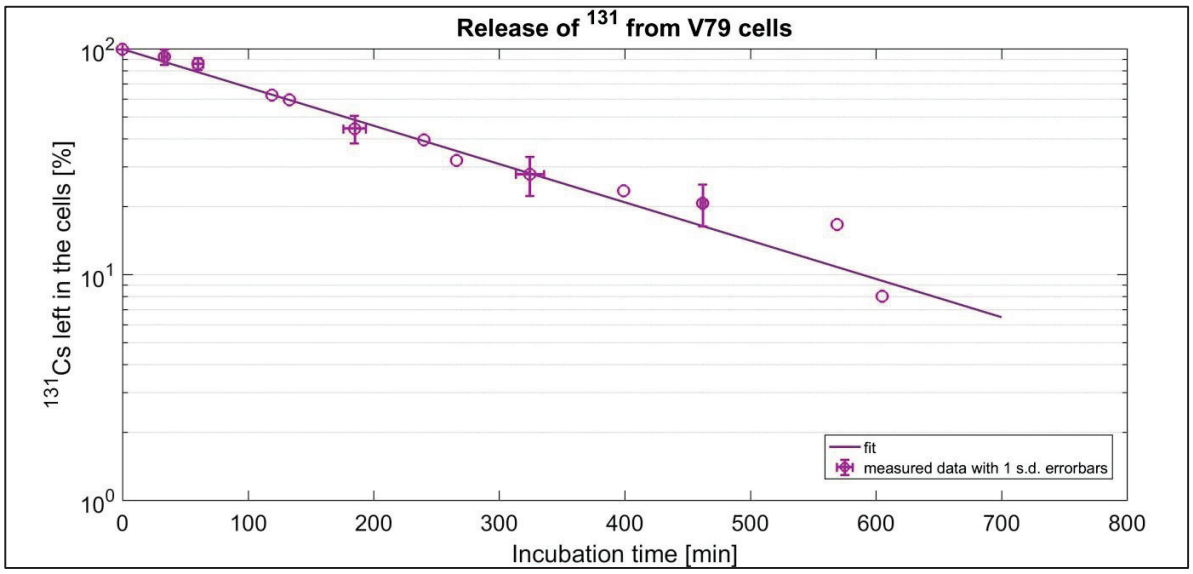

B

Figure 4.3 Release of ^{131}Cs from HeLa and V79 cells

The release of ^{131}Cs from HeLa cells (A) and V79 cells (B) over time is presented as percent ^{131}Cs left in the cells compared to the cellular activity when the ^{131}Cs containing medium was removed. ^{131}Cs is released from the cells, following an exponential decreasing course. The data are fitted to an exponential decreasing fuction ($A = A_0 * e^{-t*k_{out}}$). The fits are represented by the blue (HeLa) and purple (V79) lines. The rate constant (k_{out}) was 1/339 min^{-1} for HeLa cells and 1/256 min^{-1} for V79 cells. The data is presented as average ± s.d of 3 independent experiments. The data points (circles) without any visible error bars only include one or two observations and a standard deviation can therefore not be calculated.

4.1.4 Inhibition of ^{131}Cs uptake by ouabain

To further study the uptake of ^{131}Cs and confirm that the ^{131}Cs was transported into the cells and not bound to the cell surface, it was examined if the uptake of ^{131}Cs could be blocked. It has previously been hypothesised/reported that caesium is transported into cells by the Na^+/K^+-ATPase [115]. To examine this hypothesis HeLa and V79 cells were incubated with ^{131}Cs containing medium and ouabain, a known inhibitor of the Na^+/K^+-ATPase [116], was added at different concentrations.

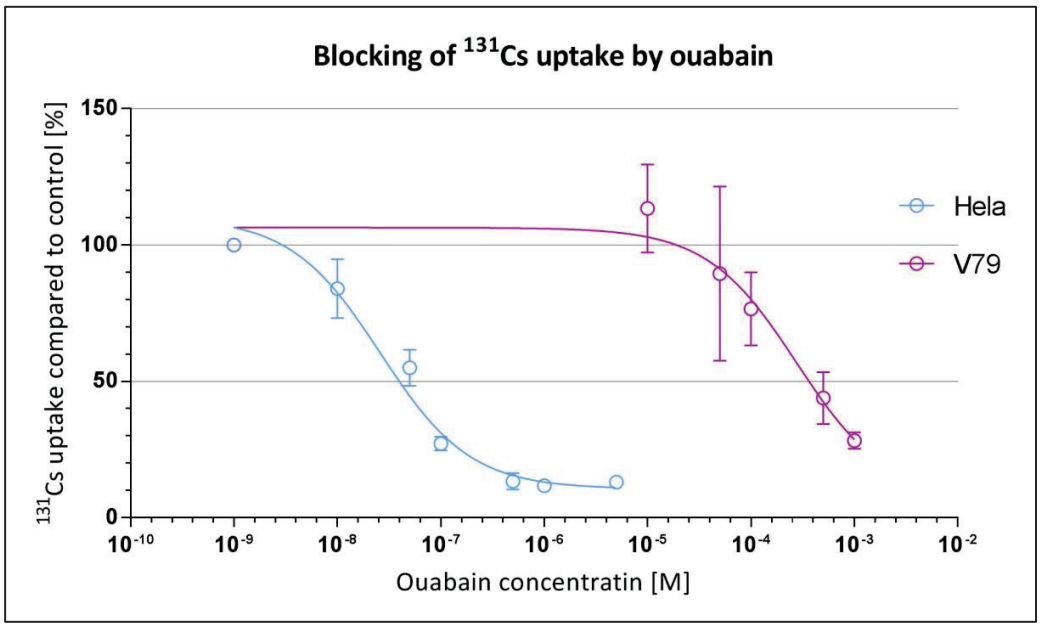

Figure 4.4 Inhibition of ^{131}Cs uptake by ouabain

The inhibition of ^{131}Cs uptake by ouabain in HeLa cells (blue) and V79 cells (purple) is shown. IC_{50} and the maximum achievable inhibition were estimated to be $2.6*10^{-8}$M and ~11 % respectively for HeLa cells, and $2.77*10^{-4}$ M and ~7 % for V79 cells. The apparent rise in V79 uptake at low ouabain concentrations is most likely just experimental variation. The data were fitted to a sigmoid curve (R^2 = 0.917 (HeLa), R^2 = 0.8904 (V79). The fitted curves and the average ± s.d. of 3 independent experiments is presented. Error bars might be too small to be seen.

As can be seen on Figure 4.4 ouabain was able to block the uptake of ^{131}Cs in both HeLa (blue) and V79 (purple) cells. An ouabain concentration of 10^{-6} M was able to maximize the decrease in ^{131}Cs

uptake in HeLa cells to ~12 %. However, an ouabain concentration of 10^{-5} M did not have any effect on the ^{131}Cs uptake in V79 cells. At the highest ouabain concentration used (10^{-3} M) ^{131}Cs uptake was decreased to ~28 % in V79 cells. However, it might have been possible to decrease the ^{131}Cs uptake in V79 cell even further, by using a higher ouabain concentration. The concentration of ouabain needed to inhibit the uptake by 50 % (IC_{50}) and the maximum achievable inhibition was estimated (using Prims GraphPad) to be $2.6*10^{-8}$ M and ~11% respectively for HeLa cells and $2.77*10^{-4}$ M and ~7 % for V79 cells. The results confirm that ^{131}Cs stays in its ionic form in the growth medium and that at least 88 % (HeLa) and 72 % (V79) of the ^{131}Cs taken up by the cells is located inside the cells and not on the cell surface. As will be explained in the discussion section 5.1.1 p. 151, the fact that ^{131}Cs is transported into the cells, while it is in its ionic form, makes it very likely that it will be homogenously distributed in the whole cell (cytoplasm and nucleus).

4.1.5 Summary & uncertainty

The homogenous distribution of ^{131}Cs is very important for the S_C-value calculations, and likewise is the accumulation of ^{131}Cs in the cells. Both cell lines were found to accumulate ^{131}Cs, reaching an accumulation factor of ~30 (HeLa) and ~70 (V79). However, the precise value of the accumulation factor is not of importance, as it is only used to see if the dose contribution from the medium can be ignored. By inhibiting the uptake of ^{131}Cs by Ouabain, it was found that 88% (±1, n=6) (HeLa) and 72% (± 3, n=3) (V79) of the ^{131}Cs was located inside the cells. This strongly indicates that ^{131}Cs stays in its ionic form in the medium, is transported into the cells by the Na^+/K^+-ATPase and is homogenously distributed throughout the cell. Whether or not ^{131}Cs was also transported into the cell by another mechanism was not examined (Figure 4.5).

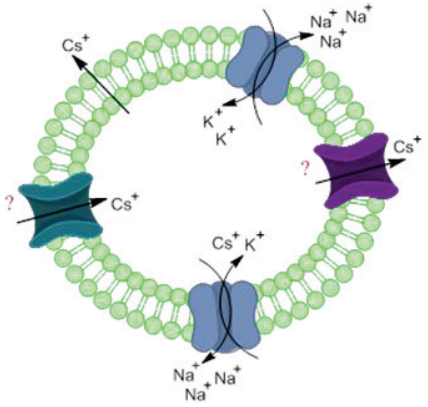

Figure 4.5 Mechanisms of Caesium uptake and release

Caesium is transported into the cells through the Na^+/K^+-ATPase, which also transports potassium into the cells in exchange for sodium. Other channels might also be involved in caesium uptake, but this was not further investigated. Caesium was also found to be released from the cells, whether this export was mediated by a channel or happened by diffusion through the bilipid-layer of the plasma membrane was not investigate. (My own figure)

The uptake and release bio-kinetics of ^{131}Cs is important for the absorbed dose and dose rate calculations. ^{131}Cs was found to be taken up by both HeLa and V79 cells. The uptake and release were fitted to the exponential equations ($A = A_0 * (1 - e^{-t*k_c})$ and $(A = A_0 * e^{-t*k_{out}})$ in Matlab and k_c and k_{out} for HeLa and V79 cells were found to be;

<u>HeLa.</u>

k_c: 1/283 min^{-1} (with 95% conf. limits 1/251 min^{-1} to 1/325 min^{-1},R^2 = 0.922)

k_{out}: 1/337 min^{-1} (with 95% conf. limits 1/304 min^{-1} to 1/381 min^{-1}, R^2 = 0.958)

1/339 min^{-1} (using solver in Excel)

<u>V79.</u>

k_c: 1/204 min^{-1} (with 95% conf. limits 1/154 min^{-1} to 1/303 min^{-1}, R^2 = 0.841)

k_{out}: 1/256 min^{-1} (with 95% conf. limits 1/237 min^{-1} to 1/280 min^{-1}, R^2 = 0.9768)

The confidence limits are not symmetric as the fitted functions are not linear.

The release data were first fitted in Excel using solver, and later in Matlab to obtain confidence intervals. The two different fitting methods used had a small influence on the obtained k_{out} for HeLa cells, but had no effect on k_{out} for V79 cells. The small difference in the fits of HeLa k_{out} is insignificant for the further use in the calculation of cumulative activity. For reasons of the chronological progression of the experimental work, the value of k_{out} =1/339 min^{-1} for HeLa was used in the further calculations.

The absolute value of the intracellular ^{131}Cs activity concentration was in each of the internal dose delivery experiments measured by taking a sample of cells at the end of the uptake period. From this sample the cellular activity concentration was obtained. The kinetic constants only served to expand this measured instantaneous activity concentration into the cumulative activity concentration.

The uncertainty in the absorbed dose and dose rate calculations from the uptake and release results was accordingly estimated to be small. A further elaboration on this argument and the entire uncertainty budget for absorbed doses and survival fractions is given in appendix 8.3 p. 198.

4.2 S_C-values

To calculate the absorbed dose, the cellular activity concentration of the Auger emitter and the S_C-value has to be known. In the above section, the bio-kinetics of ^{131}Cs was elucidated including the subcellular distribution and cellular accumulation of ^{131}Cs, which are important parameters for the S_C-values calculations. In addition to these parameters, the S_C-value is also dependent on the geometry model used and on the cell monolayer height.

In this work I have used a modified version of the MIRD cellular S-values, which I have chosen to denote S_C-value. The S_C-value was introduced earlier in section 2.5 p. 57. In this section I will elaborate on the implications of using this S_C-value and show results supporting the statements I gave in the earlier introduction.

4.2.1 S_C-values for ^{131}Cs, $S_C(N \leftarrow C)$ for HeLa and V79 cells

The geometry used in the S_C-value calculations was a 100 % confluent cellular monolayer, in which the ellipsoid nuclei were positioned. The height of the cellular monolayer was 10 µm and 8 µm for the HeLa and V79 cells respectively. The source compartment was taken as the whole cell or rather the whole cellular monolayer and the nucleus was considered the target compartment. The S_C-values have the unit Gy/(Bq*Sec)/pL (or more formal Gy * Bq^{-1} * Sec^{-1} * pL). A graphical representation of the geometry can be seen in Figure 4.6.

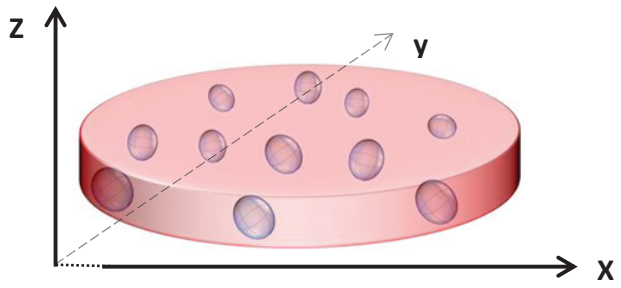

Figure 4.6 Graphical representation of the geometry used for the S_C-value calculations (not to scale)

The pink "disc" represents the 100 % confluent cellular monolayer. The blue ellipsoids dispersed within it represent the nuclei. The height of the cellular monolayer was 10 µm for HeLa cells and 8 µm for V79 cells.

The important parameters for the S_C-value calculations using this geometry turns out to be:

- The confluency of the cells
- The height of the cellular monolayer
- The size (volume), shape and orientation of the nucleus (to a lesser degree).

The average height of the cellular monolayer was found by confocal microscopy as explained in material and methods (section 3.3.6.1 p. 82). The confocal microscopy also gave us measurements of the nucleus sizes, although this is of minor importance in our model as will be show later in section 4.2.1.5 p.117.

4.2.1.1 Cell layer height, confluency (denseness) and nuclei volumes

The average height of the cellular monolayer and the volumes of the nuclei were measured using the images obtained by confocal microscopy of living cells. The cells were grown to the same level of confluency as cells used in the experiments in order to take into account any change in cell layer height due to confluency level. Figure 4.7 A (HeLa) and Figure 4.8 A (V79) show a cross section (x-y plane) through the cellular monolayers. The nuclei are red (were originally stained blue, but the colour were afterwards digitally changed to red), while the plasma membranes are green. As can be seen, the entire image plane (horizontal or x-y plane) is covered by cells lying so close together that their plasma membranes are touching each other, leaving no space in between. This denseness is central for the geometry assumed in the S_C-value calculations and its verification is important for correct absorbed dose calculations. The average heights of the cellular monolayers were estimated using the stack of image planes covering the z direction (Z stack images). Figure 4.7 B (HeLa) and Figure 4.8 B (V79) show the estimated top of the cellular monolayer (seen from above) of HeLa and V79 cultures respectively. The “picture bars” (z axis), display the (vertical) cross sections in the y-z plane (through the red line) and the x-z plane (through the green line). The blue lines indicate the estimated position of the “top” of the cellular monolayer. This estimation was based on the observation of a sudden drop in the fluorescent intensity (in the x-y plane) at this location along, with

the presence of plasma membrane "on top" of the nuclei (see arrows Figure 4.7 B and Figure 4.8 B) and the information giving in the picture bars. Due to limitations in the confocal microscopy technique, the nuclei can still be seen "through" the plasma membrane. The position of the "bottom" of the cell culture was also estimated based on the observation of a sudden drop in the fluorescent intensity (pictures not shown).

The average heights of the cellular monolayers were estimated to be 10 µm for the HeLa cells and 8 µm (round off from 7.5 shown) for the V79 cells.

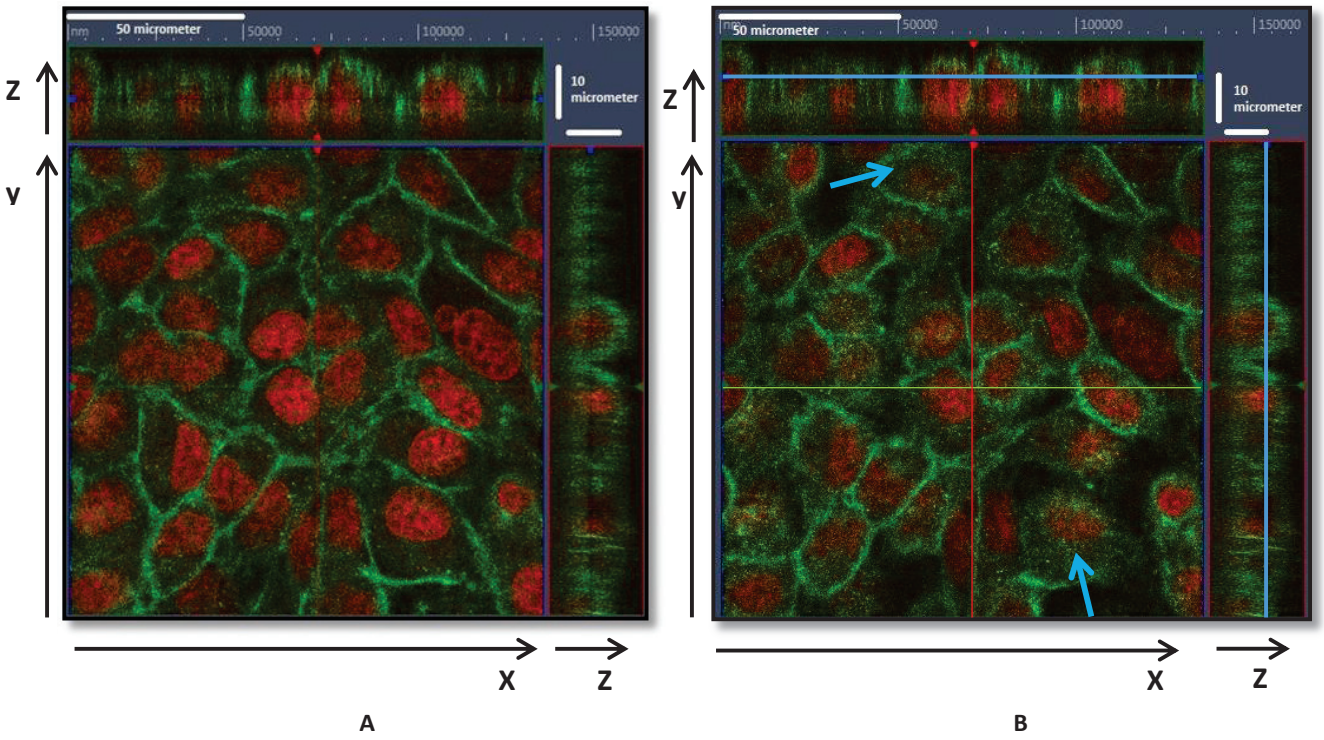

Figure 4.7 Confocal microcopy pictures (~600X magnificantion) of HeLa cells

Picture A shows a cross section (x-y plane) in the middle of the cellular monolayer. Picture B shows the estimated "top" of the cellular monolayer in the x-y plane. The red and green lines indicate the position of the cross section in the z plane visible in the "picture bars" (x-z plane (red) and y-z plane (green)).The blues lines in the "picture bars" indicate the top of the cellular monolayer and were used for estimating the average monolayer height, which was estimated to be 10µm. The blue arrows show the presence of plasma membrane (green spots) "on top" of the nuclei (red). The shown hardcopy version are only for illustration, the "real" images as handled and displayed in the Zeiss ZEN software package are more rich in contrast and details. All geometrical measurements were taken directly in ZEN as described in methods (section 3.3.6.1 p. 82). Cells were stained with WGA Oregon green 488 (5 µg/ml) (plamsammembrane) and Hoechst (20 µg/ml)(nuclei, the colour digitally changed from blue to red) for 10-20 min at 5 % CO_2, 37°C. Pictures were required by confocal laser scanning microscope (LSM 780) from Zeiss, using a 10x objective.

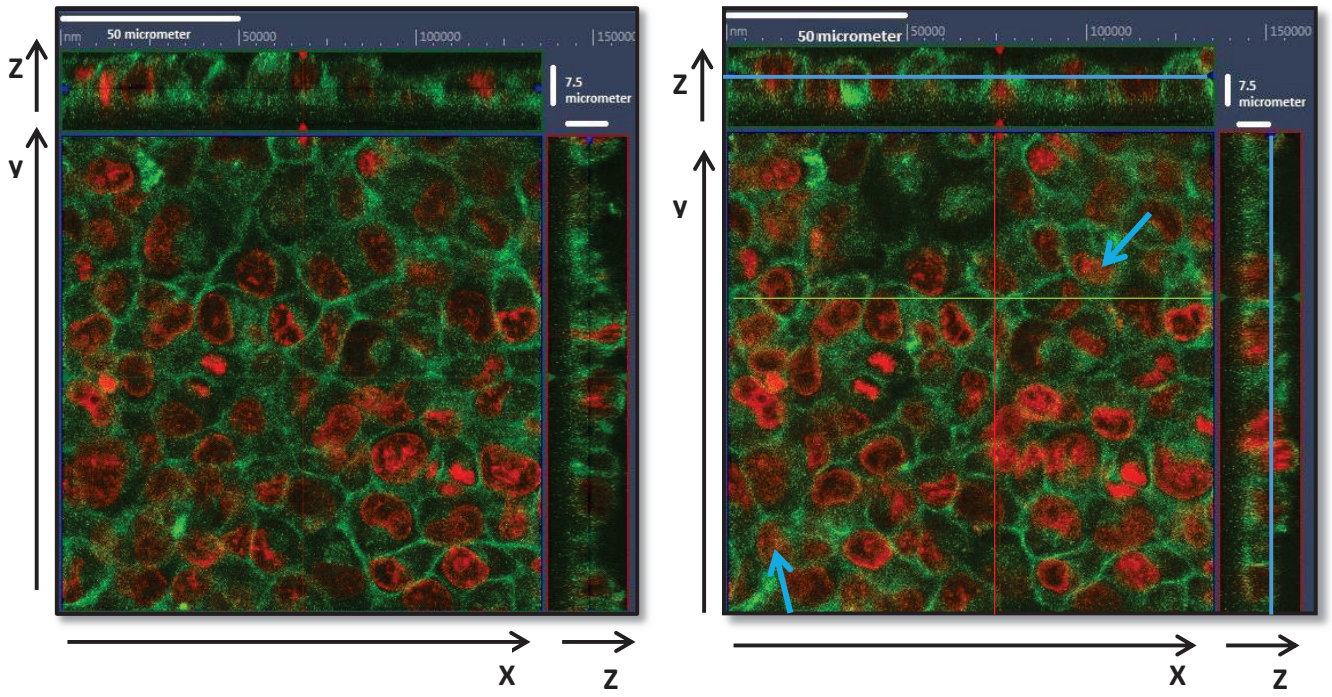

Figure 4.8 Confocal microcopy pictures (~600X magnificantion) of V79 cells.

Picture A shows a cross section (x-y plane) in the middle of the cellular monolayer. Picture B shows the estimated "top" of the cellular monolayer in the x-y plane. The red and green lines indicate the position of the cross section in the z plane visible in the "picture bars" (x-z plane (red) and y-z plane (green)).The blues lines in the "picture bars" indicate the top of the cellular monolayer and were used for estimating the average monolayer height, which was estimated to be 8 µm (round off from 7.5 µm shown in the figure). The blue arrows show the presence of plasma membrane (green spots) "on top" of the nuclei (red). The shown hardcopy version of are only for illustration, the "real" images as handled and displayed in the Zeiss ZEN software package are more rich in contrast and details. All geometrical measurements were taken directly in ZEN as described in methods (section 3.3.6.1 p. 82.) Cells were stained with WGA Oregon green 488 (5 µg/ml) and Hoechst (20 µg/ml)(nuclei, the colour digitally changed from blue to red)for 10-20 min at 5 % CO_2, 37°C. Pictures were required by confocal laser scanning microscope (LSM 780) from Zeiss, using a 10x objective.

The volumes and shapes of the nuclei were also estimated using the images obtained by confocal microscopy. It was found that the nuclei in general displayed an ellipsoid geometry, rotated at different angles in respect to the x-y plane (Figure 4.9). This rotation had only a minor influence on the calculated S_C-values.

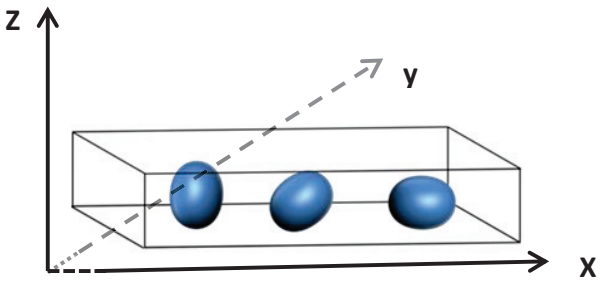

Figure 4.9 Shape and orientation of the nuclei (not to scale)

The figure shows a simpler representation of the geometry of the cellular monolayer shown in Figure 4.6. The box represents the cellular monolayer and the blue ellipsoids represent the nuclei. As shown the nuclei display an ellipsoid shape, and were rotated at different angles in respect to the x-y plane.

To determine the volume of the different nuclei, the lengths of the two axes (of the ellipsoid in the x-y plane) were measured using the image (in the Z-stack) in which each nucleus appeared largest. The length of the third ellipsoid axis was measured using the Z stack images. This was done for all nuclei that were completely contained inside the confocal image. These axes parameters of 30 HeLa cell nuclei and 50 V79 cell nuclei were thus measured. Although this axis measurement is not necessarily completely geometrical correct (the horizontal imaging planes are not necessarily aligned with the ellipsoid axes), it is a fair approximation given the otherwise big biological variation in shape. Figure 4.10 A and Figure 4.11 A show HeLa cell nuclei and V79 cell nuclei that were measured, while Figure 4.10 B and Figure 4.11 B show the distribution in volumes of the nuclei for HeLa and V79 cells respectively, as found by the standard formula for ellipsoid volume;

$$V = \frac{4}{3} * \pi abc \qquad \text{(Eq. 35)}$$

a, b and c, being the length of the three semi-axis. The volume of the HeLa cell nuclei ranged from below 0.1 pL to above 1.1 pL with an average of 0.630 pL ± 0.217, while the V79 cell nuclei ranged from below 0.1 pL to above 1.0 pL with an average of 0.400 pL ± 0.182.

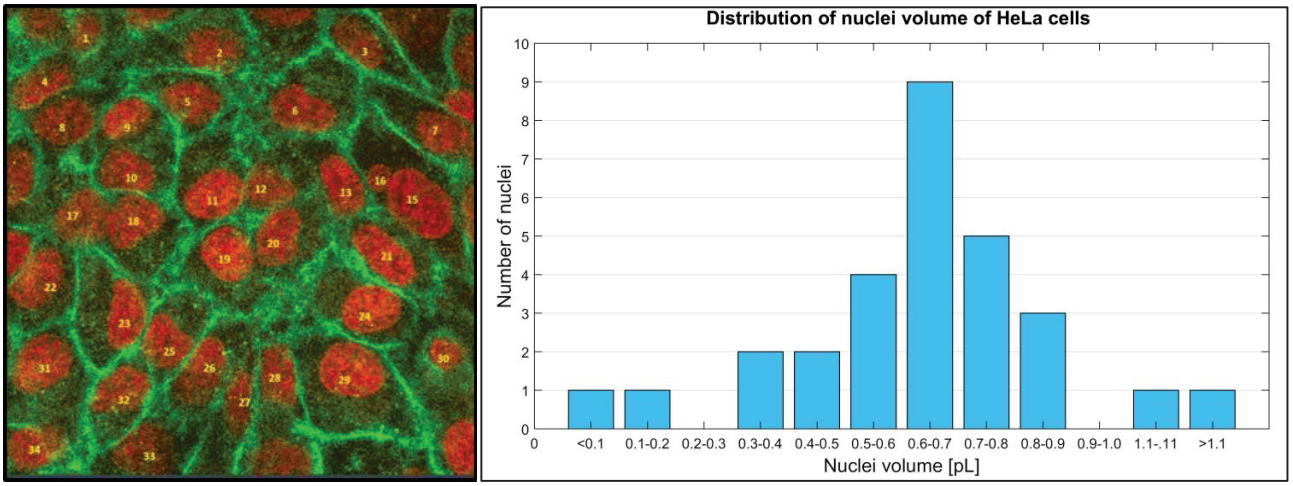

A **B**

Figure 4.10 Distribution of HeLa cell nuclei volume

The volumes of entirely visible nuclei were measured using the confocal microscopy images. The 30 numbered nuclei that were measured are displayed in (A), while (B) shows the distribution of the nuclei volumes. The nuclei volumes displayed a normal distribution and ranged from below 0.1pL to above 1.1pL, with an average volume of 0.630pL ± 0.217.(Microscopy and staining details as in Figure 4.7.

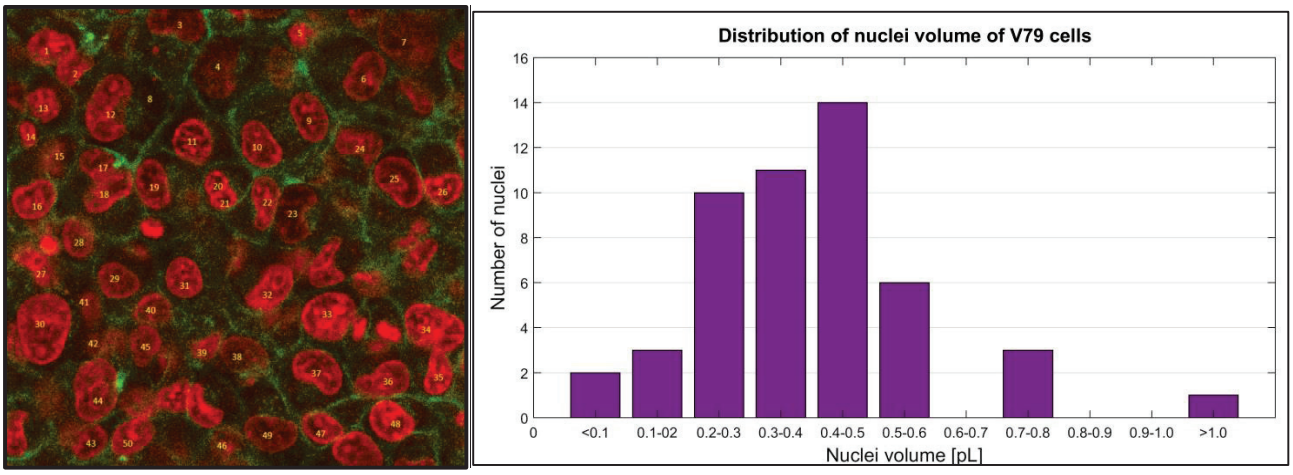

A **B**

Figure 4.11 Distribution of V79 cell nuclei volume

The volumes of entirely visible nuclei were measured using the confocal microscopy images. The 50 numbered nuclei that were measured are displayed in (A), while (B) shows the distribution of the nuclei volumes. The nuclei volumes displayed a normal distribution and ranged from below 0.1 pL to above 1.0 pL, with an average volume of 0.400 pL ± 0.182. (Microscopy and staining details as in Figure 4.8*)*

4.2.1.2 Calculation of the ^{131}Cs S_C-values.

-(S_C(C←N)) for HeLa and V79 cells in confluent, cellular monolayers

S_C-values for intracellular ^{131}Cs decays with whole cellular monolayer as source compartment and the nucleus as target compartment were calculated. The K- and L-Auger electron energies and intensities (24.6 keV (9.3 %) and 3.43 keV (79.7 %) respectively) provided by the NuDat 2.7 database were used in the calculations [25]. The absorbed dose contributions from MXY and higher shell Auger, Coster-Kronig and Super Coster-Kronig electrons were ignored and so was the X-ray contribution. Monoenergetic electron dose kernels for a point source were calculated for each of the two electrons branches, and then added, using the same method applied by MIRD for cellular S-values. In agreement with MIRD, the dose kernels were found using Cole´s inverted formula for energy versus range as a stopping power [18] [82]. As argued in appendix 8.3.2 p. 204, the total electron energy emitted per decay was normalized to a 17 % higher value than given by NuDat 2.7 numbers. This normalization can be seen as an increase in the intensities and not the energy of the individual braches, and is made to allow for the higher emission calculated by Boon Quan Lee ([93] and personal communication with B.Q. Lee).The ^{131}Cs was assumed to be homogenous distributed in the source compartment. The geometry was a confluent cellular monolayer with a respective height of 10 µm (HeLa) and 8 µm (V79). The nucleus was an ellipsoid with a volume of 0.630 pL (HeLa) or 0.400 pL (V79), dispersed in the confluent cellular monolayer. The dose contribution from the ^{131}Cs present in the medium was ignored. The S_C-values were expressed as Gy/(Bq*Sec)/pL.

4.2.1.3 Axial dose distribution

Due to the geometry (100% confluent cellular monolayer) the dose distribution in the x and y direction is constant (except for small edge effects near the wall of the cell culture well). The dose rate in the middle of the cell layer approaches the homogeneous, infinite volume value of $9.4*10^{-4}$ Gy/(Bq*Sec)/pL. The axial (z-direction) dose distribution is however not constant. Figure 4.12 shows the axial dose distributions for the HeLa and V79 cellular monolayers. As can be seen the dose

distribution remain nearly the same along most of the cell layer (depth) varying between 7.4 $*10^{-4}$ to 8.1 10^{-4} Gy/(Bq*Sec)/pL for HeLa cells and 7.2 $*10^{-4}$ to 7.8 $*10^{-4}$ Gy/(Bq*Sec)/pL for V79 cells. The dose only diminishes more drastically very close to (<1 µm) the bottom and top of the monolayer. The S_C-value is the integral of the dose distribution of the volume of the nucleus, divided by the mass (volume, because the cellular density = 1 g/cm^3) of the nucleus. As the axial dose distribution is not constant, changes in the nucleus volume and rotation, will results in variation of the S_C-values for the different nuclei. These variations are however small, due to the relatively "flat" dose distribution in the axial direction.

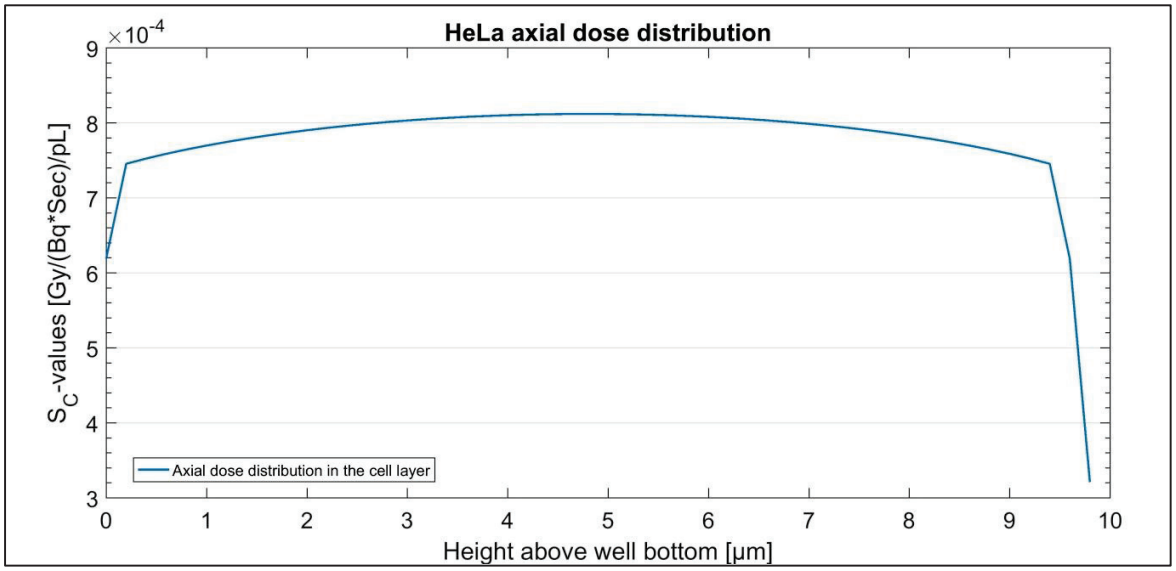

A

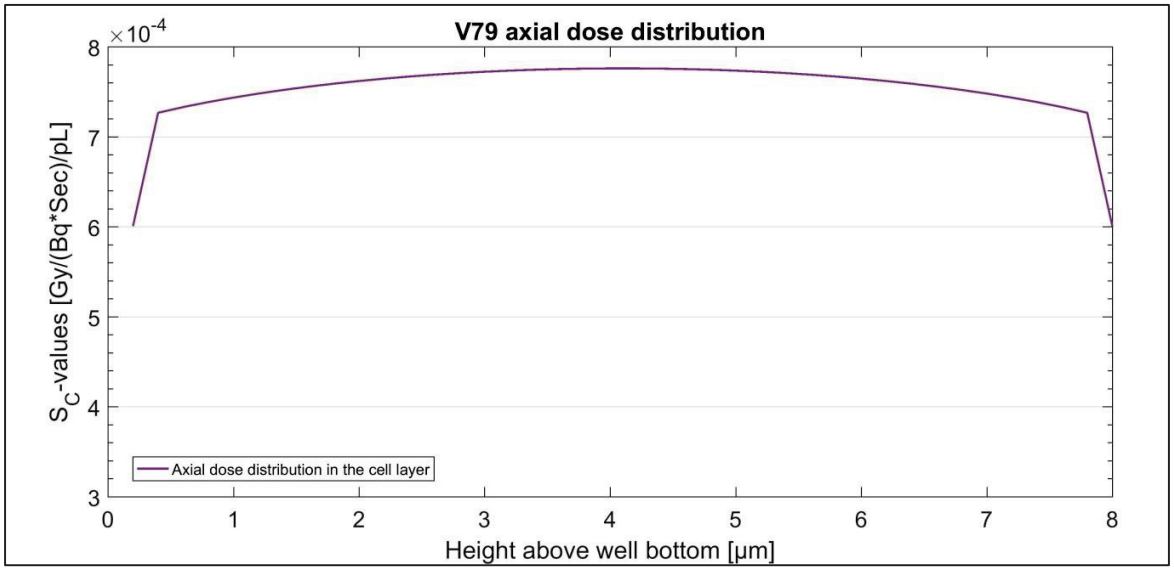

B

Figure 4.12 Axial dose distributions for HeLa and V79 cellular monolayers

The axial dose distributions for HeLa (A) and V79 (B) cellular monolayer are shown. The "bottom" of the cellular monolayers is located at 0 µm, while the top of the cellular monolayers are located at 10 µm (HeLa) and 8 µm (V79). The dose distribution remains nearly the same along most of the cell layer (depth) and only changes more drastically very close to the bottom and top of the monolayer (<1 µm).

4.2.1.4 Dose contribution from the medium.

In the calculation of the S_C-values, the ^{131}Cs located in the medium was ignored. The cells (both HeLa & V79) were shown to accumulate ^{131}Cs (see section 4.1.2 p. 98) and an accumulation factor of at least 30 (compared to the medium) was found. Due to this accumulation of ^{131}Cs in the cells, it was hypothesized that the dose contribution from the medium (to the nuclei) was neglectable, and it was therefore ignored in the S_C-value calculation. To confirm that this was indeed true, the axial (z direction) dose distributions, ignoring or including, the dose contribution from the medium were calculated for both HeLa and V79 cellular monolayers (Figure 4.13). A ^{131}Cs accumulation factor of 30 (as this was the smallest of the two accumulation factors found) was used in the calculations. Figure 4.13 shows the axial dose distribution for HeLa and V79 monolayer respectively, either ignoring (blue curve (HeLa) or purple curve (V79)) or including (green curves) the dose contribution from the medium. As can be seen the two curves are almost identical, only differing slightly towards the top of the cellular monolayer. This confirms that the dose contribution from the medium could be ignored

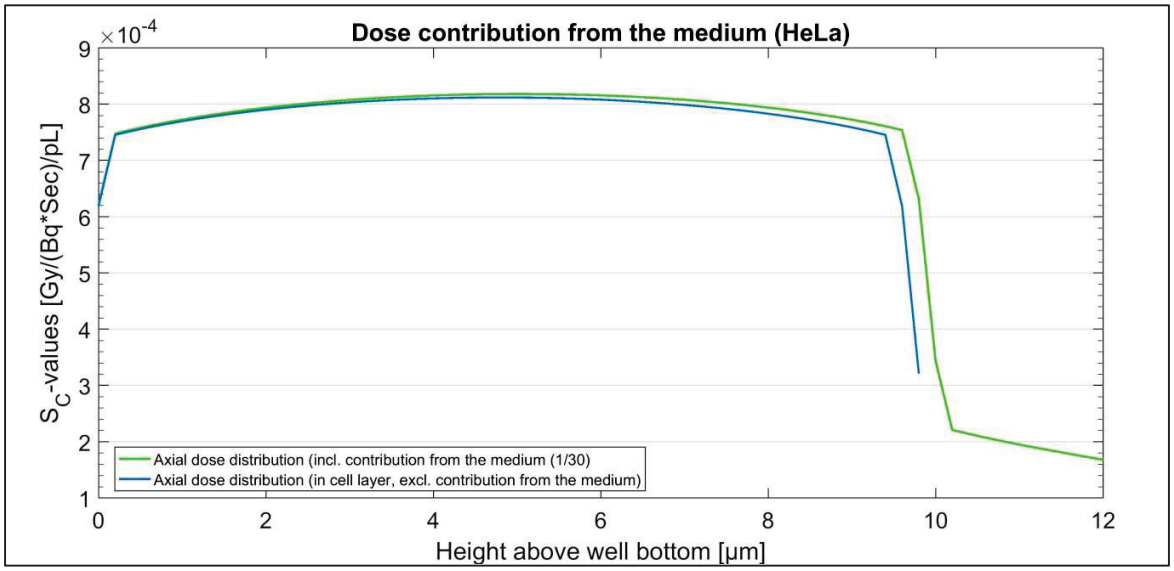

A

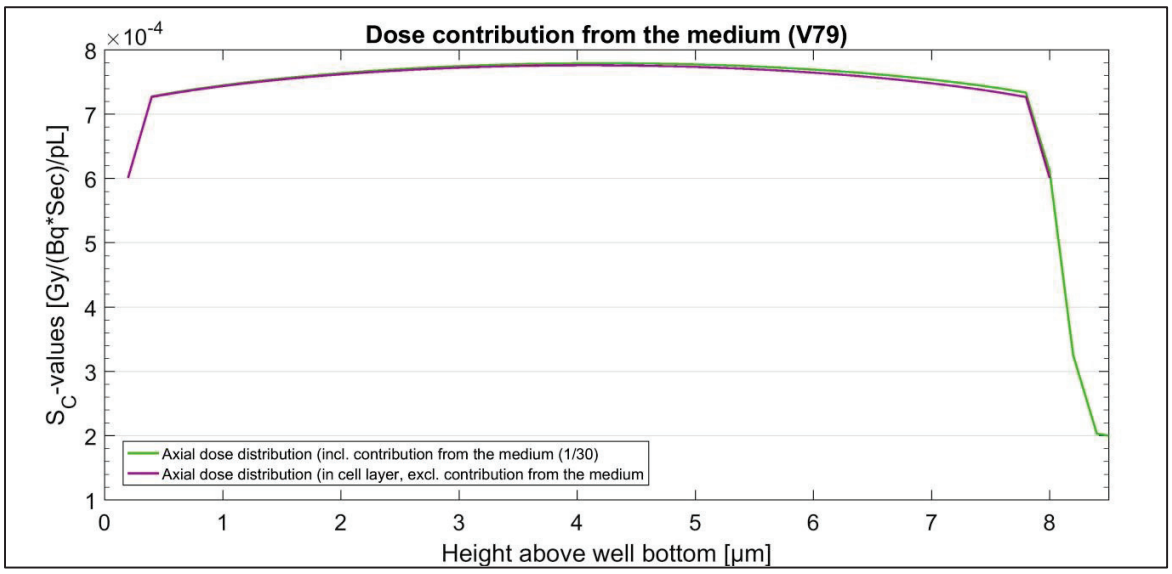

B

Figure 4.13 Dose contribution from the medium

The axial dose rate distribution for HeLa (A) and V79 (B) cellular monolayers either ignoring (blue or purple curve) or including (green curve) the dose contribution from the medium are shown. *The* "bottom*" of the cellular monolayers are located at 0 µm, while the top of the cellular monolayers are located at 10 µm (HeLa) and 8 µm (V79). The two curves are almost identical and only differ slightly towards the top of the monolayer.*

4.2.1.5 The impact of nucleus size on the S_C-value

It was hypothesized that due to the geometry used (100% confluent cellular monolayer) and the unit of the S_C-value Gy/(Bq*Sec)/pL, the S_C-values would be very robust and change very little with change in the size of the nucleus. To confirm this, S_C-values for all (except the smallest,< 0.1 pL) the different nuclei volumes of HeLa (< 0.2 pL to >1.1 pL) and V79 cells (<0.1 to >1.0 pL) found in section 4.2.1.1 (p. 107) were calculated. The S_C-values for all these 29 HeLa and 50 V79 nuclei and their distribution are shown in Figure 4.14 and Figure 4.15 respectively. As can be seen, the S_C-values for the HeLa nuclei (with volumes of 0.178 pL to 1.163 pL) ranged from $7.78*10^{-4}$ to $7.83*10^{-4}$ Gy/(Bq*Sec)/pL. The S_C-values for the V79 nuclei (with volumes of 0.080 pL to 1.080 pL) ranged from $7.45*10^{-4}$ to $7.63*10^{-4}$ Gy/(Bq*Sec)/pL. The S_C-values changes with less than 1% for HeLa cells and less than 2.5% for V79 cells even though the nucleus volume changes by a factor 10. This shows that the S_C-values are very robust and confirms that they are almost independent of the nucleus volume.

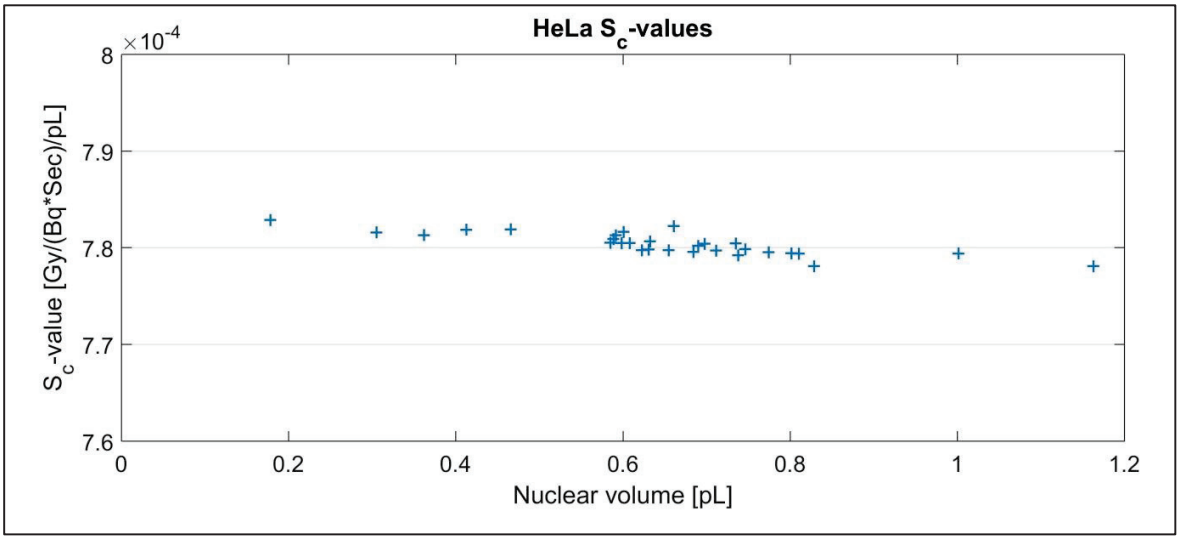

A

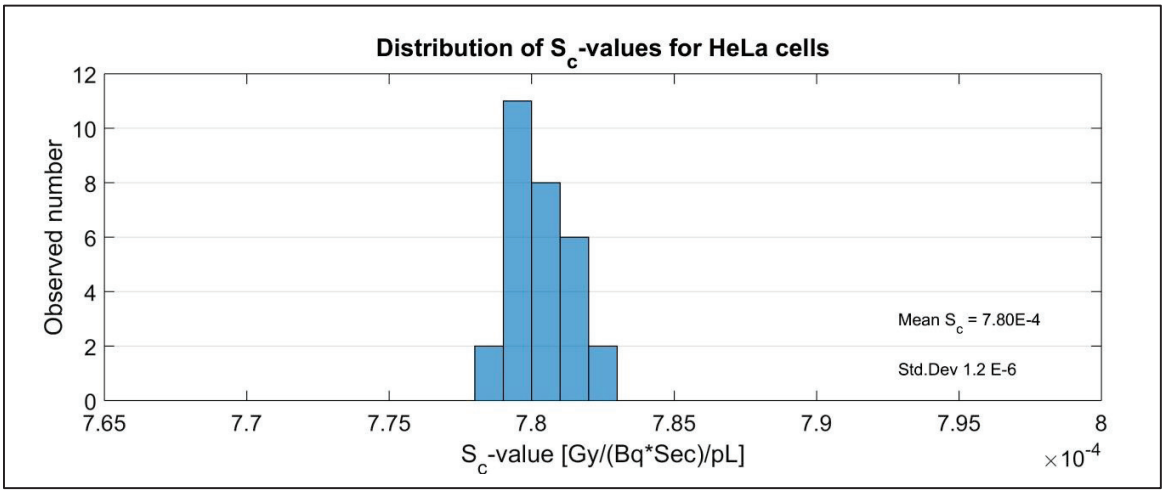

B

Figure 4.14 S_C-values and distribution for HeLa nuclei with different volumes

S_C-values (A) and their distribution (B) for HeLa cell nuclei with volumes ranging from below 0.2 pL to above 1.0 pL, positioned in the cellular monolayer, were calculated. Each blue mark in graph (A) represents the S_C-value for one of the 29 HeLa nuclei. As can be seen the S_C-values almost do not change over the big range of nuclei volumes. The S_C-values change with less than 1% even though the nuclei volume changes by a factor of 10.

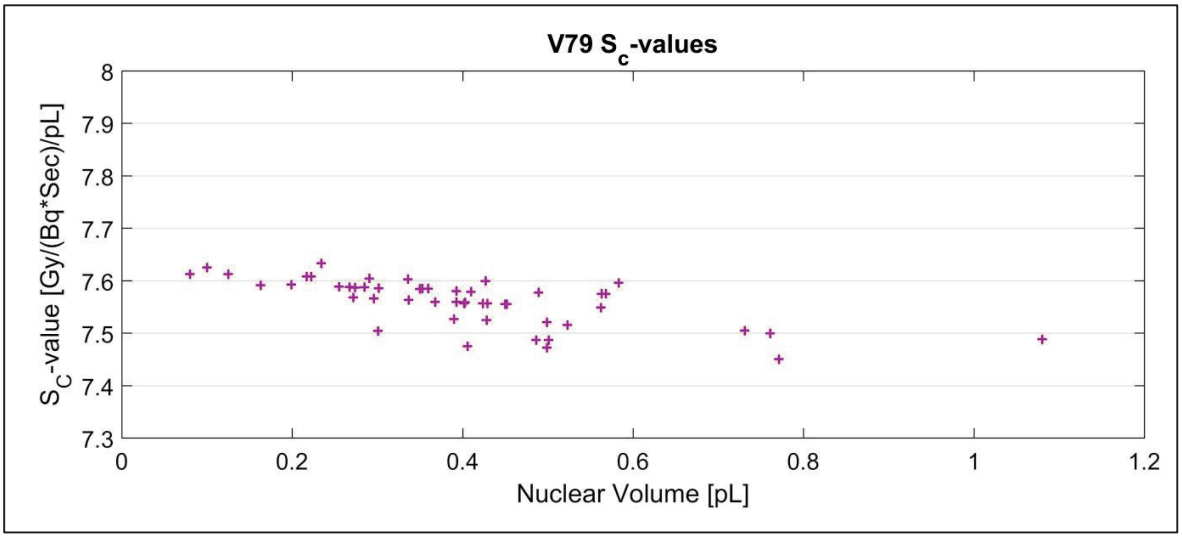

A

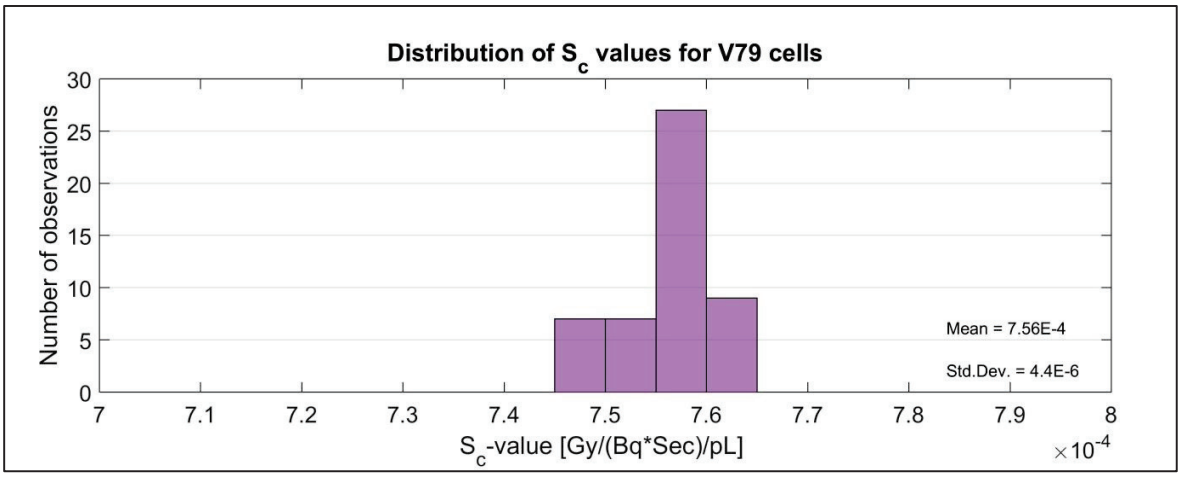

B

Figure 4.15 S_C-values and distribution for V79 nuclei with different volumes

S_C-values (A) and their distribution (B) for V79 cell nuclei with volumes ranging from below 0.1 pL to above 1.0 pL, positioned in the cellular monolayer, were calculated. Each blue mark in graph (A) represents the S_C-value for one of the 50 V79 nuclei. As can be seen the S_C-values almost do not change over the big range of nuclei volumes. The S_C-values changes with less than 2.5% even though the nuclei volume changes by a factor of 10.

4.2.1.6 S_C-value for HeLa cells

The S_C-values for HeLa cells were calculated to be between $7.78*10^{-4}$ to $7.83*10^{-4}$ Gy/(Bq*Sec)/pL , depending on the size of the nucleus. The value of $7.80*10^{-4}$ Gy/(Bq*Sec)/pL was used in dose calculations. The uncertainty of the S_C-value was estimated to be 3 %, dominated by uncertainty in cellular monolayer height. The influence of the cell layer height on S_C-values has been derived from convolutions of the dose kernel over cell layer heights of 8 µm and 10 µm and 12 µm (calculation not shown) (Figure 4.16).

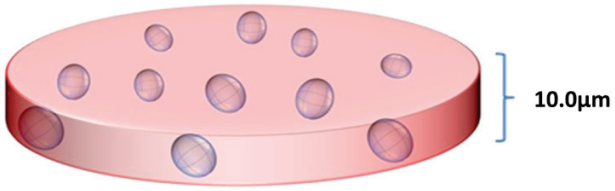

Figure 4.16 Model of the cell culture geometry for HeLa cell

A cellular monolayer height of 10 µm was used in the S_C-value calculations.

4.2.1.7 S_C-value for V79 cells

The S_C-values for V79 cells were calculated to be between $7.45*10^{-4}$ to $7.63*10^{-4}$ Gy/(Bq*Sec)/pL , depending on the size of the nucleus, for the geometry stated above. The value of $7.50*10^{-4}$ Gy/(Bq*Sec)/pL was used in dose calculations. The uncertainty of the S_C-values was estimated to be 7 %, dominated by uncertainty in the cellular monolayer height. The influence of the cell layer height on the S_C-values for V79 cells was based on the influence for S_C-values for HeLa and the influence of the nuclear volume of the V79 cells. As the V79 cellular monolayer was thinner, the influence of height on the S_C-values was thought to be bigger (Figure 4.17).

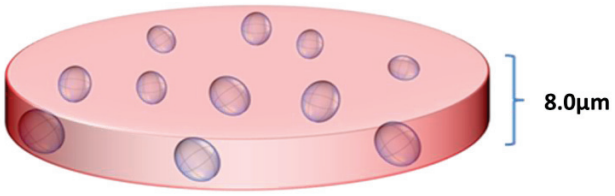

Figure 4.17 Model of the cell culture geometry for V79 cell.

A cellular monolayer height of 8 µm was used in the S_C-value calculations.

The calculated S_C-values (S_C(C←N)) for ^{131}Cs were found to be around 7.8*10^{-4}Gy/(Bq*Sec)/pL for HeLa cells, and 7,5*10^{-4} Gy/(Bq*Sec)/pL for V79 cells. These values are comfortingly close to the simple, first principle value of 9.41*10^{-4} Gy/(Bq*Sec)/pL (using our "normalised" emission rates) that is easily calculated for the absorbed dose anywhere inside an infinitely large homogenous water solution of ^{131}Cs using the decays information for the Auger electrons provided by the NuDat 2.7 database [25].

4.3 Absorbed dose calculations and dose rate profiling.

To calculate the absorbed dose, the S_C-values and the activity concentration of ^{131}Cs in the cells over time have to be known. Note that since our S_C-values are expressed as Gy/(Bq*Sec)/pL, it is the activity concentration of ^{131}Cs in the cells that is multiplied with the S_C-value, and not the activity (used in the MIRD cellular S-values).

To calculate the absorbed dose and dose rates we need;

- The S_C-value, which was determined to be $7.8*10^{-4}$ Gy/(Bq*Sec)/pL (HeLa) and $7.5*10^{-4}$ Gy/(Bq*Sec)/pL (V79)

- The uptake kinetics or rather the activity concentration of ^{131}Cs in the cells over time. This "uptake" could be described by the exponential equation ($A = A_0 * (1 - e^{-t*\frac{1}{283\ min}})$) for HeLa cells and ($A = A_0 * (1 - e^{-t*\frac{1}{204\ min}})$) for V79 cells. A_0 is the activity concentration at equilibrium.

- The cellular activity concentration of ^{131}Cs, at least at 1 time point. For experimental reasons this time point was when the cells were removed from the ^{131}Cs containing medium.

- The release kinetic could be described by the exponential equation ($A = A_0 * e^{-t*\frac{1}{339\ min}}$) for HeLa cells and ($A = A_0 * e^{-t*\frac{1}{256\ min}}$) for V79 cells. Here A_0 is the activity at the time when activity is removed from the medium. The time (t) is now the time that has passed since removal of activity.

- The combined activity expression becomes (exemplified by HeLa cells):

$$A_{up} = A_{480} * \left(1 - e^{\frac{-480\ min}{283\ min}}\right)^{-1} * \left(1 - e^{\frac{-t}{283\ min}}\right) \text{for } t \leq 480\ min$$

$$A_{out} = A_{480} * e^{-\frac{t-480\ min}{239\ min}} \text{ for } t > 480\ min \quad \text{(Eq. 36)}$$

The cumulative activity concentration (A^*) relevant to internal absorbed dose in a given experiment is now

$$A^* = \int_0^{480} A_{up} * dt + \int_{480}^{1440} A_{out} * dt \quad \text{(Eq. 37)}$$

The total internal absorbed dose to cell nuclei in such experiment is

$$D = S_c(N \leftarrow C) * A^* \quad \text{(Eq. 38)}$$

An example of the absorbed dose and dose rate calculation for cell exposed to intracellular ^{131}Cs and evaluated by γH2AX or clonogenic cell survival can be seen below (Figure 4.18). The example is based on the calculation of the absorbed dose and dose rates for HeLa cells, but they are essential the same for V79 cells (just using, the values obtained for V79 cells instead).

The activity concentration of ^{131}Cs in HeLa for this example was set to be 0.20 Bq/pL after 480 min of incubation. Using this value and the equation that described the activity concentration of ^{131}Cs over time, the cellular activity concentration at every time point was calculated (Figure 4.18 A &C). By multiplying the cellular activity concentrating (at ever time point) with the S_C-values, the dose rate (at every time point was obtained) (Figure 4.18 B & D). The absorbed dose over time was found by integration of the dose rate curve (Figure 4.18 B & D). At time point 480 min, the cells were removed from the ^{131}Cs containing medium and either prepared and fixation for the γH2AX assay (blue arrow) or seeded for clonogenic cell survival (blue arrow). Cells prepared for the γH2AX were permeabilized and fixed shortly after they were removed from the ^{131}Cs containing medium, and so intracellular ^{131}Cs decays after this point (480 min) were not considered in the absorbed dose calculations. In contrast, cells seeded for clonogenic cell survival, would still be exposed to intracellular ^{131}Cs decays, as the ^{131}Cs is slowly released from the cells. By using the equation describing the release kinetic and the activity concentrating at time point 480 min, the cellular activity concentration and so the dose

rates and absorbed dose for the cells from time point 480 min and onwards to 1440 min were calculated.

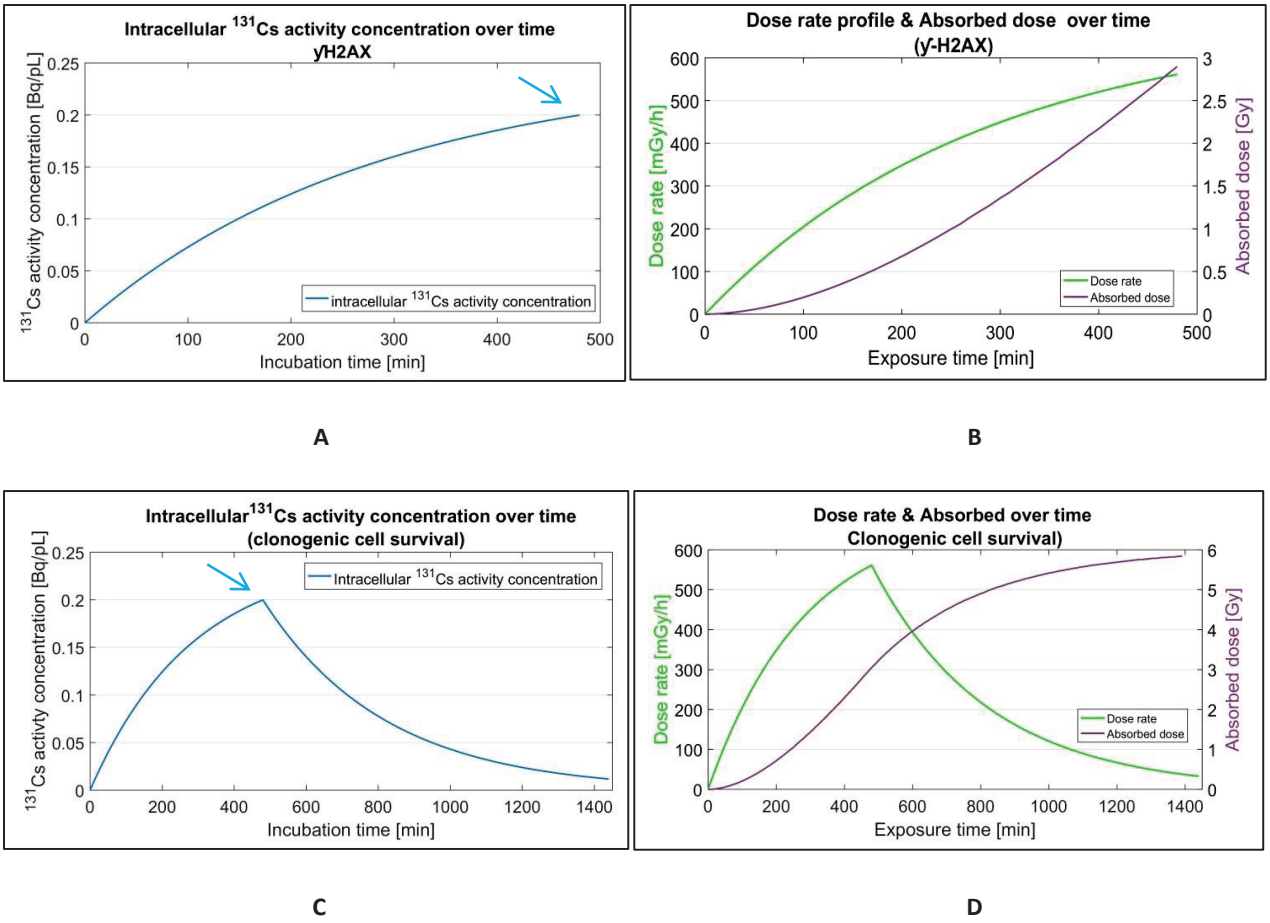

Figure 4.18 Representation of change in cellular activity concentration (Bq/pL), absorbed dose and dose rate as a function of time for HeLa cells with an activity concentration of 0.2 Bq/pL at 480 min.

The ^{131}Cs activity concentration (blue curve) increases over time until the ^{131}Cs is removed from the medium (blue arrow), whereafter it decreases exponentially. The dose rate (green curve) follows the same pattern. The absorbed dose (purple curve) increases over time but flattens out as the cellular activity concentration approaches zero. Note, that the absorbed dose after 24 hours is approximately 2 times higher than it is after 8 hours (the time where the ^{131}Cs is removed from the culture medium).

After 24 h, the activity concentration of ^{131}Cs in the cells has decrease to ~6 % (HeLa) and ~2 % (V79) of the maximum value, and the dose rate is only ~33 mGy/h (HeLa) or ~ 16 mGy/h (V79). After 24 hours, HeLa and V79 cells would also have had time to pass through the cell cycle once or twice. Therefore it was decided, that it was reasonable to end activity integration, absorbed dose calculation and dose rate profiling after 24 hours after starting the experiment.

As can be seen on Figure 4.18 the cellular ^{131}Cs activity concentration increases till 480 min, where the ^{131}Cs is removed from the medium. Thereafter it decreases exponentially. The change in dose rate over time has a similar time course and is directly proportional to the change in cellular activity concentration. The absorbed dose continues to increase over time but flattens out as the cellular activity concentration approaches zero. It is worth noticing that the absorbed dose is around a factor 2 higher at 24 h than at 8 h where the ^{131}Cs was removed.

This is how the absorbed doses and dose rate profiles for all the cells exposed to ^{131}Cs were obtained. The dose rate profiles for each independent experiment were then mimicked by the external γ-rays exposures. This was done by moving the incubator with the cells (in steps) closer to (or farther away from) the γ-rays source. The dose rates used (at each step) for the individually experiments (γH2AX and clonogenic), are show in those sections (section 4.4.2.1.1 p. 132 and section 4.4.3.1 p. 136).

4.3.1 Uncertainties and errors

Two simplifications were made in the absorbed dose and dose rate calculations. First, the physical half-life of ^{131}Cs was ignored. The cellular activity concentration measured (at time point 480 min) was used to give activity both before and after 480 min ,but as the half-life of ^{131}Cs is 9.689 days, the error introduced is small (<1 %).

Second, it was assumed that all the intracellular ^{131}Cs activity had disappeared after 24 hours and so the cellular activity concentration curve was not integrated to infinity (and the absorbed dose stated equalled the absorbed dose at time point 24 h). Likewise, the external reference γ-ray exposures were ended after 24 h. This 24 h truncation causes an error less than 1 % in the total absorbed dose.

Other uncertainties in the absorbed dose and dose rate calculations come from:

-Uncertainty in the S_C-value. The total uncertainty was estimated to be 3 % and 7 % for HeLa and V79 cells respectively. The uncertainty was dominated by:

- The height of the cellular monolayer
- Uncertainties in the decay data used. The stated uncertainties on Auger branch intensities in NuDat 2.7 are very small (<0.5%) but the calculations by Boon Q. Lee [93] indicate substantially higher Auger yields. This is discussed in appendix 8.3.2 p. 204 and has led to a 17 % higher value for the total energy released. It lead to a systematic bias of all internal doses by 17%, but it is conservative as far as the RBE measurements is concerned, and at present it is not possible to make this more accurate. The decay scheme uncertainty is not included in the internal absorbed dose uncertainty given below.

-Uncertainty in the uptake and release bio-kinetics of ^{131}Cs. This is described in appendix 8.3.1 p. 201. 1 s.d. errors in k_c and k_{out} give an error of 1.5-3.3 % in the cumulative activity ($\tilde{A}^*$) for Hela cells. Corresponding numbers for V79 are 0.23 - 4.0 %.

The span in errors reflects differences in assumptions about the nature of uncertainties in k_c and k_{out}. If they are systematic, the may well be biased in the same direction. If the uncertainty is purely statistical it is only a low (but finite) chance that they are both wrong by more than 1 standard deviation in opposing directions. In the end, I conclude that the impact of the uncertainty of the caesium kinetics on the cumulative activity is less than 4 %. As I will show below, the uncertainty on the cell counting has a much large impact (in the order of 20 %). The kinetics uncertainty is hence forward ignored.

- uncertainty in the measured cellular activity concentration. This was dominated by:

  - The estimated total cell volume. The cell concentration and the cell sizes were measured by the Sceptor (from Merck Millipore®). In addition cell concentrations (but not sizes) (from the same sample) were measured by the Muse (from Merck Millipore®). The Muse estimated on average the cell concentration to be 20 % higher than the Sceptor. However, as the Sceptor measured both cell number and their size (and this was the parameters needed), the results from the Sceptor were used.

When combining these errors in quadrature it will by far be dominated by the cell counting uncertainty. The total uncertainty in the absorbed doses and dose rate calculations were therefore estimated to be 22 % for HeLa cells and 23 % for V79 cells

For further elaboration on the calculation and estimations of the uncertainties, see appendix 8.3 p. 198.

4.4 Radiotoxicity of ^{131}Cs

The S_C-values and the bio-kinetics of ^{131}Cs in HeLa and V79 cells had now been elucidated and absorbed dose calculations and dose rate profiling was established. It was therefore time to advance to the examination of the radiotoxicity and RBE of the Auger emitter ^{131}Cs. The radiotoxicity of intracellular and extracellular Auger decays was investigated using the γH2AX assay, whereas the RBE of ^{131}Cs was studied using the γH2AX and the clonogenic cell survival assay. Due to a possible dose rate effect, it was highly prioritized to use similar dose rate profiles for both the ^{131}Cs exposed and the γ-ray exposed (reference radiation) cells when measuring RBE values. (For further elaboration on the data presentation of this specific γH2AX assay and the clonogenic cell survival assay see section 3.1 p. 59).

4.4.1 Radiotoxicity of intracellular and extracellular ^{131}Cs decays

The dosimetry model used to calculate S_C-values only considers the ^{131}Cs located inside the cells, and completely ignores the majority of ^{131}Cs which is located in the medium outside the cells. This was done to simplify the model and was justified by the relatively small dose contribution from this source (see section 4.2.1.4 p. 115). Furthermore, it is agreed on that for an Auger decay to be (highly) radiotoxic it has to occur intracellular and preferable intranuclear. Auger emitters located extracellularly are believed to cause minimum DNA damage [28]. However to investigate this assumption, HeLa cells were incubated with the same activity concentration of ^{131}Cs in the medium for the same amount of time, but in the absence or presence of 8.45 µM ouabain. Ouabain blocks ^{131}Cs uptake (see section 4.1.4 p. 102) and ouabain incubated cells were therefore exposed to much less intracellular ^{131}Cs decays, but (almost) the same amount of extracellular ^{131}Cs decays. Radiotoxicity was assessed by γH2AX assay.

The results are presented as “fold over the control levels” of the yH2AX response (percentage of activated cells) as a function of incubation time or as a function of “approximate” absorbed dose (Figure 4.19). As the HeLa cells were not 100 % confluent in this experiment (which is an assumption in the S_C-values used) the stated absorbed doses are only an approximation. The real absorbed doses might be a bit less, for all samples. Based on the intensities of the fluorescent antibodies, indicating the amount (and size) of the DNA DSBs in a cell, the cell is grouped as either activated or inactivated. The amount of activated over inactivated cells are calculated (yH2AX response) and normalised to controls to give fold over control levels. (For further elaboration see section 3.1.1 p. 59).

HeLa cells incubated with ^{131}Cs in the absent of ouabain show a steady increase in the yH2AX response with incubation time, and reached a 3.5 fold increase (compared to controls) after 480 min. In contrast, cells incubated with ^{131}Cs in the presence of ouabain did not show any significant increase in their yH2AX response after 380 min and 480 min incubation, even though the ^{131}Cs activity concentration in the medium was the same (Figure 4.19).

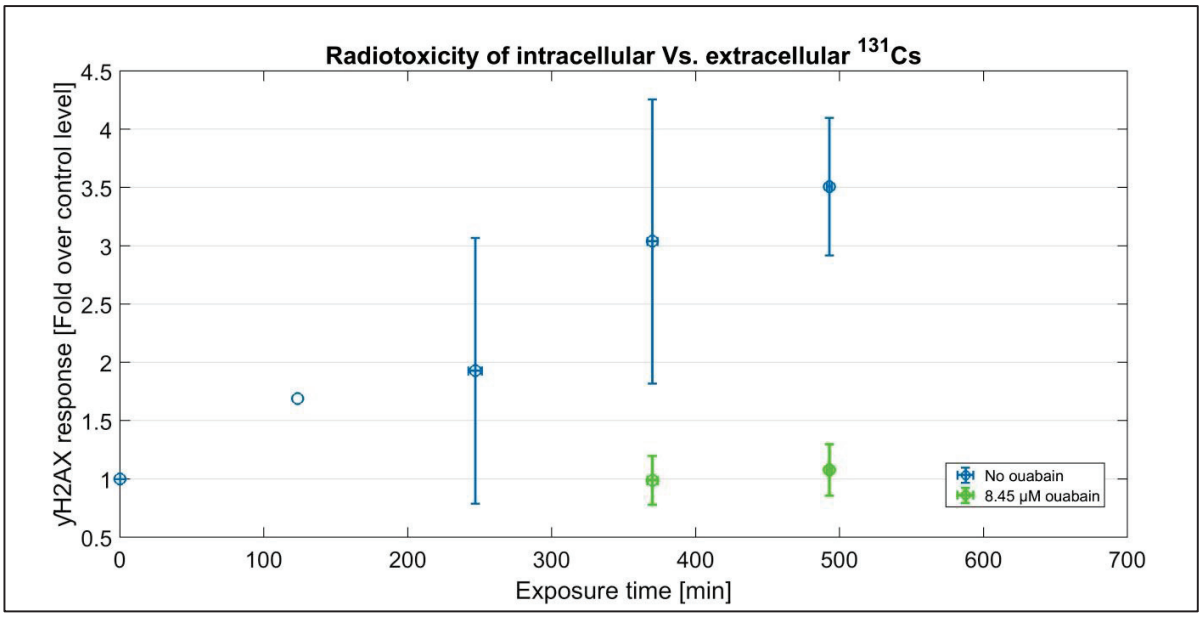

A

Figure text on next page

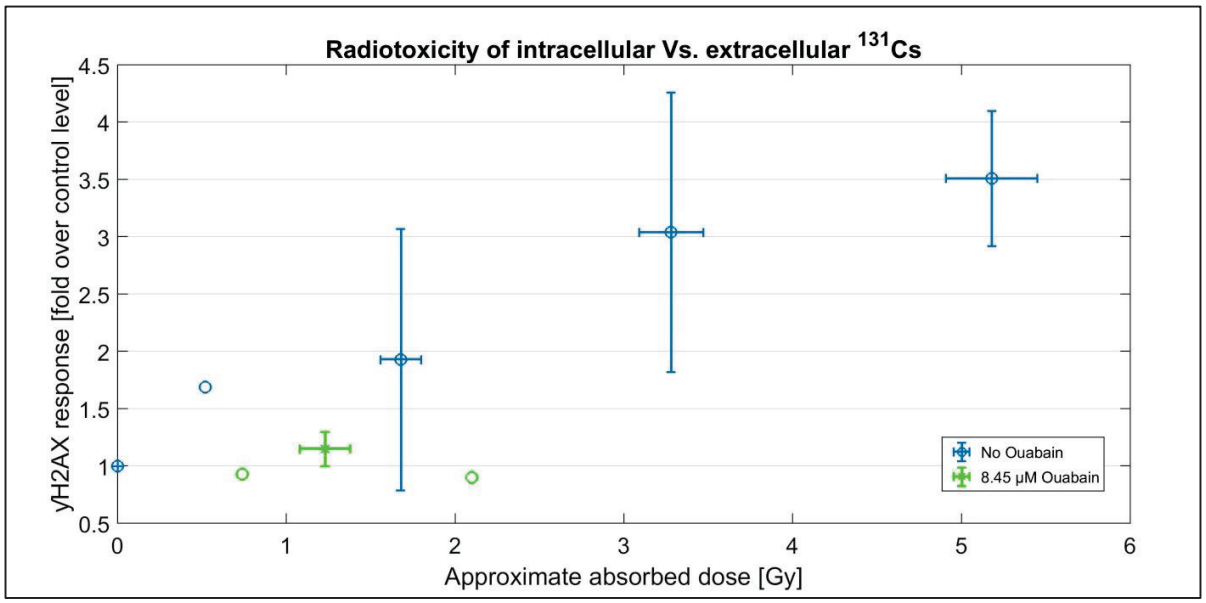

B

Figure 4.19 yH2AX response in cells after exposure to intracellular or extracellular ^{131}Cs decays

Results are presented as yH2AX response plotted as fold over the control levels as a function of incubation time (A) or approximate absorbed dose (B). As the HeLa cells were not 100 % confluent in this experiment (which is an assumption in the S_C-values used) the stated absorbed dose, is only an approximation. The real absorbed dose might be a bit less for all samples. HeLa cells were incubated with ^{131}Cs in the present (green) or absent (blue) of ouabain, and so respectively, primarily exposed to intracellular or extracellular ^{131}Cs decays. The yH2AX response increased with incubation time and absorbed dose in HeLa cells exposed to intracellular ^{131}Cs decays, reaching a 3.5 fold increase after 480 min corresponding to ~5 Gy. However, HeLa cells incubated in the presence of ouabain, (mainly exposed to extracellular ^{131}Cs) did not show any significant increase in their yH2AX response, neither with increasing incubation time or absorbed dose. Data is presented average ± s.d. of 3 independent experiments. The data points without any visible error bars only included one or two samples and a standard deviation could therefore not be calculated.

The absorbed dose stated in Figure 4.19 was calculated (as shown in the example given in section 4.3 p. 122) based on the measured activity concentration of ^{131}Cs over time in these cells (Figure 4.20). As can be seen in Figure 4.20, the "uptake" of ^{131}Cs (represented as intracellular ^{131}Cs activity concentration) over time, is much lower when cells are incubation with ouabain, than when no ouabain is present. However, still some ^{131}Cs is taken up by the cells in the presence of ouabain, resulting in the absorbed dose shown in Figure 4.19.

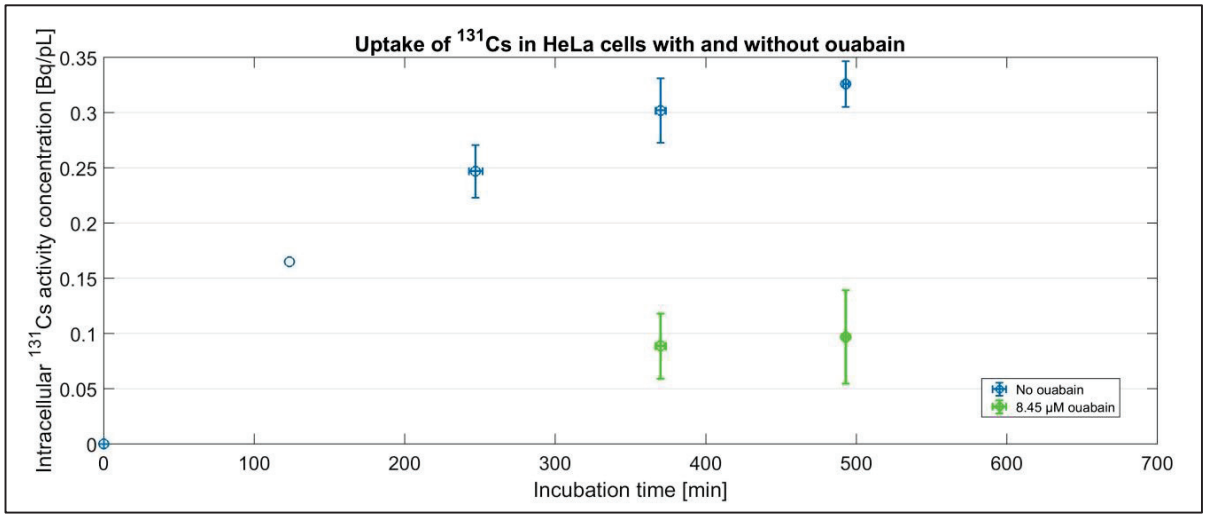

Figure 4.20 Uptake of ^{131}Cs in HeLa cells incubated with or without ouabain

The uptake of ^{131}Cs in HeLa cells over time is presented as intracellular ^{131}Cs activity concentration (Bq/pL) as a function of incubation time. The uptake of ^{131}Cs in HeLa cells incubated in the presence of 8.45 µM ouabain was significantly less compared to cells incubated in the absence of ouabain. These data is the same that were used to calculate the absorbed doses on Figure 4.19. Data is presented as average ± s.d. of 3 independent experiments. The data points without any visible error bars only included one or two samples and a standard deviation could therefore not be calculated.

Cells incubated in the absent of ouabain showed an increase in their yH2AX response and reach a 3.5 fold increase (compared to control levels) after 5 Gy, whereas cells incubated with ouabain, showed no significant increase after receiving ~2 Gy. It is however interesting, that the yH2AX response at ~2 Gy, appear to be lower in the cells incubated in the presence of ouabain, than those incubated in the absence. A possible reason for this will be discussed in the section 5.3.1 p. 161.

In summary, the results demonstrate that the cellular localisation of ^{131}Cs is important for its radiotoxicity. ^{131}Cs located extracellular did not seem to cause any significant increase in the yH2AX response compared to control levels, whereas ^{131}Cs located intracellularly showed significant increase in their yH2AX response.

4.4.2 Relative biological effectiveness of intracellular ^{131}Cs decay

The RBE of ^{131}Cs was investigated in HeLa and V79 cells using the γH2AX assay and clonogenic cell survival. As it is known that the dose rate can have a significant effect on the biological outcome, it was highly prioritized to use similar dose rate profiles for the ^{131}Cs exposed cells and the cells exposed to the reference radiation (external γ-rays).

4.4.2.1 RBE of intracellular ^{131}Cs exposure evaluated by γH2AX assay

The RBE of intracellular ^{131}Cs decay in HeLa cells was investigated using γH2AX as endpoint. The data from the γH2AX assay of cells exposed to intracellular ^{131}Cs (without ouabain) used in the above section (4.4.1 p.128) are the same data set that is used in this section (4.4.2.1). Again, as the HeLa cells were not 100% confluent in the experiment (which is an assumption in the S_C-values used), the stated absorbed doses, are only an approximation. The real absorbed doses might be a bit less for the ^{131}Cs exposed cells

4.4.2.1.1. Experimental dose rate profiles

As the dose rate of the intracellular ^{131}Cs exposure was dependent on the ^{131}Cs uptake kinetics in the cells and as this uptake could vary, dependent on the "quality" of the ^{131}CsCl solution, the dose rate profile was first calculated for these ^{131}Cs-exposed cells (as shown in the example given in section 4.3 p. 122) The obtained dose rate profile was then used to plan the external γ-ray exposure, where the dose rate was much easier to control. A representation of the experimental dose rates profiles and absorbed dose over time for the ^{131}Cs exposed cells (blue) and the externally γ-rays exposed cells (red) is pictured in Figure 4.21. To match the continuously increase in dose rate of the ^{131}Cs exposed cells, the γ-ray exposed cells were moved in steps closer to the γ-ray source. During this time in which the incubator was moved the cells were not exposed. This is the reason the area under the (step-wise)

curve in the Figure 4.21 A, appears to be somewhat larger for the γ-ray exposed cells, than the ^{131}Cs exposed cells, even though the absorbed dose in Figure 4.21 B shows that this difference between the absorbed doses is quite small. The very similar (time) course of the two curves showing the absorbed dose over time, confirms that both the dose rates and absorbed dose for the two exposures were nicely matched.

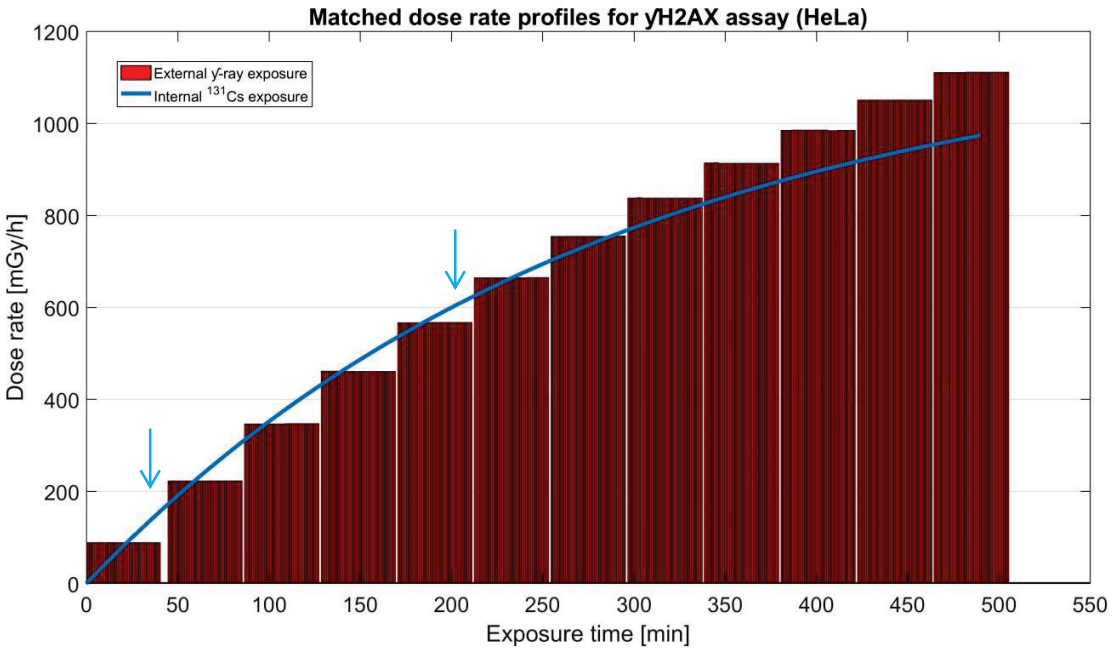

A

Figure text on next page

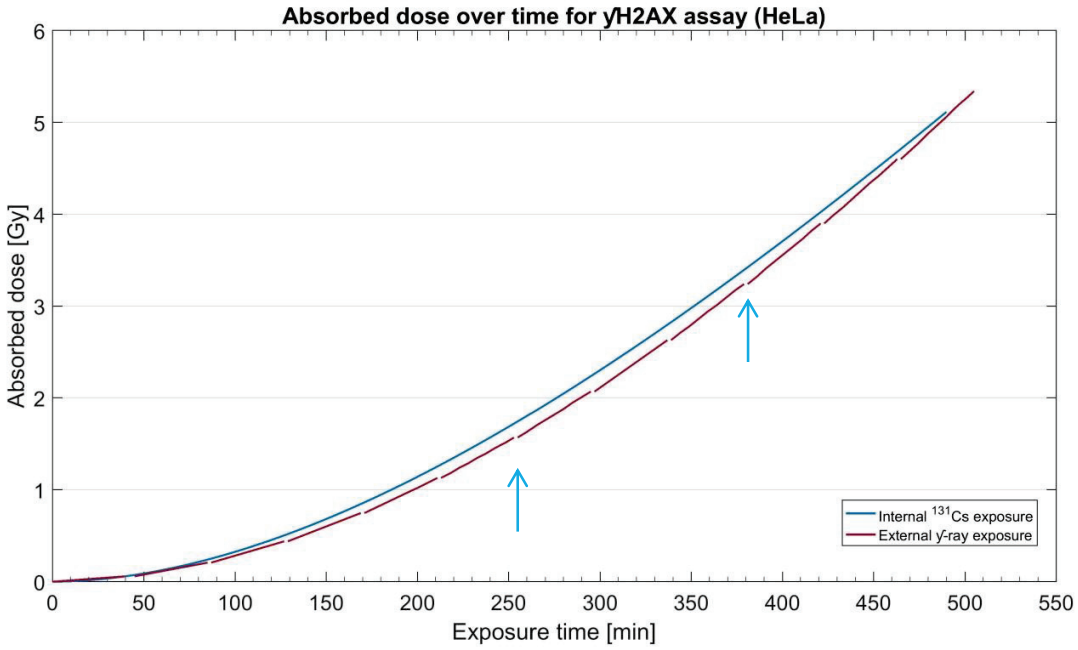

B

Figure 4.21 Representation of the dose rate profiles and absorbed doses for HeLa cells exposed to internal ^{131}Cs or external γ-rays for the γH2AX assay

The experimental dose rate profiles presented as dose rate over time (A) and absorbed dose over time (B) for the ^{131}Cs and γ-ray exposed cells are shown. To continuously get a comparable dose rate to the constantly increasing one of the ^{131}Cs exposed cells (blue), the incubator with the γ-ray exposed cells (red) were moved in steps closer to the γ-ray source. The small breaks in the red curve (blue arrow) represent the short time in which the incubator was moved and the exposure was interrupted. Therefore the areas under the curve(s) appear to be larger for the γ-ray exposed cells, than the ^{131}Cs exposed cells, even though the difference in absorbed dose is small. The curve of absorbed dose over time (B) of the ^{131}Cs (blue) and γ-ray (red) exposed cells, are very similar, confirming that both the dose rates and the absorbed dose of the two exposures were nicely match.

4.4.2.1.2. γH2AX

The biological effect was assessed by the γH2AX assay. The γH2AX response (the percentage of activated cells in a giving sample) is compared to a control sample (unexposed cells) to give the "fold over control level" value (for more information on the γH2AX assay see section 3.1.1 p. 59). The results are presented as γH2AX response of the two exposures (intracellular ^{131}Cs and external γ-ray) over absorbed dose (Figure 4.22). The γH2AX response in cells exposed to either intracellular ^{131}Cs

decay (blue) or to external γ-rays (red), increases with increasing absorbed dose and reach a 3.5 fold increase (compared to control levels) at ~5 Gy. The γH2AX response at the different absorbed doses is very similar for the two exposures showing no indication of an increased radiobiological response for the ^{131}Cs exposed cells. No increased radiotoxicity of ^{131}Cs compared to γ-rays at similar absorbed dose and dose rates could be observed and a RBE of 1 was therefore obtained. As this was evident from the standard deviations, no statistical test was performed.

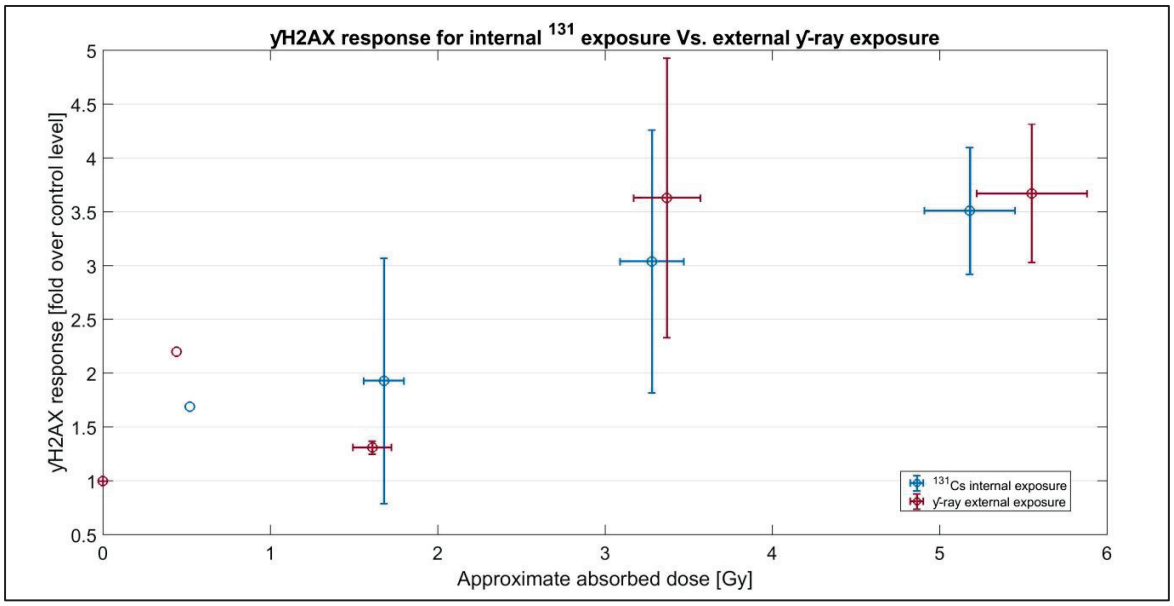

Figure 4.22 γH2AX response after exposure to intracellular ^{131}Cs decays or external γ-rays

Results are presented as γH2AX response plotted as fold over the control levels as a function of absorbed dose. As the HeLa cells were not 100% confluent in the experiment (which is an assumption in the S_C-values used) the stated absorbed doses for the ^{131}Cs exposed cells are only approximate. Cells were exposed to either intracellular ^{131}Cs decays (blue) or external γ-rays (red) at similar dose rate profiles. The γH2AX response increased with the absorbed dose, reaching a 3.5 fold increase (compared to control levels) after receiving ~5-6 Gy. The γH2AX response at the different absorbed doses was similar for the two exposures and no difference in the radiotoxicity was observed. This corresponds to a RBE of 1. Data are presented as average ± s.d. of 3 independent experiments. *The data points without any visible error bars only included one or two samples and a standard deviation could therefore not be calculated. As it was evident from the standard deviations, that there was no significant difference between biological effect of the two radiation exposures, no statistical test was performed. ^{137}Cs γ-rays was used as reference radiation.*

4.4.3 RBE of intracellular ^{131}Cs exposures evaluated by clonogenic cell survival

The RBE of intracellular ^{131}Cs decays in HeLa and V79 cells was investigated using clonogenic cell survival as an endpoint.

4.4.3.1 Experimental dose rate profiles

As the dose rate of the intracellular ^{131}Cs exposure was again dependent on the ^{131}Cs uptake kinetics in the cells and as this uptake could vary, dependent on the "quality" of the ^{131}CsCl solution, the dose rate profile was first calculated for these ^{131}Cs-exposed cells (as shown above in the example in section 4.3 p.122). The obtained dose rate profile was then used to plan the external γ-ray exposures (as these were much easier to control) so that they would resemble as closely as possible the dose rate profile of the cells incubated with ^{131}Cs. Given the restriction of our calibration facility, a dose rate above 492 mGy/h for these experiments (clonogenic cell survival) could not be achieved for the external γ-ray exposures. It was therefore prioritized (if needed) to reach the same absorbed dose (for ^{131}Cs and γ-ray exposed cells) after 24 hours, even though it compromised the dose rate match. Due to the number and size of samples (T25 flasks) placed in the incubator, it was necessary to increase the distance from the γ-ray source, to get a radiation field big enough to equally exposure all the flasks. Therefore a significant lower dose rate could be used in these experiments, compared to the dose rate used in the above "γH2AX" experiments (Figure 4.21 p. 134) (in which only a couple of 48-well plates were placed in the incubator).

Figure 4.23 and Figure 4.24 shows a representation of the experimental dose rates profiles (A) and the absorbed dose (B) for HeLa and V79 cells. The dose rate for the externally γ-ray exposed cells (red) changes in steps as the incubator is moved (closer to or further away from the γ-ray source), while the dose rate for the internal ^{131}Cs exposed cells (blue) changes continuously. During the time in which the incubator was moved the cells were not exposed. This is the reason the area or under the (step-wise) curve in Figure 4.23 A and Figure 4.24 A, appears to be larger for the γ-ray exposed cells,

than the ^{131}Cs exposed cells, even though the absorbed doses in Figure 4.23 B and Figure 4.24 B shows that the total absorbed doses for the two exposures were very similar.

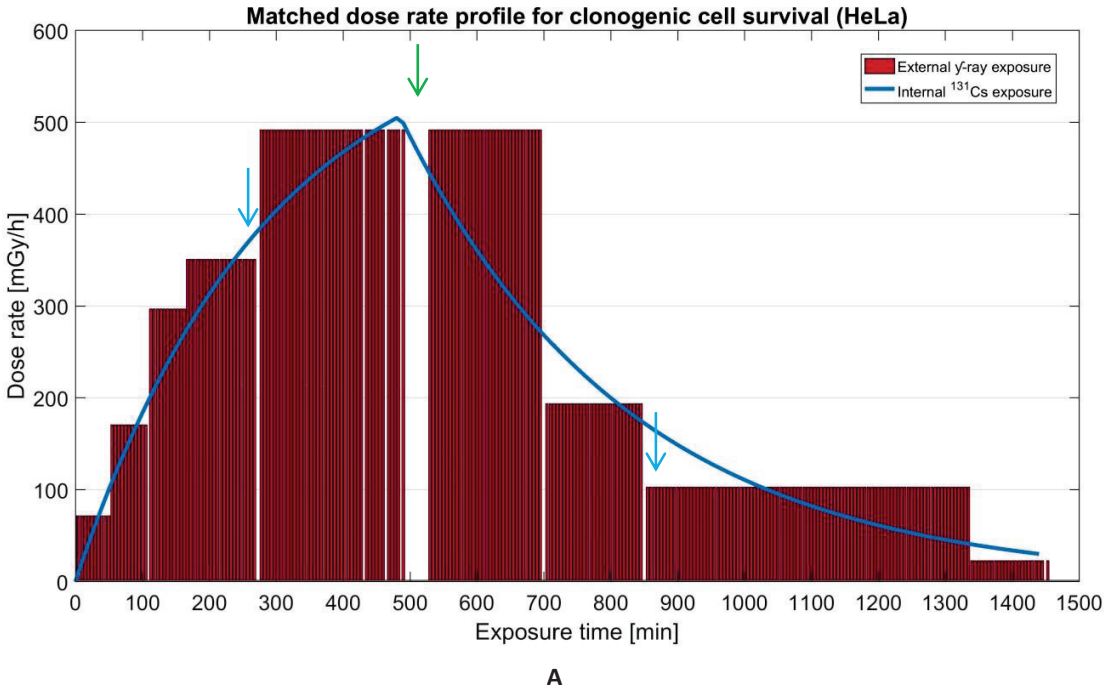

A

Figure text on next page

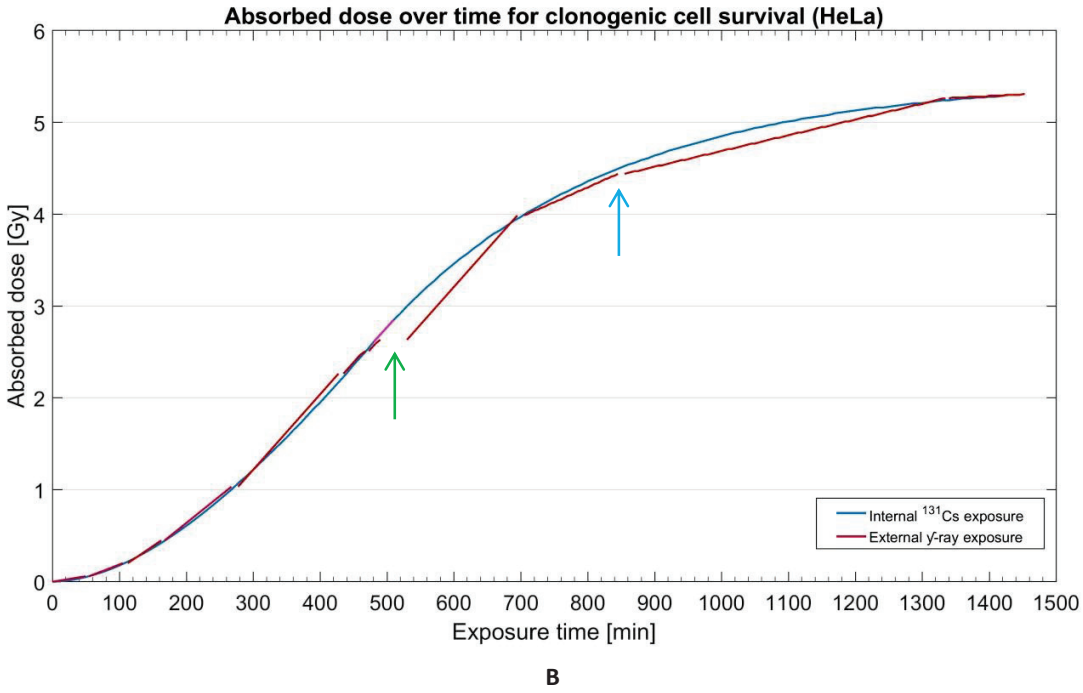

B

Figure 4.23 Representation of the dose rate profiles and absorbed dose over time for HeLa cells exposed to internal ^{131}Cs or external γ-rays (protracted) for clonogenic cell survival.

The experimental dose rate profiles presented as dose rate (A) and absorbed dose (B) over time for the ^{131}Cs (blue) and γ-ray exposed (red) cells are shown. To match the continuously increase in dose rate for the ^{131}Cs exposed cells, the incubator with the γ-ray exposed cells were moved in steps closer to the γ-ray source. The small breaks in the red curve represent (blue arrows) the short time in which the incubator was moved and the exposure was interrupted. The green arrows (and the purple line on the blue curve) indicate the time where the cells were handled for seeding for clonogenic cell survival curves. As the ^{131}Cs was located intracellularly, the exposure of these cells continued during the seeding, while the γ-ray exposed cells were not exposed during this seeding process The absorbed dose over time (B) of the ^{131}Cs (blue) and γ-ray (red) exposed cells, are very similar, confirming that both the dose rates and the absorbed dose for the two exposures were nicely match.

As the dose rate for the ^{131}Cs exposed cells did not exceed the limit of 492 mGy/h it was easily matched and so was the absorbed dose over time. At the time point where the cells were seeded for clonogenic cell survival (green arrows on Figure 4.23) the γ-ray exposed cells had received the same absorbed dose as the ^{131}Cs exposed cells.

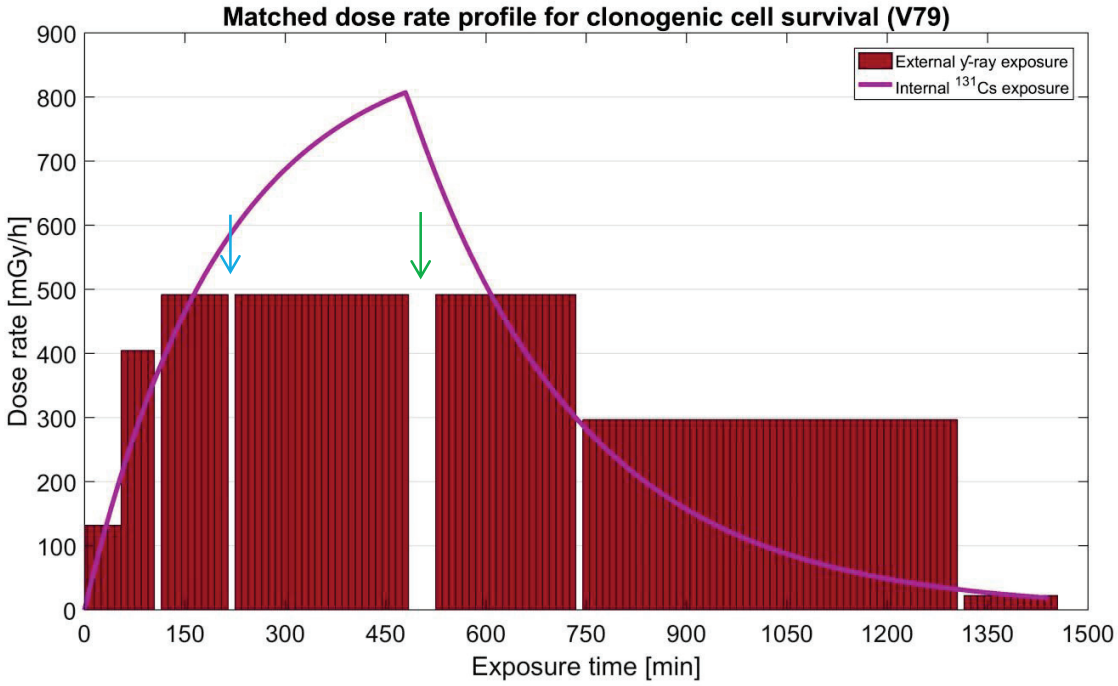

A

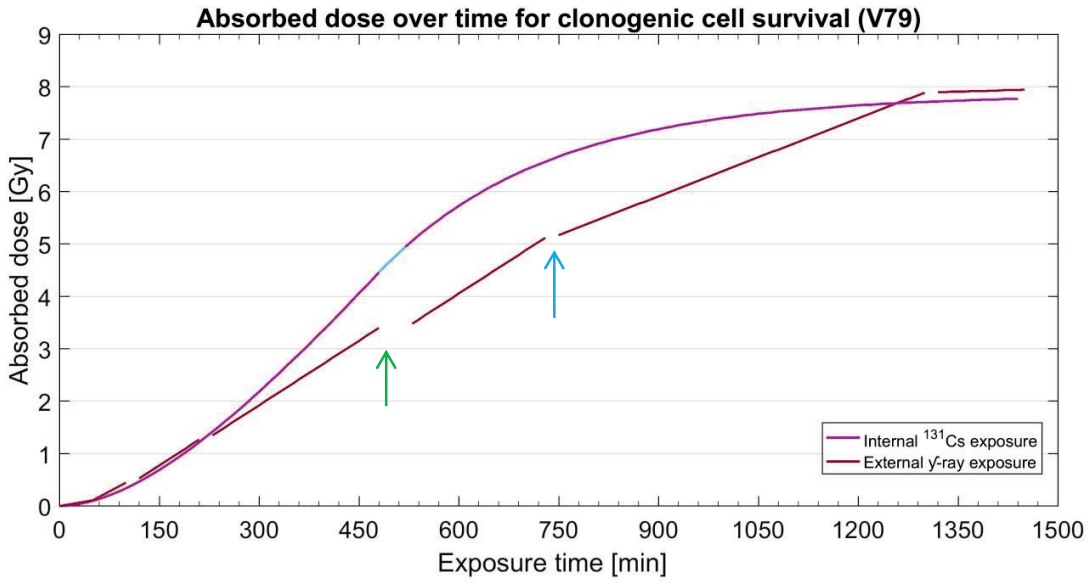

B

Figure text on next page

Figure 4.24 Representation of the dose rate profiles and absorbed dose for V79 cells exposed to internal ^{131}Cs or external γ-rays (protracted) for clonogenic cell survival.

The experimental dose rate profiles presented as dose rate (A) and absorbed dose (B) over time for the ^{131}Cs (purple) and γ-ray exposed (red) cells are shown. To match the continuously increase in dose rate of the ^{131}Cs exposed cells, the incubator with the γ-ray exposed cells were moved in steps closer to the γ-ray source. The small breaks (blue arrows) in the red curve represent the short time in which the incubator was moved and the exposure was interrupted. The green arrows (and the blue line on the purple curve) indicate the time where the cells were handled for seeding for clonogenic cell survival curves. As the ^{131}Cs was located intracellularly, the exposure of these cells continued during the seeding, while the γ-ray exposed cells were not exposed during this seeding process. At the time of seeding, the γ-ray exposed cells had received a smaller absorbed dose, than the ^{131}Cs exposed cells, due to the dose rate limit in the calibration facility. This "lack" of absorbed dose was afterwards corrected for by continuing the exposure at the highest possible dose rate. The absorbed dose over time (B) of the ^{131}Cs (purple) and γ-ray (red) exposed cells deviate some due to the lower dose rate of the γ-ray exposed cells. However, as can be seen, at the end of the experiment (time point ~1440 min) the same absorbed dose was reach for the two exposures.

For the V79 cells the dose rates could not be matched as nicely as for the HeLa cells. As can be seen in Figure 4.24, the dose rate for the ^{131}Cs exposed cells exceeded the limit of 492 mGy/h (the highest dose rate possible for these experiments (clonogenic cell survival) in our calibration facility). As a consequence the γ-rays exposed cells had received a smaller absorbed dose than the ^{131}Cs exposed cells when they were seeded for clonogenic cell survival. It was prioritized that the cells would receive the same absorbed dose after 24 hours (the end of the exposure), and so the "lack of absorbed dose" was corrected for afterwards, by continuing the exposure at the highest possible dose rate. As can be seen in Figure 4.24 B the γ-ray exposed cells reached the same total absorbed dose after 24 hours as the ^{131}Cs exposed cells.

4.4.3.2 Cellular and colony morphology of HeLa and V79 cells

4.4.3.2.1. HeLa cells

The morphology of the individual HeLa cells and the size and cell morphology of the colonies formed, in the clonogenic cell survival assay, varied within and between the samples exposed to intracellular ^{131}Cs decays and external γ-rays. This is of interest as it might elucidate possible mechanisms behind the different biological responses observed after exposure to different radiation qualities.

The two most common cell morphologies observed are showed in Figure 4.25 A B. These cells were normal in size, (~ 50-70 µm in diameter) and looked healthy (Figure 4.25 A) whereas those seen in Figure 4.25 B were much bigger than the normal cells (120-290 µm in diameter) and had a highly enlarge and flat cytoplasm. This (latter) morphology resembles that of senescence cells [117]. A small amount of the HeLa cells displayed the morphology showed in Figure 4.25 C. These cells were also highly enlarged and very elongated (~200 µm long).

The colonies formed by the external γ-ray exposed cells displayed a high variation in their size and both big and small colonies plus aborted colonies were observed. Most of the colonies, consisted only of normal looking cells as seen in Figure 4.25-A. However, some colonies made up of cells presenting a senescence like morphology (Figure 4.25 B), or a mixture of these and normal sized cells were also present. A few colonies containing the very elongated cells (Figure 4.25 C) were also observed.

Almost no colonies were formed by cells exposed to ^{131}Cs , resulting in a very low survival fraction. However, many single cells were still present in some of the samples (cultures), while other samples contained significantly fewer cells and some samples contained almost no cells. The cells that were present in the ^{131}Cs exposed samples either looked healthy and normal (Figure 4.25 A) or displayed a senescence-like morphology (Figure 4.25 B).

Most of the colonies formed in the control samples (for both the ^{131}Cs and the γ-rays exposed cells) looked healthy and contained many normal sized cells (Figure 4.25 A).

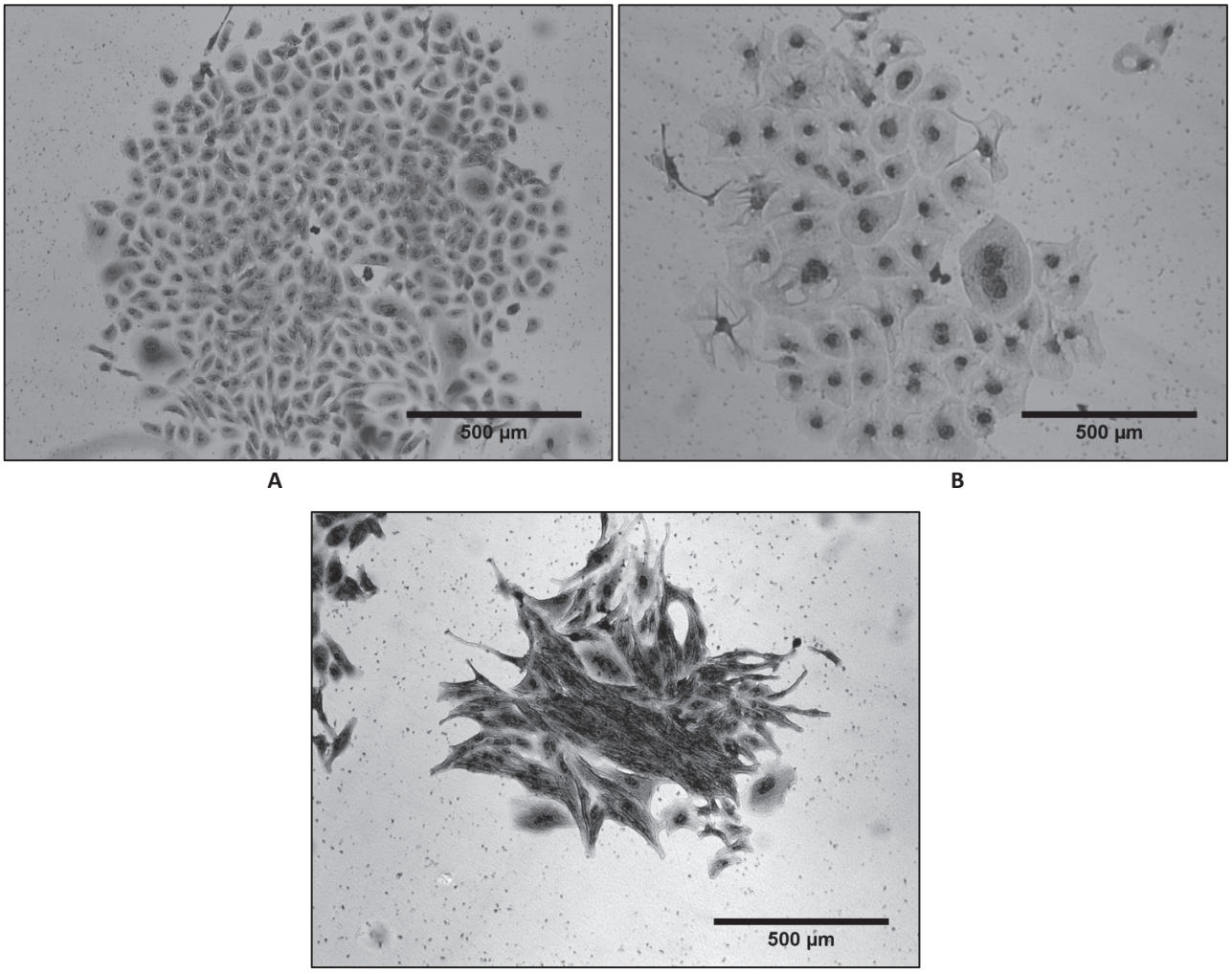

A **B**

C

Figure 4.25 Representative pictures of the different cell and colony morphologies displayed by HeLa cells. (~60X magnificantion

All pictures were acquired by the light microscopy (Axiovert 200M from Zeiss) using a 5x objective and Axiovision SE 64 software. As the cells were seeded in T25-falsk the images of the colonies had to be acquired through the thick layer of plastic (of the T25- flaks), which compromised the quality of the pictures. Still the difference in size and morphology is obvious. The morphology of the HeLa cells and the colonies formed, varied within and between samples. A colony containing mainly healthy and normal sized (~ 50-70µm in diameter) cells are pictured in **A**. A colony containing mainly cells with a senescence like morphology are pictured in **B**. These cells were much bigger than "normal" cells (120-290 µm in diameter) and had an enlarged and flat cytoplasm. The colony pictured in **C**, contained cells that were very elongated and much bigger (~200µm in length) than the "normal "cells. **Scale bar: 500 µm**.

4.4.3.2.2. V79 cells

The morphology of the V79 cells and the colonies formed did not vary between the samples exposed to ^{131}Cs, external γ-ray or the controls. Most of the colonies formed were big and consisted of much more than 50 cells (Figure 4.26). The cells in the colonies looked heathy, and had a size of around 20 µm x 10 µm, which is the normal size for these V79 cells.

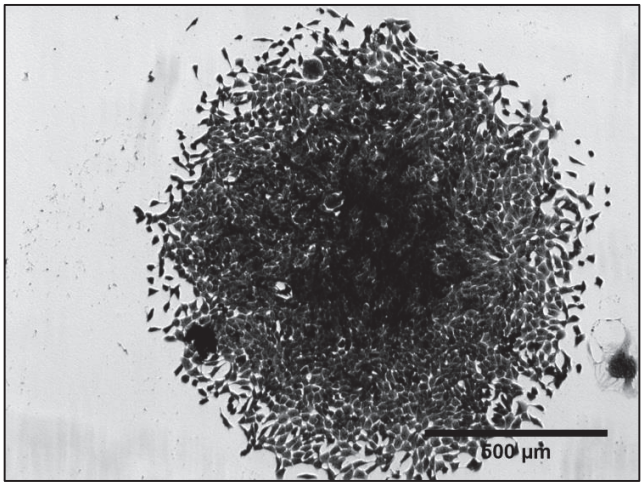

Figure 4.26 Representative picture of the cell and colony morphology displayed by V79 cells (~60X magnificantion

The picture was acquired by the light microscopy (Axiovert 200M from Zeiss) using a 5x objective and Axiovision SE64 software. As the cells were seeded in T25-falsk the image had to be acquired through the thick layer of plastic (of the T25-flaks), which compromised the quality of the picture. Still the size and morphology is obvious. The picture shows a colony with many normal and healthy looking cells with sizes around 20 µm x 10 µm. ***Scale bar: 500µm***

4.4.3.3 Clonogenic cell survival

HeLa and V79 cells were exposed to either intracellular ^{131}Cs decays, or external γ-rays using similar dose rate profiles. Absorbed doses between 4.7 Gy and 6.1 Gy were used in the HeLa cell exposures, while absorbed doses around 3 Gy, 7 Gy and 10 Gy were used in the V79 cell exposures. The absorbed dose and dose rate profiles for the ^{131}Cs exposed cells were calculated as shown in the example in section 4.3 p. 122. A representation of how the dose rate profiles of the internal ^{131}Cs exposures and the external γ-ray exposures were match were shown above in section 4.4.3.1 p. 136. HeLa cells and V79 cells were also exposed to external γ-rays using a dose rate of 1.5 Gy/min (in this context “acute

exposure"). These cells were however exposed under different conditions (low cell density) and so care should be taken in drawing conclusion from these survival curves. However they still give a good estimate of the influence of the dose rate on the biological response. For convenience these external γ-ray exposures will be referred to as acute exposures, while the other external γ-rays exposure, using matched dose rate profiles, will be referred to as protracted exposures.

4.4.3.3.1. HeLa cells

The clonogenic cell survival curves for HeLa cells can be seen in Figure 4.27. The experimentally obtained data points and their estimated uncertainties (see section 4.4.4 p. 149) for the ^{131}Cs exposed cells are shown along with the fitted survival curves. The data points with estimated uncertainties for the γ-rays exposed cells (protracted & acute), are presented in appendix 8.4 p. 206. As only a limited range of absorbed doses were received by the ^{131}Cs exposed and the protracted γ-ray exposed HeLa cells, it was not possible to deduce the presence of a potential shoulder on the survival curves. The survival curves were accordingly fitted to the linear model ($y = e^{-\propto x}$), as this model uses fewest parameters. A greater range in absorbed dose was however received by the HeLa cells exposed acutely to external γ-rays, and as the survival curve showed a clear shoulder, it was fitted to the linear quadratic model ($\mathrm{y} = \mathrm{e}^{-(\alpha \mathrm{x} + \beta \mathrm{x}^2)}$) (which is also the model most often used to fit survival curves for low LET radiation exposures [39]). α values (and β values) plus the D_{37} values for the different exposures were found to be 1.71 (α) and 0.58 Gy (D_{37}) for the ^{131}Cs exposed cells, 0.38 (α) and 2.6 Gy (D_{37}) for the protracted γ-ray exposed cells, and 0.136 (α), 0.0786 (β) and 2.8 Gy (D_{37}) for the acutely γ-rays exposed cells.

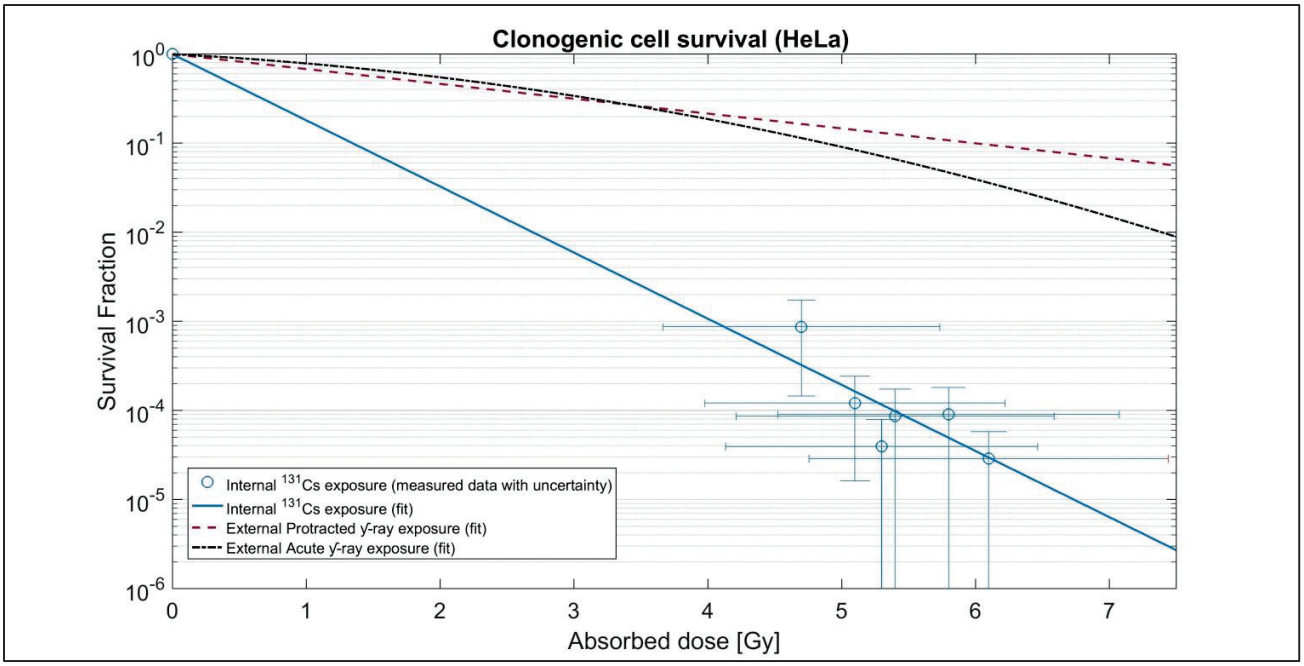

Figure 4.27 Clonogenic cell survival curves for HeLa cells exposed to ^{131}Cs or external γ-ray (protracted & acute)

Survival fraction as a function of absorbed dose for HeLa cells exposed to internal ^{131}Cs (blue) or external γ-ray *at similar dose rate profiles (red) or external γ-ray delivered acutely (black) are shown. The survival curves were fitted to either the linear model ($y = e^{-1.71x}$, ^{131}Cs exposed cells), ($y = e^{-0.384x}$, (protracted γ-ray exposed cells)), or the linear quadratic model ($y = e^{-(0.136x+0.0786x^2)}$, acute γ-ray exposed cells). The experimentally obtained data points (average of 3 replicates) for the ^{131}Cs exposed cells are presented. The vertical error bars reflect the observed standard deviation in survival fraction, while the horizontal error bars reflect the estimated uncertainty in absorbed dose. To simplify the figure the obtained data points and estimated uncertainties for the γ-ray exposed cells (protracted and acute) are only presented in appendix 8.4.1 p. 206. The difference in slope of the survival curves for the ^{131}Cs exposed and* γ-ray *(protracted) exposed cells gives a RBE of 4.5. (^{137}Cs γ-rays were used as reference radiation*).

As can be seen on the survival curves (Figure 4.27), cells exposed to intracellular ^{131}Cs decay had the lowest survival fraction, while the cells exposed to external γ-rays (protracted) had a substantially higher survival fraction, and the cells exposed to acute γ-rays had a survival fraction a bit lower than these. The presence of a possible dose rate effect was difficult to interpret due to the limited absorbed dose range used in the protracted γ-ray exposures. However, the survival fraction at 5-6 Gy,

(where survival fractions for the two γ-ray exposures (protracted and acute) were experimentally obtained), suggest that the dose rate effect was not pronounced.

As it is known that the RBE-value can dependent on the chosen endpoint, and will tend to increase with decreasing absorbed dose [13], the RBE for a survival fraction of 10 % is often stated. However, as the linear model was used to fit both the ^{131}Cs exposed and protracted γ-ray exposed cells, the calculated RBE-value will be independent on the endpoint (% survival fraction) and is simply the ratio between the slopes of the linear fits. Accordingly, the RBE will be dependent on the chosen model used to fit the survival curves. Using the linear model a RBE value of 4.5 ± 0.5 was obtained using ^{137}Cs γ-rays as reference radiation.

However, it might make more sense to compare the survival fraction after exposure of 5 Gy, where survival fractions for all the different exposures, had been obtained. At this absorbed dose, a survival fraction of only ~$4*10^{-4}$ was found for the ^{131}Cs exposed cells, while a survival fraction of ~$1.5*10^{-1}$ and ~$1*10^{-1}$ were found for the protracted and acutely γ-ray exposed cells, respectively.

4.4.3.3.2. V79 cells

The clonogenic cell survival curves for V79 cells can be seen in Figure 4.28. The experimentally obtained data points and their uncertainties (see section 4.4.4 p. 138) for the ^{131}Cs exposed cells are shown along with the fitted survival curves. The data points and estimated uncertainties for the γ-rays exposed cells (protracted & acute), are presented in appendix 8.4 p. 206. Similar to the experiments with HeLa cells, the protacted γ-rays exposed cells were only exposed to a narrow range of absorbed doses (~6-10 Gy), and the course of the survival curve and the presence of a possible shoulder was difficult to interpret. However, the one data point around 10 Gy does indicate that a shoulder was not present. The survival curve was therefore fitted to the linear model ($y = e^{-\propto x}$). In contrast, a broader range in absorbed doses were received by the ^{131}Cs exposed V79 cells, and so the absence of a shoulder was evident and the survival curve was therefore also fitted to the linear model ($y = e^{-\propto x}$). As for the HeLa cells, a greater range in absorbed doses were received by the acute γ-rays exposed

cells. The survival curve showed a clear shoulder and was fitted to the linear quadratic model ($y = e^{-(\alpha x+\beta x^2)}$). α values (and β values) plus D_{37} values for the different exposures were found to be 0.379 (α) and 2.6 Gy (D_{37}) for the ^{131}Cs exposed cells, 0.0994 (α) and 10.0 Gy (D_{37}) for the protracted γ-ray exposed cells, and 0.0983 (α),0.0266 (β) and 4.5 Gy (D_{37}) for the acutely γ-rays exposed cells.

As the survival curves reveal, cells exposed to protracted γ-rays showed the highest survival fractions, while cells exposed to ^{131}Cs or acute γ-rays showed a similar, but much lower survival fraction. At 10 Gy the survival curve for cell exposed acutely to external γ-ray, accidentally coincide with the survival curve for the ^{131}Cs exposed cells. In contrast to HeLa cells, a dose rate effect was here evident and had a great influence on the survival fraction and hence RBE.

Again the RBE was not dependent on the chosen endpoint, as the linear model was used to fit both the ^{131}Cs exposed and the cells exposed to protracted γ-ray. Still, as before, as no data was obtained (for the protracted γ-ray exposed cells) at 10 % survival (the endpoint normally used to obtain RBE values), the RBE will depend strongly on the model used to fit the survival curve. Nevertheless, a RBE of 3.8 ± 0.8 was found using ^{137}Cs γ-rays as reference radiation. However, it might make more sense to compare the survival fraction after an exposure of 7 Gy, where the survival fraction, was experimentally obtained for both exposures. At this absorbed dose a survival fraction around $8*10^{-2}$ was found for the ^{131}Cs exposed cells, while a survival fraction around $5*10^{-1}$ and $1*10^{-1}$ was found for the protracted and acutely γ-ray exposed cells respectively. In contrasts to the HeLa cells, the dose rate for the V79 cells had a big effect on the survival fraction. If the RBE had been calculated using the acutely γ-ray exposed data set instead of the protracted γ-ray exposed ones, the RBE-value at 10% survival fraction would have been 1.3.

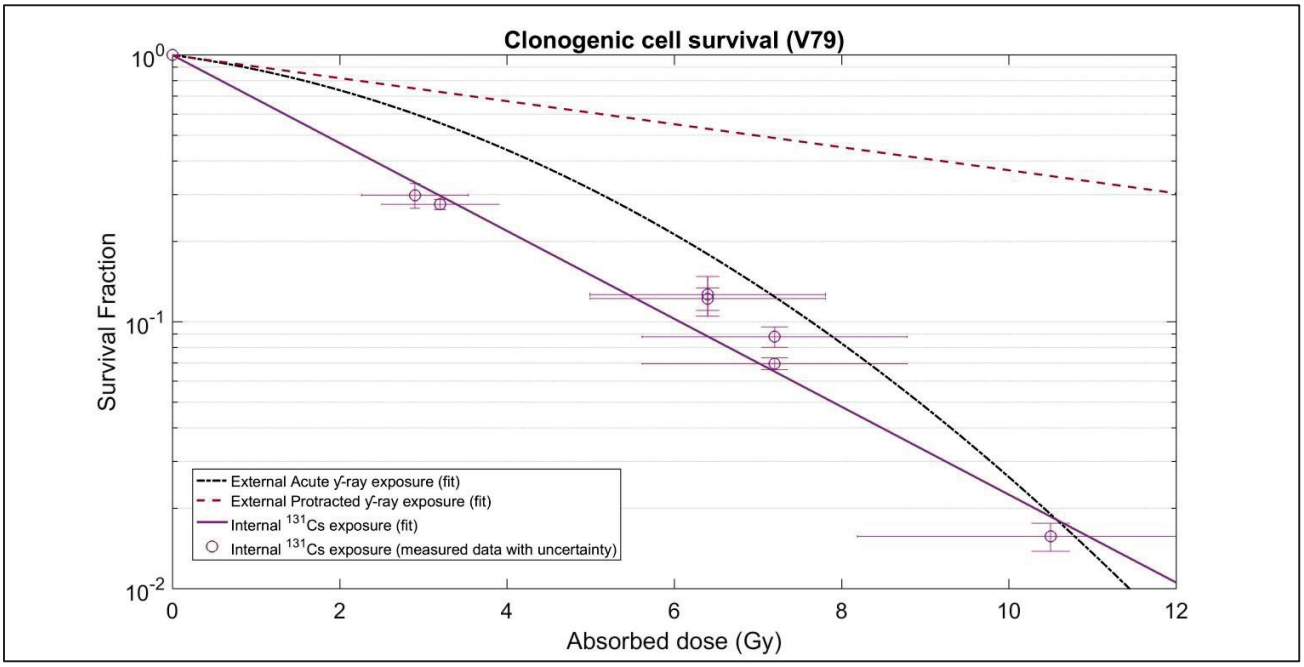

Figure 4.28 Clonogenic cell survival curves for V79 cells exposed to ^{131}Cs or external γ-ray (protracted & acute)

Survival fraction as a function of absorbed dose for V79 cells exposed to ^{131}Cs (purple) or external γ-ray *at similar dose rate profiles (red) or external γ-ray delivered acutely (black) are shown. The survival curves were fitted to either the linear model ($y = e^{-0.379x}$, ^{131}Cs exposed cells), ($y = e^{-0.0994x}$, (protracted γ-ray exposed cells)), or the linear quadratic model ($y = e^{-(0.0983x+0.0266x^2)}$, acute γ-ray exposed cells). The experimentally obtained data points (average of 3 replicates) for the ^{131}Cs exposed cells are presented. The vertical error bars reflect the observed standard deviation in survival fraction, while the horizontal error bars reflect the estimated uncertainty in absorbed dose. To simplify the figure the obtained data points and estimated uncertainties for the γ-ray exposed cells (protracted and acute) are only presented in appendix 8.4.2p. 207. The difference in slope of the survival curves for the ^{131}Cs exposed and* γ-ray *(protracted) exposed cells gives a RBE of 3.8. (^{137}Cs γ-rays were used as reference radiation*).

4.4.4 Uncertainty

The RBE-values were found by comparing the absorbed doses needed, to obtain an equal biological effect for a test and reference radiation and the uncertainties of the obtained RBE values are therefore related to the uncertainties in the dose-response curves of both the test and reference radiation. These uncertainties are again related to the uncertainties in the absorbed dose calculations and in observed biological effect.

-γH2AX

The RBE for internal ^{131}Cs exposure was investigated using the yH2Ax as endpoint. To analyse the result, a graph showing the yH2AX response relative to the control levels over the absorbed dose, was made. Results were presented as average of ± s.d. (for data points obtained by 3 independent experiments). As could clearly be seen on the graph no significant difference in the yH2AX response for the two irradiations (internal ^{131}Cs and external y-rays) could be observed. As this was evident due to the standard deviations, no statistical test was performed.

-Clonogenic cell survival

The uncertainty in the RBE –values obtained by clonogenic cell survival comes from:

- Uncertainty in the fitted survival curve for the ^{131}Cs exposed cells. This is reflected in the uncertainty in the α-values; 1.1709 (1.83, 1.587; 95% confidence bounds for HeLa cells) and 0.3792 (0.3432, 0.4153; 95% confidence bounds for V79 cells). The uncertainty is related to;
    - Uncertainty in the absorbed dose calculations. The uncertainty in the absorbed dose calculations were estimated to be 22 % of HeLa cells and 23 % in V79 cells (as explained in section 4.3.1 p. 126)

  - Uncertainty in the survival fraction. The uncertainty was dominated by the Poisson counting statistics (due to the low number of colonies counted especially for HeLa cells) and the total error was therefore assumed to be reflected by the observed variation. All clonogenic survival fractions were obtained by triplicates. The observed standard deviation in these triplicates is believed to reflect all the errors, and these standard deviations are used in the final data analysis.

- Uncertainty in the fitted survival curve for the externally protracted γ-ray exposed cells. This is reflected in the uncertainty of the α-values; 0.3838 (0.3633, 0.4043; 95% confidence bounds for HeLa cells) and 0.09936 (0.08016, 0.1186 95% confidence bounds for V79 cells). The uncertainty is related to;
  - Uncertainty in the absorbed dose calculations. The uncertainty in the absorbed dose calculations were estimated to be 2.12 % (for both cell lines) dominated by uncertainty in the distance between the cells and the γ-ray source.
  - Uncertainty in the survival fraction. The uncertainty in the survival fraction was dominated by the Poisson counting statistics. As for the internal exposure experiments, the observed standard deviations from the triplicate experiments are used in final data analysis.

The total uncertainty in the obtained RBE values can be expressed as the compounded uncertainty for a ratio, where the uncertainty of each term is known (the slopes). Using the stated uncertainty on alpha values the standard deviation for the RBE-value for Hela cells of 4.5 becomes 0.5 and the standard deviation for the RBE-value for V79 cells of 3.8 becomes 0.8, or in conclusion:

RBE (Internal ^{131}Cs, HeLa) = 4.5 ± 0.5

RBE (Internal ^{131}Cs, V79) = 3.8 ± 0.8

^{137}Cs γ-rays were used as reference radiation.

For further elaboration on the calculation and estimations of the uncertainties see appendix 8.3 p. 198.

5. Discussion

In the previous section, the RBE values for the two investigated cell types were obtained. From the outset, this was the main objective for the study. Due to the choice of experimental methods, and because the dosimetric model proves reasonably independent of cell geometry variations and target size, the measured dose-survival curves include uncertainties on the absorbed dose from internal ^{131}Cs. This allows me to state not only the RBE, but also its uncertainty. This in turn makes it evident that the RBE in my case is significantly different from 1. The surprisingly high RBE values found, necessarily demands a thorough discussion of the assumptions and methods applied with a critical comparison with literature. This is the intention in the following section.

5.1 ^{131}Cs biokinetics

As we saw in the result section (section 4.1 p. 95), the bio-kinetics of ^{131}Cs was important for both the geometrical assumptions in the S_C-value model and for the calculation of absorbed dose and dose rates. Especially the homogeneous intracellular distribution of ^{131}Cs was of importance, as it laid the ground for the use of S_C-values. Knowing the mechanism of the ^{131}Cs uptake, will help the understanding of the parameters for the uptake and release kinetics. Therefore, I will like to start the discussion with the experiment that investigated the uptake mechanism of ^{131}Cs and supported the hypotheses of its homogenous intracellular distribution.

5.1.1 Blocking of ^{131}Cs uptake by Ouabain

By this experiment the mechanism of ^{131}Cs uptake in HeLa and V79 cells was investigated. The main aim was to confirm that the ^{131}Cs was transported into the cell, and not just bound to the cell surface. In addition, the uptake mechanism strongly supported the hypothesis of a homogenous intracellular distribution of ^{131}Cs.

-the mechanism of ^{131}Cs uptake & its homogenous intracellular distribution

The HeLa and V79 cells were incubated with ^{131}Cs and different concentrations of ouabain. Ouabain is a well-known inhibitor of the Na^+/K^+-ATPase, a ubiquitous pump located in the plasma membrane of all mammalian cells. The pump normally transports three Na^+ ions out of the cell in exchange for two K^+ under the hydrolyses of one ATP-molecule [118]. The ^{131}Cs uptake by HeLa and V79 cells were significantly decreased in the presence of ouabain in the ^{131}Cs -containing medium. The maximum achievable inhibition ("bottom") was estimated to be ~11 % for HeLa cells and ~7 % for V79 cells. This strongly suggests that most of the ^{131}Cs, taken up by the cells is pumped by the Na^+/K^+-ATPase, and accordingly delivered into the cell as caesium ions. Whether the "remaining" ^{131}Cs was also transported by the Na^+/K^+-ATPase or other channels also contribute to the ^{131}Cs transport was not investigated. Several other channels in the plasma membrane (e.g. NKCC), are known to transport K^+ into the cell, and could be responsible for the uptake of the "remaining" ^{131}Cs [88]. As explained earlier (see section 2.4 p. 53), caesium (like potassium) is an alkali metal and therefore not likely to form complexes with other ions. As caesium seems to mimic K^+ in biological settings and potassium is known to only form weak bindings to biomolecules and exert its biological function primary as a charge carrier, it is reasonable to assume that intracellular ionic caesium, will behave similar to K^+ and will remain unbound and freely moveable inside the cell [88] [91][99][100].

The main compartments in a cell are the cytoplasm and the nucleus. These two compartments are separated by the nuclear envelope which is a double lipid bilayer much like the plasma membrane. However, in contrast to the plasma membrane, the nuclear envelope contains nuclear pores that allow free diffusion of smaller proteins and ions [88]. Cs^+ located intracellular will therefore be able to diffuse freely between the cytoplasm and the nucleus. No organelles are known to considerably accumulate K^+ and so, it is a fair assumption that Cs^+ will not either be accumulated in any cellular organelles [88]. This means that ^{131}Cs transported into the cell, will be freely moveable and therefore homogenously distributed throughout the cell, including the nucleus.

-IC_{50}, the ouabain concentration needed for half maximum inhibition of ^{131}Cs uptake. The differences between HeLa cells and V79 cells

In this study the ouabain concentration needed to inhibit the ^{131}Cs uptake by 50 % (IC_{50}) was found to be $2.6*10^{-8}$ M and $2.77*10^{-4}$ M for HeLa and V79 cells respectively, differing by a factor of ~10000. Similar $IC_{50(40)}$ values of ~$3*10^{-8}$ M and ~$1*10^{-4}$ M ouabain have been reported for HeLa and Chinese hamster cells respectively using ^{86}Rb, an alkali metal also transported by the Na^+/K^+-ATPase [119]. The big difference in the obtained IC_{50} values, between the HeLa and V79 cells, does therefore not reflect an experimental error. Rather this huge difference in cell sensitivity to ouabain is thought to be related to the animal species from which the cells are coming from. Similarly, a 2000 fold difference in the sensitivity to ouabain between cells originating from humans and monkeys versus hamsters and mice have been reported before, with the two latter, showing the highest tolerance. The mechanism is thought to involve differences in the binding and dissociation ability of ouabain to the α-subunit of the Na^+/K^+-ATPase [119][120][121].

5.1.2 Uptake and release of ^{131}Cs from HeLa and V79 cells.

-The rate constants k_{in}, k_{out} & k_c and their independence of the ^{131}Cs activity concentration

As said, the two main compartments in a cell are the cytoplasm and the nucleus. Because of the free diffusion of ^{131}Cs between these two compartments, the cell can be defined as one compartment. Therfore, my bio-kinetic model for ^{131}Cs (uptake and release) has only two compartments, -the cellular compartment (intracellular) and the medium (extracellular) (Figure 5.1). k_{in} and k_{out} represent the microscopic rate constants in which ^{131}Cs is transported into and out of the cell respectively. k_c represents the resulting exponential constant, describing the change in intracellular ^{131}Cs concentration. As shown in the results section (section 4.1 p. 95) the time course of ^{131}Cs release and the change in intracellular ^{131}Cs activity concentration were both fitted to the exponential equations ($A = A_0*(1 - e^{-t*k_c})$) and ($A = A_0** e^{-t*k_{out}}$) and k_c and k_{out} were respectively found to be 1/283 min^{-1} and 1/339 min^{-1} in HeLa cells and 1/204 min^{-1} and 1/256 min^{-1} in V79 cells.

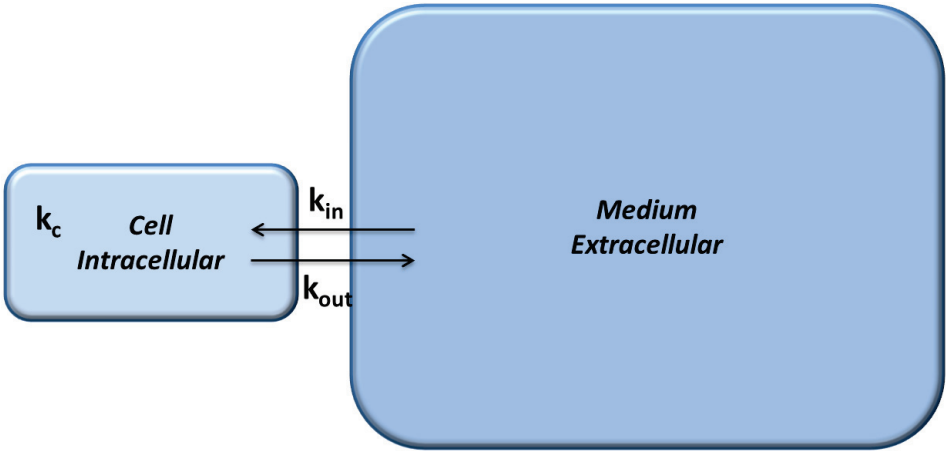

Figure 5.1 Representation of the two compartments and the constants relevant for the bio- kinetics of ^{131}Cs

Due to the free diffusion of intracellular ^{131}Cs between the cytoplasm and the nucleus, the ^{131}Cs bio-kinetics can be described by a two compartment system; an intracellular compartment and an extracellular compartment. The change in intracellular activity concentration of ^{131}Cs described by k_c, is determined by the two rate constants; k_{in} & k_{out}

The k_c and k_{out} values were obtained from experiments in which the ^{131}Cs activity concentration used was much lower (~1/500 (HeLa cells) and 1/250 (V79)) than the activity concentration used to study the radiotoxicity and RBE. As these rate constants were directly used in the absorbed dose calculations in the latter experiments, it was important to consider if the obtained rate constants (k_{in} & k_{out}) were dependent on the ^{131}Cs activity concentration, and if they would significantly change when the activity concentration was increased. Such a change could be due regulations of the "transitions rate" of the Na^+/K^+-ATPase or to saturations in ^{131}Cs uptake or release.

The transition rate of the Na^+/K^+-ATPase is mainly regulated by the intracellular Na^+ concentration [122] and since this concentration do not change with the increase in ^{131}Cs activity concentration, it seems reasonable to assume that the transition rate of this pump will not be affected. The highest ^{131}Cs activity concentration used was 17 MBq/ml which correspond to a chemical caesium concentrating of ~35 nM. (for calculations see appendix 8.1 p. 194). Due to the way ^{131}Cs was produced and the subsequent chemical separation, the specific activity of the ^{131}Cs solution added the

medium was close to the theoretical maximum. As the potassium concentration in the normal growth medium is 4-5 mM [123] the addition of ^{131}Cs will not change the combined concentration (in the medium) of the two alkali metals, K^+ and Cs^+. Accordingly, ^{131}Cs will only constitutes a very small fraction (10^{-5}) of the ions pumped into the cell by the Na^+/K^+-ATPase and the transport of ^{131}Cs should not become saturated as this concentration. It therefore seems reasonable to assume that the rate constant for ^{131}Cs uptake (k_{in}) does not change with the increase in ^{131}Cs activity concentration used.

The precise mechanism resulting in ^{131}Cs release from the cells was not investigated. However, measurements showed an exponential decrease in intracellular ^{131}Cs activity concentration (after removal of ^{131}Cs from the medium) indicating that a constant fraction of the intracellular ^{131}Cs was released from the cells per unit time. The maximum intracellular caesium concentration was only 1-2 µM (for calculations see appendix 8.1 p. 194), whereas the normal intracellular K^+ concentration is 140 mM [88]. A "release mechanism" for ^{131}Cs similar to that of potassium, should therefore not become saturated at this concentration. Together, this suggest that the rate of ^{131}Cs release from the cells, is directly proportional to the probability of a ^{131}Cs ion reaching the plasmamembrane, which again, for a homogenous distributed ion, is directly proportional to the intracellular ^{131}Cs concentration. It therefore seems reasonable to assume that the rate constant for ^{131}Cs release (k_{out}) does not change with the increase in ^{131}Cs activity concentration.

Since the rate constants, k_{in} and k_{out}, were not influenced by the increase in ^{131}Cs activity concentration and since k_c only depends on these two constants, the measured k_c and k_{out} values could be safely applied to the experiments investigated the radiotoxicity of ^{131}Cs. These k_c and k_{out} values were there used to calculate the absorbed dose by modelling the total time curve of uptake and release (and thus the cumulative activity) using only a single point of observation.

5.1.3 Chemical cytotoxicity of caesium

As ^{131}Cs was used to investigate the radiotoxicity and RBE of Auger emitters, it is of course essential that the cytotoxicity observed is due to the radiation and not direct chemical effects. Caesium is known to be cytotoxic [92]and an experimental control for this chemical cytotoxicity could have been made using stable ordinary caesium. However, the highest caesium concentration used was ~35 nM and caesium toxicity has only been reported at a much higher concentrations (119 µM) [124]. Moreover, the caesium concentrations applied in my experiments were at the level of the natural caesium concentration in seawater [125]. At this level the chemical toxicity is excluded as a confounding factor.

5.2 S_C-values

One of the purposes of this work was an effort to reduce the uncertainty in the absorbed dose calculations. By using an Auger emitter (^{131}Cs), which is homogeneously distributed throughout the cell, and by applying this to a confluent cellular monolayer, it was possible to use my so called S_C-values. The shift from a model with isolated cells to a confluent cell layer and the use of an even activity distribution throughout the cell layer made the calculated absorbed dose become almost independent of cell and nuclear sizes. It significantly reduces the uncertainty in absorbed dose calculated related to the use of the MIRD cellular S-values.

5.2.1 Calculation of the ^{131}Cs S_C-values, S_C(N←C) for HeLa and V79 cells in confluent cellular monolayers

The geometry used for the S_C-value calculations was a 100 % confluent cellular monolayer, in which the ellipsoid nuclei were located. The source compartment was the whole cellular monolayer, and the target compartment, the nucleus.

The S_C-values used for this work differ from the MIRD cellular S-values by two important features;

1. The geometry used in the S_C-value calculations is an infinite (in x and y direction) confluent cellular monolayer, and not two concentric spheres in isolation (the geometry used in the MIRD calculations)
2. The unit of the S_C-values; being Gy/(Bq*Sec)/pL, and not Gy/(Bq*Sec),which is the unit used by MIRD.

The important parameters for the S_C-value calculations using this geometry and unit turns out to be;

- The confluency of the cells
- The height of the cell layer and

- The size (volume), shape and orientation of the nucleus (to a lesser degree).

-Confluency (denseness) of the cell cultures

The geometry used in the S_C-value calculations assumes a 100% confluent cellular monolayer. This confluence/denseness was verified by confocal microscopy.

As could be in Figure 4.7 (p. 108) and Figure 4.8 (p. 109) the cells lie so close together that no space is left in between. This degree of confluency was confirmed by direct microscopy of the cell layer before all of the internal irradiation experiments. As the ^{131}Cs is equally distributed between cells and between the nucleus and the cytoplasm, it becomes irrelevant where one cell ends and the next one begin. Instead the geometry can be thought of as a continuous "sea" of cytoplasm in which the nuclei are positioned (Figure 5.2). In this way the geometry and size of the individually cells can be ignored. In addition, the dose deposition becomes constant in all x and y planes with only a small axial (z-direction) variation. As the nuclei are necessarily near the middle of the cell layer the S_c –values approaches the theoretical maximum value of $9.41*10^{-4}$ Gy/(Bq*Sec)/pL .

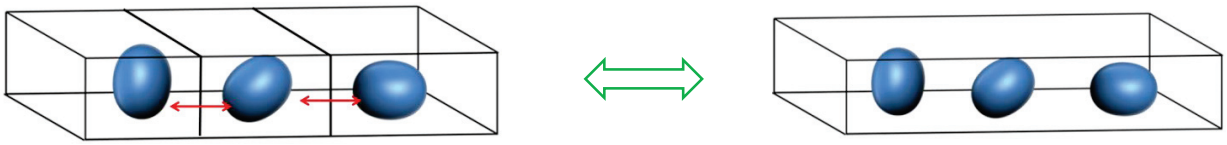

Figure 5.2 Simplification of the cell culture due to the confluency

As the cells are 100 % confluent and the ^{131}Cs is homogenously distributed throughout this cell layer, the distinction between one cell and the next becomes irrelevant. Instead the cell culture geometry can be simplified to a continuous "sea" of cytoplasm in which the nuclei are positioned. The size and shape of the individual cells can thereby be ignored.

-Height of the cellular monolayer

Inevitably, some of the Auger electrons manage to escape either the top or the bottom of the cell monolayer. Accordingly the axial (z direction) dose profile is not completely constant (Figure 4.12 p. 114). The axial dose distribution depends on the height of the cellular monolayers. These heights were measured to be 10 µm and 8 µm for HeLa and V79 cells respectively, using the Z-stack images

obtained by confocal microscopy (Figure 4.7 p. 108 and Figure 4.8 p. 109). As was shown in the results section (Figure 4.12 p. 114) the axial distribution of dose to any small voxel changes less than 10% over most of the cell layer height. The axial dose distribution for the HeLa and V79 monolayers were quite similar. The only difference between the calculations of the two axial dose distributions (HeLa and V79), were the heights of the monolayers. These heights however were not easy to measure precisely due to the fundamental limitation of resolution in the confocal microscope used. The values may have been a 1-2 µm lower or higher. However, an increase in the HeLa monolayer height from 10 µm to 12 um only increase the mid layer dose by 3 %. (found by convolution using a 12 µm high cellular monolayer). Decreasing the HeLa cellular monolayer height by 2 µm from 10 µm to 8 µm just brings us to the V79 situation and leads to a 4 % decrease of mid layer dose. Finally a reduction of V79 monolayer height by 2 µm leads to about a 5 % absorbed dose drop. When averaged over many cells and many nuclei with varying axial lengths, the total effect on the resulting S_C values is believed to be smaller than 3-5 %. In the uncertainty budget for the delivered internal doses, this has been accounted for as a 3% (HeLa), respectively 7 % (V79) uncertainty in S_C value.

-*Size, shape and orientation of the cellular nuclei*

The size and shape of the HeLa and V79 nuclei were also found using the Z-stack images obtained by confocal microscopy. In general the nuclei displayed an ellipsoid shape rotated at different angles in respect to the x-y plane. This rotation resulted in a difference in the distance to the “top” and “bottom” of the cellular monolayer and as the axial dose distribution was not constant this had a small effect on the cellular S_C -values (Figure 5.3). This rotation effect on S_C -values is actually contained in the variation of calculated S_C -values for the actual nuclei dimensions measured (see Figure 4.14 and Figure 4.15 page 118).

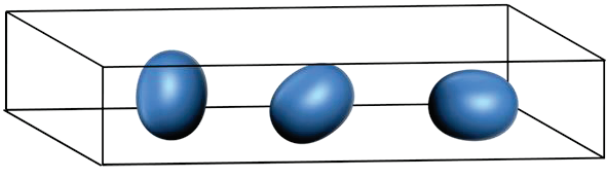

Figure 5.3 Representation of different orientations of nuclei in the cellular monolayer

Illustration of different orientations of the nuclei. The nucleus furthest to the left has sub-volumes closer to the surfaces of the monolayer and will receive a smaller dose than the nucleus to the right.

The nuclear volume for both HeLa cells and V79 cells showed large variation, ranging from below 0.1 pL to above 1.0 pL. The average nucleus volume for HeLa and V79 cells was determined to be 0.630 pL and 0.400 pL respectively. These values fit well with previously reported values of around 0.2 pL to 0.7 pL for HeLa cells [126][127][128] and around 0.5 pL and 0.8 pL for V79 cells [129][130]. The S_C-values for the 30 HeLa nuclei and the 50 V79 nuclei were calculated (Figure 4.14 p. 118 and Figure 4.15 p. 119) based on their measured axis lengths. Despite the big variation in the nuclei volumes, the S_C-values changes by less than 1% for HeLa and less than 2.5 % for V79 .This "constancy" of the S_C-values with nuclei of very different sizes is a beneficial consequence of the unit of the S_C-values.
As seen above, the S_C-values calculated turn out to be "robust". By this I mean that the final absorbed dose from internal exposure becomes relatively independent of a lot of biological variation in size, shape and volumes of cells and nuclei. In contrast, the geometry used by MIRD (two concentric spheres), makes their cellular S-values very geometry dependent and sensitive to small changes in cellular and nuclear size [17]. It can be illustrated by applying the reported variation in HeLa nuclear volumes ranging from around 0.2 pL to 0.7pL to the MIRD formalism. This will give a variation of the MIRD cellular S values by around a factor 2 (S(N←C) for ^{131}Cs (see values in appendix 8.2.1 p. 196), directly introducing a similar factor 2 variation in absorbed dose. Such an unnecessary variation could easily confound the determination of RBE by biasing the calculated internal absorbed dose.

5.3 Radiotoxicity and relative biological effectiveness of ^{131}Cs

To investigate the radiotoxicity and the relative biological effectiveness of ^{131}Cs in HeLa and V79 cells, both the γH2AX and the clonogenic cell survival assay were used. As we saw in the results section, the estimated RBE-values obtained by these two assay differed by a factor of 4, from a RBE of 1 using the γH2AX assay, to a RBE of 4.5 (HeLa cells) and 3.8 (V79 cells) using the clonogenic cell survival assay.

5.3.1 Radiotoxicity of intracellular and extracellular ^{131}Cs decays

-The importance of auger emitter location and dose rate

In this experiment the importance of the location (extracellular & intracellular) of the ^{131}Cs was investigated. The HeLa cells were incubated with ^{131}Cs either in the presence or absence of ouabain. As we saw in the results section (Figure 4.4 p. 102), ouabain significantly inhibited the ^{131}Cs uptake, and so in the cells incubated with ouabain, the uptake and consequently the intracellular ^{131}Cs activty concentration were considerably decreased. This decrease was also evident from Figure 4.20 (p.131). However, as the HeLa cells incubated with ouabain did take up a small amount of ^{131}Cs, they were also exposed to intracellular ^{131}Cs decays. The extracellular ^{131}Cs activity concentration and the incubation time were however the same for the two exposures.The radiotoxicity was evaluated by γH2AX and the results given γH2AX response over controls levels. (For further elaboration on the data presentation of this specific γH2AX assay see section 3.1 p. 59).

As was seen in Figure 4.19 (p. 130) HeLa cells in which ^{131}Cs uptake was partly blocked showed almost no increase in their γH2AX response after 380 min and 480 min of incubation with ^{131}Cs. In contrast, cells in which the ^{131}Cs uptake was not blocked showed an increase in their γH2AX response with incubation time and reached a 3.5 fold increase over control levels after 480 min. This showed that

the radiotoxicity of ^{131}Cs is very dependent on its cellular localization, having almost no effect when it is located outside the cell.

This result is in good agreement with what has previously been reported by others and with the current understanding of the underlying mechanism of the radiotoxicity of Auger emitter decays [28]. Several authors have reported a much lower radiotoxicity of various Auger emitters (^{125}I, ^{111}In, ^{201}Ti), when these are located extracellular instead of intracellular (either distributed throughout the cell or bound to the DNA) [131][132][133][134]. Due to the short range of (most of) the Auger electrons, when the decays happens extracellularly only the K-and L-Auger electrons, will be able to reach the nucleus, leaving the possibly most harmful Auger electrons (MXY, CK & SCK) to deposit their energy outside the nucleus [82] [86].

Cells incubated in the presence of ouabain were however still able to take up some ^{131}Cs (Figure 4.20 p. 131). The absorbed dose to the cells, received from this intracellular ^{131}Cs, was calculated and their yH2AX response at the different absorbed doses was shown in Figure 4.19 (p. 130). In contrast to what might be expected, these cells did not show an equivalent increase in yH2AX response (equivalent to the level shown by the cells incubated in the absent of ouabain (”non-ouabain incubated cells”)), even though they received up to 2 Gy (from intracellular ^{131}Cs decays). This “lack” in yH2AX response, might be explained by the dose rate effect. As the “non-ouabain” incubated cells received an absorbed dose of 1-2 Gy over 2-4 hours, the ouabain incubated cells received a similar absorbed dose but over 6-8 hours. The dose rate for the ouabain incubated cells (~0.2 Gy/h) was therefore 2-3 times lower than for the “non-ouabain” incubated cells. The dose rate effect is related to the repair of sublethal DNA damage [20]. It is not implausible that cells receiving a dose of 1-2 Gy with a dose rate of ~0.2 Gy/h, would be able to repair all the sublethal DNA damage and therefore not show any increase in yH2AX response level. However, the increased radiotoxicity of auger emitters are thought to be a consequence of exactly these more harmful DNA DSBs (LMDS, complex DNA damage) and therefore an inability of cells to repair these DNA DSB is also plausible. This ability (or inability) to repair DNA damage caused by Auger emitters is still open for debate[6] [28] [52]. The shoulder on clonogenic cell survival curves, characterize the repair of sublethal damage, and both

survival curves with and without shoulders (after exposure to Auger emitters) have been reported [62][20] [63][22]. The clonogenic cell survival curves (for the ^{131}Cs exposed cells) in this work (Figure 4.27 p. 145 and Figure 4.28 p. 148) did not show any shoulder, thus indicating that the repair of sublethal DNA damage was not pronounced.

Another reason for the "low" γH2AX response of the ouabain incubated cells, could be related to an interplay between a potential effect of ouabain on DNA damage repair, and the biological assay used (γH2AX). Ouabain is believed to affect the cellular sensitivity to ionising radiation. The mechanism is not yet known, but is thought to be related to the activation of DNA damage response (DDR), including cell cycle blockage and inhibition of sublethal DNA damage repair [121] [135]. The repair of sublethal DNA damage and especially the fast repair has been reported to significantly decrease in HeLa cells exposed to 10-100 nM of ouabain (8.45 µM ouabain were used in this experiment) [135]. Depending on the underlying mechanism of this inhibition of sublethal DNA damage repair, it could explain the "low" γH2AX response observed.

5.3.2 Relative biological effectiveness of ^{131}Cs

The RBE of the ^{131}Cs was investigated using two different assays; γH2AX and clonogenic cell survival assay.

5.3.2.1 RBE of intracellular ^{131}Cs evaluated using γH2AX assay

In this experiment the relative biological effectiveness of ^{131}Cs was investigated in HeLa cells using the γH2AX assay. HeLa cells were either exposed to intracellular ^{131}Cs decays or external γ-rays. The increasing dose rate, resulting from the increasing uptake of ^{131}Cs was mimicked in the external γ-rays exposure (as explained in section 4.4.2.1.1 p. 132). In order to eliminate any dose rate effects in the obtained RBE it was highly prioritized to use the same dose rate profiles for the two exposures.

As was presented in the results section (Figure 4.22 p. 135), both the ^{131}Cs exposed and the γ-ray exposed cells showed a similar increase in their γH2AX response with increasing dose. In both cases the exposed cells reached a 3.5 fold increase over the control levels after receiving 5-6 Gy. No

significant difference in radiotoxicity of intracellular ^{131}Cs decays and external γ-rays was observed using the γH2AX assay and a RBE of 1 for ^{131}Cs was found.

The increase in the percentage of activated cells only reached a 3.5 fold increase over control levels after receiving 5 Gy (from either ^{131}Cs or γ-rays exposures). This increase was lower than expected. However, a ~4.5 fold increase in the γH2AX response compared to controls after 5 Gy acute exposure (using a dose rate of 1.5 Gy/min) to external γ-rays was also observed (data obtained from positive controls and therefore not shown) and so, this 3.5 fold increase seemed reasonable, considering the lower dose rate used. However it is noteworthy that this positive control (5 Gy external acute γ-ray exposure) did indicate that a RBE below 1 might be found if the dose rate was not considered.
The proportion of H2AX (histones) of the total H2A histones, is only 2% in HeLa cells. This is quite low compared to other cell lines in which H2AX constitute between 2-20% of their total H2A histones [136]. This could explain the relatively low increase in the level of γH2AX response observed with increasing absorbed dose. HeLa cells might therefore not be the most suitable cell line, for this DNA damage assay and using a cell line with a higher proportion of H2AX (histones), might increase the validity of the obtained result.

The obtained RBE-value of 1 is in the range of what has previously been reported, when the Auger emitter is located outside the cell or in the cytoplasm [28]. Hofer et al found that radiotoxicity of ^{67}Ga located in the cytoplasm was comparable to the radiotoxicity of ^{3}H bound to the DNA [137]. However as the ^{131}Cs was homogenously distributed throughout the cell, and therefore also located in the nucleus a higher RBE value than 1 was expected. Even RBE-values of 1.4 and 1.9 for ^{125}I and ^{103}Pd respectively, were found by Ling et al when these Auger emitters were located extracellularly [138]. However, it is well known, that the RBE is an experimentally obtained value that often differs between studies using different biological assays, endpoints, cell lines etc [13]. Therefore, the "lower than expected and otherwise reported" RBE-value obtained here, could be explained by the different biological assay used. Surely, as will be seen below the γH2AX assay might not be the most suitable

for investigating the radiotoxicity of Auger emitters, and the biological assay used can have a great influence on the obtained RBE.

It is believed that the DNA damage produced by high LET radiation and Auger electrons, can be more complex and induce LMDS and so is more difficult for a cell to repair. This can result in an increase in the size of the γH2AX foci, which might also stay phosphorylated for a longer time. However, this increase in foci size and "existence" time might be difficult to identify [6][48] [52]. As explained earlier (section 3.1.1 p. 59) the γH2AX assay used in this work, measures the total intensity (per cell) of a fluorescent antibody bound specifically to phosphorylated serine 139 on histone 2AX (γH2AX). Therefore, this assay should (in theory) be able to reflect, an increase in γH2AX foci size by an increased fluorescence signal. However, due to the "grouping" of the cells in two (three) categories, any possible differences in γH2AX foci size would not be evident. The γH2AX assay still presents the overall increase in number of γH2AX foci present in a cell. However, the number of DNA DSBs (and so γH2AX foci), is not necessarily a good indicator for the severity of the DNA damage produced. This is especially evident when comparing the more detrimental complex and clustered DNA damage produced by high LET radiation, with the simple DNA damage produced by low LET radiation[52]. The γH2AX assay shows the number of the DNA DSBs produced, but tells little about the severity of the produced DNA damage and about the further fate of the cell. This assay may therefore not be the most suitable assay when investigating radiotoxicity of high LET radiation and Auger emitters, and especially not when comparing the detrimental effects of different radiation qualities.

5.3.2.2 RBE of intracellular ^{131}Cs evaluated using clonogenic cell survival

In this experiment the relative biological effectiveness of ^{131}Cs was investigated in HeLa and V79 cells using clonogenic cell survival. The HeLa or V79 cells were either incubated with ^{131}Cs or exposed to external γ-rays. The increasing dose rate, resulting from the increasing uptake of ^{131}Cs was mimicked in the external γ-ray exposures (as explained in section 4.4.3.1 p. 136). Using the same dose rate profiles was highly prioritized, in order to eliminate any dose rate effect in the obtained RBE. In addition, to see a potential effect of the dose rate, cells were also exposed to external acute γ-rays

using a dose rate of 1.5 Gy/min. However, these cells were exposed under different conditions and so care should be taken when drawing conclusions from these survival curves. Still, the data can give a good estimate for the relative importance of the dose-rate effect. To minimise confusion these external γ-ray exposure will be referred to as acute exposures, while the external γ-ray exposures using the matched dose rate profile, will be referred to as protracted exposures.

5.3.2.2.1. HeLa cells

As was shown in the results section (Figure 4.27 p. 145), there was a big difference in the survival fraction between the intracellular ^{131}Cs exposed cells and the protracted external γ-ray exposed cells. Due to the limited range of absorbed doses used for these exposures, it was difficult to interpret the shapes (shoulder or no shoulder) of the survival curves and they were therefore fitted to the linear model. Consequently, the RBE is not dependent on which endpoint (% survival fraction) is used and a RBE of 4.5 was found. The survival curve for the acutely exposed HeLa cells, show the expected shoulder and was fitted to the linear quadratic model. No pronounced dose rate effect was found, and so using the acute exposed cells as a reference radiation, would give a similar RBE.

The obtained RBE of 4.5 is a lot higher than expected. Normally, a RBE of approximate 4 is expected for Auger emitters intercalated or otherwise bound but not incorporated into the DNA [62][23][139][24]. This high RBE could not be explained by an unreasonable low survival fraction of the cells exposed to the reference radiation (protracted external γ-ray exposure), as these cells had a D_{37} of 2.6 and a 10 % survival fractions at 6 Gy. This is around the normal values seen when using an average dose rate of ~4 mGy/min for low LET exposures [20]. Furthermore, the acute (1.5 Gy/min) γ-ray exposed cells, had a similar survival fraction at 10% after receiving ~5 Gy and so, the dose rate did not seem to have any impact on the survival fraction in that absorbed dose range. The high RBE-value obtained must therefore be a consequent of the very low survival fraction of the ^{131}Cs exposed cells. This was also confirmed by the very low D_{37} of 0.58 found. A D_{37} of 0.58 is in the range of what would be expected for Auger emitters bound or incorporated into the DNA and not when the Auger emitter is distributed throughout the cell (as in this work)[22][23][140]. However, due to the narrow range of

absorbed doses used, the "D_{37}" was found by extrapolation, and are therefore sensitive to small changes in the slope of the survival curve.

Because of the low plating efficiency of the HeLa cells ($3\text{-}6*10^{-1}$) and their radiation sensitivity, the amount of cells seeded (for the clonogenic cell survival assay) was very high. This sometimes made it difficult to separate the colonies from each other, and two sub-colonies (less than 50 cells each), lying close to each other, could have been mistaken as one colony, and therefore included in the survival fraction. Furthermore, the high amount of dead cells, and the lack of a midway medium change, could have affected the cells and their ability to form colonies. Yet, a similar amount of cells was seeded after the different exposures and so if these conditions had an influence on the number of colonies formed, they should have affected the survival fraction of both the ^{131}Cs and the γ-ray (protracted) exposed cells.

However, it is noteworthy that the clonogenic cell survival assay only scores the fraction of cells able to form colonies. Cells that have survived, but lost their ability to divide continuously e.g. cells in senescence, are thereby not contributing to the survival fraction. Almost no colonies were observed in the ^{131}Cs exposed samples, but many single cells, which displayed a senescence-like morphology were still present (Figure 4.25 p. 142). These senescence-like cells were also present (however fewer) in the samples exposed to the reference radiation (protracted external γ-ray exposure), but were almost missing in both controls. If these cells were indeed cells in senescence, the very low clonogenic survival fraction observed (for the ^{131}Cs exposed cells) and the high RBE obtained, could be a cause of an increased ability of ^{131}Cs over γ-rays, to drive cells into senescence.

5.3.2.2.2. V79 cells

As was shown in the results section (Figure 4.28 p. 148), there was a big difference in the clonogenic cell survival of the intracellular ^{131}Cs exposed and protracted external γ-rays exposed cells. As three different absorbed doses around 3 Gy, 7 Gy and 10 Gy were used in the intracellular ^{131}Cs exposure it was possible to deduce the shape of the survival curve, being a straight line (on a semi-log plot) with

no shoulder. It was therefore fitted to the linear model. In contrast, a narrower range of absorbed doses were used for the protracted external γ-ray exposures (reference radiation), and so the shape of this survival curve was less clear. However, as the few data points do suggest a linear curve with no shoulder, and as this model uses the fewest parameters, the survival curve was also fitted to the linear model. Again, the obtained RBE-value is not dependent on which endpoint (% survival fraction) is used and a RBE-value of 3.8 was calculated. The survival curve for the acutely exposed V79 cells, showed the expected shoulder and was fitted to the linear quadratic model. Using the acutely exposed cells as reference radiation, would give a RBE-value of 1.3 at 10 % survival fraction.

Again, the obtained RBE-value of 3.8 is a lot higher than expected. A RBE-value of 3.8 is in the order of what has previously been reported for Auger emitters bound (but not incorporated) to the DNA [62][23][139][24]. This high RBE-value could again not be explained by an exceptionally high survival fraction of the protracted γ-ray exposed cells (reference radiation). These cells had a survival fraction of 60 % after 5 Gy and a D_{37} of 10 Gy which seems reasonable giving the average dose rate of ~ 5 mGy/min [141][142]. However, the cells exposed to acute (1.5 Gy/min) γ-rays had a much lower survival fraction of only 30 % after 5 Gy and a D_{37} of 4.5 Gy, showing a significant dose rate effect in V79 cells. As so, if the dose rate effect had not been considered and the acute γ-ray exposures with a dose rate of 1.5 Gy/min would have been used for comparison, the obtained RBE value would have been only 1.3. These results demonstrate the importance of using similar dose rates for the test and reference radiation when studying the RBE.

Unfortunately the γ-ray exposed (protracted) cells were allowed to from colonies for 8-9 days, whereas the ^{131}Cs exposed cells were incubated for 7 days, which could have had an influence on the obtained survival fraction. However, as the cell cycle time of V79 cells is ~12 hours [114], the ^{131}Cs exposed cells would still have had time to produce a colony of 50 cells, even if they had experience an extensively cell cycle delay. Moreover, most of the colonies produced by V79 cells, consisted of significantly more than 50 cells (the minimum amount of cells in a colony to be considered a survivor), and so a “extended” incubation time of 1-2 more days was not thought to influence the result significantly.

5.3.2.3 The difference between HeLa cells and V79 cells and the results obtained.

The RBE-values obtained for HeLa and V79 cells using clonogenic cell survival were very similar, being 3.8 and 4.5 respectively. Yet, comparing the data from the two different cell lines, several differences were observed. The HeLa cells generally displayed a much lower survival fraction than the V79 cells, while the V79 cells show a significant dose rate effect, which was not observes in HeLa cells. In addition, the senescence like morphology, which was seen in the HeLa cell samples, was not present in the V79 cell samples.

5.3.2.2.3. Colony and cellular morphology

Many of the HeLa cells showed a senescence like morphology, which was not seen in V79 cells. The induction of senescence in HeLa cells, but not in V79 cells might be due to difference in their cell cycle check points and response to DNA damage [143][144]. In response to DNA damage, the DNA damage response mechanism (DDR) will be activated in both cell lines. This will in turn activate p53, an important effector that is involved in cell cycle arrest and induction of senescence. However both cell lines lack a well-functioning p53 protein. Other proteins are however also involved in cell cycle checkpoints, cells cycle arrest and induction of senescence. The protein Retinoblastoma (pRb) plays an important role in the restriction point present in the G1 cell cycle phase and may also be a downstream effector in the DNA damage response [69]. Studies have shown that human cell lines and cell lines from mice differ in their ability to surpass senescence upon DNA damage. This difference may lie in a difference in activation of two different pathways, one involving p53 and one involving pRb. Human cell lines, have shown to still undergo senescence after DNA damage, if just one of these two proteins (p53 or pRb are present). In contrast, if not both proteins are functional, murine cells line are able to surpass senescence [143][144]. As murine cells and hamster cells are quite similar, it is likely that this mechanism is also present in V79 cells. This could explain why we observe senescence cells in the HeLa cell samples but not in V79 cell samples.

5.3.2.2.4. Dose rate effect

Another difference between the two cell lines was the effect of dose rate on clonogenic survival. For HeLa cells no significant difference in survival fraction between the cells exposed to γ-rays, acutely or protracted were observed. However, if a broader absorbed dose range had been applied in the protracted γ-ray exposure, a dose rate effect might have been observed). In contrast, the survival fraction of V79 cells decreased dramatically, when the dose rate was increased. It has been shown that a dose rate of 0.372 Gy/h is needed to arrest to HeLa cells while a dose rate of 2.7 Gy/h was needed to arrest V79 cells [142]. This might explain the difference in dose rate effect between the two cell lines. The highest dose rate used for the protracted γ-ray exposure was 0.492 Gy/h. This dose rate is above the one needed to arrest HeLa cells, and so both the HeLa cells exposed to the lower (protracted) and the higher (acute) dose rate, could be arrested. In contrast, the dose rate needed to arrest V79 cell was much higher than the 0.492 mGy/h used in the protracted γ-ray exposures (and in the ^{131}Cs exposed cells, (~0.8 Gy/h)), and so these V79 cells would not become arrested. In contrast the acute γ-ray exposed cells received a much higher dose rate (1.5 Gy/min or 90 Gy/h), which could arrest the cells and significantly decrease their clonogenic cell survival fraction.

5.4 Relative Biological Effectiveness of Auger emitters

The RBE for ^{131}Cs homogenously distributed throughout the cell were found to be 1 when using the γH2AX assay and around 4 (4.5 for HeLa cells and 3.8 for V79 cells), when using the clonogenic cell survival assay. Based on earlier reported RBE values for Auger emitters located intracellularly, a RBE-value around 2 had been expected. The RBE-value of 1 was therefore lower than expected, while the value around 4 was much higher than expected. Due to the distinct qualities of the two biological assays used, the RBE-values obtained by clonogenic cell survival assay were considered to most accurately reflect the radiotoxicity of intracellular Auger decays. These RBE-values are even conservative, as a 17 % higher (compared to NuDat 2.7) total energy per decay was used in the absorbed dose calculations. If this normalisation had not been applied, the calculated absorbed dose would have been 17 % lower and accordingly the obtained RBE- values 17 % higher.

Unfortunately, not many (if any) have investigated the RBE for Auger emitters distributed homogenously throughout the cell and no one has used ^{131}Cs. It is therefore a bit difficult to compare the RBE-values obtained in this work, with previously reported ones. In addition, the dependency of the RBE on the biological assay and endpoint used, makes the comparison (of RBE values) only more complicated. A big difference in obtained RBE-values for seemingly similar experiments, using different biological assays have also been reported before, and is an inherent property of the RBE concept [145][24]. Nonetheless, the RBE value of 1 (found in this work) is in the range of what would be expected (and has previously been reported), for Auger emitters located either extracellularly or purely in the cytoplasm [28][137][138]. As the ^{131}Cs in this work was also located in the nucleus and not only in the cytoplasm, a RBE value above 1 had been expected. In contrast the RBE-values around (3.8 & 4.5), also obtained in this study, were much higher than expected as these are in the range of what have previously been reported for Auger emitters bound to (but not incorporated into) the DNA [21] [62][24] [23]. Together with RBE-values for Auger emitter located throughout a cell (however not homogenously) [146][147][148], a RBE-value around 2 had been expected in this work.
As the RBE is dependent on several parameters, the cause of the difference in the obtained RBE-values in this work, and the ones reported in the literature can be many. However, one clear possible

cause could lie in the absorbed dose calculations. For Auger emitters the absorbed dose is difficult to estimate, and so a big uncertainty these calculation must be incorporated into the obtained RBE-values. Often the tabulated MIRD cellular S-values are used for the absorbed dose calculations and several combinations of source and target compartments are calculated and listed for several radioisotopes [17]. However, the MIRD cellular S-values are especially sensitive to changes in the cellular or nuclear size. Unfortunately, as also showed in this work, the size of a nucleus in a cell population varies greatly, which raises a problem in deciding which nucleus size and consequently cellular S-value to use, for the absorbed dose calculation. The volume of the nuclei measured in this work, varied from below 0.1 pL to above 1 pL. The corresponding tabulated MIRD cellular S-values for this range in nucleus size differs by several factors (1.3-6,5) (for ^{131}Cs, S(N←C), (for these cellular S-values see appendix 8.2.1 p. 196)), which will result in a similar variation in the calculated absorbed doses. The cellular S-values as tabulated by MIRD might thereby give a very big uncertainty in the absorbed dose calculations and hence the obtained RBE-value. This could also be an explanation for the diverse RBE-values reported in the literature and might be one of the reasons why we obtained a higher than expected RBE-value.

In relation to the absorbed dose, the dose rate is known to influence the biological response and hence the RBE. When using radiochemicals the bio kinetics (uptake and release of the radiochemical), often results in a chronic or protracted exposure of the cells, and the dose rate between the test and reference radiation can be very different (if not matched). As pointed out by Howel et al [149] and Rao et al [150], this difference in dose rate and especially acute versus chronic (protracted) exposures, can have a big influence on the obtained RBE. A RBE-value of ~20 for DNA incorporated ^{125}I, were for example reported by Howel et al, when matching the dose rate with chronic exposure, in contrast to the RBE-value of ~9 he obtanied, when acute exposure was used (as the reference radiation) [149]. Rao et al though, found the reverse effect, in which the radiotoxicity increased by a factor 3, when the dose rate decreased [150]. Both results illustrates that the dose rate can have a big influence on the RBE-value obtained. Likewise, this work also showed a difference in the radiotoxicity obtained when acute exposures instead of protracted exposures were used (as the reference radiation). A RBE-value of ~4 were found when the dose rates were matched (protracted exposure), in contrast to the RBE-

value of 1.3 when acute exposure was used. The effect was visible for V79 cells, but not for HeLa cells, which most likely is due to the chosen dose rates and the inherent differences between the cell types, as explained in section 5.3.2.2.4 (p. 170). Interestingly, the "RBE-value" of 1.3 obtained in this work, when using acute exposure as the reference radiation, is closer to what I initially expected based on previous reported RBE-values. Unfortunately, matching the dose rate or at least using a chronic exposure as the reference radiation, when investigating the RBE of Auger emitters is often not applied [22] [23][24] [151]. This, feature could also be an explanation for the higher than expected RBE-value obtained in this study. In addition, it might also explain some of the seemingly paradoxical RBE-values below 1, that has been obtained in some studies [151][148].

However, more interesting is it that Auger emitters are often referred to as a homogenous group, even though their decay characteristics are very different [13][25]. Paradoxically, it is the very low energy electrons (MXY Auger and higher shell branches, plus CK and SCK), which can safely be ignored in conventional absorbed dose calculations , that are believed to be responsible for the severe DNA damage and high biological effectiveness of Auger emitter decays [15]. The number of electrons emitted and their energy distribution will have a great impact on the obtained RBE-value. Most experiments have investigated the RBE of ^{125}I, ^{111}In and ^{99m}Tc, which on average emits 24.9, 14.7 and 4.0 electrons per decay with average energies of 849 eV, 2215 eV and 3159 eV respectively [86][152]. The great range in number of electrons released and their average energies (or rather energy distribution), might also explain some of the variations in the reported RBE-values. In comparison, ^{131}Cs releases on average 10.1 electrons with an energy average of 613eV (Personal communication with Boon Q. Lee). The combination of a high number of electrons released per decay and low average electron energy, is believed to cause the most severe DNA damage. Hence ^{125}I is thought to be the most potent Auger emitter of the four [152]. This also corresponds with studies showing a lower radiotoxicity of ^{99m}Tc compared to the ^{111}In [153],and the general lower radiotoxicity obtained for ^{99m}Tc [150][154]. However, in order to better understand this complexity and biological response following Auger emitter decays, there is a need for microdosimetry. The use of microdosismetry is also the official recommendation from ICRP in assessing risk estimation from Auger emitters [13]. Unfortunately, there are several factors needed for proper microdosimetric

calculations/simulations, for which the details are not known. These include the distribution of the actual number of electrons and their energies emitted per individual decay, along with the angular correlations in which these electrons are emitted. In addition, the size of the "true" biological target needed to convert energy deposition into dose is unknown, and might even dependent on cell type [87]. Before these questions have been answered, microdosimetry might not be able to precisely calculate the energy deposition distribution and predict the biological effect of from Auger emitter decays. However, even if all these factors were known, the biological response would still dependent on several factors (just like the RBE), including cell type, dose rate, endpoint etc. As also showed in this work, the biological response was very dependent on the cell type and the biological assay used. Even though almost the same RBE-value were obtained for HeLa and V79 cells, using the clonogenic cell survival assays, their respective survival fractions (at similar absorbed doses) differed by a factor 10^3. The biological response, showed a huge dependency on cell type (here sought to be explained by differences in pathway activations, see section 5.3.2.3 p. 169) which could never be explained purely by microdosimetry.

The biological response can be evaluated using different biological assays each showing a different "aspect" of the biological response. Dependent on the purpose of the study, the chosen biological endpoint can be more or less relevant. If wishing to ascertain Auger emitters as a future cancer therapy, the fate of a cell after irradiation is of highest importance. The clonogenic cell survival assays tells exactly the information that is relevant; is the cancer cell still able to continuously divide or not. However, if the issue is radiation protection, the risk of stochastics effects, e.g. cancer, will be related to the mutagenic and carcinogenic properties of the radiation, and biological assays with focus on this, e.g. in vitro mammalian gene mutation test or fluorescence in situ hybridizations, ((FISH), which looks at translocations and deletions) might give more useful information.

In retrospect, the RBE concept might be dependent on too many parameters, which precise effect is unclear, and the obtained RBE-values (for Auger emitters) will therefore become too complicated to extract the relevant information. Especially, the high uncertainty in calculated absorbed doses, resulting from big variations in the MIRD cellular S-values, makes the obtained RBE-value so

dependent on the chosen cellular and nuclear size, that they can "change" the obtained RBE considerable. In addition, as showed by microdosimetry, the energy deposition density and "track structure" of different Auger emitters vary so much that they should not be considered as equally potent or harmful. Microdosimetry could elucidate these differences, but the calculated dose will still be dependent on the chosen target volume, resulting in a similar issue with high dependency and uncertainty in the target size, as confronted with, when the MIRD cellular S-values are used in the absorbed dose calculations. To obtain reliable results of the radiotoxicity of Auger emitters, it might be better to disregard the absorbed dose all together and just use the activity of the Auger emitter instead. In this way ones effort could be concentrated on investigating the delivery of the individual Auger emitters and their respective potentials in cancer therapy or detrimental effects for radiation protection. In addition, the classical way of calculating equivalent dose using radiation weighting factors, based on RBE-values (not using microdosimetry), does not make much sense for Auger emitters, since a higher absorbed dose of one Auger emitters will not necessarily result in a greater biological effect than a lower absorbed dose from another Auger emitter. As so, a higher absorbed dose from ^{99m}Tc will not necessarily result in a greater biological effect compared to a lower absorbed dose from ^{125}I.

A few studies have already been carried out in humans studying the pharmacokinetics, toxicity profile and therapeutic potential of various ^{111}In-radiopharmaceuticals [155][156][157][158]**,** that were originally approved for diagnostic use (except [155]). Due to the complex nature of the energy deposition distribution after Auger emitter decays, and the even more complex nature of the following biological response, a pragmatic approach investigating the potential of various radiopharmaceutical candidates, using a steady increase in the administered activity, might be the most effective methodology. This suggests that animal experiment might be the most reasonable choice in assessing the potential of a radiopharmaceutical. If this approached is chosen, the differences between human cells and the cells from the chosen animal, should be highly considered, especially if using human xenograft. As showed in this work (and also supported by the literature [20][119][141][142]), several difference between the human (HeLa) and hamster (V79) hamster cells

were found, including a factor 10^3 difference in their sensitivity to radiation. Such a difference would be of vital importance in assessing the radiation response using animal models.

However if one still wish to investigate the RBE of Auger emitters, certain aspect of the experimental setup should be highly prioritized. First, a reliable method to calculate absorbed dose should be used. Using the MIRD cellular S-values for these calculations, will most likely result in an uncertainty of the absorbed dose and hence RBE, that is too big to draw any conclusions. In this work, I have developed and showed one possible method to calculate the absorbed dose (for homogeneously distributed Auger emitters), which are very robust and almost independent on the cellular and nuclear sizes. Second, using comparable dose rates for the test and reference radiation should also be highly prioritized. As also showed in this work, the dose rate effect can significantly change the RBE-value. Ignoring this dose rate effect, can again influence the obtained RBE so much, that it losses its validity. A lot of effort has been put into the investigation of the radiotoxicity and RBE of Auger emitters, and it is unfortunately that the validity of many of these RBE-values are compromised due to unfortunate mistakes in the experimental setup and the absorbed dose calculations.

5.5 Summary

In the present study the radiotoxicity and relative biological effectiveness of Auger emitters were investigated. For this purpose the pure Auger emitter ^{131}Cs was chosen, as it had some beneficial bio-chemical characteristic. The cellular experiments were carried out using two cell lines; HeLa and V79 cells. By investigating the bio-kinetics of ^{131}Cs in these two cell lines, it was found that at least ~80 % of the ^{131}Cs, taken up by the cells, was transported across the plasmamembrane through the Na^+/K^+-ATPase. The uptake of ^{131}Cs resulted in an accumulation of intracellular ^{131}Cs compared to the external cell culture medium, of at least a factor 30. ^{131}Cs was also found to be released from the cells again, although this mechanism was not further studied. The increase in intracellular ^{131}Cs activity concentration and the release of ^{131}Cs from the cells over time could both be described by exponential functions. The bio-kinetics of ^{131}Cs plus its chemical characteristics, as an alkali metal, leads us to strongly believe that ^{131}Cs was not intracellularly chemically bound , but freely diffusible and homogeneously distributed throughout the cell.

The intracellular homogeneous distribution of ^{131}Cs, allowed us to establish an experimental setup and develop new cellular S-values, denoted S_C-values. The geometry applied for these S_C-values was a confluent cellular monolayer, in which ellipsoidal nuclei were located. The source compartment for these S_C-values was the whole cellular monolayer and the nucleus the target ($S_C(C \leftarrow N)$). The S_C-values were dependent on the height of the cellular monolayer, which was estimated using confocal microscopy to be 10 µm and 8 µm respectively, for the two cell lines used (HeLa & V79). Using the experimental setup, the S_C-values turned out to be very robust, and almost independent of the nuclear size. The S_C-value changed with less than 2.5 % for nuclear sizes ranging from below 0.1 pL to above 1.1 pL.

The S_C-values were expressed as Gy/(Bq*Sec)/pL, and so the intracellular ^{131}Cs activity concentration over time was used in the absorbed dose calculations. As the bio-kinetics of ^{131}Cs had been elucidated, the activity concentration of ^{131}Cs at only one time point was needed, in order to calculate the absorbed dose and dose rates over time. This was a huge advantage as the total amount of ^{131}Cs

available to us was spares. In addition, the intracellular accumulation of ^{131}Cs, allowed us to ignore the dose contribution from the cell culture medium.

In the end the radiotoxicity and RBE of ^{131}Cs was investigated. Using the obtained knowledge of the ^{131}Cs transport across the plasmamembrane, we were able to block most of this uptake using ouabain, which is known to inhibit the Na^+/K^+-ATPase. This allowed me to study the radiotoxicity of intracellular and extracellular located ^{131}Cs. In line with the belief, the radiotoxicity of ^{131}Cs was markedly reduced, when it was located extracellularly compared to intracellularly. The RBE of intracellular ^{131}Cs was investigated using two different biological assays; the γH2AX assay and the clonogenic cell survival assay. As several factors are known to influence the biological response to radiation, it was highly prioritized to apply similar experimental conditions for the cells exposed to intracellular ^{131}Cs (test radiation) and external γ-rays (reference radiation). A special focus was on the dose rate effect and the dose rate profiles for the two exposures were therefore matched as closely as possible. A RBE-value of 1 was obtained for HeLa cells, using the γH2AX assay. In contrast much higher RBE-values of 4.5 ± 0.5 and 3.8 ±0.8 respectively, were obtained for HeLa and V79 cells using the clonogenic cell survival assay and ^{137}Cs γ-rays as reference radiation. In addition, a "RBE"-value using acute exposure for the reference radiation instead of the matched dose rate profiles was also obtained. Here, a significant dose rate effect was found for V79 cells (but not for HeLa cells) decreasing the obtained "RBE"-value from 3.8 to 1.3. Nevertheless, due to the distinct qualities of the two biological assays used (γH2AX & clonogenic cell survival) the RBE-values obtained by clonogenic cell survival assay were considered to more accurate. These RBE-values (4.5 & 3.8) were higher than would be expected for Auger decays located intracellularly, as long as it is not intercalated or bound to the DNA. However, our robust S_C-value, the simple homogeneous intracellular distribution of ^{131}Cs, the elucidated ^{131}Cs bio-kinetics and especially the matched dose rate profiles, make our obtained RBE-values reliable. It is very unlikely that our absorbed dose calculations would be are so incorrect as to account for this high RBE-value. In addition, we know that the obtained RBE-values are conservative, as a 17 % higher (compared to NuDat 2.7) total energy per decay was used in the absorbed dose calculations. If this normalisation had not been applied the calculated absorbed dose would have been 17 % lower and accordingly the obtained RBE-values would be 17 % higher.

Summary

A possible explanation for the high RBE-values obtained, could be related to a dose rate effect, which in this study, when ignored, decreased the obtained “RBE- value from 3.8 to 1.3. All in all, this study have established an experimental setup and developed new cellular S-values, named S_C-values, which are very robust and almost independent of nuclear volumes. Using this setup, RBE-values of 1 (HeLa cells) and 4.5 ± 0.5 (HeLa cells) and 3.8 ± 0.8 (V79 cells) for intracellular ^{131}Cs decays, were obtained using the γH2AX and clonogenic cell survival respectively.

6. Conclusions and Outlook

The outcome of this study is twofold. The first outcome relates to the RBE values found, while the second relates to the experimental model and S_C-values that were developed.

RBE-values of 1 (HeLa) and 4.5 ± 0.5 (HeLa) and 3.8 ± 0.8 (V79) were found for intracellular ^{131}Cs decays, using the γH2AX and clonogenic cell survival assay respectively and ^{137}Cs γ-rays as reference radiation. Due to the distinct qualities of the two biological assays used, the RBE-values obtained by clonogenic cell survival assay were considered to most accurately reflect the radiotoxicity of intracellular Auger decays. Due to the experimental model, the very robust S_C-values and the matched dose rates profiles, these obtained RBE-values are seen as very reliable. The high RBE-values obtained, raise both hope and concerns. One of the struggles in developing Auger therapy is related to getting the radioisotope close enough to the DNA to achieve a high radiotoxicity. With the RBE-values obtained in this study, it may be enough to get the radioisotope into the nucleus, not being forced to bind it to the DNA. On the other hand, these RBE-values of ~4, should raise concerns in the way Auger emitters are treated in radiation protection and especially in the risk assessment of diagnostic procedures. At the moment Auger electrons release by the Auger emitters e.g. ^{111}In, ^{99m}Tc, which are extensively used in everyday diagnostic procedures are treated as “regular electrons”, having a radiation weighting factor of 1. This might have been justified by the belief that Auger emitters should bind to the DNA to be highly radiotoxic. However, the RBE-values of ~4 obtained in this study, show that the radiotoxicity of intracellularly located Auger decays (when not bound to the DNA), are significantly higher than otherwise thought, and should not be ignored. Even though the precise radiotoxicity of ^{99m}Tc, ^{111}In and other Auger electron emitting radioisotopes is most likely not identical to ^{131}Cs, due to their individual energy deposition density, the high RBE-value obtained in this study should be taken very serious. Luckily, studies have indicated that ^{99m}Tc might not be as radiotoxic as ^{111}In and ^{125}I, which correspond to their lower number of electrons released per decay. However, as the average number of electrons released per decay and their energy average for ^{131}Cs are not that different from ^{111}In, it could be feared that the RBE-values obtained in this study reflect that of ^{111}In. If this is true, we could be severely miscalculating the risk posed by Auger electron

emitting radioisotopes. The risk associated with diagnostic procedures, could therefore very well, be significantly underestimated, affecting a substantial amount of people.

This leads to the second outcome of this study: The radiotoxicity of Auger emitter decay clearly needs to be further investigated. I believe that the experimental model and the S_C-values developed and applied in this study, is highly suitable for this purpose. The cell culture geometry, the homogenous distribution of ^{131}Cs and the use of intracellular activity concentration, makes our S_C-values very robust. This along with the known bio-kinetics of ^{131}Cs, makes the calculated absorbed doses and dose rates very reliable. The high uncertainty in dosimetric calculations often inherent in other experimental setups can thereby be overcome. In addition, the matching the dose rate profiles, overcomes the dose rate effect, which is known to greatly impact the biological response and hence the RBE. Other endpoints (e.g. micronuclei formation) or other cellular responses to Auger decays, including changes in gene expression and DNA damage repair pathways can also be studied using this model and could help to further elucidate the biological differences between Auger emitter decay exposures and exposure from other types of ionising radiation.
Importantly, this experimental model and calculation of the S_C-values can if wished to also be applied to other radioisotopes, as long as they are homogeneously distributed in the cells.

Lastly, as ^{131}Cs is transported into the cells by the Na^+/K^+-ATPase, which is a ubiquitous pump present in all mammalian cells, the experimental model can be applied to all cell types. Differences in sensitivity to Auger emitter decays between cells originating from different tissues (e.g. cancerous or normal) can be investigated. In addition, because of the resemblance of caesium to potassium this can be expanded to include investigation the radiotoxicity of Auger emitter decays in cells of non-mammalian origin, including microorganism such as bacteria and fungi.

However, most importantly, this study unequivocally demonstrates a high RBE for Auger emitter decays located intracellular, but not bound to the DNA. This high radiotoxicity of Auger emitters shows that Auger electrons released by radioisotopes should not be ignored, but rather taken very seriously. The detrimental effects and risks associated with Auger emitter decays should be further investigated, regardless of the experimental model used.

7. References

[1] Clarke RH, Valentin J. The History of ICRP and the Evolution of its Policies. Ann ICRP 2009;39:75–110. doi:https://doi.org/10.1016/j.icrp.2009.07.009.

[2] World Nuclear Association. http://www.world-nuclear.org/information-library/non-power-nuclear-applications/radioisotopes-research/radioisotopes-in-medicine.aspx n.d. http://www.world-nuclear.org/info/Safety-and-Security/Safety-of-Plants/Chernobyl-Accident/#.UfW2y6wWbw8.

[3] Mettler FA, Bhargavan M, Faulkner K, Gilley DB, Gray JE, Ibbott GS, et al. Radiologic and Nuclear Medicine Studies in the United States and Worldwide: Frequency, Radiation Dose, and Comparison with other radiation sources-1950-2007. Radiology 2009;253:520–31. doi:10.1148/radiol.2532082010.

[4] Hoefnagel AC. Radionuclide therapy revisited. Eur J Nucl Med 1991;18:408–31. doi:10.1007/BF02258432.

[5] Buchegger F, Perillo-Adamer F, Dupertuis YM, Delaloye AB. Auger radiation targeted into DNA: a therapy perspective. Eur J Nucl Med Mol Imaging 2006;33:1352–63. doi:10.1007/s00259-006-0187-2.

[6] Kassis AI, Adelstein S. J. Radiobiologic Principles in Radionuclide Therapy. J Nucl Med 2005;46:4S–12S.

[7] International Commission on Radiological Protection. Radiation Dose to Patients from Radiopharmaceuticals. Addendum 3 to ICRP Publication 53. ICRP 106 Publication. Ann ICRP 2008;38.

[8] Howell RW. Auger processes in the 21st century. Int J Radiat Biol 2008;84:959–75. doi:10.1080/09553000802395527.

[9] Fairlie I. RBE and wR values of Auger emitters and low-range beta emitters with particular reference to tritium. J Radiol Prot 2007;27:157–68. doi:10.1088/0952-4746/27/2/003.

[10] United Nations Scientific Committee on the Effects of Atomic Radiation (UNSCEAR). SOURCES AND EFFECTS OF IONIZING RADIATION. UNSCEAR REPROT 2008. vol. I. 2008.

[11] Feinendegen LE. PROBLEMS ASSOCIATED WITH THE USE QF LABELLED MOLECULES IN BIOLOGY AND MEDICINE. General review. Biol. Eff. Transmutat. Decay Inc. Radioisot. IAEA, n.d., p. 1–17.

[12] Feinendegen LE. Biological toxicity associated with the auger effect. J Chem Inf Model 1971;53:1689–99. doi:10.1017/CBO9781107415324.004.

[13] International Commission on Radiological Protection. Relative Biological Effectiveness (RBE), QualityFactor (Q), and Radiation Weighting Factor (wR). ICRP Publication 92. Annals of the ICRP

33(4). 2003.

[14] Pomplun E, Booz J, Dydejczyk A, Feinendegen LE. A microdosimetric interpretation of the radiobiological effectiveness of ^{125}I and the problem of quality factor. Radiat Environ Biophys 1987;26:181–8. doi:10.1007/BF01213704.

[15] Humm JL, Howell RW, Rao D V. Dosimetry of Auger-electron-emitting radionuclides: Report No. 3 of AAPM Nuclear Medicine Task Group No. 6. Med Phys 1994;21:1901–15. doi:10.1118/1.597227.

[16] Humm JL, Howell RW, Rao D V. ERATUM:"Dosimetry of Auger-electron-emitting radionuclides: Report no. 3 of AAPM Nuclear Medicine Task Group No. 6" [Med. Phys. 21, 1901-1915 (1994)]. Med Phys 1995;22:1837.

[17] Goddu SM, Howel RW, Bouchet LG, Bloch W, Dandamudi WR. MIRD Cellular S values. Reston, VA: Society of Nuclear Medicine; 1997.

[18] Goddu SM, Howel RW, Rao D V. Cellular Dosimetry: Absorbed Fractions for Monoenergetic Electron and Alpha Particle Sources and S-values for Radionucleides Uniformly Distributed in Different Cells Compartments. Jounal Nucl Med 1994;35.

[19] Hofer KG, Hughes WL. Radiotoxicity of Intranuclear Tritium, 125 Iodine and 131 Iodine. Radiat Res 1971;47:94–109.

[20] Hall EJ, Brenner DJ. THE DOSE-RATE EFFECT REVISITED: RADIOBIOLOGICAL CONSIDERATIONS OF IMPORTANCE IN RADIOTHERAPY. Int J Radiat Oncol Biol Phys 1991;21:1403–14. doi:10.1016/0360-3016(91)90314-T.

[21] Howell RW, Rao D V, Hou DY, Narra VR, Sastry KS. The Question of Relative Biological Effectiveness and Quality Factor for Auger Emitters Incorporated into Proliferating Mammalian Cells. Radiat Res 1991;128:282–92.

[22] Kassis AI, Fayaad F, Kinsey BM, Sastry KSR, Taube RA, Adelstein SJ. Radiotoxicity of ^{125} I in Mammalian Cells. Radiat Res 1987;111:305–18. doi:10.2307/3574245.

[23] Kassis AI, Fayad F, Kinsey BM, Sastry KSR, Adelstein J, May N. Radiotoxicity of an 125I-Labeled DNA Intercalator in Mammalian Cells. Radiat Res 1989;118:283–94.

[24] Yasui LS, Hughes A, DeSombre ER. Relative Biological Effectiveness of Accumulated ^{125}IdU and ^{125}I-Estrogen Decays in Estrogen Receptor-Expressing MCF-7 Human Breast. Radiat Res 2001;155:328–34.

[25] NUDAT2. http://www.nndc.bnl.gov/nudat2/chartNuc.jsp n.d.

[26] Meitner L. Das β-Strahlenspektrum von UX_1 und seine Deutung. Zeitschrift Für Phys 1923;17:54–66. doi:10.1007/BF01328663.

[27] Auger P. Sur les rayons b secondaires prodiuts dans un gaz par des rayons x. Comptes Rendues

Hebdomadaires des Seances de l'Academie des Sciences 1925;180:65–8.

[28] Kassis AI. The Amazing World of Auger Electrons. Int J Radiat Biol 2004;80:789–803. doi:10.1080/09553000400017663.

[29] Persson L. THE AUGER ELECTRON EFFECT IN RADIATION DOSIMETRY. Health Phys 1994;67:471–6.

[30] Lee BQ, Kibédi T, Stuchbery AE, Robertson KA. Atomic Radiations in the Decay of Medical Radioisotopes: A Physics Perspective. Comput Math Methods Med 2012. doi:10.1155/2012/651475.

[31] Podgorsak EB. Radiation Physics for Medical Physcists. Berlin, Heidelberg: Springer-Verlag; 2006. doi:10.1007/978-3-642-008745-7.

[32] Krause MO. Atomic Radiative and Radiationless Yields for K and L shells. J Phys Chem Ref Data 1979;8:307–27. doi:10.1063/1.555594.

[33] Kortright JB. X-Ray Data Booklet. Section 1.3 FLUORESCENCE YIELDS FOR K and L SHELLS. http://xdb.lbl.gov/Section1/Sec_1-3.html n.d. http://xdb.lbl.gov/Section1/Sec_1-3.html (accessed May 5, 2017).

[34] Kahoul A, Abassi A, Deghfel B, Nekkab M. K-shell fluorescence yields for elements with 6≤Z≤99. Radiat Phys Chem 2011;80:369–77. doi:10.1016/j.radphyschem.2010.11.011.

[35] Podgorsak EB. Radiation Oncology Physics: A Handbook for Teachers and Students. Vienna: International Atomic Energy Agency; 2005.

[36] Ertl HH, Feinendegen LE, Heiniger HJ. Iodine-125, a Tracer in Cell Biology: Physical Properties and Biological Aspects. PHYS MED BIOL 1970;15:447–56. doi:10.1088/0031-9155/15/3/005.

[37] Carlson TA, White RM. Formation of Fragment Ions from CH3Te125 and C2H5Te125 Following the Nuclear Decays of CH3I125 and C2H5I125. J Chem Phys 1963;38:2930–4. doi:10.1063/1.1733622.

[38] ICRU. ICRP Report of the RBE Committee of the International Commissions on Radiological Protection and on Radiological Units. Health Phys 1963;9:375–84.

[39] Hall EJ, Giaccia AJ. Radiobiology for the Radiologist. vol. 7 Edition. Wolters Kluwer; 2012.

[40] Hofer KG. Biophysical aspects of Auger processes. Acta Oncol 1996;35:789–96. doi:10.3109/02841869609104028.

[41] Charlton DE. The Range of High LET Effects from ^{125} I Decays. Radiat Res 1986;107:163–71.

[42] Wright HA, Hamm RN, Turner JE, Howell RW, Rao D V., Sastry KSR. CALCULATIONS OF PHYSICAL AND CHEMICAL REACTIONS WITH DNA IN AQUEOUS SOLUTION FROM AUGER CASCADE. Radiat Prot Dosimetry 1990;31:59–62. doi:10.1093/oxfordjournals.rpd.a080639.

[43] Agency IAEA. Radiation biology: A Handbook for Teachers and Students. 2010.

[44] Lomax ME, Folkes LK, O'Neill P. Biological Consequences of Radiation-induced DNA damage: Relevance to Radiotherapy. Clin Oncol 2013;25:578–85. doi:10.1016/j.clon.2013.06.007.

[45] Lobachevsky PN, Martin RF. Iodine-125 Decay in a Synthetic Oligodeoxynucleotide. II. The Role of Auger Electron Irradiation Compared to Charge Neutralization in DNA Breakage. Radiat Res 2000;153:271–8. doi:10.1667/0033-7587(2000)153[0271:IDIASO]2.0.CO;2.

[46] Kassis AI, Harapanhalli RS, Adelstein S. J. Strand Breaks in Plasmid DNA after Positional Changes of Auger Electron-Emitting Iodine-125 : Direct Compared to Indirect Effects. Radiat Res 1999;152:530–8.

[47] Balagurumoorthy P, Xu X, Wang K, Adelstein SJ, Kasis A. Effect of distance between decaying 125I and DNA on Auger-electron induced double-strand break yield. Int J Radiat Biol 2012;88:998–1008. doi:10.3109/09553002.2012.706360.

[48] Magnander K, Elmroth K. Biological consequences of formation and repair of complex DNA damage. Cancer Lett 2012;327:90–6. doi:10.1016/j.canlet.2012.02.013.

[49] Ward JF. Some Biochemical Consequences of the Spatial Distribution of Ionizing Radiation-Produced Free Radicals. Radiat Res 1981;86:185–95. doi:10.2307/3575500.

[50] Georgakilas AG. Processing of DNA damage clusters in human cells: current status of knowledge. Mol Biosyst 2008;4:30–5. doi:10.1039/b713178j.

[51] Eccles LJ, O'Neill P, Lomax ME. Delayed repair of radiation induced clustered DNA damage: Friend or foe? Mutat Res 2011;711:134–41. doi:10.1016/j.mrfmmm.2010.11.003.

[52] Hada M, Georgakilas AG. Formation of Clustered DNA Damage after High-LET Irradiation: A Review. J Radiat Res 2008;49:203–10. doi:10.1269/jrr.07123.

[53] Dependence of yield of DNA Damage Refractory to Enzymatic Repair on Inization & Excitation Density of Radiation- Exploring the Induction Mechanims of Clustered DNA Damage. JEAE R&D Rev 2007:71. http://jolisfukyu.tokai-sc.jaea.go.jp/fukyu/review_en/2007/pdf/6-5.pdf.

[54] Krokan HE, Nilsen H, Skorpen F, Otterlei M, Slupphaug G. Base excision repair of DNA in mammalian cells. FEBS Lett 2000;476:73–7. doi:10.1016/S0014-5793(00)01674-4.

[55] Caldecott KW. DNA single-strand break repair. Exp Cell Res 2014;329. doi:10.1016/j.yexcr.2014.08.027.

[56] Gulston M, de Lara C, Jenner T, Davis E, O'Neill P. Processing of clustered DNA damage generates additional double-strand breaks in mammalian cells post-irradiation. Nucleic Acids Res 2004;32:1602–9. doi:10.1093/nar/gkh306.

[57] Harper J V., Anderson JA, O'Neill P. Radiation induced DNA DSBs: Contribution from stalled replication forks? DNA Repair (Amst) 2010;9:907–13. doi:10.1016/j.dnarep.2010.06.002.

[58] Datta K, Neumann RD, Winters TA. Characterization of a complex ^{125}I-induced DNA double-strand break: implications for repair. Int J Radiat Biol 2005;81:13–21. doi:10.1080/09553000400017713.

[59] Sundell-Bergman S, Johanson KJ. Repairable and Unrepairable DNA Strand Breaks Induced by Decay of 3H and <sup<125</sup>I Incorporated into DNA of Mammalian Cells. Radiat Environ Biophys 1980;18:239–48.

[60] Painter R. ., Young RB, Burki HJ. Non-Repairable Strand Breaks Induced by 125 I Incorporated into Mammalian DNA. Proc Nat Acad Sci USA 1974;71:4836–8. doi:10.1073/pnas.71.12.4836.

[61] Pastwa E, Neumann RD, Mezhevaya K, Winters TA. Repair of radiation-induced DNA double-strand breaks is dependent upon radiation quality and the structural complexity of double-strand breaks. Radiat Res 2003;159:251–61. doi:10.1667/0033-7587(2003)159[0251:RORIDD]2.0.CO;2.

[62] Dahmen V, Pomplun E, Kriehuber R. Iodine-125-labeled DNA-Triplex-forming oligonucleotides reveal increased cyto- and genotoxic effectiveness compared to Phosphorus-32. Int J Radiat Biol 2016. doi:10.3109/09553002.2016.1160157.

[63] Kassis AI, Sastry KS, Adelstein SJ. Kinetics of Uptake , Retention , and Radiotoxicity of ^{125} IUdR in Mammalian Cells : Implications of Localized Energy Deposition by Auger. Radiat Res 1987;109:78–89. doi:DOI: 10.2307/3576869.

[64] Deckbar D, Jeggo P a, Löbrich M. Understanding the limitations of radiation-induced cell cycle checkpoints. Crit Rev Biochem Mol Biol 2011;46:271–83. doi:10.3109/10409238.2011.575764.

[65] Sancar A, Lindsey-Boltz LA, Unsal-Kaçmaz K, Linn S, Ünsal-Kaçmaz K, Linn S. Molecular Mechanism of Mammalian DNA Repair and the DNA Damage Checkpoints. Annu Revi Biochem 2004;73:39–85. doi:10.1146/annurev.biochem.73.011303.073723.

[66] Pawlik TM, Keyomarsi K. ROLE OF CELL CYCLE IN MEDIATION SENSITIVITY TO RADIOTHERAPY. Int J Radiat Oncol Biol Phys 2004;59:928–42. doi:10.1016/j.ijrobp.2004.03.005.

[67] Cancer Information & supportNetwork. http://cisncancer.org/research/what_we_know/biology/the_cell_cycle.html n.d.

[68] Goodarzi AA, Jeggo P, Lobrich M. The influence of heterochromatin on DNA double strand break repair: Getting the strong, silent type to relax. DNA Repair (Amst) 2010;9:1273–82. doi:10.1016/j.dnarep.2010.09.013.

[69] Campisi J, d'Adda di Fagagna F. Cellular senescence: when bad things happen to good cells. Nat Rev Mol Cell Biol 2007;8:729–40. doi:10.1038/nrm2233.

[70] Fridlyanskaya I, Alekseenko L, Nikolsky N. Senescence as a general cellular response to stress: A mini-review. Exp Gerontol 2015;72:124–8. doi:10.1016/j.exger.2015.09.021.

[71] Vilenchik MM, Knudson AG. Inverse radiation dose-rate effects on somatic and germ-line

mutations and DNA damage rates. Proc Nat Acad Sci USA 2000;97:5381–6. doi:10.1073/pnas.090099497.

[72] Brenner DJ, Hall EJ, Randers-Pehrson G, Miller RC. Mechanistic Considerations on the Dose-Rate / LET Dependence of Oncogenic Transformation by Ionizing Radiations. Radiat Res 1993;133:365–9. doi:10.2307/3578223.

[73] Brenner DJ, Hall EJ. The inverse dose-rate effect for oncogenic transformation by neutrons and charged particles: a plausible interpretation consistent with published data. Int J Radiat Biol 1990;58:745–58. doi:10.1080/09553009014552131.

[74] Liu C, Lin Q, Yun Z. Cellular and Molecular Mechanisms Underlying Oxygen-Dependent Radiosensitivity. Radiat Res 2015;183:487–96. doi:10.1667/RR13959.1.

[75] Schneewiess FHA, Meyers D., Tisljar-Lentulis G, Feinendegen l. E. LOW OXYGEN ENHANCEMENT RATIO FOR STRAND BREAKS INDUCED BY DECYAS OF ^{125}I IN DNA OF HHUMAN T1 CELLS STORED AT 0^{o}C. Radiat Prot Dosimetry 1985;13:237–9. doi:10.1093/oxfordjournals.rpd.a079586.

[76] Koch CJ, Burki HJ. The oxygen-enhancement ratio for reproductive death induced by ^{3}H or ^{125}I damage in mammalian cells. Int J Radiat Biol 1975;28:417–25. doi:10.1080/09553007514551241.

[77] Bolch WE, Eckerman KF, Sgouros G, Thomas SR. MIRD Pamphlet No. 21: A Generalized Schema for Radiopharmaceutical Dosimetry-Standardization of Nomenclature. J Nucl Med 2009;50:477–84. doi:10.2967/jnumed.108.056036.

[78] Howell RW. The MIRD Schema: From Organ to Cellular Dimensions. J Nucl Med 1994;35:531–3.

[79] Loevinger R, Budinger T., Watson EE. MIRD Primer for Absorbed Dose Calculations. Revised ed. Revied Ed. New York: The Society of Nuclear Medicine; 1991.

[80] ICRP. Adult Reference Computational Phantoms. ICRP Publication 110. Ann. ICRP 39 (2). 2009.

[81] Emfietzoglou D, Kostarelos K, Hadjidoukas P, Bousis C, Fotopoulos A, Pathak A, et al. Subcellular S-factors for low-energy electrons: a comparison of Monte Carlo simulations and continuous-slowing-down calculations. Int J Radiat Biol 2008;84:1034–44. doi:10.1080/09553000802460180.

[82] Cole A. Absorption of 20-eV to 50,000-eV Electron Beams in Air and Plastic. Radiat Res 1969;38:7–33. doi:10.2307/3572707.

[83] Palmans H, Rabus H, Belchior AL, Bug MU, Galer S, Giesen U, et al. Future development of biologically relevant dosimetry. Br J Radiol 2015;88. doi:10.1259/bjr.20140392.

[84] ICRU. Fundamental Quantities And Units For Ionizing Radiation (Revised) ICRU-report No 85. vol. 11. 2011. doi:10.1093/jicru/ndr012.

[85] Nikjoo H, Emfietzoglou D, Charlton DE. The Auger effect in physical and biological research. Int J Radiat Biol 2008;84:1011–26. doi:10.1080/09553000802460172.

[86] Howell RW. Radiation spectra for Auger-electron emitting radionuclides: report No. 2 of AAPM Nuclear Medicine Task Group No. 6. Med Phys 1992;19:1371–83. doi:10.1118/1.596927.

[87] Howell RW. Physical Considerations for Understanding Responses of Biological Systems to Low Doses of Ionizing Radiation. Health Phys 2016;110:283–6. doi:10.1097/HP.0000000000000467.

[88] Aabert B, Johnson, Alexander Lewis J, Raff M, Roberts K, Walter P. Molecular Biology of The Cell. fourth. New York: Garland Science; 2002.

[89] Sastry KSR. Biological effects of the Auger emitter Iodine-125: A review. Report No 1 of AAPM Nuclear Medicine Task Group No. 6 a). Med Phys 1992;19. doi:10.1118/1.596926.

[90] Avery S V., Codd G a., Gadd GM. Caesium accumulation and interactions with other monovalent cations in the cyanobacterium Synechocystis PCC 6803. J Gen Microbiol 1991;137:405–13. doi:10.1099/00221287-137-2-405.

[91] Avery S V. Caesium accumulation by microorganisms: uptake mechanisms, cation competition, compartmentalization and toxicity. J iIdustrial Microbiol 1995;14:76–84. doi:10.1007/BF01569888.

[92] Agency for Toxic Substances & Disease Registry. Toxicological Profile for Cesium. 2004.

[93] Lee BQ, Nikjoo H, Ekman J, Jönsson P, Stuchbery AE, Kibédi T. A stochastic cascade model for Auger-electron emitting radionuclides. Int J Radiat Biol 2016;3002:1–13. doi:10.3109/09553002.2016.1153810.

[94] Zhang P, Idota Y, Yano K, Negishi M, Kawabata H, Arakawa H, et al. Characterization of Cesium Uptake Mediated by a Potassium Transport System of Bacteria in a Soil Conditioner. Biol Pharm Bull 2014;37:604–7. doi:10.1248/bpb.b13-00871.

[95] Avery S V, Codd GA, Gadd GM. Transport kinetics, cation inhibition and intracellular location of accumulated caesium in the green microalga Chlorella salina. J Gen Microbiol 1993;139:827–34. doi:10.1099/00221287-139-4-827.

[96] Latorre R, Miller C. Conduction and Selectivity in Potassium Channels. J Membr Biol 1983;71:11–30.

[97] Juri Ayub J, Rubio Valverde L, Garcia-Sanchez MJ, Fernandez JA, Velasco RH. Kinetics of caesium and potassium absorption by roots of three grass pastures and competitive effects of potassium on caesium uptake in Cynodon sp. AIP Conf Proc 2008;1034:269–72. doi:10.1063/1.2991224.

[98] Whittam R, Ager ME. Vectorial Aspects of Adenosine-Triphosphatase Activity in Erythrocyte Membranes. Biochem J 1964;93:337–48.

[99] Williams R. Tilden Lecture. The biochemistry of sodium, potassium, magnesium, and calcium. Q Rev Chem Soc 1970;3:331–65. doi:10.1039/qr9702400331.

[100] Ussing HH, Kruhoffer P, Thaysen HJ, Thorn NH. The Alkali Metal Ions in Biology. 1st ed. Berlin, Heidelberg: Springer-Verlag Berlin Heidelberg; 2011. doi:10.1007/978-3-642-49246-4.

[101] Kuo LJ, Yang L-X. γ-H2AX - A novel biomarker for DNA double-strand breaks. In Vivo (Brooklyn) 2008;22:305–10.

[102] Bonner WM, Redon CE, Dickey JS, Nakamura AJ, Sedelnikova OA, Solier S, et al. γH2AX and cancer. Nat Rev Cancer 2008;8. doi:10.1038/nrc2523.

[103] Pearson Education Inc. Pearson education. http://www.mun.ca/biology/desmid/brian/BIOL2060/BIOL2060-18/18_21.jpg n.d.

[104] Pilch DR, Sedelnikova OA, Redon C, Celeste A, Bonner WM. Characteristics of -H2AX foci at DNA double- strand breaks sites. Biochem Cell Biol 2003;129:123–9. doi:10.1139/O03-042.

[105] Muslimovic A, Johansson P, Hammarsten O. Measurement of H2AX Phosphorylation as a Marker of Ionizing Radiation Induced Cell Damage. Aida Muslimovic, Pegah Johansson and Ola Hammarsten (2012). Measurement of H2AX Phosphorylation as a Marker of Ionizing Radiation Induced Cell Damage, Current Topic. Curr Top Ioniz Radiat Res 2012. doi:10.5772/33257.

[106] Merck Millipore. http://www.merckmillipore.com/DK/en/life-science-research/cell-analysis/muse-cell-analyzer/hb2b.qB.lI0AAAE_vzlkifKv,nav?ReferrerURL=https%3A%2F%2Fwww.google.dk%2F n.d.

[107] Puck TT, Marcus PL. ACTION OF X-RAYS ON MAMMALIAN CELLS. J Exp Med 1956;103:653–66. doi:10.1084/jem.103.5.653.

[108] Munshi A, Hobbs M, Meyn RE. Clonogenic cell survival assay. vol. 110. Springer; 2005. doi:10.1385/1-59259-869-2:021.

[109] Franken N a P, Rodermond HM, Stap J, Haveman J, van Bree C. Clonogenic assay of cells in vitro. Nat Protoc 2006;1:2315–9. doi:10.1038/nprot.2006.339.

[110] Tweedale G. HeLa cells 50 years on: the good, the bad and the ugly. Nat Rev Cancer 2002;2:311–5. doi:10.1038/nrc775.

[111] The Lacks Family. http://www.lacksfamily.net/henrietta.php n.d.

[112] Munger K, Scheffner M, Huibregtse JM, Howley PM. Interactions of Hpv E6 and E7 Oncoproteins With Tumor Suppressor Gene-Products. Cancer Surv 1992;12:197–217.

[113] ATCC. https://www.lgcstandards-atcc.org/Products/All/CCL-2.aspx#characteristics n.d.

[114] ATCC. https://www.lgcstandards-atcc.org/Products/All/CCL-93.aspx#characteristics n.d.

[115] Leggett RW, Williams LR, Melo DR, Lipsztein JL. A physiologically based biokinetic model for cesium in the human body. Sci Total Environ 2003;317:235–55. doi:10.1016/S0048-9697(03)00333-4.

[116] Pubchem. https://pubchem.ncbi.nlm.nih.gov/compound/ouabain#section=Top n.d.

[117] Carnero A, Blanco C, Blanco F, Castro ME, Guijarro M V, Fominaya J, et al. Exploring cellular senescence as a tumor suppressor mechanism. Rev OnCol 2003;5:249–65. doi:10.1007/BF02711481.

[118] Suhail M. Na^+, K^+-ATPase: Ubiquitous Multifunctional Transmembrane Protein and its Relevance to Various Pathophysiological Conditions. J Clin Med Res 2010;2:1–17. doi:10.4021/jocmr2010.02.263w.

[119] Gupta RS, Chopra A, Stetsko DS. Cellular Basis for the Species Differences in Sensitivity to Cardiac Clycosides (Digitalis). J Cell Physiol 1986;127:197–206. doi:10.1002/jcp.1041270202.

[120] Schultheis PJ, Wallick ET, Lingrel JB. Kinetic Analysis of Ouabain Binding to Native and Mutated Forms of Na,K- ATPase and Identification of a New Region Involved in Cardiac Glycoside Interactions. J Biol Chem 1993;268:22686–94.

[121] Verheye-Dua F., Böhm L. Influence of Ouabain on Cell Inactivation by Irradiation. Strahlenther.apie Und Onkol 1996;172:156–61.

[122] Pollack LR, Tate EH, Cook JS. Na^+, K^+-ATPase in HeLa cells after prolonged growth in low K^+ or ouabain. J Cell Physiol 1981;106:85–97. doi:10.1002/jcp.1041060110.

[123] Sigma-Aldrich. http://www.sigmaaldrich.com/content/dam/sigma-aldrich/docs/Sigma/Formulation/d6546for.pdf n.d.

[124] Ghosh A, Sharma A, Talukder G. CLASTOGENIC EFFECTS OF CAESIUM CHLORIDE ON H U M A N PERIPHERAL BLOOD LYMPHOCYTES I N V I T R O. Toxic Vitr 1993;7:137–40. doi:10.1016/0887-2333(93)90123-M.

[125] Standford. https://web.stanford.edu/group/Urchin/mineral.html n.d.

[126] Fujioka A, Terai K, Itoh RE, Aoki K, Nakamura T, Kuroda S, et al. Dynamics of the Ras/ERK MAPK cascade as monitored by fluorescent probes. J Biol Chem 2006;281:8917–26. doi:10.1074/jbc.M509344200.

[127] Maul GG, Deaven L. QUANTITATIVE DETERMINATION OF NUCLEAR PORE COMPLEXES IN CYCLING CELLS WITH DIFFERING DNA CONTENT. J Cell Biol 1977;73:748–60.

[128] Monier K, Armas JC, Etteldorf S, Ghazal P, Sullivan KF. Annexation of the interchromosomal space during viral infection. Nat Cell Biol 2000;2:661–5. doi:10.1038/35023615.

[129] Ottolenghi A, Monforti F, Merzagora M. A Monte Carlo calculation of cell inactivation by light ions. Int J Radiat Biol 1997;72:505–13. doi:10.1080/095530097143004.

[130] Kassis AI, Adelstein SJ, Haydock C, Sastry KSR. Radiotoxicity of ^{75} Se and ^{35} S : Theory and Application to a Cellular Model Author (s): A . I . Kassis , S . J . Adelstein , C . Haydock and K . S . R . Sastry Published by : Radiation Research Society Stable URL : http://www.jsto. Radiat Res 1980;84:407–25. doi:10.2307/3575480.

[131] Kiess AP, Minn I, Chen Y, Hobbs R, Sgouros G, Mease RC, et al. Auger Radiopharmaceutical Therapy Targeting Prostate-Specific Membrane Antigen. J Nucl Med 2015;56:1401–7. doi:10.2967/jnumed.115.155929.

[132] Cai Z, Chen Z, Bailey KE, Scollard D a, Reilly RM, Vallis K a. Relationship between induction of phosphorylated H2AX and survival in breast cancer cells exposed to ^{111}In-DTPA-hEGF. J Nucl Med 2008;49:1353–61. doi:10.2967/jnumed.108.051805.

[133] WARTERS RL, HOFER KG. Radionuclide Toxicity in Cultured Mammalian Cells : Elucidation of the Primary Site for Radiation-Induced Division Delay. Radiat Res 1977;69:348–58. doi:10.2307/3574442.

[134] Kasis A, Adelstein JS. Thallium-201 : An Experimental and a Theoretical Radiobiological Approach to Dosimetry. J Nucl Medc 1983;24:1164–75.

[135] Verheye-Dua F, Bohm L. Na^+, K^+-ATPase Inhibitor, Ouabain Accentuates Irradiation Damage in Human Tumour Cell Lines. Radiat Oncol Investig 1998;6:109–19. doi:10.1002/(SICI)1520-6823(1998)6:3<109::AID-ROI1>3.0.CO;2-1.

[136] Rothkamm K, Horn S. γ -H2AX as protein biomarker for radiation exposure. Ann Ist Super St 2009;45:265–71.

[137] Hofer KG, Harris CR, Smith JM. Radiotoxicity of Intracellular ^{67} Ga, ^{125} I and ^{3} H. Int J Radiat Biol 1975;28:225–41. doi:10.1080/09553007514550991.

[138] Ling CC, Li WX, Anderson LL. The relative biological effectiveness of I-125 and Pd-103. Int J Radiat Oncol Biol Phys 1995;32:373–8. doi:10.1016/0360-3016(95)00530-C.

[139] Hofer KG. Biophysical aspects of Auger processes. Acta Oncol 1996;35:789–96. doi:10.3109/02841869609104028.

[140] Makrigiorgos AGM, Kassis AI, Mcelvany KD, Welch J, Sastry KSR, Adelstein SJ, et al. Radiotoxicity of 5 -[^{123}I]Iodo-2'-deoxyuridine in V79 Cells: A Comparison with 5-[^{125}I]Iodo-2'-deoxyuridine. Radiat Res 1989;118:532–44. doi:10.2307/3577411.

[141] Mitchell JB, Bedford JS, Bailey SM. Dose-Rate Effects in Plateau-Phase Cultures of S3 HeLa and V79 Cells. Radiat Res 1979;79:520–36.

[142] Mitchell JB, Bedford JS, Bailey SM. Dose-Rate Effects in Mammalian Cells in Culture : III . Comparison of Cell Killing and Cell Proliferation during Continuous Irradiation for Six Different Cell Lines. Radiat Res 1979;79:537–51.

[143] Qian Y, Chen X. Tumor suppression by p53: Making cells senescent. Histol Histopathol

2010;25:515–26. doi:10.14670/HH-25.515.

[144] Kennedy AL, McBryan T, Enders GH, Johnson FB, Zhang R, Adams PD. Senescent mouse cells fail to overtly regulate the HIRA histone chaperone and do not form robust Senescence Associated Heterochromatin Foci. Cell Div 2010;5:16. doi:10.1186/1747-1028-5-16.

[145] Kriehuber R, Riedling M, Simkó M, Weiss DG. Cytotoxicity, genotoxicity and intracellular distribution of the Auger electron emitter ^{65}Zn in two human cell lines. Radiat Environ Biophys 2004;43:15–22. doi:10.1007/s00411-004-0234-y.

[146] Rao D V, Sastry KS, Grimmond HE, Howell RW, Govelitz GF, Lanka VK, et al. Cytotoxicity of some indium radiopharmaceuticals in mouse testes. J Nucl Med 1988;29:375–84.

[147] Howell RW, Kassis AI, Adelstein SJ, Rao D V, Harvel A, Hamm RN, et al. Radiotoxicity of Platinum-195m-Labeled trans-Platinum (ll) in Mammalian Cells. Radiat Res 1994;140:55–62. doi:10.2307/3578568.

[148] Narra V, Sastry KSR, Goddu SM, Howell RW, Strand S-E, Rao D V. Relative biological effectiveness of ^{99m}Tc radiopharmaceuticals. Med Phys 1994;21:1921–4. doi:10.1118/1.597230.

[149] Howell R, Rao D, Hou D, Narra V, Sastry K. The question of relative biological effectiveness and quality factor for Auger emitters incorporated into proliferating mammalian cells. Radiat … 1991;128:282–92. doi:1961925.

[150] Rao D V, Narra VR, Howell RW, Lanka VK, Sastry KS. Induction of sperm head abnormalities by incorporated radionuclides: dependence on subcellular distribution, type of radiation, dose rate, and presence of radioprotectors. Radiat Res 1991;125:89–97.

[151] Kriehuber R, Kadenbach K, Schultz F, Weiss DG. Study on cell survival, induction of apoptosis and micronucleus formation in SCL-II cells after exposure to the auger electron emitter ^{99m}Tc. Int J Radiat Biol 2004;80:875–80. doi:10.1080/09553000400017705.

[152] Chen J. A compilation of microdosimetry for uniformly distributed Auger emitters used in medicine. Int J Radiat Biol 2008;84:1027–33. doi:10.1080/09553000802499253.

[153] Chan C, Cai Z, Su R, Reilly RM. ^{111}In- or ^{99m}Tc-labeled recombinant VEGF bioconjugates: in vitro evaluation of their cytotoxicity on porcine aortic endothelial cells overexpressing Flt-1 receptors. Nucl Med Biol 2010;37:105–15. doi:10.1016/j.nucmedbio.2009.10.001.

[154] Pomplun E, Terrissol M, Kummerle E. Estimation of a radiation weighting factor for Tc-99m. Radiat Prot Dosimetry 2006;122:80–1. doi:10.1093/rpd/ncl405.

[155] Vallis K a, Reilly RM, Scollard D, Merante P, Brade A, Velauthapillai S, et al. Phase I trial to evaluate the tumor and normal tissue uptake, radiation dosimetry and safety of (111)In-DTPA-human epidermal growth factor in patients with metastatic EGFR-positive breast cancer. Am J Nucl Med Mol Imaging 2014;4:181–92.

[156] Limouris GS, Dimitropoulos N, Kontogeorgakos D, Papanikolos G, Koutoulidis V, Hatzioannou A,

et al. Evaluation of the therapeutic response to In-111-DTPA octreotide-based targeted therapy in liver metastatic neuroendocrine tumors according to CT/MRI/US findings. Cancer Biother Radiopharm 2005;20:215–7. doi:10.1089/cbr.2005.20.215.

[157] Anthony LB, Woltering EA, Espenan GD, Cronin MD, Maloney TJ, McCarthy KE. Indium-111-pentetreotide prolongs survival in gastroenteropancreatic malignancies. Semin Nucl Med 2002;32:123–32. doi:10.1053/snuc.2002.31769.

[158] Valkema R, De Jong M, Bakker WH, Breeman WAP, Kooij PPM, Lugtenburg PJ, et al. Phase I Study of Peptide Receptor Radionuclide Therapy With [lllIn-DTPA~ The Rotterdam Experience. Semin Nucl Med 2002;32:110–22. doi:S0001299802500155 [pii].

[159] Bambynek W, Crasemann B, Fink RW, Freund HU, Mark H, Swift CD, et al. X-ray fluorescence yields, auger, and coster-kronig transition probabilities. Rev Mod Phys 1972;44:716–813. doi:10.1103/RevModPhys.44.716.

[160] Babenkov MI, Bobykin B V., Zhdanov VS, Petukhov VK. KMM-AUGER TRANSITIONS IN 131Xe. Phys Lett 1976;56:363–5.

8. Appendix

8.1 Calculations of chemical caesium concentrations in the medium and intracellular

Chemical caesium concentration in the medium

The number of ^{131}Cs nuclei present can be calculated if the activity is known, by the formula below:

$$\text{Number of nuclei/Bq} = \frac{T(\frac{1}{2})}{\ln(2)} \quad \text{(Eq. 39)}$$

$$\text{Number of nuclei/Bq} = \frac{9.689*24*3600}{\ln(2)} = 1{,}21 * 10^6\ nuclei/Bq \quad \text{(Eq. 40)}$$

Because of the production of ^{131}Cs and the subsequent chemical separation, the specific concentration is very high and close to 100%. The highest activity concentration of ^{131}Cs used was 17MBq/ml and assuming a specific activity of 100%, maximum chemical concentration of caesium in the medium was found to be:

$$\text{chemical concentration of Cs131} = \frac{\text{number of nuclei per beqaurel} * \text{activity cocentration}}{\text{avogadro constant}} \quad \text{(Eq. 41)}$$

$$\text{chemical concentration of Cs131} = \frac{\frac{1.21*10^6 \text{nuclei}}{\text{Bq}} * \frac{17*10^9 \text{Bq}}{\text{L}}}{6.022*10^{23}} \quad \text{(Eq. 42)}$$

$$\underline{\approx 35\text{nM}}$$

-Intracellular chemical caesium concentration

Given a maximum caesium concentration in the medium of ~35nM, as obtained above, the maximum intracellular ^{131}Cs concentration was calculated using the accumulation factor. The accumulation factor of caesium in the HeLa and V79 cells were found to be around 30 and 70 respectively. This gives a maximum caesium concentration inside the HeLa and V79 cells of 1µM and 2µM respectively. As the highest ^{131}Cs activity concentration in the medium used in experiments with V79 cells was significantly lower, the maximum intracellular ^{131}Cs concentration in these cells, will also be lower, however a more precise estimate was not necessary. For comparison the normal concentration of potassium inside mammalian cells is around 140mM [88] , a factor 10^5 higher.

8.2 Cellular S-values

8.2.1 MIRD Cellular S-values for ^{131}Cs

The published MIRD cellular S-values for ^{131}Cs are show in the table below [17]. In addition, the cellular S-value with the whole cell as source and nucleus as target, (which have not been tabulated by MIRD), have been calculated and is shown in the last column (blue column) in the table. These cellular S-values have been calculated using only the already given cellular S-values. As can be seen by below equation (Eq. 43) given by MIRD for calculation of absorbed dose when the radionuclide is located in one or more of the source compartment [17], the cellular S-value for source and target combination S(N←C) is easily calculated using equation (Eq 45)

$$\bar{D}_N = \tilde{A}_C \left[f_N \, S(N \leftarrow N) + f_{Cy} \, S(N \leftarrow Cy) \right] \qquad \text{(Eq. 44)}$$

$$S(N \leftarrow C) = \frac{S(N \leftarrow N) * \text{nuclear volume} + S(N \leftarrow Cy) * \text{cytoplams volume}}{\text{volume of the whole cell}} \qquad \text{(Eq. 45)}$$

Each S(N←C) for the different cellular geometries (cytoplasm and nuclear size), shall of course be calculated using the S(N←N) and S(N←Cy) for those respective geometries.

Radionuclide: ^{131}Cs		Half-Life: 9,69 d			Decay Mode: EC		
Cell radius (µm)	Nucleus radius (µm)	S(C←C) (Gy / Bq s)	S(C←CS) (Gy / Bq s)	S(N←N) (Gy / Bq s)	S(N←Cy) (Gy/ Bq s)	S(N←CS) (Gy/ Bq s)	S(N←C) (Gy/ Bq s)
3	2	5,94E-03	3,09E-03	1,91E-02	1,01E-03	1,72E-04	1,71E-02
3	1	5,94E-03	3,09E-03	1,36E-01	1,42E-03	1,60E-04	1,07E-01
4	3	2,59E-03	1,35E-03	5,94E-03	4,00E-04	1,04E-04	5,47E-03
4	2	2,59E-03	1,35E-03	1,91E-02	4,25E-04	9,64E-05	1,66E-02
5	4	1,37E-03	7,15E-04	2,59E-03	2,09E-04	7,14E-05	2,42E-03
5	3	1,37E-03	7,15E-04	5,94E-03	2,02E-04	6,62E-05	5,31E-03
5	2	1,37E-03	7,15E-04	1,91E-02	2,44E-04	6,35E-05	1,61E-02
6	5	8,13E-04	4,29E-04	1,37E-03	1,28E-04	5,33E-05	1,29E-03
6	4	8,13E-04	4,29E-04	2,59E-03	1,19E-04	4,96E-05	2,35E-03
6	3	8,13E-04	4,29E-04	5,94E-03	1,31E-04	4,74E-05	5,16E-03
7	6	5,26E-04	2,80E-04	8,13E-04	8,83E-05	4,31E-05	7,69E-04
7	5	5,26E-04	2,80E-04	1,37E-03	8,01E-05	3,99E-05	1,25E-03
7	4	5,26E-04	2,80E-04	2,59E-03	8,43E-05	3,79E-05	2,28E-03
7	3	5,26E-04	2,80E-04	5,94E-03	9,51E-05	3,67E-05	5,02E-03
8	7	3,62E-04	1,94E-04	5,26E-04	6,50E-05	3,51E-05	5,00E-04
8	6	3,62E-04	1,94E-04	8,13E-04	5,95E-05	3,38E-05	7,44E-04
8	5	3,62E-04	1,94E-04	1,37E-03	6,08E-05	3,28E-05	1,21E-03
8	4	3,62E-04	1,94E-04	2,59E-03	6,54E-05	3,13E-05	2,21E-03
9	8	2,61E-04	1,40E-04	3,62E-04	4,91E-05	2,83E-05	3,45E-04
9	7	2,61E-04	1,40E-04	5,26E-04	4,58E-05	2,75E-05	4,83E-04
9	6	2,61E-04	1,40E-04	8,13E-04	4,72E-05	2,75E-05	7,20E-04
9	5	2,61E-04	1,40E-04	1,37E-03	4,97E-05	2,77E-05	1,17E-03
10	9	1,95E-04	1,04E-04	2,61E-04	3,80E-05	2,29E-05	2,50E-04
10	8	1,95E-04	1,04E-04	3,62E-04	3,55E-05	2,24E-05	3,34E-04
10	7	1,95E-04	1,04E-04	5,26E-04	3,71E-05	2,24E-05	4,68E-04
10	6	1,95E-04	1,04E-04	8,13E-04	3,94E-05	2,27E-05	6,97E-04
10	5	1,95E-04	1,04E-04	1,37E-03	4,22E-05	2,33E-05	1,13E-03

8.3 Uncertainties

-Clonogenic cell survival

The aim of this experimental study was to compare the survival fraction as function of the absorbed dose for the two different exposures (intracellular^{131}Cs and external γ-rays), while keeping all other experimental conditions as similar as possible (e.g. cell density, dose rates). Each of the two exposures has its own sources of experimental errors that generate an inherent uncertainty in the actual doses delivered. This means that each data point (absorbed dose versus survival fraction) in each of the two data sets from the two exposures will have an uncertainty in the calculated absorbed dose. In addition there are important sources of uncertainty in the observed survival fraction. Not only from the normal liquid handling and pipetting error sources, but also, more fundamentally from the inherent Poisson statistical nature of the cell colony counting. This was especially pronounced in the internal ^{131}Cs exposures, for HeLa cells, due to the very low number of colonies formed. It is a combination of all errors in the survival fraction that gives rise to the uncertainty in the calculated survival fraction.

In the sections below, the different error sources will be treated individually, and then later combined.However, from the starting point it should be made clear, that the aim is to compare the two clonogenic cell survival curves, each having their statistics and confidence limits.

-External γ-ray exposure (protracted)

The integrated external absorbed doses contain the following error terms:

- Uncertainty in calibrated dose rate at fixed distance from the γ-ray source (^{137}Cs), (0.63 %).
- Uncertainty in dose rate decrement due to the decay of the ^{137}Cs source since time of calibration caused by uncertainties in the half-life of ^{137}Cs (0.29 %).
- Uncertainty and experimental errors in the distance adjustments between the cells and the γ-ray source (2 %)

- Uncertainty in timing of the individual exposures (small).
- Dose rate effects (deviation from attempted curve) (neglected)

When these errors are combined in quadrature (because they are independent) the total uncertainty in external absorbed dose becomes: 2.12 %

-Intracellular ^{131}Cs exposures

The integrated internal absorbed doses contain the following error terms:

- Calibration of LSC efficiency for ^{131}Cs (6%), (Uncertainty mainly coming from the Ge-detector)
- Counting statistics in LSC (small)
- Average cell volume determination by the Scepter (Estiamted to be 15%)
- Cell concentration (cell number/uL) (20 %)
- Exposure time (2%)
- LSC counting sample pipetting (5%)
- Error in intracellular cumulative activity due to exponential fit of uptake and release curves (small, further elaborations can be seen below. Less than 4% and ignored compared to the other, larger uncertainties.
- Error in S_C-values from geometry variations (cell layer Height) HELA 3%
- Error in S_C-values from geometry variations (cellular monolayer height) V79 7%

Cummulative internal absorbed dose error: 22 % HeLa cells

Cummulative internal absorbed dose error: 23 % V79 cells

-Survival fraction for both exposures

The survival fraction calculations contain the following sources of error terms:

- Cell concentration counting (5 %) observed
- Number of cells seeded in the controls samples (pipetting, (5 %) systematic)
- Number of cells seeded in the test samples (pipetting, (5 %) observed)
- Counting statistics in the control experiment : (small, is ignored)
- Counting statistics in the exposed arm of the experiments. The uncertainty in the number of counted colonies N is √N, and the relative error then √N / N.

The only "unobserved, systematic" error source is the pipetting (number of cell seeded) of the control samples. However, these seedings are done in triplicates, and the resulting number of colonies counted is used to define the plating efficiency. Therefore, this error is seen as "small" compared to the cell colony number errors. The relative standard deviation of the observed survival fraction varies between 5 % and 21 %. The largest Poisson statistical error for a single observation is in each of the internal dose experiments leading to high absorbed dose for HeLa. Here only 9-10 survivors are counted, giving a Poisson error close to 30 %. However, when all survivors in the triplicate are counted, the sum of survivors is 29 and the Poisson error then 19 %.

The observed error in the survival fractions seem to be in accordance with the error sources listed, as the cumulative relative survival fraction error becomes dominated by the Poisson counting statistics. The total error is therefore assumed to be reflected in the observed variation.[2]

[2] The statistical analysis of the survival fraction from clonogenic cell survival is done by supervisor Mikael Jensen.

8.3.1 The influence of time constant uncertainty for cumulative activity concentration

The cumulative activity concentration (A^*) of intracellular ^{131}Cs could be calculated by equation 48;

$$A^* = \int_0^{480} A_{up} * dt + \int_{480}^{1440} A_{out} * dt \quad \text{(Eq. 46)}$$

Where $A_{up}$and A_{out} are calculated by equation…;

$$\mathrm{A_{up}} = \mathrm{A_{480}} * \left(1 - \mathrm{e}^{-480\,\mathrm{min} * \mathrm{k_c}}\right)^{-1} * \left(1 - \mathrm{e}^{-\mathrm{t} * \mathrm{k_c}}\right) \text{for t} \leq 480 \text{ min}$$

$$\mathrm{A_{out}} = \mathrm{A_{480}} * \mathrm{e}^{-(\mathrm{t} - 480\,\mathrm{min}) * \mathrm{k_{out}}} \; for\; t > 480\; min \quad \text{(Eq. 47)}$$

Using an arbitrary activity concentration of 1 Bq/pL at 480 min, the resulting difference in cumulative activity concentration after 1440 min for the different combinations of k_c and k_{out}, could be calculated.

8.3.1.1 HeLa

k_c and k_{out} were found to be;

k_c: 1/283 min^{-1} (with 95% conf. limits 1/251 min^{-1} to 1/325 min^{-1},R^2 = 0.922)

k_{out}: 1/337 min^{-1} (with 95% conf. limits 1/304 min^{-1} to 1/381 min^{-1}, R^2 = 0.958)

1/339 min^{-1} (using solver)

Worst case (2 s.d.):

The biggest impact of errors in the k_c and k_{out} arises from a situation when one of them is determined too short and the other too long, or vice versa.

Having an error exceeding 2 standard deviations on both k_c and k_{out} at the same time is very unlikely (p=0.05*0.05 = 0.0025), but it can used to graphically illustrate the impact as shown in the curves below (Figure 8.1). This "unlikely" combination leads to an error in A* of 6.5% for HeLa.

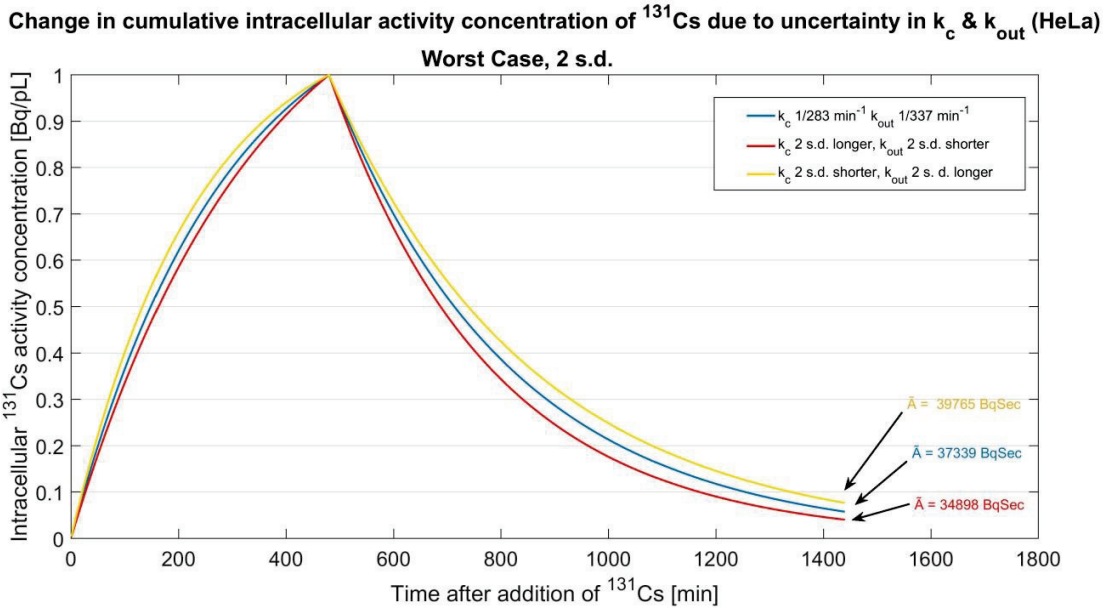

Figure 8.1 Uncertainty in cumulative activity concentration due to variations in k_c & k_{out}

The graph shows the cumulative activity concentration ($\tilde{A}^*$) for three scenarios; the blue line represent the the case used in the dose calculations in which k_c and k_{out} have the values obtanied by the fit. The yellow and red lines represent the case in with the constants (k_c & k_{out}) are 2 standard deviations shorter or longer in opposite directions, resulting in the biggest difference in the cumulative activity. The cumulative activity using an arbitrary activity concentration of 1 Bq/pL at 480 min, calculated for the three situations are shown.

Below are given the change in the cumulated activity concentration (A^*) for different errors in k_c and k_{out}, calculated as shown above

Worst case at 1 s.d.:

Looking at the 1.s.d. limit , I get :

3.3 % increase in A^* if k_c is 1 s.d. shorter, and k_{out} is 1 s.d. longer

2.8 % decrease in A^* if k_c is 1 s.d. longer and k_{out} is 1 s.d. shorter

Less than worst case: 1 s.d. change in k_c and k_{out} in the same direction

1.5% decrease in A^* if time constants are 1 s.d. shorter

2.1% increase in A^* if times constant are 1 s.d. longer

8.3.1.2 V79 cells

K_c and K_{out} were found to be;

k_c: 1/204 min^{-1} (with 95% conf. limits 1/154 min^{-1} to 1/303 min^{-1}, $R^2 = 0.841$)

k_{out}: 1/256 min^{-1} (with 95% conf. limits 1/237 min^{-1} to 1/280 min^{-1}, $R^2 = 0.9768$)

Worst case (2 s.d.):

7.0 % decrease in A^* if k_c is 2 s.d. longer, and k_{out} is 2 s.d. shorter

7.5 % increase in A^* if k_c is 2 s.d. shorter, and k_{out} is 2 s.d. longer

Worst case (1 s.d.):

4.0 % decrease in A^* if k_c is 1 s.d. longer, and k_{out} is 1 s.d. shorter

3.5 % increase in A^* if k_c is 1 s.d. shorter, and k_{out} is 1 s.d. longer

Less than worst case : 1 s.d. change in k_c and k_{out} in the same direction

0.23 % increase in A^* if time constants are 1 s.d. shorter

0.75 % decrease in A^* if time constants are 1 s.d.longer

8.3.2 Normalization of the dose kernel.

The dose kernel used to calculate the absorbed dose to cell nuclei was based on known electron emission energies and rates. The dose kernel was computed using the Cole stopping power approximation, which may be slightly incorrect [82]. However, under all circumstances should the total energy released in the dose kernel be equal to the sum of energies of the intensity weighted electron emissions.

When only using NuDat 2.7 data, this sum is 5.02 keV. However, NuDat 2.7 lists only K- and L- Auger electrons [25]. We know that more electrons are emitted (MXY-Auger, CK-, SCK-electrons).

Bambynek et al (1972) discusses in depth the emission rates of Auger electrons, and compare with experiments available at the time of writing. Bambynek argues for a high emission probability (more than 1 per decay) for CK and M shell Auger electrons for Z around 50, but he has no relevant experimental data for ^{131}Cs [159].

Babenkov (1975) show significant deviation between calculated and measured KMM emission probabilities for ^{131}Cs [160].

Finally, Boon Q. Lee in ref. [93] and in private communication has done a detailed Monte-Carlo calculation of the ^{131}Cs Auger yields. When using his data, the total Auger electron energy released per decay is around 6.20 keV (20-24 % higher than NuDat 2.7). The main differences are slightly higher total K-Auger yields (because KMX are taken into consideration) and higher L-Auger yields. Finally, the inclusion of CK and SCK branches adds a few percent to the total energy release.

We cannot decide if Boons data are the most correct, but the use of Boons total Auger energy release as normalization gives the highest total absorbed dose in our confluent cellular monolayer model, irrespectively of the detailed shape of the dose kernel.

As such a higher absorbed dose will lead to a conservative measurement of the RBE values (by a possible overestimation the absorbed dose) we have chosen to use a normalization of 5.87 keV per decay throughout the S_C-value calculations in this study. This is 17% higher than NuDat 2.7, but

slightly below the value given by Boon. This normalization gives total KMM rates consistent with the experimental measurement given by Babenkov [160].

8.4 Clonogenic cell survival curves

8.4.1 HeLa cells

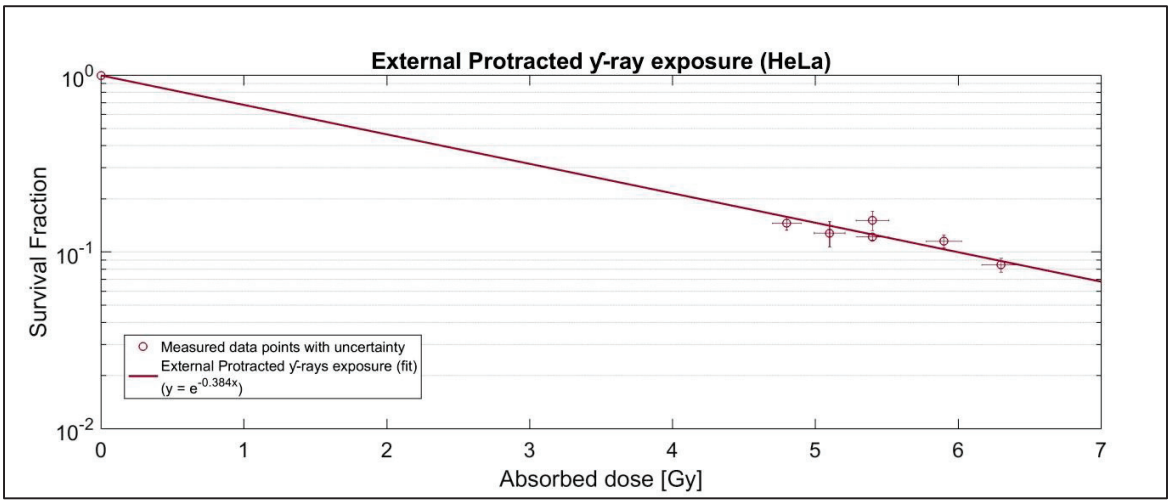

A

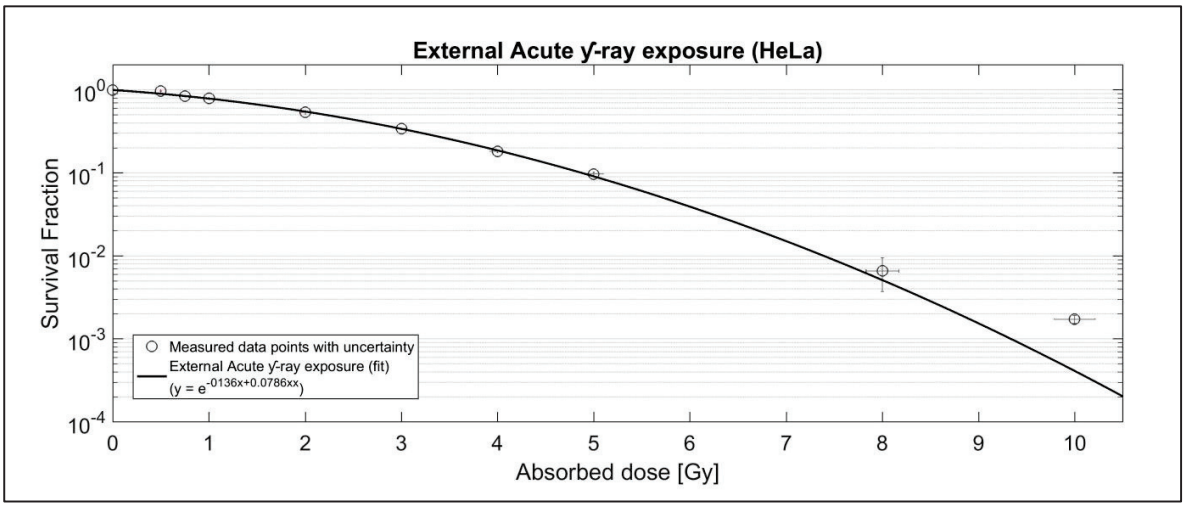

B

Figure 8.2 Clonogenic cell survival curves for HeLa cells external γ-ray (protracted & acute)

Survival fraction as a function of absorbed dose for HeLa cells exposed external γ-ray at similar dose rate profiles (A) or external γ-ray delivered acutely (B) are shown. These survival curves are the same survival curves that are shown in Figure 4.27*p. 145. The survival curve for the protracted γ-rays exposed cell were fitted the linear model,* ($y = e^{-0.384x}$)*, while the survival curve for the acutely γ-exposed cells were fitted to the linear quadratic model* ($y = e^{-(0.136x+0.0786x^2}$)*. The experimentally obtained data points (average of 3 replicates) for the two exposures are shown. The vertical error bars reflect the observed standard deviation in survival fraction, while the horizontal error bars reflect the estimated uncertainty in absorbed dose.*

8.4.2 V79 cells

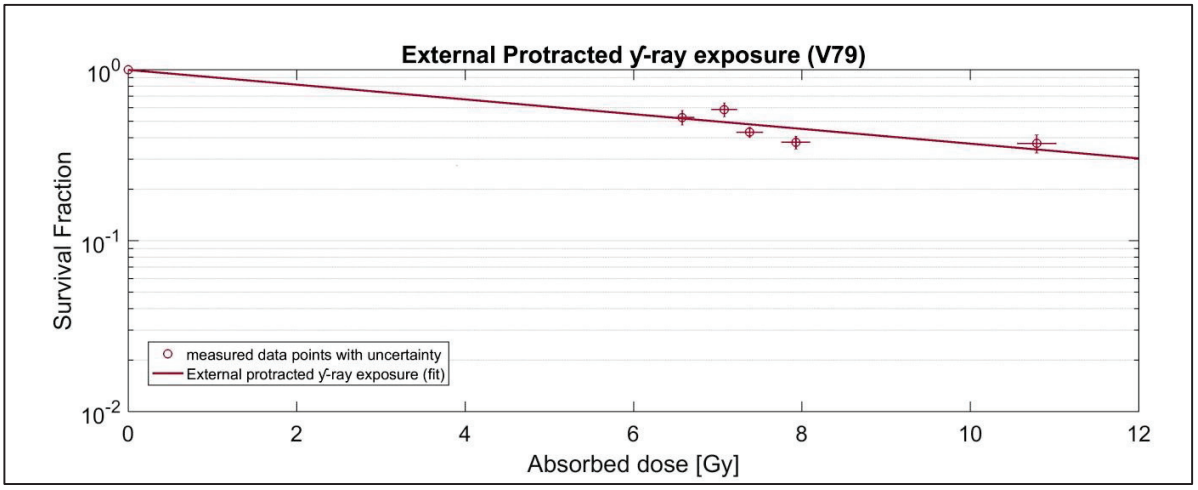

A

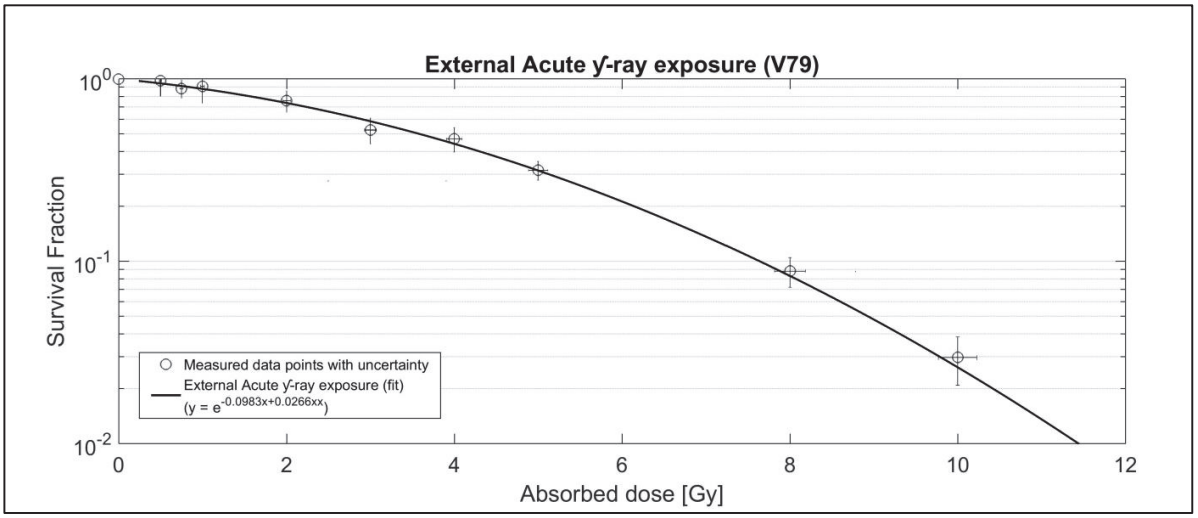

B

Figure 8.3 Clonogenic cell survival curves for V79 cells external γ-ray (protracted & acute)

Survival fraction as a function of absorbed dose for V79 cells exposed external γ-ray *at similar dose rate profiles (A) or external γ-ray delivered acutely (B) are shown. These survival curves are the same survival curves that are shown in* Figure 4.28 *p. 148. The survival curve for the protracted γ-rays exposed cell were fitted the linear model, ($y = e^{-0.0994x}$),while the survival curve for the acutely γ-exposed cells were fitted to the linear quadratic model ($y = e^{-(0.0983x+0.0266x^2)}$. The experimentally obtained data points (average of 3 replicates) for the two exposures are shown. The vertical error bars reflect the observed standard deviation in survival fraction, while the horizontal error bars reflect the estimated uncertainty in absorbed dose.*